Nationalpark
Berchtesgaden

Modelling of the mountain snow cover in the Berchtesgaden National Park

Forschungsbericht 55

Nationalpark
Berchtesgaden

Die Modellierung der Gebirgsschneedecke im Nationalpark Berchtesgaden

Modelling of the mountain snow cover in the Berchtesgaden National Park

Ulrich Strasser

Department für Geographie
(Ludwig-Maximilians-Universität München)

Berchtesgaden, Juli 2008

Forschungsbericht 55

Impressum:

Nationalpark Berchtesgaden
Forschungsbericht 55/2008

Herausgeber:
Nationalparkverwaltung Berchtesgaden, Doktorberg 6,
D-83471 Berchtesgaden, Telefon 0 86 52/96 86-0, Telefax 0 86 52/96 86 40,
e-Mail: poststelle@npv-bgd.bayern.de
Internet: http://www.nationalpark-berchtesgaden.de
im Auftrag des Bayerischen Staatsministeriums für Umwelt, Gesundheit und Verbraucherschutz

ISSN 0172-0023
ISBN 978-3-922325-62-8
EAN-Code 9783922325628

Druck: Berchtesgadener Anzeiger, Berchtesgaden

Gedruckt auf chlorfrei gebleichtem Papier

Titelbild:
Ulrich Strasser

Fotos:
Peter Neusser, Ulrich Strasser

Vorwort

Dieser Bericht ist das Ergebnis von mehreren Jahren wissenschaftlicher Untersuchung der Schneedecke im Nationalpark Berchtesgaden. Die Arbeiten wurden in Kooperation zwischen der Nationalparkverwaltung und der Ludwig–Maximilians–Universität München durchgeführt.

In der Einführung wird ein Überblick über die spezifischen Herausforderungen der Modellierung hydrologischer Systeme im Gebirge gegeben. Dazu werden Skalenaspekte diskutiert und Überlegungen zur Auswahl geeigneter Modelle angestellt. Die Heterogenität der alpinen Schneedecke wird durch Akkumulations–, Umverteilungs– und Ablationsprozesse verursacht. Die genannten Prozesse sind durch vielfache Interaktionen aufgrund der besonderen Topographie und meteorologischen Bedingungen des Hochgebirges geprägt. Die zur Beschreibung dieser Prozesse entwickelten Modelle wurden in das modulare, physikalisch basierte framework *AMUNDSEN*[1] (**A**lpine **MU**ltiscale **N**umerical **D**istributed **S**imulation **EN**gine) integriert. Das Systemdesign und seine technische Funktionsweise werden im zweiten Abschnitt dieses Forschungsberichtes beschrieben, gefolgt von einer Darstellung des Testgebietes: die zentralen Berchtesgadener Alpen (Südostbayern/Deutschland).

Als Nächstes wird die verwendete Datenbasis dargestellt. Es wird gezeigt, wie die meteorologischen Variablen unter Berücksichtigung der Topographie auf die Fläche verteilt werden. Zudem wird die Modellierung der einzelnen, für die Heterogenität der Gebirgsschneedecke relevanten Prozesse erläutert. Diese umfassen die Energie– und Massenbilanz der Schneeoberfläche, Schnee–Vegetations–Wechselwirkungen, gravitative Schneerutschungen und wind–induzierten Schneetransport. Letzterer wird unter Verwendung einer Bibliothek simulierter Windfelder modelliert. Die Validierung der Modellergebnisse wird durch den Vergleich mit Messungen auf der Punktskala, und durch die qualitative Gegenüberstellung des Musters der modellierten Schneedecke mit einer entsprechenden, aus Satellitendaten abgeleiteten Schneebedeckungskarte durchgeführt.

Im ersten Ergebnisabschnitt wird gezeigt, in welchem Ausmaß die Prozesse der Akkumulation, Umverteilung und Ablation die Heterogenität der Schneedecke beeinflussen, und wie sie die Menge des als Schnee gespeicherten Wassers und seine Schmelzdynamik steuern. In einem nächsten Schritt werden mögliche zukünftige Entwicklungen der Schneedecke unter Verwendung zweier Klimawandel–Szenarien simuliert, welche durch Anwendung eines stochastischen Wettergenerators erzeugt werden.

Der letzte Abschnitt beinhaltet Schlussfolgerungen, Vorschläge zu möglichen Weiterentwicklungen und Verbesserungen der Modellrechnungen, sowie eine Diskussion zu zukünftigen Forschungsprioritäten im Bereich der alpinen Schneedeckenmodellierung.

Die Synthese der Modellalgorithmen, ihre Entwicklung, Integration, Validierung und Anwendung wurde von vielen Kollegen und Freunden unterstützt. Die Ludwig–Maximilians–Universität (München) stellte ein exzellentes Umfeld für die Forschungsarbeiten zur Verfügung. Wolfram Mauser, Inhaber des Lehrstuhls für Geographie und Geographische Fernerkundung, förderte die wissenschaftlichen Untersuchungen und setzte sich für den Alpine*Snow*Workshop[2] ein, welcher im Oktober 2006 in Kooperation mit der Nationalparkverwaltung in München durchge-

[1] Ein offensichtlicher Grund zur Wahl dieses Akronyms ist, an den berühmten Norwegischen Polarforscher Roald Amundsen (1872-1928) zu erinnern. Siehe letzte Seite.
[2] http://www.alpinsnowworkshop.org

führt wurde. Der Workshop diente dazu, die internationale Gemeinschaft der Schneewissenschaftler zusammenzubringen und war eine hervorragende Plattform zum Diskutieren, zum Ideen austauschen und um Erfahrungen und Visionen zu teilen (siehe den Forschungsbericht 53 dieser Reihe). Meine Kollegen am Department für Geographie haben mit ihrer Kompetenz und mit ihrer praktischen Unterstützung tatkräftig zur Entwicklung und Anwendung der beschriebenen Modelle beigetragen. Ihnen allen sei hier ganz besonders gedankt. Matthias Bernhardt hat seine Ergebnisse zum wind-induzierten Schneetransport beigesteuert und mit seiner Erfahrung zahllose Diskussionen bereichert. Seine Doktorarbeit, durchgeführt im Nationalpark Berchtesgaden, wird einen wertvollen Kenntnisgewinn zur Heterogenität der alpinen Schneedecke darstellen.

Die Nationalparkverwaltung Berchtesgaden hat die Aktivitäten immer großzügig unterstützt, professionelle Feldarbeit durchgeführt und freien Datenzugang gewährt. Insbesondere sei an dieser Stelle Helmut Franz gedankt, der mit seinem unermüdlichen Einsatz die Arbeiten erst ermöglicht hat. Die verwendeten Daten beinhalten auch Messungen der Bayerischen Lawinenwarnzentrale (München), des Deutschen Wetterdienstes (Offenbach) sowie des Salzburger Lawinenwarndienstes (Salzburg), denen dafür auch herzlich gedankt sei.

Besonderer Dank für die fruchtbare Zusammenarbeit gebührt meinen Kollegen Markus Weber (München), Javier Corripio (Innsbruck) und Stephan Gruber (Zürich), die ihr Wissen, ihre Erfahrung und ihre technischen Fähigkeiten in passionierende Diskussionen zur Weiterentwicklung von AMUNDSEN einfließen haben lassen. Markus Weber verbesserte auch das erste Manuskript dieses Berichtes und kontrollierte die mathematischen Formeln.

Die Entwicklung von AMUNDSEN wurde von der großzügigen Förderung durch die Projekte Arolla[3] und GLOWA-Danube[4] sowie Brahmatwinn[5] unterstützt.

Um diesen Forschungsbericht einer möglichst breiten, internationalen Gemeinschaft zugänglich zu machen, ist der inhaltliche Teil in Englisch verfasst. Die Zusammenfassung und Ausblick sind in Deutsch und in Englisch. Das Englisch wurde vom zweisprachigen Schneehydrologen Stefan Pohl (Freiburg) korrigiert. Ihm sei an dieser Stelle dafür herzlich gedankt.

[3] http://ww.arolla.ethz.ch/ (funded by ETH)
[4] http://www.glowa-danube.de/ (funded mainly by bmb+f)
[5] http://www.brahmatwinn.uni-jena.de (funded by EC)

Zusammenfassung

Im Hochgebirge wird ein beträchtlicher Anteil der Niederschläge temporär in der Schneedecke gespeichert. Die Dynamik dieser Schneedecke unterliegt dabei einer Reihe von spezifischen Prozessen, die zu einer ausgeprägten räumlichen Heterogenität der Schneebedeckung führen. Diese Prozesse umfassen die stark von der Topographie beinflussten meteorologischen Vorgänge in der Grenzschicht, die Massenbilanz der Schneedecke am Boden, die Wechselwirkungen zwischen Schnee und Vegetation sowie die laterale Verlagerung von Schnee aufgrund von gravitativen Rutschen und wind–induziertem Transport.

Im vorliegenden Forschungsbericht wird eine kontinuierliche, räumlich sowie zeitlich hochaufgelöste Modellierung dieser Prozesse mit einer Reihe von flächenverteilten Modellen dargestellt. Die Prozessbeschreibungen orientieren sich, soweit möglich und sinnvoll, an physikalischen Gegebenheiten, so dass aufwendige Kalibrierungen nicht notwendig sind und das Modellsystem prinzipiell in Ort und Zeit übertragbar ist. Dadurch und durch die Berücksichtigung der wesentlichen, die Heterogenität der hochalpinen Schneedecke verursachenden Prozesse werden Szenariosimulationen zukünftiger Schneedeckenentwicklung für verändertes Klima ermöglicht sowie eine Vorhersage der Verteilung und Verfügbarkeit der Wasserressource Schnee in Hochgebirgs–Einzugsgebieten. Anhand der Modellergebnisse wird eine detaillierte Diskussion der sich aus den einzelnen Prozessbeschreibungen ergebenden Muster durchgeführt. Testgebiet ist die hochalpine Region des Nationalparks Berchtesgaden (Bayerische Alpen, Süddeutschland).

Die Prozesse zur Akkumulation, der Wechselwirkungen zwischen Schnee und Vegetation, der gravitativen Umverteilung sowie der Ablation von Schnee werden mit dem physikalisch basierten, flächenverteilten Modell AMUNDSEN (**A**lpine **MU**ltiscale **N**umerical **D**istributed **S**imulation **EN**gine) simuliert, welches zur Simulation der Schneedeckendynamik in Hochgebirgsräumen kleiner bis mittlerer Skala konzipiert wurde. Das Modell berechnet stündliche meteorologische Eingabefelder aus Punktmessungen von möglichst repräsentativ im Raum und in der Höhe verteilten Stationen. Aus den Messwerten werden unter Einsatz eines integrierten stochastischen Wettergenerators Szenarien zukünftigen Klimas produziert. Die Prozesse und Auswirkungen von wind–induziertem Schneetransport werden mit einem separaten Modell unter Verwendung einer Bibliothek modellierter Windfelder simuliert.

Bei der Aufbereitung der meteorologischen Felder, dem Modellinput, wird den spezifischen Charakteristika hochalpiner Gebiete Rechnung getragen. Dazu zählen dynamische, höhenabhängige Gradienten der meteorologischen Variablen, der Einfluss der Topographie auf die kurz– und langwelligen Strahlungsflüsse sowie deren Modifikation durch Schatten, multiple und Geländereflexionen und Wolken. Das räumliche Muster der Strahlungsflüsse, welche zur Schneeschmelze wesentlich Energie beitragen, ist außerordentlich komplex. Sie spielt aber eine entscheidende Rolle für das Verständnis der zeitlichen Dynamik und der räumlichen Heterogenität der hochalpinen Schneedecke.

Die Energiebilanz der Schneeoberfläche wird mit einem physikalisch basierten Ansatz bestimmt, einschließlich der expliziten Formulierung des beteiligten Austausches von Masse, d.h. der Akkumulations– und Ablationsprozesse. Beide Bilanzen sind für den betrachteten Schneespeicher zwischen Boden und Atmosphäre geschlossen.

In vielen gemäßigten Berggebieten ist Bergwald der dominante Landnutzungstyp. Mit AMUNDSEN wird der Einfluss des Bestandes auf die mikrometeorologischen Verhältnisse über dem Schnee am Boden explizit behandelt. Außerdem wird die Sublimation von zuvor interzipiertem Schnee zurück in die darüberliegenden Luft-

schichten berücksichtigt, sowie Schmelze und Herunterfallen von Schnee aus dem Interzeptionsspeicher. In den höheren Bereichen vieler hochalpiner Gebiete dominieren steile Felswände und bilden zusammen mit scharfen Gipfelgraten das prägende Landschaftselement. Die hier wirkenden Prozesse der lateralen Umverteilung von Schnee aus den steilen Hangbereichen in die darunter befindlichen Verflachungen, meist Karflächen, bedingen einen Großteil der in Hochgebirgsregionen typischen räumlichen Muster der Schneedecke. Um diese realistisch wiedergeben zu können, werden die dafür relevanten Prozesse explizit modelliert. Es entspricht der visuellen Erfahrung, dass in den Kar- und Muldenbereichen die höchsten Akkumulationsraten vorkommen und die lokale Schneebedeckung bis in das späte Frühjahr hinein andauern kann, während die Gipfelgrate und steilen Felsflanken weitgehend schneefrei bleiben.

Die wind-induzierten Prozesse der Erosion, des Transportes, der Deposition sowie der Sublimation von Schnee aus einer Schicht turbulenter Suspension werden mit dem physikalisch basierten, flächenverteilten Modell SnowTran-3D quantifiziert. Dabei finden mit dem Atmosphärenmodell MM5 simulierte Felder von lokaler Windgeschwindigkeit und -richtung Verwendung. Die Windfelder wurden zuvor berechnet und in einer Bibliothek gespeichert, auf die zur Laufzeit der Schneedeckenmodellierung zugegriffen wird. Der Zugriffsschlüssel zu dieser Bibliothek wird durch DWD-Lokalmodell-Rechnungen dargestellt, die die Kopplung zwischen der Schneemodellzeit und -skala und dem synoptischen Status der Atmosphäre erlauben.

Mit Hilfe eines stochastischen Wettergenerators, der direkt mit AMUNDSEN gekoppelt ist, können auf sehr effiziente Weise meteorologische Zeitreihen potentieller zukünftiger Klimaentwicklung generiert werden. Dies geschieht durch Aufteilung der vorhandenen meteorologischen Messreihen in zeitlich begrenzte Perioden und anschließendes Umsortieren unter Berücksichtigung eines vorgegebenen klimatischen Trends. Daraus wird eine zukünftige, physikalisch konsistente Zeitreihe meteorologischer Daten unter Reproduktion dieses Trends konstruiert. Die anschließende Modellierung der Schneedeckendynamik unter Verwendung der generierten zukünftigen Zeitreihe meteorologischer Eingabedaten erlaubt dann eine Quantifizierung der potentiellen Veränderung des Wasserspeichers Schnee unter den veränderten Klimabedingungen, sowie die Abschätzung der entsprechenden Auswirkungen auf die Hydrologie eines Hochgebirgs-Einzugsgebietes.

Die Validierung des Modellsystems auf der Punktskala zeigt die gute Übereinstimmung der Ergebnisse mit den Messungen. Ein Vergleich mit einer aus Satellitendaten abgeleiteten Schneebedeckungskarte zeigt die generelle Übereinstimmung der Modellergebnisse mit der Beobachtung auch auf der Flächenskala, und insbesondere die Verbesserung des modellierten Schneebedeckungsmusters durch die Berücksichtigung der gravitativ bedingten Schneerutsche. Insgesamt ist aber anzufügen, dass trotz der guten Übereinstimmung in Anbetracht der Anzahl und Verflechtung der betrachteten Prozesse ein Vergleich zwischen Rechenergebnis und Messung zu nur einem einzelnen Zeitschritt kein aussagekräftiges Maß für die Güte eines so komplexen Modells sein kann. Erst eine Zeitserie von aus Fernerkundungsdaten abgeleiteten Validierungskarten wird diesem Anspruch gerecht werden können. Ein terrestrischer Sensor wäre hierzu ein geeignetes Instrument mit hinreichender räumlicher und zeitlicher Auflösung. Die Anwendung des beschriebenen Modellsystems wird für die saisonale Schneedeckenentwicklung im Gebiet des Nationalparks Berchtesgaden durchgeführt. Als Ergebnisse werden die einzelnen verteilten Größen der Massenbilanz diskutiert. Hauptaugenmerk der Analyse liegt bei den speziellen Eigenschaften der räumlichen Muster der Schneedecke. Deren Heterogenität ist im Wesentlichen bedingt durch den hochalpinen Charakter der Topographie. Darüber hinaus wird der jährliche Beitrag der Wasserbilanzgrößen quantifiziert und die mittlere jährliche Evapotranspiration mit Hilfe gemessener Abflüsse abgeschätzt.

Als Ergebnis der Modellierungen zeigt sich, dass auf lokaler Skala der Niederschlag, die Schneeschmelze und die Sublimation während wind–induziertem Schneetransport bedeutende Bilanzgrößen darstellen, während der Anteil von Kondensation und Sublimation von Schnee am Boden bzw. aus dem Bestand mäßig ist. Auf regionaler Skala dagegen stellen Niederschlag und Schneeschmelze bedeutende Bilanzgrößen dar, Sublimation aus dem Bestand einen mäßigen, und Kondensation und Sublimation von Schnee am Boden sowie aus wind–induziertem Schneetransport geringe. Laterale Umverteilung von Schnee beinflusst die Wasserbilanz des Einzugsgebietes nicht, ist lokal aber hochsignifikant.

Unter Einsatz des stochastischen Klimagenerators werden sodann zwei zukünftige Szenarien veränderten Klimas konstruiert und für prognostische Modellläufe verwendet, um die zukünftige saisonale Entwicklung der Schneedeckendynamik im betrachteten Hochgebirgsgebiet unter veränderten klimatischen Bedingungen abzuschätzen. Die Ergebnisse zeigen für einen angenommenen mäßigen Trend zu höheren Temperaturen einen prinzipiell deutlichen und räumlich stark differenzierten Rückgang der Schneedeckendauer. Dies gilt auch für das Szenario, das zusätzlich zur Erwärmung eine Verschiebung von Sommerniederschlägen in den Winter berücksichtigt. Obwohl letztere überwiegend als Schnee fallen, wird der Effekt der zusätzlichen Akkumulation vom angenommenen Temperaturtrend und den damit einhergehenden veränderten meteorologischen Bedingungen weitgehend kompensiert.

Das vorgestellte Modellsystem ist ein Schritt hin zur Entwicklung von Landoberflächenmodellen, welche den Anforderungen an eine vollständige und realistische Darstellung von Schneedeckenprozessen in Hochgebirgsräumen gerecht werden. Damit können auch Simulationsrechnungen für längerfristige Szenarien zukünftiger Klimaentwicklung durchgeführt werden. Darüberhinaus stellt dies eine wesentliche Voraussetzung für die korrekte Wiedergabe von zukünftiger Gletscherdynamik dar, welche wegen der Bedeutung der Eisressourcen v.a. für die Hydrologie, die Wasserwirtschaft und den Tourismus in hochalpinen Einzugsgebieten von besonderem Interesse ist.

Die wichtigsten Eingabedaten für AMUNDSEN, welche für ein betrachtetes Gebiet vorliegen müssen, umfassen stündliche Zeitreihen der meteorologischen Variablen, ein digitales Geländemodell, den sky view factor sowie LAI bzw. Wuchshöhe der Bäume. Mit der zu erwartenden weiteren Steigerung verfügbarer Rechenleistung wird es bald möglich sein, das Modell für ganze Gebirgseinheiten auf regionaler Skala anzuwenden. Durch die bidirektionale Kopplung der Landoberflächen–Prozesse mit entsprechenden Klimamodellen wird dann eine verbesserte Abschätzung der Menge, Verteilung und Verfügbarkeit zukünftiger Wasserressourcen in hochalpinen Gebirgseinzugsgebieten möglich sein.

Contents

Modelling of the mountain snow cover in the Berchtesgaden National Park

Modelling of the mountain snow cover in the Berchtesgaden National Park

Ulrich Strasser

1 Introduction

In terms the availability of water for mankind, snow dominated regions are crucial for downstream inhabitants in their function of collecting, storing, and releasing water resources: More than one sixth of the earth's population is relying on seasonal snowpacks and glaciers for their water supply (Barnett et al. 2005). With some exceptions, these regions are at latitudes greater than ~45° North and South and mountains where water resources are accumulated and stored during winter, and released into the rivers during the ablation season generally in late spring and summer. Beneficial effects of such runoff regimes include increased precipitation amounts due to the topographical effect of mountain ridges on the amosphere, and the fact that the release of meltwater generally coincides with periods of high water demand. Thus, a mountain snow cover represents a natural storage system of considerable importance in terms of availability and distribution of the water resources for the forelands (Burlando et al. 2002). The meltwater release from the snow storage system is therefore of much higher importance for the forelands than melting glacier ice, at least in the streamflow of foreland rivers. Only at the headwater spatial scale, and during particular melting situations on high-radiation days in summer, does the water originating from melting ice represent a significant portion of runoff.

Generally, the prediction of the availability of meltwater resources from a mountain snow cover is complicated by the fact, that it is characterized by a heterogeneity that is highly variable in space and time, originating from the various processes of accumulation, ablation, and redistribution of snow (Marsh 1999, Pomeroy et al. 1998). A proper representation of these processes in model algorithms is still a significant challenge in mountain hydrology since the predictive capabilities of a model strongly depend on the accuracy with which the main processes are represented (Klemes 1990). This is a particularly important issue when it comes to future scenario simulations.

1.1. Snow cover processes in mountain regions

Large differences in snow accumulation can be caused by an increase in precipitation with elevation. It is still a great challenge to measure this phenomenon and moreover to account for it when distributing measured precipitation over a region with complex topography (Lang 1985). Furthermore, a critical role for snow distribution is represented by the phase change between rain and snow: although clearly visible in the landscape as a distinct line, this transition is not an easy task to model. For an accurate recording of both, precipitation amount as well as its phase, representative meteorological stations at higher elevations are required to provide a picture of the respective differences which may, on top of that, also vary considerably in time (Strasser et al. 2004). Furthermore, since the phase of precipitation is determined by the temperature of the entire boundary layer, the 2 m temperature, as recorded by most meteorological sensors, only gives a vague estimate whether precipitation falls as rain or snow (the typical range of transition is between –1 °C and +4 °C). Hence, attempts have been made to better represent the physical processes in the surface layer, e.g. by considering humidity and related energy transfer at the snow crystal surfaces (Weber 2005).

Ablation patterns are very sensitive to radiation input, and thus to topography at the local scale. In high mountain regions many steep North-facing slopes are shaded most of the daytime, at particular sunlight-protected locations even in summer, and a proper consideration of this effect is crucial to predict local melt rates. On the other hand, shortwave radiation is reflected (mostly) from South-facing, snow-covered slopes with the effect, that global radiation input can be additionally increased by this effect at certain locations on the opposite side of a valley, leading to an accelerated melt there. Hence, a detailed consideration of the radiative fluxes is an important prerequisite for an adequate modelling of the snow cover in mountain regions.

In forested mountain areas significant variations in snow coverage can develop by the pro¬cesses of canopy interception and sublimation (Marsh 1999, Pomeroy et al. 1998). Snow falling on forest canopies is partitioned into interception by the canopy, and melt unload to the forest floor. Intercepted snow has a large exposed surface area and can be subject to high sublimation rates especially in dry continental environments. It can on the other hand also be removed from the canopy by direct unloading and dripping of meltwater to the ground (Liston and Elder 2006, Pomeroy et al. 2002). Depending on the efficiency of interception, its duration, and the atmospheric conditions, the local losses can be as large as up to 30 % of snow precipitation (Pomeroy and Gray 1995). To quantify the water balance as accurately as possible, such additional fluxes of moisture back into the atmosphere have to be considered (Pomeroy and Essery 1999). The snow cover beneath the canopy, in contrast to open areas, is mostly sheltered from wind and solar radiation but receives increased thermal radiation emitted from the trees (Link and Marks 1999a, b), influencing both quantity and timing of runoff of meltwater from forested catchments. Forest canopies strongly modify the interactions between snow-covered surfaces and the atmosphere. The extensive areas of boreal forests have thus been found to have important effects on weather and climate at hemispheric scales. Even the litter on the forest floor has a significant effect on the radiative properties of the snow cover beneath a canopy (Melloh et al. 2001, Hardy et al. 2000).

A specific feature of the snow cover in areas with steep topography is the process of gravitational redistribution of snow. Snow either immediately slides down during the precipitation event, or it is later entrained in a snow slide and then deposited at the base of the hillslopes. From the steep summit region of an alpine mountain almost all precipitation that fell as snow is laterally removed and accumulated at the base of the surrounding slopes (STRASSER et al. 2008c). Whereas the adjacent rock faces and ridges, although higher, can be almost or totally snow-free, such zones of very high winter snow accumulation can form perennial snow patches which are significant elements of the summer mountain landscape (GRUBER 2007, STRASSER et al. 2008c, MACHGUTH et al. 2007). Where the topography allows the collection of snow in a funnel-like surface feature, often in conjunction with effective shading of the surface, accumulation rates can be such that glaciers are formed even in an elevation where they could otherwise not exist, e.g. the Blaueis glacier or the Höllental glacier in the Bavarian Alps (KUHN 1995, KUHN 1993a, b).

Finally, wind-induced snow transport can lead to small scale redistribution of snow (MARSH 1999, POMEROY et al. 1998). Due to their complexity, the processes of lateral transport of both, falling as well as already deposited snow, are mostly neglected in the practice of hydrological modelling. However, in mountain terrain the local snow cover evolution can be highly dependent on wind-induced erosion and deposition. The resulting modification of the snow cover subsequently affects the temporal dynamics of runoff generation during melt. Furthermore, sublimation of transported snow is of importance. Under certain conditions, it can be the cause for a significant loss of snow mass, amounting to up to 45 % of the local winter precipitation (MARSH 1999). However, in mountainous terrain it is very difficult, if not impossible, to model wind-induced snow transport due to the difficulty of properly distributing the recordings of wind speed and direction. Bernhardt et al. (2008a, b) have recently developed a technique to model wind-induced snow transport using a library of simulated wind fields, a new way to provide meaningful windfields in complex terrain. Results show that in very steep alpine topography, wind-blown snow is mostly deposited in areas where it is later entrained by snow slides, the combined processes being very efficient in removing the snow from the highest regions and accumulating it in the cirques beneath (STRASSER et al. 2008c).

1.2. Requirements for modelling the mountain snow cover

The modelling of all these effects is strongly dependent on the resolution of the available input data which (BLÖSCHL 1999, CLINE et al. 1998). The resolution also determines the accuracy with which the topographical features of a certain domain can be reproduced. An important demand on the accurate modelling of snow patterns at proper resolutions is represented by the steadily increasing needs of *Global Circulation Models* (GCM's) in terms of an adequate land surface representation (LISTON 2004). The algorithms that describe snow processes in these models are important components because much of the earth's land surface is at least temporally covered with snow. On top of that, strong snow–climate feedbacks have been identified from model output and measurements (POMEROY et al. 1998). Much effort is therefore invested in the development of sophisticated, physically realistic descriptions of the snow processes across all scales.

In very high mountain regions characterized by extremely wind-exposed ridges and steep slopes (i.e., such as the summit crests in the Himalayas), the modelling requirements get particularly demanding. For long-term simulations and when glacier response to a changing climate is of interest, it is mandatory to include the removal of snow from high mountain crests in the modelling. If this process is not considered, the modelled snow heights become unrealistically high. In nature, accumulated solid precipitation is removed by the combined effects of sublimation, blowing snow, and avalanches. As a result, and in accordance with visual experience, the snowpack does not infinitely accumulate in areas where no melt occurs. In contrast, snow mass-balance models which do not include the mentioned effects, underestimate snow removal and lead to unrealistic snow depths in long-term simulations. These considerations are supported by the observation of reduced snow cover in high mountain areas due to changes in climate: More and more rocks become visible in areas where no melt occurs as a results of increased snow sublimation due to higher radiative energy input and/or reduced precipitation. The 1999 *Mallory and Irvine Research Expedition* found the remains of George L. Mallory at 8200 m a.s.l., lost on Mount Everest in 1924. In the exceptionally dry and sunny spring season of 1999 he had been released from snow which had covered him the previous 75 year (MountainZone.com[6], ANKER and ROBERTS 1999).

From all the aspects hitherto mentioned follows, that physically based descriptions of snow accumulation, ablation, and redistribution are important components of any hydrological process modelling in mountain areas. Not only have the dynamics of a seasonal snowpack with all the related vertical and lateral fluxes of mass and energy direct effects on the runoff regime; they also determine ecological habitat characteristics, seasonal vegetation evolution, aspects of agricultural practices, the local climate, and tourism (HECHT and HUBER 2002, Eberhardt 2002, Marsh 1999, Pomeroy et al. 1998). Furthermore, the estimation and prediction of avalanche risk is of crucial importance in mountain regions, particularly for the respective measures of blocking, prevention, and construction (BARTELT and LEHNING 2002).

[6] http://www.classic.mountainzone.com/everest/99/north/

1.3. Theoretical background

1.3.1. Modelling mountain hydrology – an ultimate challenge

With regard to the specific challenges of modelling mountain hydrology, a groundbreaking paper has been published in 1990 by the former President of the *International Association of Hydrological Sciences* (IAHS) (KLEMES, 1990): This comprehensive description of the manifold difficulties in assessing mountain hydrology processes is of particular relevance for the snowmelt component of any landsurface model for a mountainous domain, and, hence, for what is important here. In the following, „hydrological modelling" (and synonymously „snowmelt modelling") is regarded as a synthesis of observed empirical facts and their theoretical understanding, expressed in terms of general and internally consistent quantitative relationships formulated in computationally feasible algorithms. Continuous observations of the states of nature in mountainous terrain are the most difficult to carry out, and the processes governing mountain hydrology cover the widest range, thus posing the greatest demands on the theoretical understanding. Therefore, to call the challenge of modelling mountain hydrology *ultimate* is justified even from today's perspective. Since in this work a simulation tool for modelling mountain–specific snow processes is developed at a scale which promises to overcome many of the existing limitations, it is adequate to position it in the framework of this theoretical background and to put the respective modelling aspects into a proper perspective.

1.3.2. Observation of the states of nature

In mountainous terrain, continuous *accessibility* is a great challenge. As a result, weather stations are often located in the more accessible valleys which only allows the estimation of a rough sketch of the course of a meteorological variable across a mountain ridge especially when considering the topography of alpine mountains. The measurement of any snow–related variable at higher elevations requires a skiing expedition, or the service of a helicopter. Of course, many mountain sites can nowadays be comfortably reached with the help of a cablecar – but as a consequence these locations are more or less affected by human activities and far away from a natural state. A great step forward has been achieved by using remote sensing techniques, e.g. for the mapping of snow (an overview of snow–related remote sensing techniques is given in König et al. 2001). However, the problem of accessibility will remain a permanent one since ground measurements will be required for the validation of remotely sensed data. Furthermore, for some phenomena (e.g., the inside state of a snowpack) they will remain the only source of information.

The second challenge is *accuracy*, or less generally speaking the *signal–to–noise ratio*. Not only can the rough environmental conditions cause malfunctions or complete failures of the instruments, resulting in inhomogeneities and gaps in the records. Furthermore, long slopes and strong winds affect the catch of precipitation gauges or a cork of snow may congest the aperture of the device in winter. Subsequent melt cause an „extreme event" when the cork drops onto the sensor, mostly on sunny days with high radiative energy input (making such artificial events at least easier detectable). Recordings of the 2 m temperatures over snow without radiation shielding and artificial ventilation are quite unreliable due to the radiation error and cannot be corrected (GEORGES and KASER 2002). Generally, an inverse relationship exists between the accuracy of measurements and the large scale roughness of the terrain, e.g. for the systematic error of precipitation measurements (SEVRUK 1985).

The third aspect in this respect is *representativeness*. Even if assumed to be accurate, any specific observation is only representative for a small areal extent, representing a significant obstacle in accurately describing the state of nature in the surrounding area. The distribution from point measurements to the spatial scale is a general research issue in hydrological sciences, but it becomes most serious in mountain areas which are characterized by the most significant heterogeneities in all hydrological and meteorological components. Again, remote sensing is a promising technique able to supply spatially distributed or at least averaged quantities which can be used to validate and improve spatial interpolates of point observations.

The overall conclusion of the major effects described herein is the fact that in many mountain catchments the components of a long–term water balance cannot be reliably established; this also holds true for the catchment considered in the present investigation.

1.3.3. Theoretical understanding

The variety of the physical conditions over which the processes range and which are relevant for mountain hydrology increases the difficulty in *theoretically understanding* them; e.g., in terms of vegetation, surface temperature, or surface and groundwater regime a single mountain slope includes conditions which spread over thousands of kilometers and tens of degrees of latitudes in flat regions. Surface water velocities range over the whole spectrum, from vertical rock walls to alluvial plains. Response times to precipitation input may vary from some minutes to centuries depending on whether it falls on exposed slopes or on a glacier. The influence of topography on the distribution of precipitation surpasses the highest extremes observable in flat terrain. Sharp and stable discontinuities in irradiation form cloud reservoirs on the one side of a mountain ridge, while the other is sunny. All this intrinsic theoretical complexity makes it necessary for mountain hydrology to employ an interdisciplinary approach for a better understanding of the observed phenomena.

1.3.4. Implications for modelling mountain hydrology

In the context of modelling mountain hydrology, the height of the mountains themselves becomes important with respect to the term *scale*: very different processes will affect runoff in the glacierized central Alps compared to a forested catchment in a pre–alpine region. The vertical dimension of a modelling domain has a direct relevance to the design and setup of a model for this region, its parameterization, and the representation of scale, i.e. the extent of lumping. In this respect it should be noted here that the differentiation in lumped and distributed is relative, stemming from the fact that every element of a distributed model is itself a lumped representation of smaller scale elements (KLEMES 1990). On the other hand, a lumped model may become an element of a distributed model at a larger scale (this aspect becomes of particular importance for communications in the scientific community, where the members all have different backgrounds of education and origin).
Precipitation is not the only important component in mountain hydrology models with respect to *model input;* the energy input represents an indispensable component as well, i.e. to separate liquid from solid precipitation. Secondly, many inputs into mountain hydrology models must first be modelled themselves, since many measurements cannot be made where they are most needed. Thus, the general input processing becomes *input modelling* in mountain hydrology models (the ones described and applied in the following are typical examples). The required modelling of model input data can become more complex and elaborate than the mountain hydrology model itself. A simplification of this aspect can only be achieved if the model provides its own input data, e.g. the snow cover area which is used as input in the SRM model (MARTINEC et al. 1998).

With respect to the *resolution of modelling* in mountain areas, their nature generally suggests the use of finer–grid models than flat basins of comparable size would require to obtain comparable results. However, the „optimum" resolution depends on the purpose of the applied model, the available data and its quality, and the type of parameterizations implemented. Conceptual models have the advantage that, due to the intensive use of proxies, they are relatively insensitive to the various systematic errors in the input data, and the existing ones can be filtered out by the process of calibration. This, however, comes at the cost of limited applicability and credibility of the model. If errors in the data and in the model compensate each other, the model may give plausible results for the wrong reasons but fails under conditions other than the ones prevailing in the calibration data (WMO 1986). Where the representation of physical processes and their interactions are replaced by postulated ones, and where calibration parameters are just regression variables, the „accuracy" achieved by model calibration may be increased, but not the understanding of the underlying physics, as well as the general applicability and transferability of the model. Appropriate parameterization and inputs of the right kind may significantly increase a model's parsimony in terms of parameters required without necessarily sacrificing its performance. Furthermore, there is also no apparent reason to assume the various storage components of a hydrological mountain system (snowpack, glacier, and groundwater) are linear systems; actually, there are many inherent nonlinearities and also threshold effects, e.g. the lateral transfer of large snow masses by avalanches into low elevation zones with consequent acceleration of respective local melting rates in spring.

With respect to *model output*, it is often the case that the stream gauge against which the mountain hydrology models are validated, or which is used in model optimization (be it calibration or a proper adaptation of the model's parameters) is far away from the ridges and slopes where the snowmelt and runoff generation processes are internally represented in the model, and the runoff is generated. Hence, by „improving" the performance of the models their conceptual soundness may even be corrupted, since many components generating the streamflow observed at the stream gauge may not be internally represented by the model, e.g. heterogeneities in the snow cover or a glacier matrix, or the features of the channel characteristics. As a consequence, a systematic improvement of models and the understanding of the processes relying on single–point, output–based optimization is difficult. This is particularly true for mountain hydrology models, where there are more unknowns and where the physical setting is more complex than in other environments.
No rule without exception: surface melt infiltrating into the deeper layers of a mountain snow cover will always follow the local slope, according to the laws of flow through porous media. On the other hand, in the snow covers of flat areas liquid water will accumulate which leads to the very complex processes of energy and mass exchange at the water–snow crystal interfaces. In this particular aspect, snow modelling in mountain areas is actually easier than in flat regions.

1.4. Scale issues for modelling the mountain snow cover

1.4.1. Process scale, measurement scale, and model scale

In hydrological modelling, the concept of scale is generally used to quantify the three characteristic lengths of (i) a natural process, (ii) a measurement, and (iii) a model (Blöschl 1999, 1996). In the case of snow modelling, (i) could be, e.g., the correlation length of the spatial snow water equivalent (SWE) variability, (ii) the characteristic sample size of a sensor recording or the footprint of a satellite sensor, and (iii) the grid size of a distributed model. The three different scales are usually denoted as *process scale*, *measurement scale*, and *model scale*, respectively. Operations like interpolation, extrapolation, aggregation or disaggregation are interpreted as a

change in measurement and/or model scale. Such transitions in scale make it a complex task to choose an adequate parameterization for each specific process. As an example, the scale of turbulent mixing in an unstable surface layer is different from the scale of turbulent mixing in a layer of katabatic flow where the assumption of the similarity theory of a constant flux layer is violated. The katabatic flow layer can be of very different local thickness – but its existence is a frequent phenomenon in mountain regions. The footprint area of most fluxes also depends on the height of the instrument above the surface, and on the altitude of the surface above sea level. On top of that, it can be characterized by a distinct daily course and, hence, can be also variable in time (the typical footprint increasing with stability and mean windspeed). The location of the actual footprint is also of concern: whereas measured radiative fluxes can be resolved at relative great detail, the turbulent fluxes observed at a sensor are approximately representative for areas with an extent of 500 to 500 m and more, and located upwind (Weber 2008). It can be generally stated that if the scales of the components of a considered system are different, then the surface energy balance cannot be closed.
Campbell et al. (2004) give an overview of the characteristic lengths of typical snow processes, ranging from the size of individual snow grains (e.g., relevant for metamorphosis) to that of an entire mountain range (e.g., relevant for windward/lee effects or shading). The existence of a mathematical representation of these processes in any model is crucial: for mountain regions this includes a proper simulation of the snow surface energy balance, snow–vegetation effects, snow slides from steep slopes and wind–induced snow transport (Marsh 1999, Pomeroy et al. 1998). The reason why so many attempts to simulate streamflow in Himalayan headwaters using conceptual models fail is that the processes of wind–induced and gravitational snow transport with the related sublimation losses and avalanches are not represented in these models (Weber 2007, Strasser et al. 2008c).

1.4.2. Support, spacing and extent

With respect to the measurement scale, Blöschl and Sivapalan (1995) have introduced the three scale attributes *support, spacing,* and *extent* for a set of observations: Support is defined as the area integrated into a single measurement, spacing is the distance between the measurements, and extent is the distance spanned by a set of measurements. In order to accurately capture the heterogeneity of a high alpine snow cover, all three have to be chosen according to the natural scale characteristics of the related phenomena. This can become extraordinarily difficult in mountain regions. With respect to support, meteorological recordings of temperature and humidity are generally representative for a certain larger area, but wind speed, precipitation and radiation can vary at very small scales. Spacing is limited by the fact that the number of observation sensors is limited, and the extent is given by the size of the domain which encloses the chosen set of stations – any extrapolation outside this domain is characterized by high uncertainty. Obviously, the topography is the main reason for the high spatial variability of meteorological variables, and for the snow cover distribution as produced by the respective processes.
It is an important question what model scale should be chosen for proper snow cover representation in mountainous terrain. Again according to Blöschl and Sivapalan (1995), the three scale attributes support, spacing, and extent also exist for modelling and should correspond with their counterparts in the measurement scale, enabling specific phenomena to be reflected adequately in the model's predictions.

1.4.3. Model resolution

The length of each side of a raster element (pixel) of a model grid is the so–called *resolution* of the model. This resolution determines the area for which the pixel or cell value is considered representative, i.e. the support: A digital elevation model (DEM) with a resolution of 50 m represents topography with one elevation value for each 2500 m^2 spatial element. In mountainous regions where slopes are steep, the range of elevations aggregated into one single cell value is much larger than in flat areas. The range represented by one single value strongly depends on the DEM resolution: e.g., assuming a mountain side with 45 degree of steepness (which is not extraordinary), a 1000 m high slope is represented with a single (its mean) elevation in a 1 km resolution DEM. Increasing resolution to 50 m reduces the elevation range to be averaged into one value for the same site to 50 m, but the number of pixels to cover the same spatial domain (the extent) now equals 400. This increase of data equals a corresponding increase of computational demand for the modelling, but can greatly improve the accuracy of the results if the chosen parameterizations are adequate at that scale.

Fig. 1 illustrates the within–cell altitudinal elevation differences for a high alpine model domain at an eight km resolution (upper Durance catchment, French Alps). In this example, three subareas of equal size have been derived by averaging the respective elevations from a one km fine scale resolution grid. The hydrological modelling of streamflow runoff was significantly improved by distributing the meteorological variables to the three elevation zones, and computing the relevant processes of runoff generation separately (Strasser and Etchevers 2005, Etchevers et al. 2001a). It is interesting to note that the vertical differences between the subarea elevations within one eight km cell can exceed 1000 m due to the local relief gradient. The geographical distribution of the standard deviation (sigma) of the pixel elevations in the cells shows that the highest values can be found in the valley grounds, and the summit region of the Ecrins massif (NW region of the catchment). Both areas are characterized by very steep terrain. The smallest stan-

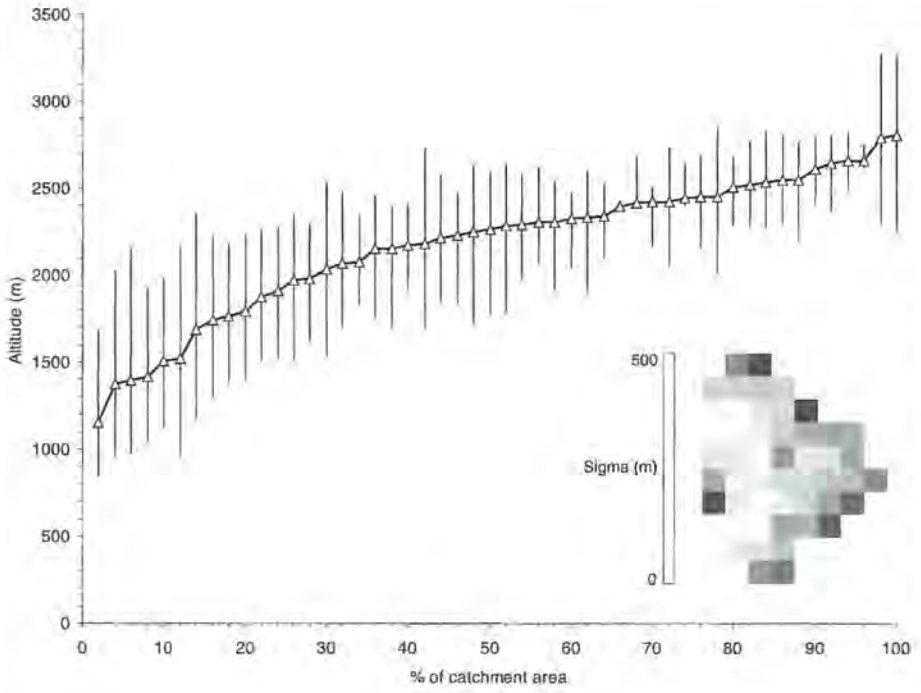

Fig. 1: Distribution of three equal-size subgrid elevation areas in model cells with eight km resolution (large graph). Small map: regional distribution of the standard deviation (= sigma) of one km resolution pixel elevations in each eight km resolution cell of the upper Durance catchment (French Alps). From STRASSER and ETCHEVERS (2005).

dard deviations are found close to the eastern borderline of the watershed where the summit regions are obviously flatter than the deep valleys at that particular scale.

The range of elevations covered by each single pixel element is crucial for the variance of the computed meteorological variables which are spatially distributed over the domain usually by applying an interpolation scheme which considers the elevations as represented in the DEM. E.g., assuming an adiabatic saturation temperature lapse rate of –0.65 °C for every 100 m elevation increase, the range of temperatures covered by the 1000 m elevation range cell of the above example is +/–3.25 °C of the mean represented by the pixel value. This is much higher than what can be assumed to be the accuracy of the point measurements and the subsequent spatial distribution technique (and neglects the fact that the temperature at a snow surface cannot exceed 0 °C). However, the accuracy of the temperature has significant consequences for the modelling, e.g. with respect to the phase change of precipitation or runoff generation dynamics: In nature, snow generally first melts in the lower regions and only later in the upper ones, no matter whether at the subpixel or domain scale.

Finally, the aspects of scale-dependent model errors have to be considered. At the domain scale the model results can be compared to snow cover maps derived from satellite imagery with similar coverage and spatial resolution. The simulated spatial pattern of a melting snow cover gives a valuable, integrative information of the model's capability to realistically reproduce both accumulation and ablation processes. The optimal dates for a comparison between model result and any satellite data derived snow cover map are cloudless days in the middle of the melt season when significant portions of the image are snow-covered while others are snow-free. Nevertheless, it must be kept in mind that snow detection in satellite data is a difficult task in itself, with respective uncertainties, and such a validation only covers a single date – the one of image acquisition. Continuous series of satellite images with proper resolutions are mostly not available. To overcome this, time series of model results can be compared with continuous observations at the local scale. This is mostly realized for one or more station recordings and the corresponding grid cell(s) within the modelling domain (e.g., Prasch et al. 2008). Although this comparison gives a good impression of model accuracy at the local scale and the range of processes that force the observed course of the measurements, its value suffers from some serious issues. Firstly, station locations are often chosen for reasons other than process representativeness: a reliable meteorological station in a steep, leeward slope with frequent deposition of wind-blown snow and avalanche activity still has to be invented, due to obvious reasons. Secondly, the number of stations (and hence evaluated model results) is always very small compared to the number of model cells: even with 10 stations in a 400 · 400 domain, only 0.00625 % of the grid cells are validated. Finally, the model does not consider the intricate small scale conditions around the station in the respective model cell.

1.4.4. Subgrid variability

It is a common feature of snow modelling to assume that all model cells are either snow-covered or snow-free, whereas in nature, especially in mountainous terrain, the

respective areas are only partly snow–covered. This spatial variability, called subgrid variability with respect to model resolution, is considered by a number of parameterizations, e.g. *distribution functions or effective parameters* (BLÖSCHL and SIVAPALAN 1995). It is especially important for the representation of a modelled snow–covered land surface when coupled to atmospheric models (LISTON 2004). Furthermore, subgrid variability of snow in a grid cell has tremendous effects on the modelling of snowmelt–induced runoff generation. The more the amount of snow in a cell is concentrated in a certain within–cell area fraction, the less melt per time is produced by a specific amount of available energy at the snow surface in that cell. Consequently, the duration of the melt period and the release of meltwater into runoff is correspondingly dependent on subgrid variability (Fig. 2): a) complete snow coverage of the cell results in a consistent, terminated impulse b) a slight heterogeneity in the snow cover (a small fraction of the cell area is snow–free) results in a slightly damped and delayed impulse and c) a strong heterogeneity in the snow cover (at least one half of the cell area is snow–free) results in a strongly damped and delayed impulse.

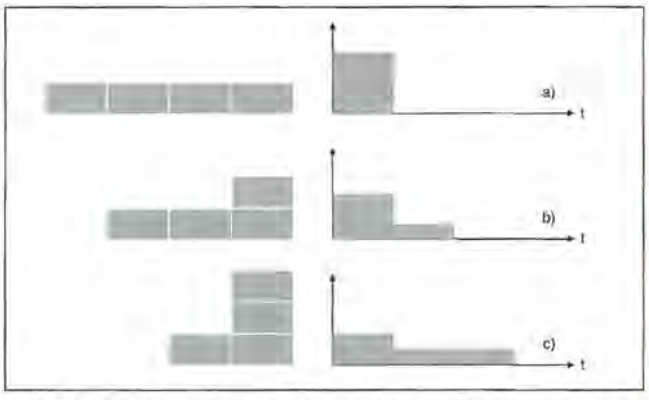

Fig. 2: Heterogeneous snow coverage in a conceptual model cell (left), and respective runoff generation impulse under melting conditions (right).

As a consequence, a snowmelt model assuming complete snow coverage of the cell will produce too much melt in a too short period. In all applications where the parameters of snowmelt models are fitted to observed runoff records, this effect (as many others) is compensated for by calibration. The result is a deceleration of the simulated temporal snowmelt dynamics for the wrong reason as the erroneous assumption of a too large snow–covered area is not addressed by this process. Consequently, if a strong spring snowfall covering the entire model cell occurs, the succeeding snowmelt flood will be underestimated in extent and timing. The assumed snow–covered area is now correct, but the dynamics of the melting process are underestimated.

1.4.5. Practical considerations

Wood et al. (1988) have suggested that there may be an optimum grid size for snowmelt modelling which is determinable by rational means. In reality, however, the selection of the grid size is often determined by practical considerations (BLÖSCHL 1999). This is also true for the present study: a 50 m model resolution was chosen as a practical compromise between all the restrictions and requirements described herein. On the one hand, it was assumed that even for high mountain topography the main atmosphere–snow surface interaction processes which force the evolution and distribution of the snow cover can be realistically reproduced at that spatial resolution; this includes the provision of meteorological forcing, e.g. a proper distribution of local recordings, and the sophisticated modelling of topographic effects. On the other hand, a 50 m resolution allows the dissolving of the typical patterns of lateral processes of snow redistribution, be it wind–induced snow transport or gravitational snow slides. Finally, a manageable number of model cells ensures fast computer processing even for a larger domain and long–term scenario simulations. In Fig. 3, the chosen model resolution of 50 m is illustrated by means of a TERRA–ASTER satellite data derived snow cover map, and compared with a much coarser resolution of one km.

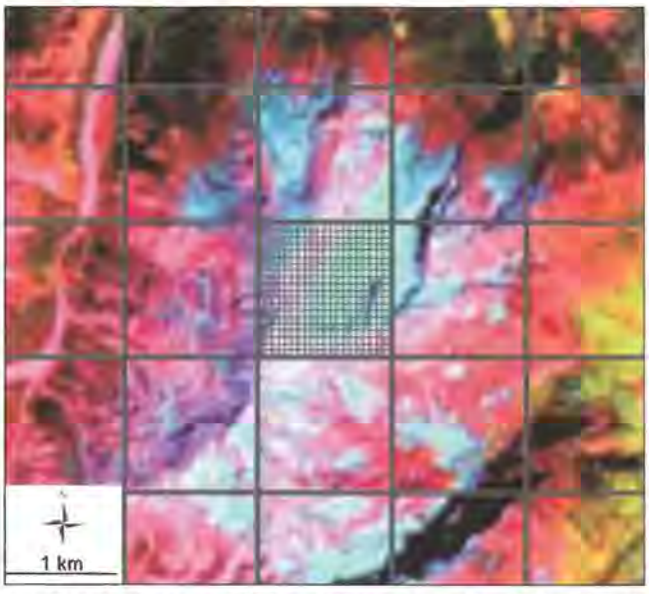

Fig. 3: Satellite scene of Mount Watzmann in the National Park Berchtesgaden (center at 47.49 N, 13.21 E), created from data recorded by the Advanced Spaceborne Thermal Emission and Reflection Radiometer (ASTER) flying onboard the TERRA satellite, 26 May 2005. Spatial resolution of the satellite data is 30 m. By combining visible and shortwave infrared bands (2, 4 and 5) the snow–covered areas (bright blue) can be distinguished from the rocks appearing in pink. The two raster grids represent model resolutions of one km (coarse) and 50 m (fine), respectively.

It is clearly evident that the observed snowmelt pattern is not reproducible at the coarser (one km) model scale; however, the effects of all important processes for snow cover heterogeneity can be recognized in the satellite data: wind–induced erosion (in the very West of the one km cell) and deposition (in the East), snow slides (left half), respective accumulation (right half), as well as various sun exposition/shading zones. For the 50 m reso-

lution, a considerably larger amount of model cells are either completely snow-covered, or snow-free and hence, a proper consideration of scale-dependent processes in the modelling becomes feasible.

1.5. The right model for the right purpose

With respect to the computation of snowmelt processes in high mountain regions, a lot of effort has been invested by the scientific community into the discussion of which type of model to use for what purpose (FERGUSON 1999, KLEMES 1990, WMO 1986). Generally, snowmelt models can be divided into three different types: The simple *conceptual* models only require few input variables and are fitted to a certain location and time by means of parameter calibration. Thereby, the most essential proxy for the energy budget of a snow cover surface is provided by the surface layer temperature which (i) can be reliably measured, (ii) is comparably easy to distribute over a spatial domain due to its continuous nature, and (iii) is available even in many remote areas where recordings of other meteorological variables are very sparse or simply do not exist. Ohmura (2001) gives a thorough explanation of why temperature is a physically meaningful replacement of three important energy sources at the snow surface (incoming longwave radiation, absorbed global radiation and sensible heat flux). Typical representatives of this kind of temperature index model include the *SRM* (Martinec et al. 1998), *HBV* (Bergström 1992) or Anderson's (1973) *combination approach* which assumes radiation melt for dry days and advection melt for wet days. The derivatives and successors of these models, mostly running at a daily timestep, are in wide use by a broad community. In an advanced version of the temperature index approach the modelled potential solar radiation is considered (Hock 1998, Brubaker et al. 1996), as solar radiation represents the most important source of energy for snowmelt. This type of model allows a computation with sub-daily time steps. Recently, a successful attempt has been made to enhance this model by including absorption of energy by adding an albedo parameterization scheme (Pellicciotti et al. 2005).

A critical step in the application of the temperature index models remains the calibration procedure (KLEMES 1990). The tuning of conceptual models increases their performance for the catchment under investigation. However, model accuracy achieved by calibration is only a poor indicator of the quality of the model results in other catchments, since model parameters are fitted to a specific location including all features of its natural environment, and not necessarily valid elsewhere (ZAPPA et al. 2003). Moreover, the calibration process introduces a certain bias of the model to the period for which it was calibrated; hence, the parts of the natural system's status which change over time (e.g., saturation of the soil or liquid water content in the snowpack) might not be accurately reproduced in another period. On the other hand, one of the advantages of conceptual models is that they are quite robust with respect to the accuracy of the input data. The fact that for applying a temperature index model temperatures at one height above the ground (usually 2 m) are used as input (and not the local vertical temperature gradients in the surface layer) represents an intrinsic correction moment since the lateral differences of temperature at this height are the result of the processes that are represented in the model. It is often overseen or neglected that measured variables in the boundary layer are the result of surface processes, and not vice versa.

The second type of snowmelt models is the *physically based one-layer model* which assumes the snow cover to be a single and homogeneous pack and which solves the energy and mass balance equations for the snow surface. These models comprise detailed parameterizations of the relevant physical processes and only require minimum calibration, if any. Since the underlying physics are independent of space and time, they can be generally transferred to other regions. Furthermore, they represent adequate tools to be applied for simulations of the effects of future climate change. However, energy balance models require a comprehensive set of input data, namely (hourly) recordings or interpolations of temperature, humidity, precipitation, wind speed, and radiation. The provision of these variables at the distributed scale requires a set of representative stations and is often a modelling task itself. This type of snowmelt model is often utilized as a component of a *Soil-Vegetation-Atmosphere Transfer scheme* (SVAT) (STRASSER and MAUSER 2001, GURTZ et al. 1999), or as a component of a land surface scheme (LISTON 2004, SLATER et al. 2001, POMEROY et al. 1998). It has proved its applicability and robustness for many different environments. Nevertheless, simulation accuracy for a specific site can vary between consecutive seasons if the evolution of the meteorological conditions changes, and hence the effect of single processes not considered in the modelling, e.g. sintering or constructive metamorphosis (ZAPPA et al. 2003, STRASSER et al. 2002). Recently, efforts have been undertaken to systematically compare and document various available energy balance schemes for snowmelt simulations within the framework of the SnowMIP[7] programme.
Finally, the third type of snowmelt model is the *multi-layer model* which comprises a physical description of metamorphism and the status of each single stratigraphic layer in a snowpack, and the thermophysical as well as mechanical processes of energy and mass exchange between them. These models are computationally demanding, require detailed measurements of input variables, and are mostly applied at experimental plots at the local scale. Prominent representatives of this type of model are *SNTHERM* (JORDAN 1991), *CRO-*

[7] http://www.cnrm.meteo.fr/snowmip/

CUS (*Brun* et al. 1992) or *SNOWPACK* (Bartelt and Lehning 2002). Usually such models are applied for research purposes or with respect to risk issues such as avalanches. Recently, sustained success has been achieved in applying multi-layer snowmelt models at the distributed scale and for hydrological applications (Etchevers et al. 2001b, Lehning et al. 2006). These studies show that model accuracy strongly depends on the quality with which the detailed input data can be provided.

1.6. Existing modelling systems for the mountain snow cover

Only few model systems exist which include physical descriptions of the main processes which affect the heterogeneity of a high alpine snow cover. E.g., *Snowmodel* (Liston and Elder 2006) includes modules to define meteorological forcing conditions, to calculate surface energy exchanges, to simulate snow depth and water equivalent evolution, and to account for snow redistribution by wind. Additionally, modifications made to the submodels for forested areas are provided. Snowmodel's blowing snow module *SnowTran-3D* allows the application of the model in arctic, alpine, and grassland environments (Liston et al. 2007, Liston and Elder 2006). Recently, Snowmodel has been adapted to the domain investigated hereafter in conjunction with a regional climate model which provides meaningful fields of wind speed and direction (Bernhardt et al. 2008a, b), an indispensable prerequisite for snow transport modelling in high alpine areas. The physically based modelling system *ALPINE3D* is designed for the high resolution simulation of alpine surface processes, in particular snow processes (Lehning et al. 2006). The core three-dimensional *ALPINE3D* modules consist of a radiation balance model (which uses a view factor approach and includes shortwave scattering and longwave emission from terrain and tall vegetation), and a drifting snow model solving a diffusion equation for suspended snow and a saltation transport equation. The processes in the atmosphere are thus treated in three dimensions and are coupled to the distributed model of vegetation, snow, and soil *SNOWPACK* (Bartelt and Lehning 2002, Lehning et al. 2002a, b). The model is completed by a conceptual runoff module *PREVAH* (Gurtz et al. 2003) which routes the water from each grid element through a linear storage cascade before it reaches the basins outlet. ALPINE3D has been successfully applied to numerous alpine study sites[8].

Applications of both Snowmodel and ALPINE3D in domains with steep topography have shown that besides the effects of blowing snow, the lateral gravitationally driven redistribution of snow is an important process to explain the observed snow cover heterogeneity, and to properly quantify snow accumulation on glaciers (Bernhardt et al. 2008b, Michlmayr et al. 2008, Kuhn 1995). This aspect becomes of specific interest with respect to plausibility of long-term simulations. Here an explicit model will be used to include the modelling of gravitational snow slides for an entire winter season and discuss the resulting snow patterns.

1.7. Content and final goal

The goal of the investigation described in this report is to improve today's snow cover modelling with respect to the mountain-specific accumulation, redistribution, and ablation processes which affect the heterogeneity of a high alpine snow cover. These particular processes include: the snow surface energy and mass balance, snow-canopy interaction, gravitational snow slides, and wind-induced snow transport. In this report, a set of distributed models will be applied to describe the spatially heterogeneous pattern of a high alpine snow cover, and to quantify the contribution of each individual process to the alpine winter water balance. The models will be applied for historical and for future climate conditions.

The test site which is chosen for the model application is the high alpine area of the Berchtesgaden National Park (Bavarian Alps, Germany). There, two important conditions are fulfilled: the natural environment is such that the snow cover is strongly affected by each of the mentioned processes, and a comprehensive dataset of meteorological recordings, a high resolution DEM, and detailled maps of canopy parameters are available as input for the modelling.

The effects of the complex alpine topography is thoroughly considered for the spatial distribution of the local meteorological measurements to the area of the investigation. Therefore, dynamic elevation-dependent lapse rates of the meteorological variables are derived, and the incoming radiative fluxes are modelled with a sophisticated scheme including the effects of shadows, multiple and terrain reflexions, and clouds.
The energy balance of the snow cover is modelled with an explicit formulation of the related mass balance, i.e. accumulation and ablation. Both balances are closed for the considered snow storage system between the atmosphere and the ground.
Snow-vegetation interaction is simulated with a model that includes physical descriptions of sublimation and melt unload of snow previously intercepted in the canopy. The effects of the trees on the micrometeorological conditions at the ground are also considered.
The entrainment, transport and deposition of gravitational snow transport is simulated with a snow slide model. Hydrologically meaningful flow paths are derived from the DEM, and the masses of sliding snow are transported from slopes steeper than a critical threshold value along couloir gullies to the flatter deposition zones.

[8] http://www.wsl.ch/staff/manfred.staehli/projects/alpine3d.ehtml

The modelling of these processes is integrated into the modular, physically based, distributed modelling system AMUNDSEN (**A**lpine **MU**ltiscale **N**umerical **D**istributed **S**imulation **EN**gine). AMUNDSEN has been designed to specifically address the requirements of snow modelling in mountain regions (Strasser et al. 2008a, 2008c; Strasser et al. 2004, Strasser 2002). The functionality of the system includes:

- adequate interpolation routines for scattered point meteorological measurements (Strasser et al. 2004)
- rapid computation of topographic parameters from a DEM
- simulation of shortwave and longwave radiative fluxes including consideration of topography with shadows and cloudiness (Corripio 2003, Greuell et al. 1997)
- parameterization of snow albedo depending on age and temperature (Rohrer 1992)
- modelling of snowmelt with either an energy balance model (Strasser et al. 2008c) or an enhanced temperature index model considering radiation and albedo (Pellicciotti et al. 2005)
- modelling of the forest snow processes interception, sublimation, and melt unload (Liston and Elder 2006) as well as consideration of the effect of the trees on the micrometeorological conditions at the ground (Strasser et al. 2008c), and
- simulation of gravitational redistribution of snow (Gruber 2007) along couloir courses which are derived from the DEM.

Finally, wind-induced snow transport including the processes of erosion, saltation, sublimation from a layer of turbulent suspension, and deposition of blowing snow are modelled with the physically based model SnowTran-3D (Liston et al. 2007, Liston and Sturm 1998). Distributed fields of wind speed and direction are therefore provided by a library of wind fields simulated with the atmospheric model MM5 (Grell et al. 1995). DWD-Lokalmodell simulations are used to provide a key to access the windfield library during the snow modelling (Bernhardt et al. 2008a, b).
The models AMUNDSEN and SnowTran-3D are applied for the Berchtesgaden National Park area using continuous meteorological recordings for the one-year period 1 August 2003 to 31 July 2004. The results include a discussion of the spatial heterogeneity of the modelled snow cover and a numerical quantification of the contribution of the individual processes to the winter water balance.
The models which are described and applied are mostly based on physical process descriptions. Therefore and by consideration of the relevant processes affecting the heterogeneity of the mountain snow cover, the modelling system is generally transferable in space and time. No site-specific calibrations are required. In particular, the system facilitates application for scenario simulations with a long-term temporal horizon.
To predict the future snow cover evolution under changing climatic conditions, a stochastic climate generator is developed and applied to provide time series of meteorological input data for the modelling. The produced time series of meteorological input data represents a predetermined trend of future climate conditions (Strasser et al. 2008a, Mauser et al. 2007, Strasser and Mauser 2006). Two scenarios are produced: one solely with increasing temperature, and a second one with increasing temperature combined with a shift of precipitation from summer to winter. The temporal horizon of both scenarios is 50 years and the reference is represented by the period 1998-2006. Then AMUNDSEN is applied for the two scenarios and the results are again discussed with respect to the resulting heterogeneity of the modelled snow cover and with respect to the contribution of the individual processes to the winter water balance – both in comparison to the reference period.
All in all, the goal of the study and the modelling system presented here is to adequately quantify the spatial heterogeneity of the high mountain snow cover with mostly physically based, distributed, transferable models. It includes descriptions of the relevant processes of accumulation, redistribution and ablation of snow, and facilitates continuous application at the small to regional scale for historical and future time series of meteorological input. The modelling tools developed and applied improve the quantification and prediction of the amount, the distribution, and the release of water resources stored as snow in high mountain regions.

2 Amundsen - program concept

The scientific software tool AMUNDSEN (**A**lpine **MU**lti-scale **N**umerical **D**istributed **S**imulation **EN**gine) for the continuous modelling of the alpine snow cover provides distributed time series of snow process variables in high mountain regions employing a wide range of interpolation, parameterization, and simulation procedures.
Basic considerations for the design of the program framework were: mostly physically based process representation, consideration of temporal and spatial variability, a simple interface to plug in existing models, raster and vector data capability, real–time visualization of the computed fields (i.e., during simulation) and platform independence. AMUNDSEN is coded in the *Interactive Data Language*[9] (IDL), a programming environment, that enables a very efficient coding of vector and array manipulations, and that offers a large variety of pre– and postprocessing as well as visualization possibilities. IDL runs on UNIX/LINUX, Windows and Mac OS and can call external FORTRAN or C routines.

In the current version, the functionality of AMUNDSEN includes: several interpolation routines for scattered meteorological measurements, rapid computation of topographic parameters from a digital elevation model, simulation of shortwave and longwave radiative fluxes including consideration of topography with shadows and cloudiness, parameterization of snow albedo, modelling of snowmelt and icemelt with either an energy balance model or an enhanced temperature index model considering radiation and albedo, modelling of the forest snow processes interception, sublimation and melt unload including the effect of the trees on the micrometeorological conditions at the ground, and simulation of gravitational redistribution of snow along couloir courses which are derived from the digital elevation model. Finally, AMUNDSEN incorporates a built–in stochastic weather generator that can be used to produce synthetic future meteorological data for climate change scenario simulations of any length if a respective time series of measurements is available. Potential applications of the program cover the simulation of physical processes in hydrology, glaciology, climatology, ecology and other alpine research fields. The code is continuously updated.

The data requirements for AMUNDSEN consist of:
- hourly meteorological recordings of temperature, relative humidity, precipitation, wind speed and global radiation (one file for each station)
- a digital terrain model of the investigation domain as an array of elevations, preferably including some area surrounding the intended model domain for the computation of the sky view factor, shadows, and the effect of reflections from the surrounding terrain. The resolution and spatial extent of the DEM determines the geometry of all output fields
- a sky view factor file with the same geometry as the DEM
- a watershed area file with the same geometry as the DEM, defining a region of interest (ROI) for which the processes will be simulated
- files of minimum and maximum LAI , a file with the cortex area index (CAI) as well as a file with the canopy height, all with the same geometry as the DEM.

All these files are read only once in the beginning of a model run, the required format is ASCII. Missing values in the meteorological recordings are replaced by the spatial interpolation for the respective location if at least one station within the domain provides a value. If no recording is available for a certain time step, missing values are put in place and the model continues with the next time step. Finally, a setup file is used for the parameters, constants, and factors used in the different submodels of AMUNDSEN. This file is commented and can be edited with specific values for the domain under investigation. After reading in all input fields the geometry of all intermediate and output fields is determined, and computation enters a time step loop in which the single simulation modules are called one after each other, writing their results into the output files. Computation of daily fields (e.g. the counting of snow days or the modelling of snow slides) are performed after a model day is completed at 24:00, after the computation of mean daily temperature. When leaving the time step loop at the end of the modelling period, cumulative fields are calculated, files are written and closed, and finally simulation stops. The AMUNDSEN output files comprise (in ASCII where not stated otherwise):
- hourly time series files for the locations of the meteorological recordings including meteorological variables and important simulation results
- one hourly time series file for the locations of the meteorological recordings including meteorological variables and important simulation results
- one hourly time series file with the spatial mean of temperature, relative humidity, precipitation, wind speed, and global radiation for the domain
- total (seasonal) aggregates of water balance, transported snow, deposited snow, snowmelt, snowfall, rainfall, precipitation, potential global radiation, melt unload, ground condensation, ground sublimation, and canopy sublimation with the same geometry as the DEM for the domain; apart from ASCII, these files are also written in TIFF
- files for the variables of the radiation, the canopy, and the snow module.

All point output files start with a header that includes the coordinates, elevation (from the DEM), sky view factor, and effective LAI and canopy height of the specific location. The ASCII versions of the distributed array output

[9] http://www.ittvis.com/idl/

files include an *ArcGIS*[10]–type header with the number of columns and rows, the coordinates of the lower left corner, the cell size, and the no–data–value. Finally, a so–called journal file is written in which all system prompt outputs are stored, allowing for fast detection of errors after a model run. The error level to be stated by IDL can be set in the beginning of a model run. Fig. 4 illustrates a model run with AMUNDSEN.

The system of units for all values read and written by AMUNDSEN is the *International System of Units* (SI). Time system is Universal *Time Coordinated* (UTC). During runtime, AMUNDSEN displays a color, real time view of the distributed fields of rainfall, snowfall, temperature, global radiation, longwave radiation, cloudiness, canopy interception storage, canopy sublimation, canopy melt unload, snow albedo, SWE, and snowmelt in a 1024 · 768 window, including scaling bars for the units (Fig. 5). All fields are scaled by a factor of five to fit them into the screen window. This display can be automatically screen–captured and an animation produced in MPEG–4 format which illustrates the hourly change of the fields during the entire season. On a standard PC (2.2 GHz core 2 duo CPU, 2 GB RAM), the modelling of one year for the Berchtesgaden National Park domain (810.000 DEM pixels, size of the ROI 205.105 pixels) requires 11 hours of computing time, approximately.

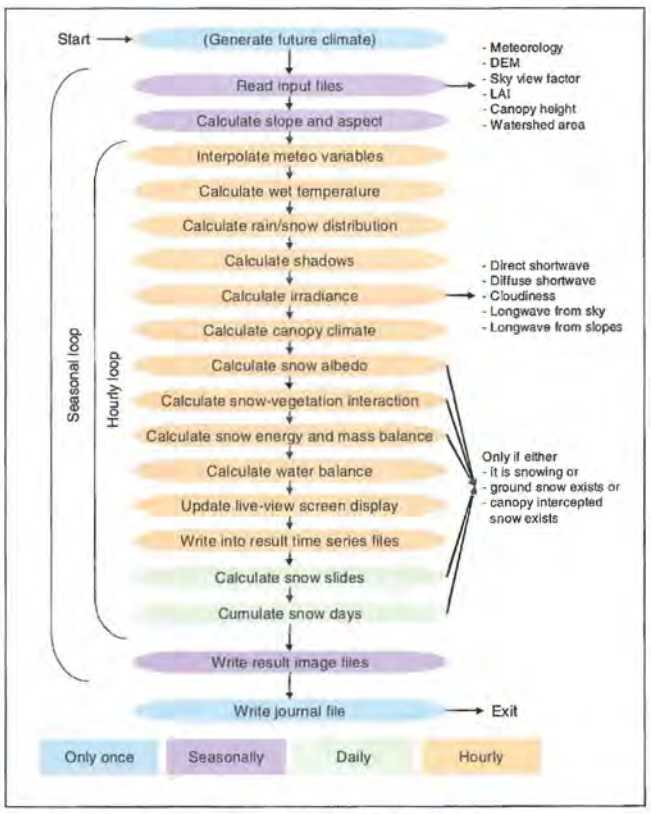

Fig. 4: Flow diagram of an AMUNDSEN model run.

Fig. 5: AMUNDSEN real time view during simulation for the Berchtesgaden National Park area.

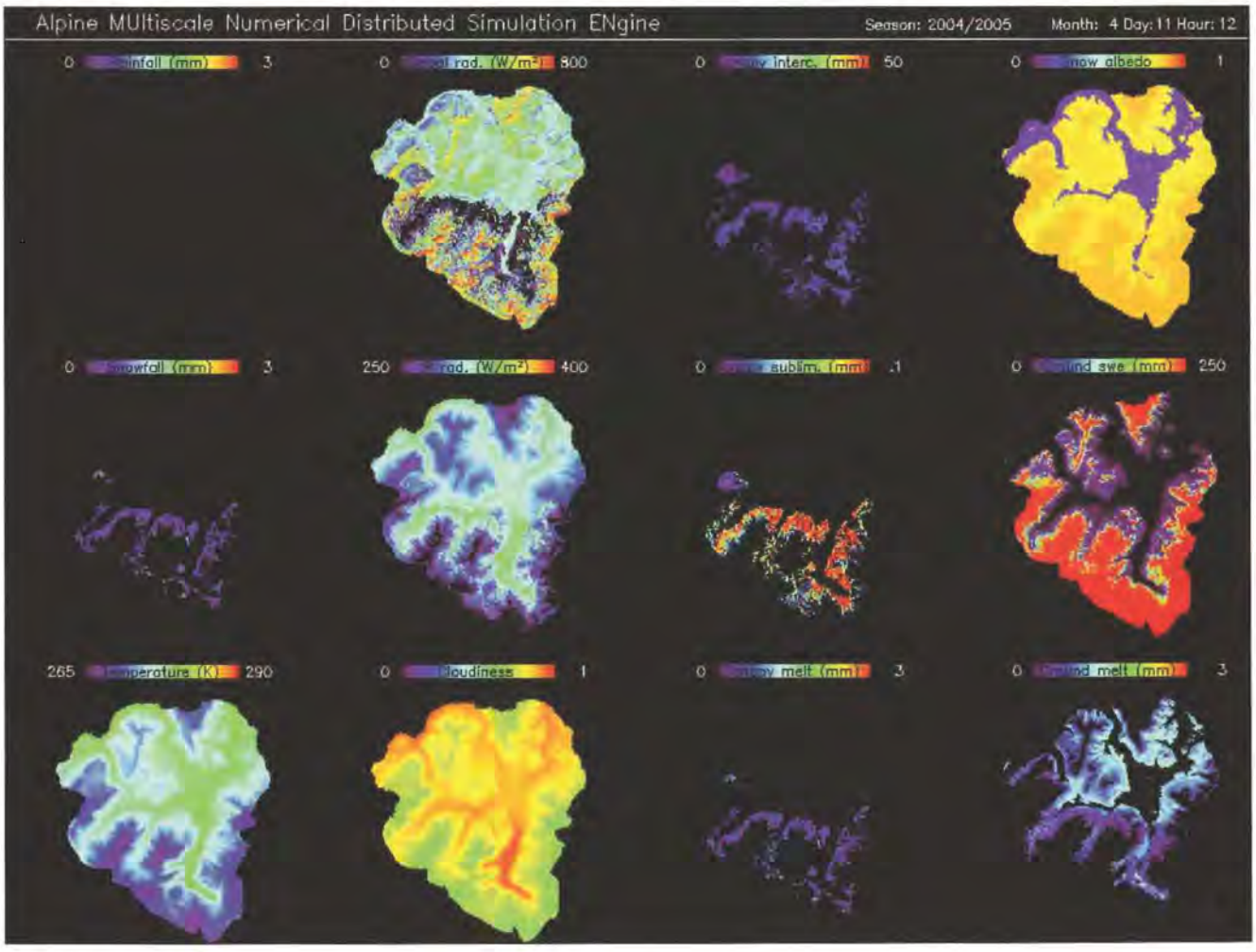

[10] http://www.esri.com/

3 The test site

In terms of adequate application of AMUNDSEN and SnowTran-3D, a test site is required which provides all the challenges for the modelling with respect to relief, variability of the meteorological variables and land surface types as well as small scale heterogeneity of the relevant processes for the evolution of the snow cover. On top of that, a continuous time series of adequate input data should is required. With respect to all this, an ideal test site could be found: The central Berchtesgaden Alps in the area of the Berchtesgaden National Park.

3.1. Site description

The Berchtesgaden National Park[11] is located in Southeast Germany in the state of Bavaria, in the southern corner of the administrative district Berchtesgadener Land (Fig. 6).

Fig. 6: Location of the Berchtesgaden National Park.

The park was founded in 1978 and covers an area of 210 km². For the most part, the boundary of the National Park is represented by the national border between Germany and Austria. In the North, the National Park adjoins the settlement areas of the communities Berchtesgaden, Schönau at the Königssee, as well as Ramsau. The valley areas are characterized by extensive forests with larch, spruce, and mountain pine stands (Konnert 2004), subordinated to the National Park authority since 1987. The high alpine area of the National Park includes the massifs Watzmann (2713 m a.s.l.) and Hochkalter (2606 m a.s.l.), as well as parts of the massifs Hoher Göll, Hagengebirge, Steinernes Meer, and Reiter Alm. The massifs are separated from each other by deep valleys stretching from South to North. Lakes within the park cover an area of approximately 6 km². The hydrological drainage system of the area is represented by the rivers Bischofswieser Ache, Ramsauer Ache, and Königsseer Ache. Below their confluence the water leaves the area of the National Park flowing into the Salzach which is part of the Danube river system.

The mountain massifs of the central Berchtesgaden Alps are characterized by an extreme topography, even for a high alpine area. The East face of Watzmann is one of the highest rock faces in the Alps with an elevation difference of approximately 2000 m. Several rock faces are almost vertical, e.g. in the Reiter Alm (South sides of Mühlsturzhorn and Grundübelhorn), at Untersberg (South and East side), or at the Kleiner Watzmann (West face). As an effect of local topography, some small glaciers still exist in elevations where their specific mass balance would always be strongly negative if only the climatological processes are taken into account. The Blaueis glacier, the northernmost glacier of the Alps, is shaded by the surrounding steep rock walls and fed by avalanches sliding down from them. The Watzmann glacier receives additional accumulation by wind-blown snow originating from the West-facing slopes of Watzmann. In 2000, the mean elevation of these two glaciers was 2146 and 2047 m a.s.l., respectively (Weber 2008). Finally, the Eiskapelle (ice chapel) at 920 m a.s.l., a perennial snowfield at the base of the Watzmann East face, is fed by both wind-blown snow from the Watzmann crest and frequent avalanches from the rock face above, which effectively is a snow funnel depositing masses of snow at a location far from where it has fallen. Nevertheless, the glaciers in the Berchtesgaden Alps have retreated dramatically during the past decades and are at risk to completely disappear in the near future (Winkler 2005). Only the Eiskapelle, due to the completely different character of its accumulation process, has shown little reaction on the changing climate.

The climate of the National Park area is subject to great spatial variability, particularly in response to the over 2000 m relief gradient. In addition, small scale local differences are mainly caused by the general position within the mountainous landscape: the windward or lee position relative to the prevailing winds and solar exposure. Mean annual temperature in the valleys is around +8 °C, while it is as low as -6 °C in the highest regions (Enders 1994), with generally January being the coldest

[11] http://www.nationalpark-berchtesgaden.de/

and July the warmest month. Mean measured annual rainfall in the valleys is approximately 1500 mm with a July maximum. At Kühroint (1420 m a.s.l.), an annual precipitation of approximately 1800 mm has been recorded since the station has been installed, over 40 % of which falls as snow. In the highest regions where no meteorological variables are recorded, annual precipitation is estimated to be in the range of 2700 mm (ENDERS 1994).
The extreme topography and the high alpine meteorological conditions make it particularly interesting and challenging to initiate the considered modelling in this domain.

3.2. Data

The input data required for the distributed modelling of snow processes using AMUNDSEN consist of a series of raster–based maps, and the time series of meteorological recordings from the stations in the domain. Most important is the digital elevation model (Fig. 7), from which the topographical parameters (sky view factor, slope, and aspect) are derived. These are used in the radiation modelling (including the determination of shadows), the interpolation of the meteorological variables and the modelling of gravitational snow slides.
The projection and resolution of the DEM defines the geometry of the model input datasets, as well as the model results. Here, a 50 m resolution dataset in *Gauß–Krüger projection* is used (900 · 900 raster elements, lower left corner at UTM *coordinates* E 4546250 and N 5249450). *The sky view* factor (portion of the hemisphere which is visible at each location) has to be derived only once, in advance of the modelling. since it is not variable in time. It is determined for each raster element using an algorithm which scans the horizon in all directions. Hence, for that purpose it is beneficial if the DEM covers a larger area than the modelling domain. The same is the case for the computation of solar shading effects. Here sightlines between each (pixel) location and the position of the sun have to be determined for all solar elevations and azimuth positions.
Canopies in the National Park area are described by maps of effective *leaf area index* (LAI) and canopy height datasets, both available as GIS datasets for the center zone of the park area.
Finally, fields of simulated wind directions are derived using the *Penn State University – National Center for Atmospheric Research MM5 model*, and downscaled with an energy conserving procedure considering small scale topography (Bernhardt et al. 2008a).

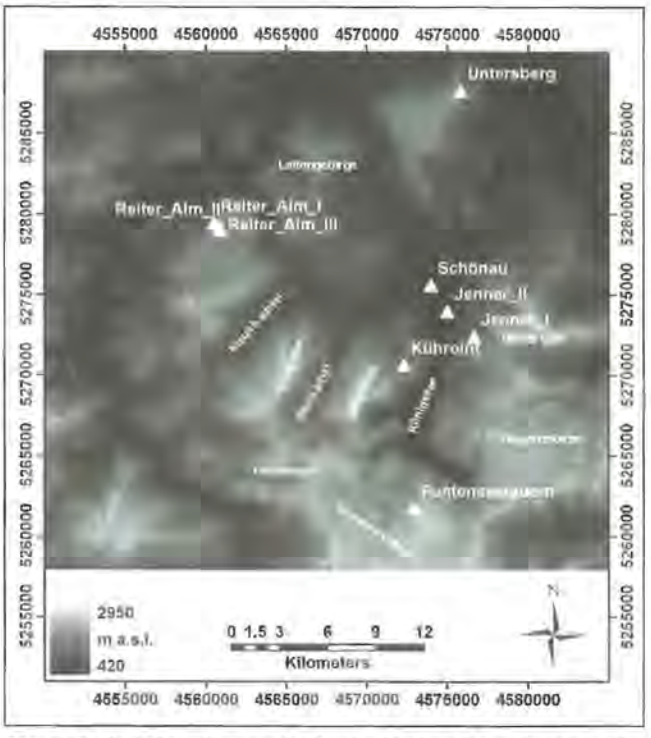

Fig. 7: Digital elevation model for the National Park area and its surrounding. The triangles represent the locations of the automatic stations comprising the operational network of meteorological stations. The spatial resolution of the DEM is 50 m.

3.2.1. Meteorological data

Meteorological forcing data to run the AMUNDSEN model consist of hourly recordings of precipitation, global radiation, temperature, humidity, and wind speed. These datasets are provided by the operational network of automatic meteorological stations located in the National Park. The stations are part of the infrastructure maintained by the Bavarian Avalanche Warning Service (LWZ)[12] of the State Office for Environment (stations Jenner, Reiter Alm, Kühroint, and Funtenseetauern), the Administration of Salzburg[13] (station Untersberg), and the German Weather Service[14] (DWD) (station Schönau). The locations of the stations and their position with respect to surrounding topography are illustrated in Fig. 7. The data recorded at these automatic stations is polled at regular intervals by means of a wireless radio transmission connection, and stored in a central database for further distribution and use. Subsequently, the recordings are aggregated from the 10 and 30 min recording intervals to hourly values and first quality checks are performed. To disseminate the data to the users, an interface has been developed which allows automated, regular network connection to the database with respective download of the most recently recorded datasets.
By means of this central database, composed of the recordings from the automatic stations of the different providers, a data pool is made available by the Administration of the National Park, which allows the continuous running of distributed models in an operational

[12] http://www.lawinenwarndienst-bayern.de/
[13] http://www.lwz-salzburg.org/
[14] http://www.dwd.de/

mode with a high temporal resolution. Table 1 gives an overview of the variables recorded at each station. All data are aggregated to hourly means (i.e., average for temperature, humidity, wind speed, radiation and air pressure; sum for precipitation; maximum for maximum wind speed).

Table 1: Meteorological stations and variables recorded in the Berchtesgaden National Park. The level of the temperature recordings is given with respect to the ground level.

Station	Elevation [a.s.l.]	Easting [m]	Northing [m]	Variables	Sampling rate
Reiter Alm I	1755 m	4560494	5279436	W, W_{max}, WD	10 min
Reiter Alm II	1670 m	4560835	5279235	T_a, T_s, T_{s20}, T_{s40}, T_{s60}, T_s, RH, H_s	10 min
Reiter Alm III	1615 m	4560950	5278982	T_a, RH, G, G_{ref}, P, H_s	10 min
Kühroint	1407 m	4572314	5270625	T_a, RH, G, G_{ref}, W, WD, P, H_s	10 min
Funtenseetauern	2445 m	4572939	5261755	T_a, RH, W, WD	10 min
Jenner I	1200 m	4576659	5272417	T_a, T_{s0}, T_{s20}, T_{s40}, T_s, RH, H_s	10 min
Jenner II	660 m	4575000	5273988	T_a, RH, P	15 min
Schönau	617 m	4573987	5275597	T_a, T_{a05}, RH, G, G_{dir}, SS, W, WD, P, p	10 min
Untersberg	1776 m	4575822	5287649	T_a, RH, W, W_{max}, WD, P	30 min

W	=	wind speed	T_s	=	snow temperature (at the surface)
W_{max}	=	maximum wind speed	RH	=	relative humidity
WD	=	wind direction	H_s	=	snow height
T_a	=	air temperature (2 m)	SS	=	sunshine duration
T_{a05}	=	air temperature (0.05 m)	G	=	global radiation
T_{s0}	=	snow temperature (0.0 m)	G_{dir}	=	direct radiation
T_{s20}	=	snow temperature (0.2 m)	G_{ref}	=	reflected radiation
T_{s40}	=	snow temperature (0.4 m)	P	=	precipitation
T_{s60}	=	snow temperature (0.6 m)	p	=	atmospheric pressure

The available data is characterized by a set of features which make them especially useful and suitable for the purpose of the modelling considered in this report:

- the spatial distribution as well as the coverage of the elevation range occuring in the National Park area are much more complete than in most other mountain regions
- an almost continuous time series covering several years including all winter seasons is available
- most of the stations (in particular all those maintained by the LWZ) are designed to deliver reliable and very accurate winter measurements, and finally
- the temporal resolution of the recordings is higher than required for the modelling, i.e. no temporal interpolation is required. The necessary aggregation is by far an easier and more accurate task.

3.2.2. Forest canopy data

Data fields of leaf area index (LAI) and canopy height are required as model inputs for the simulation of snow–canopy interaction processes. These datasets have been derived from a combination of forest inventory data, a color infrared aerial photograph interpretation, and by application of the relations to provide local estimates of LAI developed by Hammel and Kennel (2001). They are now stored together with a wide variety of other spatial datasets in the Geographical Information System (GIS) of the National Park administration[15] (Franz 1995). For snow cover modelling, an effective LAI including stems, leaves, and branches is required (Chen et al. 1997). To account for that, values for the cortex area index are added in the modelling. During winter, when the vegetation

[15] http://www.nationalpark-berchtesgaden.bayern.de/

is not active, minimum LAI values have been derived by multiplying the values for spruce *(picea abies)* with a factor of 0.8, and the one for pine *(pinus cembra)* with 0.6, while for the mountain pine shrubs *(pinus mungo)* the LAI is assumed to be 3.2 (KONNERT 2006).

The resulting effective winter LAI and tree heights of the canopies in the center zone of the National Park area as used for the modelling are illustrated in Fig. 8.

Like the meteorological data, the maps of the canopy parameters represent unique, valuable datasets for the intended modelling. The entirety of the described data features make the Berchtesgaden National Park a most suitable test site for model development and application especially with respect to the particular capabilities such a model is supposed to include in order to consider the snow cover characteristics of high alpine topography.

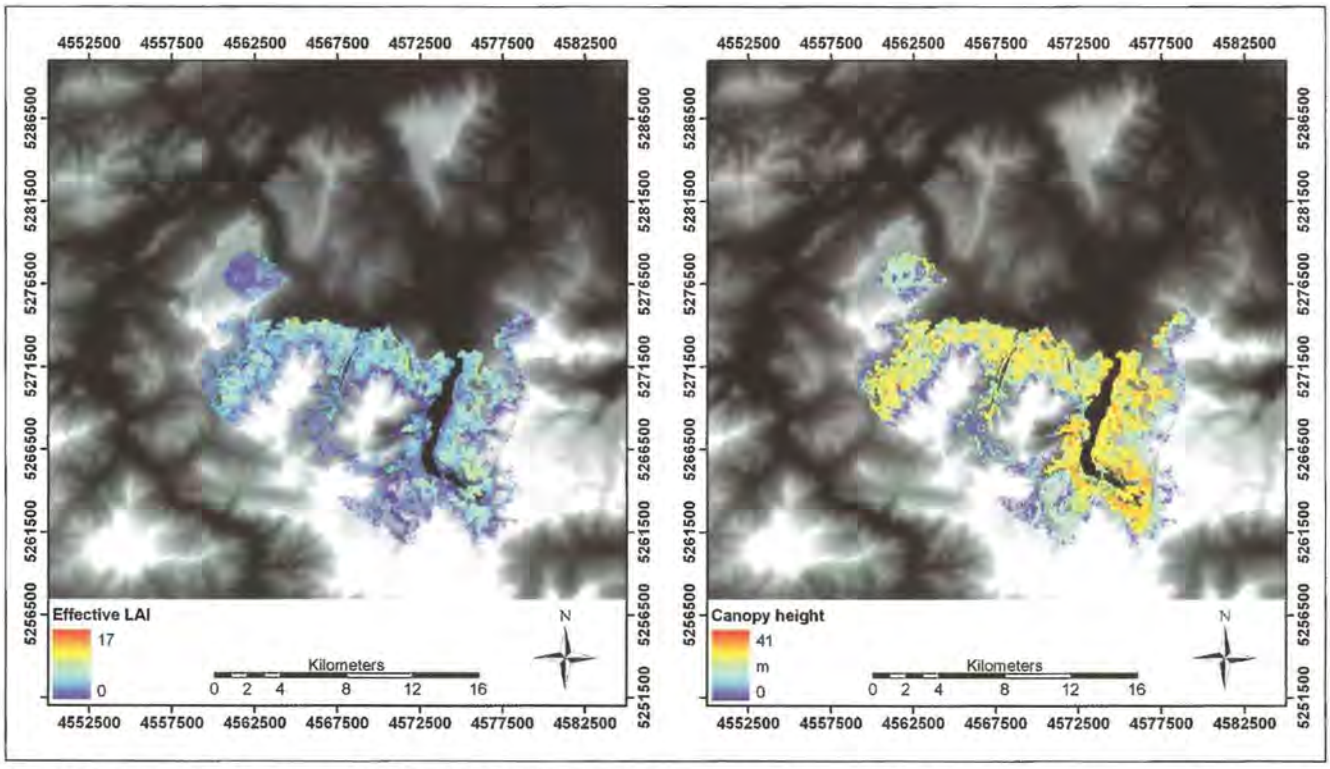

Fig. 8: Effective LAI (left) and tree heights (right) for the canopies in die Berchtesgaden National Park (data is only available for the center zone of the park).

4 Distribution of meteorological variables

It is crucial for an accurate simulation of the mountain snow cover heterogeneity and dynamics to have both, adequate model algorithms and parameters as well as all fields of meteorological input variables required for the modelling.

For the current application, this comprises the variables temperature, humidity, precipitation, wind speed and direction, and incoming shortwave radiation. Theses variables need to be available in a spatially distributed form, either provided by the application of an appropriate model (implicating that represented physics in such a model are in accordance with the snow modelling), or derived from point measurements by means of more or less robust statistical assumptions. An adequate verification of the validity of such statistical models is set aside in many applications for reasons of pragmatism.

In this study, physical relationships between topography and meteorological variables are preferred and used as much as reasonably possible and described after the general overview. The provision of wind direction fields by means of a regional climate model is part of the section on the simulation of wind-induced snow transport. A considerable part of the contents in this section has been published in Strasser et al. (2004).

4.1. The variability of meteorological variables in mountainous terrain

The understanding of the temporal and spatial variations of meteorological variables is a prerequisite for the description of the relationship between climate and the energy and mass balance of a mountain snow cover. Increasing efforts are therefore invested into the tasks of regionalization and exploiting the existing data sources for distributed model applications (Blöschl 1999, Greuell and Böhm 1998). The spatial and temporal variability of meteorological variables relevant for the snow accumulation and ablation processes are often extrapolated from measurements available at a single station in the modelling domain or from observations available at stations in the surrounding areas. Alternatively, the output from a meteorological model can be used. For the distribution of the variables from a local point measurement to the area of investigation, many methods of varying sophistication can be applied.

Temperature is often indicated as the most important variable for the determination of snowmelt (e.g., Ohmura 2001), and probably the most readily available from operational observation networks (Hock 1998). Its close correlation to elevation allows for a quite reliable spatial interpolation if a representative number of stations is available.
Many model applications assume a constant temperature lapse rate for all conditions, ranging from −0.0055 to −0.0065 °C m^{-1} (e.g. Brock et al. 2000, Hock 1998). A predefined lapse rate, however, predetermines the magnitude of the fluxes over snow (with snow having a $Ts \leq 0$ °C): the smaller the lapse rate, the larger the flux. However, measurements reveal that the temperature lapse rate can vary considerably depending on the meteorological conditions (mainly cloudiness) and on topographical effects (Fig. 9).

Taking this into account, Escher-Vetter (2000) used diurnally variable lapse rates for three ranges of cloudiness: a smaller lapse rate during morning hours, a higher variation of amplitude during cloudless conditions, and −0.006 °C m^{-1} for rainy days. If two or more meteorological stations are available in the domain, a dynamic temperature lapse rate with the temporal resolution of the recordings can be derived.

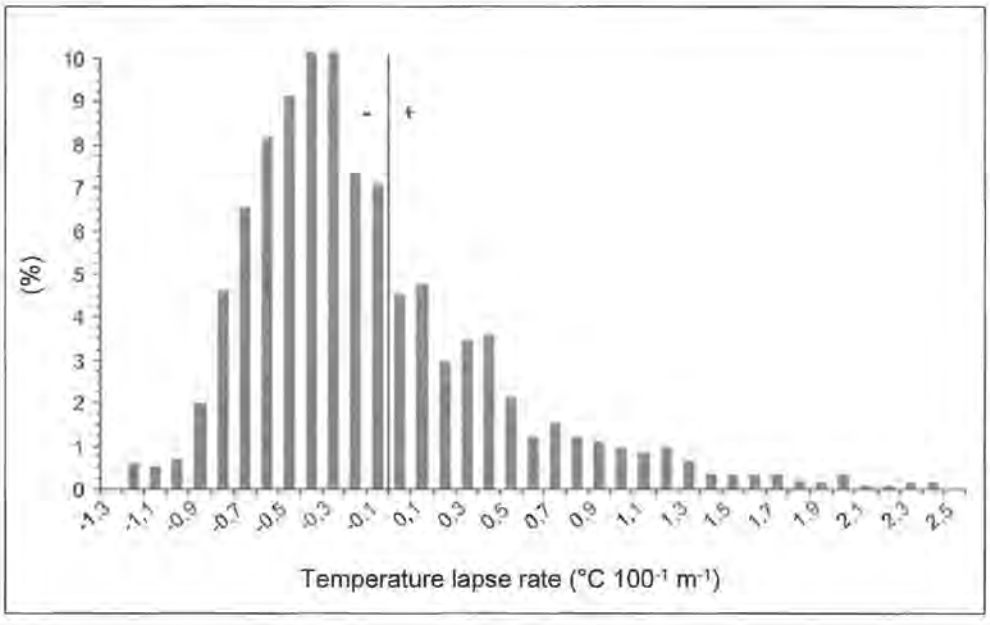

Fig. 9: Fraction, in %, of mean hourly temperture lapse rates between two sites (2813 and 3005 m a.s.l.) on Haut Glacier d' Arolla (Switzerland) during the snowmelt soeason 2001. From Strasser et al. (2004).

Precipitation is known to generally increase with elevation (Schwarb 2001), although the increase has an upper elevation limit from which on the lapse rate may decline again. Due to the lack of rain gauges and the difficulties in accurately measuring precipitation at higher elevations, this phenomenon is hard to quantify. The *phase of precipitation* plays an important role for the energy balance of the snow surface, especially during the melt season. Liquid rain represents an additional energy input into the snow cover, whereas additional snow mostly increases albedo and, therefore, reduces absorption of solar radiation. Hence, both distribution of precipitation over the site, as well as the distinction between rain and snow can significantly affect the simulation accuracy.

This aspect is of greatest importance in mountain regions. Not only is the measuring of precipitation falling as snow a challenge, but moreover, the distribution of the meteorological observations across the domain is extremely difficult. Usually, the solid/liquid precipitation transition is assumed to occur at a fixed threshold temperature ranging between +1 and +2 °C (Klok and Oerlemans 2002, Escher-Vetter 2000, Brock et al. 2000, Hock 1998), but recently new techniques to consider latent energy transfer at the snowflake surfaces improved the determination of phase transition (Weber 2005).

Global radiation, i.e. the sum of direct and diffuse radiative fluxes on a horizontal surface, is the most important energy source for snow- and icemelt (Hock 1998). Today, digital elevation models and sophisticated algorithms are used in distributed energy balance snowmelt models to simulate its temporal and spatial variability by incorporating the interaction with the local terrain (e.g. Lehning et al. 2006, Klok and Oerlemans 2002, Brock et al. 2000, Arnold et al. 1996). Under cloudless conditions, shortwave radiation can be reliably simulated using a high resolution digital terrain model and considering the exact position of the sun as well as the attenuation of the radiation by the atmosphere (Corripio 2003, Iqbal 1983, Kondratyev 1969, Garnier and Ohmura 1968). To account for the effect of clouds, measurements of global radiation are often included.

Besides global radiation, *cloudiness* affects the temperature lapse rate and the longwave radiation. Since the cloud cover is spatially highly variable and cannot easily be interpolated, especially in mountainous regions, respective measurements from a local station are of high value. The influence of cloudiness on the increase of longwave radiation can be reliably simulated by means of empirical formulas (Brutsaert 1975, Brunt 1932, Ångström 1916), and applying correction coefficients to account for the type of cloud cover, e.g. following the classification by Bolz (1949).
Incoming *longwave radiation from the atmosphere* is usually estimated with empirical relations based on standard meteorological measurements and using the correlation of air temperature with vapour pressure at screen level (Ohmura 2001, Kondratyev 1969). Longwave *emission* is generally calculated applying the *Stefan Boltzmann law*, assuming that the radiative characteristics of snow are similar to those of a black body, with the emissivity being close to one. The implicit uncertainty in this is small compared to the uncertainity associated with an accurate determination of atmospheric emissivity (Weber, 2008).

Wind speed and direction also play an important role with respect to both, the redistribution of precipitation and the interchange of momentum and heat with the surface. However, the synoptic wind field widely differs from the local conditions at a specific, snow-covered site in mountainous terrain, e.g. a meteorological measurement station. The influence of the cold snow surface, boundary layer effects and topographic disturbances produce a local wind field (*Bernhardt* et al. 2008a). The distribution of observed wind directions to a spatial scale for distributed modelling of e.g., wind-induced snow transport by means of interpolation techniques is very inaccurate in complex terrain, if local exposition and curvature are not considered (*Bernhardt* et al. 2008a, *Liston* and *Elder* 2006).
Finally, *humidity* influences the emission of longwave radiation from the atmosphere and controls the latent heat flux. As for the wind, humidity at the local scale can differ considerably from the synoptic field due to topography and the effect of the local wind, especially under melting conditions.

4.2. Spatial interpolation

In AMUNDSEN, distributed meteorological fields are computed hourly from station recordings as follows: firstly, a so-called *trend field* is derived by calculating linear regressions of the meteorological observations with elevation; this regression is then applied to the entire area represented by the DEM. Optionally, this step can be restricted to the elevation range covered by the stations in the study area (above and below this range, the trend is set to Zero). Then, the residuals (i.e., the deviations of the measurements from the trend field) are spatially interpolated by applying an *Inverse Distance Weighting* (IDW) approach, resulting in a so-called residual *field* representing the local deviations of a certain meteorological variable from its value in the trend field. The weights are the inverse distances between any location defined by a DEM pixel and the stations; the weighting power of the distances is set to two in this study. In a last step, the trend and residual fields are added up.

This algorithm, applied for each time step, ensures that the station observations are reproduced and it can be applied irrespective of whether a relation of the meteorological variable with elevation exists; e.g., the important temperature lapse rate is dynamically adjusted according to the observations in each time step. Nevertheless, it should be noted, that not all energy exchange processes in the area between the stations are conside-

red with this procedure (e.g., local turbulences due to an obstacle). However, for snow-covered surfaces the representativeness of meteorological recordings is comparably high. The described procedure is applied to the meteorological variables temperature, wind speed, shortwave incoming radiation, and precipitation. Relative humidity (%) is converted to absolute humidity ($kg \cdot m^{-3}$) prior to spatial interpolation, and re-converted afterwards. All interpolates within a timestep can be limited to the range between the minimum and the maximum value of the observations in the current timestep to avoid the generation of unrealistic extrapolates.
As an example for the described interpolation procedure, the annual aggregate of the precipitation distribution 2003/2004 is illustrated in Fig. 10.

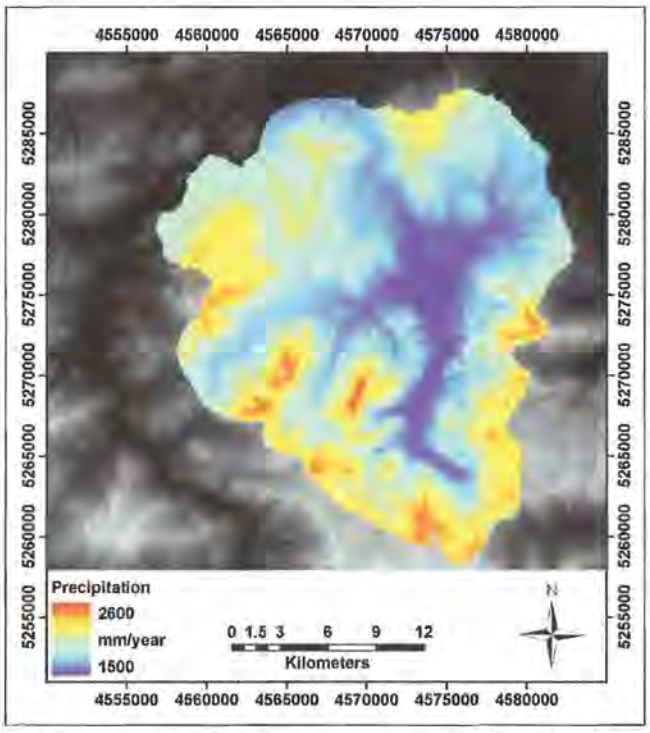

Fig. 10: Annual precipitation for the area of the Berchtesgaden National Park, derived from hourly interpolation of station recordings and aggregaton for the 8784 timesteps of the period 1 August 2003 to 31 July 2004.

The general increase of precipitation with elevation is clearly visible in the Figure: whereas in the valleys the mean annual precipitation for this season amounts to approximately 1500 mm, maximum values of almost 2600 mm are obtained for the summit regions of the highest mountains. These results are slightly less than the estimates of Enders (1994) derived from the recordings of the DWD network of meteorological stations in and around the domain. However, these stations are mostly situated in the lower regions of the area, and it can be assumed that the precipitation increase with elevation diminishes upwards since elevation dependency of measured precipitation for the domain is best fitted by a convex-shaped curve (according to the results of Enders 1994). The sharp delineation of the obtained values around the mountain massifs is attributable to the availability of forest canopy data (see section 3.2.2), and, consequently, the result of the modelled interception processes in the canopies. Sublimation losses of snow intercepted by the canopy are simulated only in the areas where a forest canopy is represented in the modelling (i.e., in the center zone of the park).

4.3. Radiation modelling

4.3.1. Incoming shortwave radiation

All shortwave radiation components are derived from local terrain characteristics as well as from physical and empirical relations with the parameterization scheme outlined in the following section. The algorithms compute the effects of shading by the surrounding terrain, the decrease of atmospheric transmittance due to the individual processes of scattering, and multiple reflections between the atmosphere and the ground as well as reflections from surrounding terrain. The latter aspect is of particular importance for high mountain regions, where slope reflections can considerably increase incoming shortwave radiation, in particular if these slopes are covered with snow (Corripio 2003).
Direct and diffuse shortwave radiative fluxes for each grid cell are parameterized using efficient vectorial algebra algorithms, the principles of which are described in detail in Corripio (2003). First, potential direct solar radiation for a clear sky is determined for each grid cell for its specific geographical position and date of simulation. Then, slope and aspect as well as cell surface area are represented as a vector normal to the surface and calculated using the minimum area unit of the DEM which is enclosed between four data points. This vector is half the sum of the cross products of the vectors along the sides of the grid cell. The position of the sun is calculated by applying rotational matrices to a unit vector defined at noon as a function of latitude and declination. The rotation matrix is dependent on the hour angle ω for given latitude and declination:

$$\omega = \pi \cdot \left(\frac{t}{12} - 1 \right)$$

with t being the local apparent time in hours and decimal fraction. The declination ‰ is computed after Bourges (1985) with a Fourier series approximation:

$$\delta = 0.3732 + 23.2567 \cdot \sin(D) - 0.758 \cdot \cos(D) + 0.1149 \cdot \sin(2 \cdot D) + 0.3656 \cdot \cos(2 \cdot D) - 0.1712 \cdot \sin(3 \cdot D) + 0.0201 \cdot \cos(3 \cdot D)$$

with D being the day number:

$$D = \left(\frac{2 \cdot \pi}{365.25} \right) \cdot (J - 79.346)$$

J is the Julian day, 1 on the first of January and 365 on 31 December.

The direct component of insolation intercepted by each cell surface is then calculated as a dot product between the unit vector in the direction of the sun and the unit vector normal to the surface, multiplied by direct normal irradiation, i.e. the solar constant (1367 W · m^{-2}) which is corrected with a multiplicative factor c for excentricity after Spencer (1971), Γ being the day angle:

$$\Gamma = \frac{2 \cdot \pi \cdot (J-1)}{365}$$

Hence, excentricity correction c gets:

$$c = 1.000110 + 0.034221 \cdot \cos(\Gamma) + 0.001280 \cdot \sin(\Gamma) + 0.000719 \cdot \cos(2 \cdot \Gamma) + 0.000077 \cdot \sin(2 \cdot \Gamma)$$

Shading by adjacent terrain is computed by scanning the projection of cells onto a solar illumination plane perpendicular to the sun direction. By checking the projection of a grid cell over this plane following the direction of the sun, it is determined whether a point is in the sun or in the shade of another cell. To increase computational efficiency of the algorithm, an array of cells is defined for every cell on the illuminated side of the grid border. The length of this array is given by the nearest intersection of a line along the vector opposite to the sun and the DEM boundaries.

Horizon angles and estimated sky view factor are calculated using a more computationally efficient algorithm than a rigorous evaluation of all the angles subtended by every grid cell to each other (Corripio 2003). The sky view factor is an important parameter for the computation of incoming diffuse and multiple scattered shortwave radiation, especially in areas of high albedo like snow-covered mountains, and for the net balance of longwave radiation. Following Iqbal's (1983) unit sphere method, the sky view factor is computed as the ratio of the projected surface of visible sky onto the projected surface of a sphere of unit radius (Nunez, 1980). For the computation of the horizon zenith angles for selected azimuths, a modification of Corripio's (2003) shading algorithm is used. As the sky view factor is temporally invariant, it is computed only once for all grid cells of the domain and then stored in a file which is read in at the beginning of each simulation run (Fig. 11).

The actual direct shortwave radiation at normal incidence I is computed accounting for the total transmittance of the atmosphere, given as the product of the individual transmittances. An additional correction β_e for elevation after Bintanja (1996) is introduced to account for the increase of transmittance with elevation (W · m^{-2}):

$$I = 1367 \cdot c \cdot (\tau_r \cdot \tau_o \cdot \tau_g \cdot \tau_w \cdot \tau_a + \beta_e)$$

with τ_r being the transmittance due to Rayleigh scattering, τ_o the transmittance by ozone, τ_g the transmittance by uniformly mixed trace gases, τ_w the transmittance by water vapour and τ_a the aerosol transmittance, all of them referring to sea level.

The correction for elevation ,e is assumed to be linear up to 3000 m a.s.l. (and kept constant for higher elevations) and given by:

$$\beta_e = 2.2 \cdot 10^{-2} \cdot km^{-1}$$

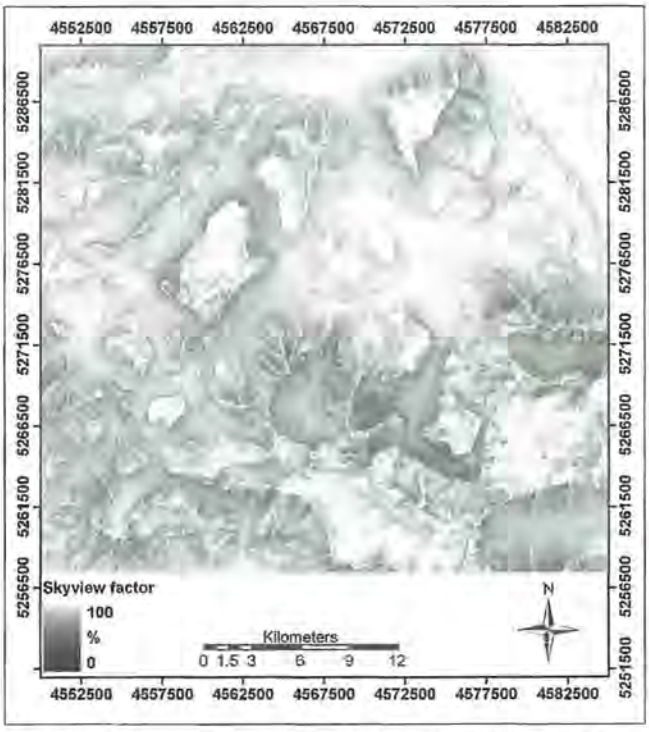

Fig. 11: Modelled sky view factor for the Berchtesgaden Alps.

The individual transmittances are computed as described in the followinig (Iqbal 1983, Bird and Hulstrom 1981). The relative optical path length m is computed after Kasten (1966) and corrected for elevations other than sea level, thereby p being the local pressure (hPa) and ız the solar zenith angle:

$$m = \left(\frac{p}{1013.25} \cdot \frac{1}{\cos\theta_z + 0.15 \cdot (93.885 - \theta_z)^{-1.253}} \right)$$

1013.25 is the sea level pressure (hPa). The transmittance due to Rayleigh scattering, τ_r, is given by:

$$\tau_r = e^{\left[-0.0903 \cdot m^{0.84} \cdot \left(1 + m - m^{1.01}\right)\right]}$$

The transmittance by ozone τ_o can be computed with l being the vertical ozone layer thickness, assumed to be 0.35 cm according to measurements from the *Total Ozone Mapping Spectrometer–Earth Probe* (TOMS–EP 2001):

$$\tau_o = 1 - \left[0.161 \cdot l \cdot m - \frac{1}{(1 + 139.48 \cdot l \cdot m)^{0.3035}} - 0.02715 \cdot l \cdot m \cdot \frac{1}{1 + 0.044 \cdot l \cdot m + 0.0003 \cdot (l \cdot m)^2} \right]$$

The transmittance by ozone is the only transmittance, that is spatially invariant for the area.

The transmittance by uniformly mixed trace gases Ùg is computed with:

$$\tau_g = e^{\left(-0.0127 \cdot m^{0.26}\right)}$$

τ_w, the transmittance by water vapour, is computed with w being the precipitable water in cm:

$$\tau_w = 1 - 2.4959 \cdot w \cdot m \cdot \frac{1}{\left(1 + 79.034 \cdot w \cdot m\right)^{0.6828} + 6.385 \cdot w \cdot m}$$

Thereby, the precipitable water is computed after Prata (1996) with e_0 being the actual water vapour pressure at the site and T_a the air temperature (K):

$$w = 46.5 \cdot \frac{e_0}{T_a}$$

Finally, the aerosol transmittance τ_a is calculated as follows, v being the (prescribed) clear sky atmospheric visibility, here assumed to be 25 km:

$$\tau_a = \left(0.97 - 1.265 \cdot v^{-0.66}\right)^{m^{0.9}}$$

For the computation of the diffuse component of the shortwave radiative fluxes the following processes are taken into account: Rayleigh and aerosol scattering, multiple reflections between the atmosphere and the ground, and reflections from the surrounding terrain. The transmittance due to Rayleigh scattering τ_{rr} is given by:

$$\tau_{rr} = \frac{0.395 \cdot \cos\left(\theta_z\right) \cdot \tau_o \cdot \tau_g \cdot \tau_w \cdot \tau_{aa} \cdot \left(1 - \tau_r\right)}{\left(1 - m + m^{1.02}\right)}$$

with τ_{aa} being the transmittance of scattered direct radiation due to aerosol absorptance, computed using $\omega_0 = 0.9$ as assumed single scattering albedo:

$$\tau_{aa} = 1 - \left(1 - \omega_0\right) \cdot \left(1 - m + m^{1.06}\right) \cdot \left(1 - \tau_a\right)$$

Transmittance due to aerosol scattering, τ_{as}, is given by:

$$\tau_{as} = \frac{\cos\left(\theta_z\right) \cdot \tau_o \cdot \tau_g \cdot \tau_w \cdot \tau_{aa} \cdot S_{f/l} \cdot \left(1 - \frac{\tau_a}{\tau_{aa}}\right)}{\left(1 - m + m^{1.02}\right)}$$

$S_{f/l}$ is the ratio of forward scattering to total scattering. It is computed as regression from the tabulated values given by Robinson (1963) as:

$$S_{f/l} = 0.9067 + 0.1409 \cdot \theta_z - 0.2562 \cdot \theta_z^2$$

Now, the effect of multiple reflections between the atmosphere and the ground is calculated. For this, the sum of the radiative fluxes as computed with eq. (6) to (18) is increased by a factor mr which is given with effective ground albedo ag by:

$$m_r = \frac{a_g \cdot a_a}{1 - a_g \cdot a_a}$$

a_a is the atmospheric albedo, computed as:

$$a_a = 0.0685 + \left(1 - S_{f/l}\right) \cdot \left(1 - \frac{\tau_a}{\tau_{aa}}\right)$$

with 0.0685 being the assumed clear sky albedo. Since slopes not visible from the site but located in its vicinity do contribute to diffuse radiative fluxes by multiple scattering, effective ground albedo can be estimated as the mean albedo of a (not too large) modelling domain. It is computed in each time step as the area weighted sum of rock albedo (assumed to be 0.15) and snow albedo (parameterized as described later).

As an alternative to the surface energy balance method as described in the following section, the estimation of the area fraction of the different surface types can also be conducted by means of a temperature index snowmelt model considering simulated (clear sky) solar radiation G* and parameterized albedo a (Pellicciotti et al. 2005):

$$melt = tf \cdot T_a + af \cdot G^* \cdot \left(1 - \alpha\right) \quad \text{for} \quad T_a > 1°C$$

tf and af are empirical coefficients, called temperature and albedo factor, expressed in mm $h^{-1} \cdot °C^{-1}$ and $m^2 \cdot mm \cdot h^{-1} \cdot W^{-1}$, respectively. Calibration with melt rates computed with an energy balance model (Brock and Arnold 2000) yielded tf = 0.00021 mm $h^{-1} \cdot °C^{-1}$ and af = 0.0094 $m^2 \cdot mm \cdot h^{-1} \cdot W^{-1}$ (Pellicciotti et al. 2005).

Finally, the sum of the direct and diffuse radiative fluxes is corrected for the visible portion of the hemisphere by multiplying their sum with the sky view factor for each pixel in the domain. In a last step, direct reflections from the surrounding terrain are added by considering the shortwave radiation, the ground view factor and the fraction as well as albedo of the reflecting surfaces after Corripio (2003).

The influence of clouds is accounted for through the use of the cloud factor which is computed as fraction of observed global radiation to the respective simulation result representing the clear sky situation. If more than one recording is available in a single model timestep, then the cloud factor is spatially distributed over the domain in the same way as the meteorological variables (see section 4.2).

The presented solar radiation model is parametric and not truly physical. Nevertheless, it gives good estimates of the individual atmospheric transmittances (Niemelä et al. 2001). It can be applied for any mountainous domain if an appropriate DEM is available. To enable the consideration of surrounding mountains in the computation of diffuse radiative fluxes by multiple scattering as well as of shadowing, the actual area covered by the DEM should be considerably larger than the modelling domain itself.

Strasser et al. (2004) have quantified the effect of the different processes considered in the radiation model on the extraterrestrial flux for five different locations in a high mountain region (Fig. 12): On average, a gain of approximately 10 % of energy could be attributed to terrain reflections and multiple reflections, most effective

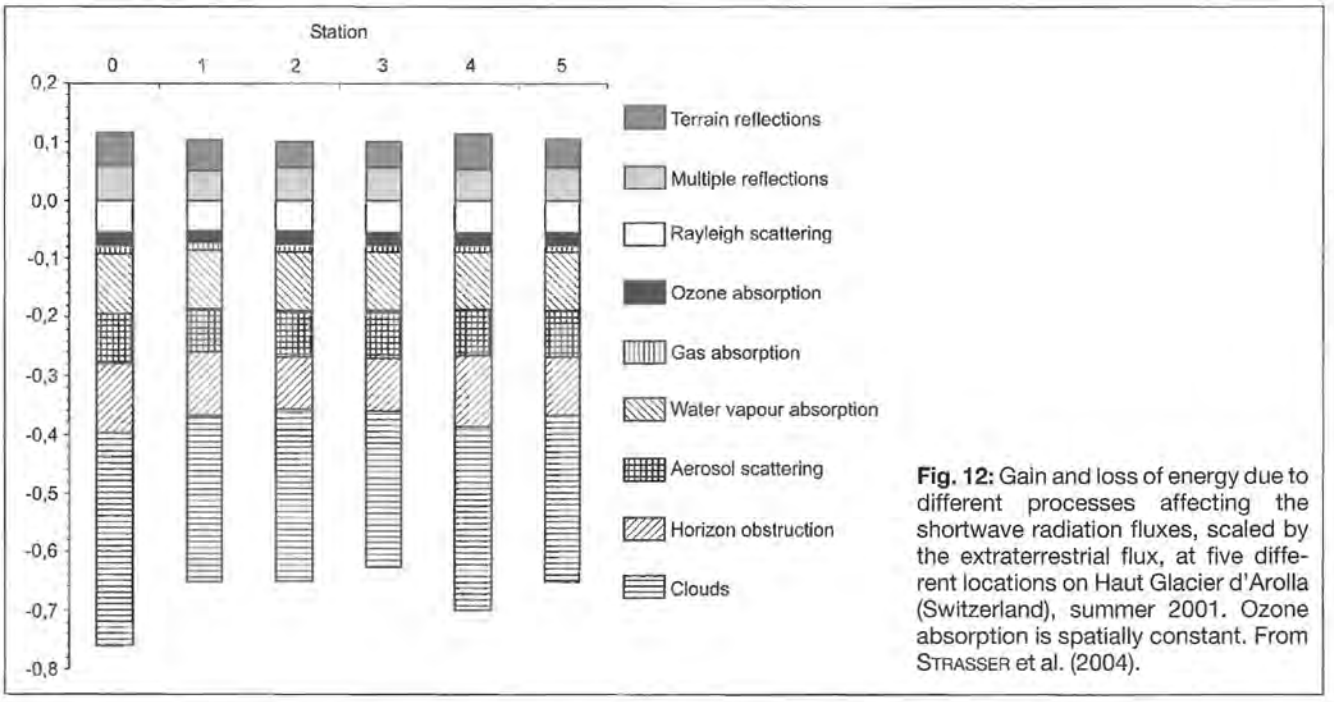

Fig. 12: Gain and loss of energy due to different processes affecting the shortwave radiation fluxes, scaled by the extraterrestrial flux, at five different locations on Haut Glacier d'Arolla (Switzerland), summer 2001. Ozone absorption is spatially constant. From STRASSER et al. (2004).

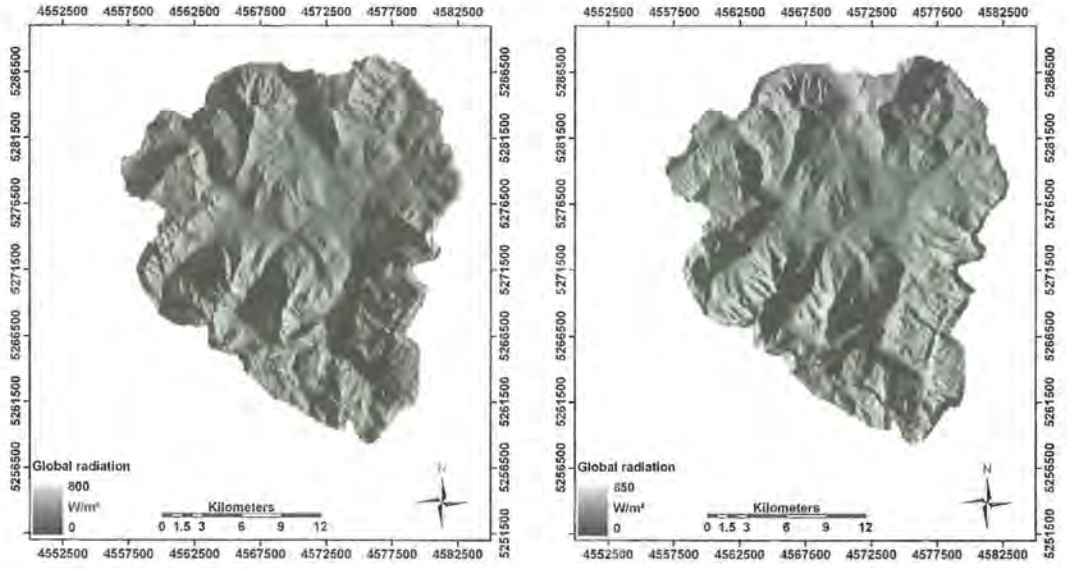

Fig. 13: Simulated (clear sky) global radiation for the National Park Berchtesgaden domain at 1 August, 8 CET (up left) and 18 CET (up right), as well as potential mean annual global radiation (left).

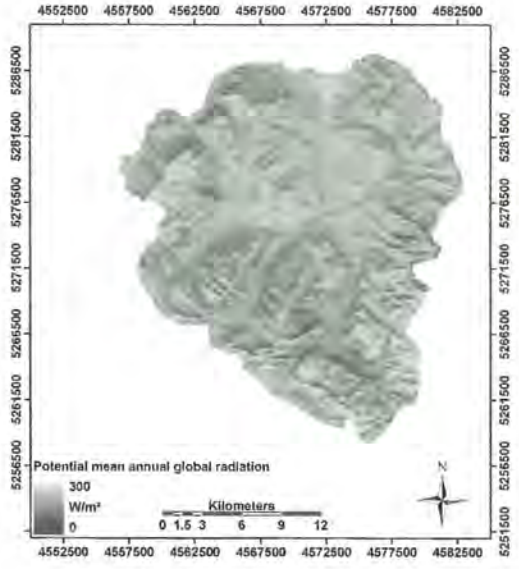

at sites surrounded by steeper slopes. Solar energy losses due to horizon obstruction (12 %), scattering processes (8 %) and absorption by water vapour, ozone and trace gases (19 %) were calculated. Of all factors affecting shortwave radiation the cloud factor was the most effective. On average, clouds accounted for 30 % of the loss of energy of the extraterrestrial flux. Overall, potential shortwave radiation during the (summer) observation period was reduced by the significant amount of 57 %, attributable to the local weather conditions (frequent cloudy situations) and pronounced horizon obstructions, both typical for high mountain areas.

As an example of a spatially distributed modelling of the shortwave radiative fluxes, Fig. 13 shows the result of the described computation in the National Park area for single time steps, and accumulated for an entire year: in the

morning, the mountain shadows fall to the left (West) of the mountains, whereas in the evening, they fall to the right (East). In the annual map, the distinction between the generally more sun–exposed and the more shadowed areas becomes obvious. In the shadowed areas only diffuse radiation reaches the ground.

4.3.2. Incoming longwave radiation

Spatial differences in the incoming longwave radiative flux can be attributed to three main phenomena: (i) differences in air temperature and its vertical profile, (ii) differences in the effect of upper hemisphere slopes, and (iii) differences in the effect of clouds. These three phenomena represent the processes which have to be quantified by a parameterization scheme for high mountain areas. In the following section, the respective algorithm as implemented in AMUNDSEN is described.

The majority of the longwave radiation reaching the surface is emitted from the lowest layers of the atmosphere which are not necessarily correctly represented by measurements of temperature at the 2 m level (OHMURA 2001). Therefore, the longwave radiative flux emitted can be different from one location to another, depending on the mixture conditions in the boundary layer, the height of a potential inversion layer, and a respectively different temperature profile. To quantify the effect of (i), Strasser et al. (2004) have selected clear sky situations from the data of Haut Glacier d'Arolla (Switzerland) defining a cloud factor threshold of 0.975. The cloud factor was computed as the ratio of measured to simulated clear sky shortwave radiation for the time step, while longwave emission from the atmosphere was computed with recorded air temperatures. For these conditions, and without consideration of the effect of upper hemisphere slopes (ii) and clouds (iii), the difference of incoming longwave radiative fluxes between two locations at different elevations, which can only be attributed to temperature and its profile, was computed applying the Stefan Boltzmann law and resulted in an average of –0.0325 W m^{-2} m^{-1}. The emissivity of the clear sky atmosphere ε_{cs} depends on the precipitable water content w (and hence on the air temperature, see eq. (13)) and can be estimated in AMUNDSEN with several approaches, e.g. after Prata (1996):

$$\varepsilon_{cs} = 1 - (1 + w) \cdot e^{-\sqrt{(1.2 + 3 \cdot w)}}$$

The effect of upper hemisphere slopes on the longwave radiative fluxes (ii) is taken into account by considering the sky view factor in each pixel. Upper hemisphere slopes increase longwave radiative fluxes since radiances received from adjacent slopes are larger than the ones received from the sky. Generally, snow–free slopes are likely to have higher mean surface temperatures than slopes covered with snow. Therefore it is necessary to consider whether the surrounding area of a location is snow–covered or not. In AMUNDSEN, the modelled incoming longwave radiative flux from surrounding slopes is partitioned into a fraction emitted by rocks, and a remaining part emitted by snow. The temperature T_r of the emitting rocks is set equal to the air temperature during night time. During daytime it is assumed to be higher than the air temperature by a factor T_+ which is dependent on the amount of the incoming shortwave radiation G (W m–2):

$$T_+ = j \cdot G$$

Greuell et al. (1997) determined j from measurements of slope temperature by means of a Heymann IR sensor. Relating these measurements to simultaneous values of the global radiation yielded j = 0.01 °C m^2 W^{-1}, indicating that during maximum insolation conditions (approximately 1000 W m^{-2}) the mean temperature of those parts of the slopes not covered by snow is 10 °C higher than the temperature above the snow surface. For the fraction of surrounding slopes which is covered by snow, the temperature is set equal to T_a, but cannot exceed 0 °C. Whether a cell is snow–covered or not is determined hourly either by means of the surface energy balance model described in the following section, or with the temperature index melt model developed by Pellicciotti et al. (2005), considering simulated (clear sky) solar radiation and parameterized albedo. Interactions between the atmosphere and clouds with the surrounding slopes and the cell under consideration are neglected. Taking into account the effect of the surrounding slopes with the described procedure leads to an increase of longwave radiative fluxes of approximately 30 % in high mountain locations that have adjacent rock massifs. The previously described simulations do not consider the effect of clouds (iii), which, in principle, should enhance the incoming longwave radiative flux due to their water content. Since observations of the cloud amount are mostly not available, cloudiness C is derived from the cloud factor cF by inverting the best–fit function found by Greuell et al. (1997) for the Pasterze glacier (Austria). They concluded that their data is in line with monthly values for the cloud factor for different elevations based on data from Austrian climate stations. Here, it is assumed that this relation is transferable for nearby areas that have similar mountain topography:

$$C = 0.997 + 0.4473 \cdot cF - 1.4059 \cdot cF^2$$

According to the Stefan Boltzmann law, the incoming longwave radiative flux from the sky is estimated by the Stefan Boltzmann constant, the fourth power of the air temperature, and the emissivity of the sky. It is then further modified by the skyview factor. Therefore, the emissivity of the sky ε_{sky} is computed as:

$$\varepsilon_{sky} = \varepsilon_{cs} \cdot (1 - C^2) + \varepsilon_{oc} \cdot C^2$$

ε_{oc}, the emissivity of totally overcast skies, is assumed to be 0.976 (after Greuell et al. 1997). Simulating the effect of the clouds using equations (24) and (25) leads to an increase of the longwave radiative fluxes of approximately 7 %. This process counteracts the effects of temperature and slopes since, generally, higher elevations are characterized by lower temperatures and smaller slopes, but increased clouds.

5 Modelling the snow surface energy balance

The core of AMUNDSEN is a physically based description of the energy and mass balance of the snow surface. The respective algorithm, called *ESCIMO* (**E**nergy balance **S**now **C**over **I**ntegrated **MO**del), has been developed as a modular point model for the simulation of the energy balance, the water equivalent. and the melt rate of a snow cover. Through a simple, documented interface ESCIMO can easily be adopted by any distributed modelling framework which provides data fields for the required variables. Consequently, it has already been implemented and applied for numerous geographical positions and climatic conditions at scales ranging from a particular site up to regional catchments (100.000 km²). E.g., ESCIMO has been integrated in

(a) the SVAT scheme *PROMET* (**P**rocesses of **R**adiation, **M**ass and **E**nergy **T**ransfer) for distributed, physically based water balance simulations including sophisticated formulations of the matter and energy fluxes in the soil, plants and in the atmospheric boundary layer (MAUSER and BACH 2008, STRASSER and MAUSER 2001, MAUSER and SCHÄDLICH 1998, STRASSER 1998, TASCHNER et al. 1998)

(b) the integrative decision support system *DANUBIA–Light*[16] developed to simulate the effects of global change on the water balance of the upper Danube river basin (PRASCH et al. 2008, MAUSER et al. 2007, MAUSER 2003, LUDWIG et al. 2003, MAUSER and LUDWIG 2002)

(c) the hydrological model *PREVAH* (GURTZ et al. 2003) to compute distributed snowmelt rates, e.g. for the Goldbergkees (Austria) (Koboltschnig 2007) or in a comparative application for the Dischma catchment (Switzerland) (ZAPPA et al. 2003)

For the purpose of validation, ESCIMO has been compared with the sophisticated, multi-layer snowmodel *CROCUS* (Brun et al. 1992, STRASSER et al. 2002), and tested within the framework of the international SNOWMIP[17] programme (ETCHEVERS et al. 2002, 2004), including comparison with observations at sites with very different climate. ESCIMO is fully integrated in AMUNDSEN and mutually exchanges variables with the other modules in both directions. Alternatively, AMUNDSEN also allows the computation of snowmelt and icemelt rates applying a temperature index model, which can be driven at an hourly time step and which is considering potential direct radiation and albedo (Pellicciotti et al. 2005) – see eq. (21). The index model is faster in terms of computational performance, but has to be properly calibrated to the site of consideration (see the remarks in sections 1.3 and 1.5).

5.1. General model structure

The energy balance of the snow surface is modelled hourly considering shortwave and longwave radiation, sensible and latent heat fluxes, energy conducted by solid or liquid precipitation, sublimation/resublimation, and a constant soil heat flux. First, a distinction is made between melting conditions (air temperature ≥ 273.16 K) and no melt conditions (air temperature < 273.16 K). In the first case, a snow surface temperature of 273.16 K is assumed and melt occurs if the energy balance is positive. The melt amount is determined by the simulated available excess energy. If the air temperature < 273.16 K, an iterative procedure to compute the snow surface temperature needed for closing the energy balance is applied. In this procedure, the snow surface temperature is altered until the residual energy balance passes Zero. The parameter values and constants used in ESCIMO are listed in the symbols section in the appendix.
Generally, the energy balance for a snowpack can be expressed as:

$$Q + H + E + A + B + M = 0$$

where Q is the shortwave and longwave radiation balance, H the sensible heat flux, E the latent heat flux, A the advective energy supplied by solid or liquid precipitation, B the soil heat flux and M the energy potentially available for melt in the considered time step. All energy flux densities are expressed in W · m^{-2}. In the following, the computation of the individual energy balance components as algorithmically implemented in AMUNDSEN is described. The soil heat flux B is small compared to the contribution of the other energy fluxes in most alpine environments. It is assumed to be constant in space and time and has a value of 2 W · m^{-2}.

5.2. Radiation balance

To determine Q, incoming shortwave and longwave radiation fluxes are computed by means of the radiation model as described in section 4.3. Subsequently, the reflected shortwave radiation as well as the longwave emission from the snow surface has to be calculated. The amount of shortwave radiation that is reflected by the snow surface is determined by the albedo which depends on many factors (mainly grain size, density and impurity content) and varies with incidence angle and for different spectral bands. In ESCIMO, snow albedo a is modelled using the *ageing curve approach* (modified for operational use after Rohrer 1992 and U.S. Army Corps of Engineers 1956) which integrates the change of the physical properties of the surface grain during its ageing:

$$a = a_{\min} + \left(a_{t-1} - a_{\min}\right) \cdot e^{-k \cdot \frac{1}{24}}$$

[16] http://www.glowa-danube.de
[17] http://www.cnrm.meteo.fr/snowmip

where a_{min} is the minimum albedo of (old) snow, a_{t-1} is the albedo in the previous time step, k is a recession factor depending on air temperature (which determines snow surface temperature). The factor 1/24 is required to scale the result to the hourly progression of the computations. Each time a considerable snowfall occurs (at least 0.5 mm · h^{-1}), the snow albedo is reset to its maximum value $a_{min} + a_{add}$. It should be noted that the theoretical maximum albedo of 1.0 for fresh snow is never realized in nature. Observations at Kühroint (1420 m a.s.l.) revealed maximum albedos of 0.75, while higher values of up to 0.95 are reported by Strasser et al. (2004) for Haut Glacier d'Arolla (Switzerland).
The longwave emission from the snow cover $Q_{l\uparrow}$ is calculated with snow emissivity Â (usually set to values between 0.98 and 1) and the Stefan Boltzmann constant σ:

$$Q_{l\uparrow} = -\sigma \cdot \varepsilon \cdot T_s^4$$

where Ts is the snow surface temperature.

5.3. Turbulent transfer

Next is the computation of the turbulent fluxes H and E. In general, the *Monin–Obukhov similarity theory* or the *eddy flux correlation* can be considered adequate physically based methods to accurately determine the surface fluxes (Weber 2005). However, the application of the former presupposes a constant flux layer which is definitely not realized within the stable surface layer during the occurrence of a low level jet; the theory results in a Zero momentum flux at the wind maximum level. Furthermore, profile measurements of temperature, humidity and wind speed at 3 or more levels are required. Hence, bulk formulations based on the eddy flux correlation method are implemented here. In areas where the contribution of the turbulent fluxes to the energy balance of the snowpack is small, the induced loss of accuracy is negligible. In AMUNDSEN, two different parameterizations of varying complexity are implemented. The simpler one has been proposed by Kuchment and Gelfan (1996), and is valid for neutral or stable conditions at the local scale. The sensible heat flux H is expressed with wind speed W in m · s^{-1} as

$$H = 18.85 \cdot (0.18 + 0.098 \cdot W) \cdot (T_a - T_S)$$

and the latent heat flux E is calculated as

$$E = 32.82 \cdot (0.18 + 0.098 \cdot W) \cdot (e_l - e_s)$$

where W is the measured wind speed (m · s^{-1}), e_l is the water vapour partial pressure at measurement level and es the water vapour saturation pressure at the snow surface, with the water vapour pressures being calculated by using the *Magnus formula*, for positive air temperatures:

$$e_s = 6.1078 \cdot e^{\left(\frac{17.08085 \cdot (T_a - 273.16)}{234.175 + (T_a - 273.16)}\right)}$$

Similarly, for negative air temperatures (e.g., over a snow or ice surface) water vapour pressure is calculated with:

$$e_s = 6.1071 \cdot e^{\left(\frac{22.4429 \cdot (T_a - 273.16)}{172.44 + (T_a - 273.16)}\right)}$$

The water vapour partial pressure e_l is then obtained by multiplying e_s with the relative humidity.
A more physically based new formulation of turbulent exchange, particularly adapted to high mountain conditions (namely the frequent high wind speeds, its dependency on elevation and changing surface roughness), has been developed and thoroughly evaluated with extensive measurements by Weber (2008, 2005). This new formulation considers the efficiency of the turbulent exchange according to the stability and wind speed within the surface layer and can be applied in AMUNDSEN alternatively to the simpler approach (at the cost of higher computational demand). The two flux densities are thereby expressed as

$$H = \cdot \rho_a \cdot C_p \cdot 0.01182 \cdot RWT \cdot W \cdot (T_a - T_S)$$

and, respectively,

$$E = \rho_a \cdot L_v \cdot 9.2 \cdot RWT \cdot W \cdot (SH - SH_s)$$

with C_p being the specific heat capacity of moist air:

$$C_p = C_{p,dry} \cdot (1 + 0.84 \cdot SH)$$

$C_{p,dry}$ is the specific heat capacity of dry air and p_a its density, given by:

$$\rho_a = \frac{p \cdot 100}{R_d \cdot T_a}$$

with R_d being the gas constant for dry air. Atmospheric pressure p is computed (assuming a linear temperature gradient in the free atmosphere) by:

$$p = 1013.25 \cdot \left(1 - \frac{g_a \cdot h_e}{280}\right)^{\frac{M_a \cdot g}{R \cdot g_n}}$$

M_a is the molecular mass of dry air, R the universal gas constant, h_e the elevation above sea level, g the gravitational constant and g_a the atmospheric temperature gradient. Specific humidity SH is calculated with:

$$SH = \frac{0.622 \cdot e_l}{p - 0.378 \cdot e_l}$$

For the computation of the specific humidity for saturated conditions at the snow surface SH_s, e_l is replaced by e_s. The latent heat of vaporization Lv is calculated as:

$$L_v = 2501 - 2.361 \cdot (T_a - 273.16)$$

RWT is a spatially variable correlation coefficient describing the efficiency of turbulent mixing according to the different stability criteria. Unstable conditions are assumed for a negative surface temperature gradient g_s,

defined as the difference between the 2 m temperature and the snow surface temperature. Then, RWT is set to 0.4 under these conditions according to observations (Weber 2005). For stable conditions ($g_s \geq 0$), RWT is set to 0.2 if g_s exceeds or is equal to a certain threshold. The threshold value is a factor with which wind speed W is multiplied. Its value of 3.68 was empirically derived from measurements by WEBER (2005). If g_s is below this threshold, RWT is computed by:

$$RWT = \left(0.119 \cdot \frac{g_s}{W}\right) - 0.438$$

This equation is valid for smooth (snow) surfaces (roughness length < 0.001 m). This more complex scheme to calculate the turbulent fluxes gives more realistic estimates of the energy transferred during periods of high wind speeds in which mixing efficiency does not linearly increase (Weber 2008). The additional computational demands are moderate. The advantages of this approach compared to simpler, empirically derived approaches include that (i) it is based on a physically sound theory (turbulence), (ii) it considers dependency on elevation which is important in mountain regions, (iii) it compares favourably with (the few existing) measurements, (iv) it is optimized for snow and ice surfaces and (v) it can be applied for both the sensible and the latent flux, respectively. On the other hand, it should be applied only for surfaces with moderate roughness, its representativeness is limited to areas larger than 300 · 300 m and the utilized empirical constants are not yet thoroughly validated.
The latent heat flux E is accompanied by small mass changes δe, generated by sublimation or resublimation of moisture from or to the snow surface and expressed in mm water equivalent. ‰e is simulated with dt being the time between two model time steps (s):

$$\delta e = \frac{E \cdot dt}{l_s}$$

where ls is the sublimation/resublimation heat of snow.

5.4. Advective heat

The advective energy A that is supplied by the precipitation P depends mainly on its phase. If not measured, a threshold wet temperature T_w of 2 °C is assumed for the distinction between snow and rain. The wet temperature is determined by iteratively solving the psychrometer formula with ew being the saturated vapour pressure for the wet temperature ($\Delta e = 0$):

$$\Delta e = e_l - \left(e_w - \gamma \cdot \left(T_a - T_w\right)\right)$$

The psychrometric constant γ depends on the elevation above sea level, and is given by:

$$\gamma = C_p \cdot \frac{p}{L_v}$$

Next, the energy advected by precipitation P (in mm) is calculated for rainfall on snow with:

$$A = P \cdot c_{sw} \cdot \left(T_a - 273.16\right)$$

where c_{sw} is the specific heat of water. For snowfall, the advective energy is computed with:

$$A = P \cdot c_{ss} \cdot \left(T_W - 273.16\right)$$

where c_{ss} is the specific heat of snow. If the air temperature is below 0 °C, then a freezing of the rain in the snow cover is assumed, and A is increased by the melting heat of ice ($3.375 \cdot 10^5$ J · kg^{-1}).

5.5. Snowmelt

Finally, the available energy M for melt can be computed for the case of melt condition ($T_a \geq 273.16$). For those conditions, all fluxes are calculated with an assumed snow surface temperature of 273.16 K, and M_w is the remainder of the energy balance equation. If $M > 0$, the melt amount in mm is calculated with

$$melt = \frac{M \cdot dt}{c_i}$$

where c_i is the melting heat of ice.
In the case of no–melt condition ($T_a < 273.16$ K), an iterative scheme to close the energy balance is applied; thereby, the snow surface temperature is altered with respective recalculation of longwave emission and turbulent fluxes until eq. (26) passes Zero. After that, the mass balance is updated by the amount of δe (sublimation or resublimation, eq. (41)).

6 Modelling snow-canopy processes

Mountain forests are primarily composed of evergreen conifer species which retain their needles throughout the year and, therefore, intercept snow efficiently throughout the winter. Snow interception and sublimation in a canopy have been identified as important hydrological processes with complex mass and energy exchanges (MARSH 1999, POMEROY et al. 1998). The processes affecting a snow cover beneath a forest canopy are distinct from those in the open: on one hand, the meteorological conditions relevant for the energy transfer at the snow surface beneath the canopy are different, and on the other hand, a certain amount of precipitation is retained in the interception storage of stems, branches and needles. Snow that is intercepted in the canopy can melt, fall down, or sublimate into the air masses above the canopy. This latter process leads to a reduction of precipitation accumulated and stored in the ground snowpack (Fig. 14).

A forest canopy can have opposing effects on the snow cover beneath the trees, depending on many factors such as canopy density, gap size and distribution, geographical position and meteorological conditions (Pomeroy et al. 2002). Since vegetation canopies strongly affect the snow surface energy balance the result can be less SWE and a shorter duration, or more SWE and longer snow coverage. The canopy alters both the shortwave and the longwave radiation balance of the snow cover and affects the turbulent fluxes of sensible and latent heat by re¬ducing the wind speed at the snow surface (Link and Marks 1999a, b). Likewise, humidity and temperature underneath a canopy differ from those in the open. All the snow–canopy interaction processes have significant effects on the amount and timing of meltwater release from forested areas. Strasser and Etchevers (2005) have shown that the consideration of meteorological conditions at the ground beneath a canopy considerably improves the simulated amount and timing of meltwater release and in the hydrological modelling of a high alpine catchment.

Pomeroy et al. (1998) report that interception by forest canopies can store up to 60 % of cumulative snowfall resulting in a 30 – 40 % annual loss of snow cover in many coniferous forest environments. Due to its large surface area to mass ratio, and the fact that the snow remaining in the canopy is exposed to a relatively dry and warm atmosphere, relatively high rates of sublimation can occur. For an accurate determination of exposure times, it is important to know the amount of snow intercepted. Snow interception efficiency increases with canopy density, increasing size of falling snow crystals, decreasing density of the falling snow, decreasing temperature and decreasing wind speed (Marsh 1999). The capacity of the interception storage of a canopy is in the range of approximately 10 mm, according to field measurements (HEDSTROM and POMEROY 1998, POMEROY and GRAY 1995).

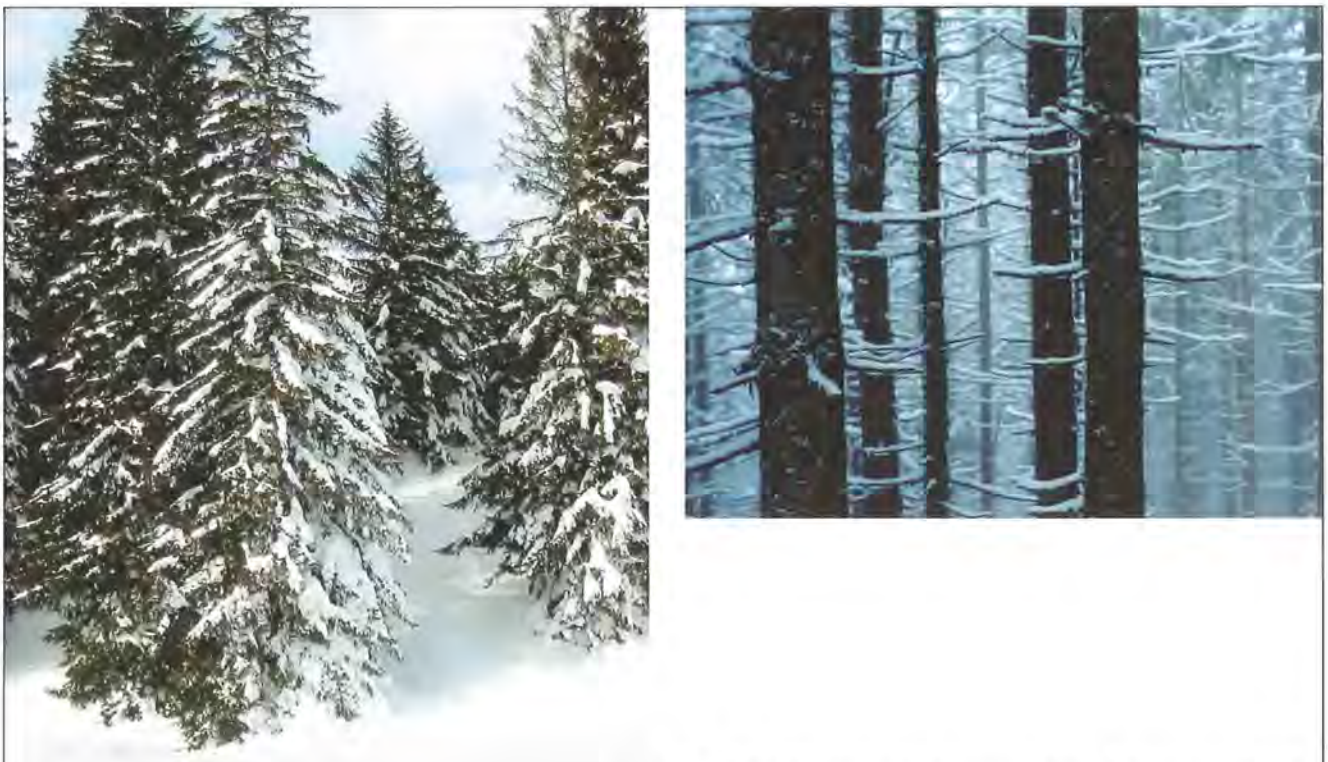

Fig. 14: Left: Intercepted snow an alpine fir trees one day after a heavy snowfall.
Right: Inside-canopy snow interception on the branches of subalpine firs. Both sites in the Bavarian Alps (Germany).
Photos: U. Strasser

Various modelling approaches have been developed to simulate snow–vegetation interaction (see HEDSTROM and POMEROY 1998, POMEROY et al. 1998, HARDY et al. 1997 and POMEROY and GRAY 1995 for reviews). Recently, an effort has been undertaken to compare the existing schemes in the framework of the SnowMIP2[18] program, including the one presented here. In AMUNDSEN the processes of interception, sublimation as well as unloading by melt and fall down are calculated depending on effective LAI and canopy height, using well documented parameterizations from the literature, mostly following the scheme of LISTON and ELDER (2006) which in itself is based on the work of POMEROY et al. (1998).

6.1. Modifications for beneath canopy climate variables

An existing forest canopy changes the micrometeorological conditions at the surface of the ground snow cover. Shortwave radiation, precipitation and wind speed are reduced, whereas longwave radiation and humidity are increased and the course of temperature is attenuated (STRASSER and ETCHEVERS 2005, TRIBBECK et al. 2004, LINK and MARKS 1999a, b). Consequently, latent fluxes and the associated sublimation rates at the snow surface inside a forest canopy differ from those in the open. Additionally, snow interception in a forest canopy affects the optical properties of a canopy which is important for remote sensing applications; the implications for snowmelt modelling are discussed by Pomeroy and Dion (1996).
In AMUNDSEN, the micrometeorological conditions for the ground beneath a forest canopy are derived from the interpolated measurements (if all stations are located in the open) by applying a set of modifications for solar and thermal radiation, temperature, humidity and wind speed. Required stand characteristics for the modelling include effective leaf area index (LAI) and tree height, the provision of which for the National Park area is described in section 3.2.2.
Following the principles of the *Beer–Lambert law*, the reduced amount of solar radiation reachinig the ground surface beneath a canopy $Q_{sc\downarrow}$ (W · m^{-2}) is determined by calculating the fraction of top-of-canopy incoming solar radiation $Q_{s\downarrow}$ transmitted through the trees depending on LAI (HELLSTRÖM 2000):

$$Q_{sc\downarrow} = Q_{s\downarrow} \cdot e^{-0.71 \cdot LAI}$$

with 0.71 being a dimensionless extinction coefficient which has been fitted to two years of hourly observations in a spruce, fir, pine and aspen stand in the USDA *Fraser experimental forest* at an elevation of 2800 m a.s.l. (LISTON and ELDER 2006). This formulation takes the multidimensional character of solar radiation interaction including the variation of the solar zenith angle into account (HELLSTRÖM 2000).

Incoming longwave radiation reaching the snow underneath the canopy $Q_{lc\downarrow}$ (W · m^{-2}) consists of a fraction of the top-of-canopy incoming longwave radiation $Q_{l\downarrow}$ and a fraction of longwave radiation emitted by the forest canopy itself:

$$Q_{lc\downarrow} = (1 - F_c) \cdot Q_{l\downarrow} + F_c \cdot \sigma \cdot T_c^4$$

where σ is the Stefan Boltzmann constant, T_c the air temperature inside the canopy, and F_c the canopy density which can be calculated with:

$$F_c = 0.55 + 0.29 \cdot \ln(LAI)$$

This relationship has been derived by POMEROY et al. (2002) by means of a logarithmic best fit between leaf area index and canopy density measurements.
Canopy air temperature T_c can either be set to equal the air temperature or be modified to include a dampening inside the canopy which accounts for the shading effect during the day, and for the emission of thermal radiation during the night (Fig. 15).

Assuming linear dependency on canopy density, T_c is given by (OBLED 1971):

$$T_c = T_a - F_c \cdot (T_a - (R_c \cdot (T_a - T_{mean}) + T_{mean} - \delta T))$$

with Ta the top-of-canopy air temperature, T_c a dimensionless scaling parameter (= 0.8), T_{mean} the mean daily air temperature and δT a temperature offset depending on T_{mean} and limited to the range -2 K ≤ δT ≤ +2 K (DUROT 1999):

$$\delta T = \frac{(T_{mean} - 273.16)}{3}$$

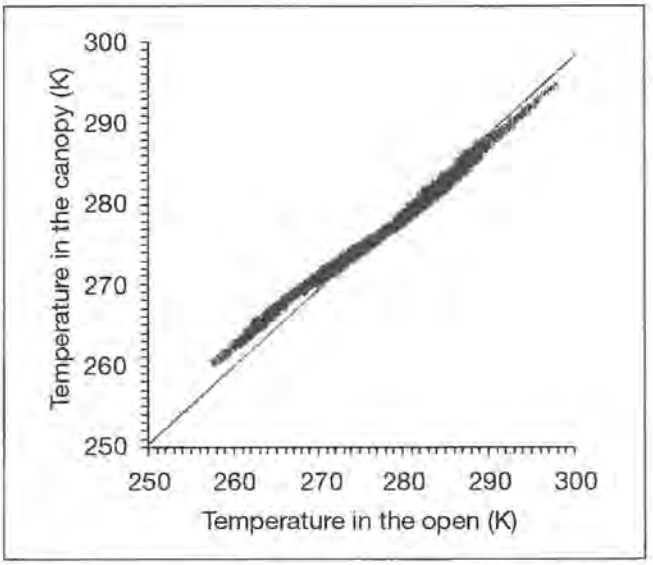

Fig. 15: Dampening of the simulated beneath canopy temperature compared to the observed air temperature in adjacent open areas. Data from Col de Porte (1325 m a.s.l., France) for the winter season 1998/1999.

[18] http://xweb.geos.ed.ac.uk/~ressery/SnowMIP2.html

The relative humidity RH_c (%) inside a canopy is often slightly higher than in the open (Durot 1999), due to sublimation and evaporation of melted snow. In the model, it is modifield, again uncluding linear dependency on the canopy density:

$$RH_c = RH \cdot (1 + 0.1 \cdot F_c)$$

For melt conditions, RH_c is set to saturation.
The wind speed W_c (m · s^{-2}) inside a canopy with the height h (m) and 0.6 being the canopy wind speed reference level (Essery et al. 2003, Cionco 1978) is calculated with:

$$W_c = W \cdot e^{-f_i\left(1-\frac{0.6}{h}\right)}$$

where f_i is the canopy flow index:

$$f_i = \beta \cdot LAI$$

with β = 0.9 being a dimensionless scaling factor that adjusts LAI values to be compatible with canopy flow indices defined by Cionco (1978) (Liston and Elder 2006).

6.2. Simulation of canopy snow interception and sublimation

In recent years, numerous models have been developed and applied to quantify the rates at which snow sublimates from evergreen forest canopies (Liston and Elder 2006, Essery et al. 2003, Pomeroy et al. 2002, Link and Marks 1999a, b, Hedstrom and Pomeroy 1998, Pomeroy et al. 1998). These models comprise a detailed simulation of the interception and sublimation processes, depending on meteorological forcing data and parameters for tree characteristics like effective leaf area index (LAI) and canopy height. Pomeroy et al. (1998) reported modelled seasonal intercepted snow sublimation to range from 13 % of annual snowfall for a mixed *spruce–aspen,* to 31 % for mature *pine* and 40 % for a mature spruce stand in the southern boreal forest of central Canada *(Waskesiu Lake, Prince Albert National Park, Saskatchewan).* Measurements of sublimation from intercepted snow within a subalpine forest canopy at a U.S. continental site amounted to 20 – 30 % of total snowfall accumulated at the site (Montesi et al. 2004).
The snow interception and sublimation model implemented in AMUNDSEN applies the physical understanding of snow interception from the branch scale to the canopy, and scales the corresponding understanding of snow sublimation of a single snow crystal to the intercepted snow in the canopy similar to Pomeroy et al. (1998). When canopy air temperatures are above freezing, intercepted snow is melted and transferred to the ground storage. Snow unloading by wind is a complex process that depends on canopy structure and spacing, branch and trunk flexibility, snow temperature and precipitation history, and wind speed and direction (Liston and Elder 2006). Numerical quantification of these processes awaits a field study and is not implemented yet.

Absorbed solar radiation SR_{abs} (W) by a snow particle in the canopy is defined by:

$$SR_{abs} = \pi \cdot r^2 \cdot (1 - a) \cdot Q_{s\downarrow}$$

with r (m) being the radius of a spherical ice particle, assumed to be 500 µm (Liston and Elder 2006) and a the intercepted snow particle albedo, which is assumed to be equal to the simulated snow surface albedo in the open (eq. (27)). $Q_{s\downarrow}$ (W · m^{-2}) is the top–of–canopy incoming solar radiation (see 4.3.1).
For the description of the mass loss rate, the *Reynolds, Nusselt and Sherwood numbers* are required in the model. The particle Reynolds number R_e with $0.7 < R_e < 10$ is given by (Lee 1975):

$$R_e = \frac{2 \cdot r \cdot W_c}{\nu}$$

with ν being the kinematic viscosity of air
(1.3 · 10^{-5} m^2 · s^{-1}). The Sherwood number S_h is assumed to equal the Nusselt number Nu which is given by

$$N_u = 1.79 + 0.606 \cdot \sqrt{R_e}$$

The saturation vapour pressure E_s (Pa) over ice is estimated with Buck (1981):

$$e_s = 611.15 \cdot e^{\frac{22.452 \cdot (T_a - 273.16)}{T_a - 0.61}}$$

This equation is analogous to eq. (32) but produces slightly larger saturation vapour pressure results accounting for the fact that the assumed surface of the canopy–intercepted snow is curved, whereas the ground snow cover is flat.
The absolute humidity at saturation ρν (kg · m^{-3}), is computed after Fleagle and Businger (1980) as

$$\rho_v = 0.622 \cdot \frac{e_s}{R_d \cdot T}$$

R_d is the gas constant for dry air (287 J · K^{-1} · kg^{-1}). The diffusivity of water vapour in the atmosphere D_v (m^2 · s^{-1}) is given by (Thorpe and Mason 1966):

$$D_v = 0.0000206 \cdot \left(\frac{T_c}{273}\right)^{1.75}$$

Now, the mass loss rate dm/dt from an ice sphere, given by the combined effects of humidity gradients between the particle and the atmosphere, absorbed solar radiation, particle size and ventilation influences can be computed. For this, both temperature and humidity are assumed to be constant with height through the canopy:

$$\frac{dm}{dt} = \frac{2 \cdot \pi \cdot r \cdot \left(\frac{RH_c}{100} - 1\right) - SR_{abs} \cdot \Omega}{l_s \cdot \Omega + \frac{1}{D_v \cdot \rho_v \cdot S_h}}$$

with l_s being the latent heat of sublimation
(2.838 · 10^6 J · kg^{-1}). ø is computed as:

$$\Omega = \frac{1}{\lambda_t \cdot T_c \cdot N_u}\left(\frac{l_s \cdot M_W}{R \cdot T_c} - 1\right)$$

λ_t being the thermal conductivity of the atmosphere (0.024 J · m^{-1} · s^{-1} · K^{-1}), M_w the molecular weight of water (0.018 kg · mole^{-1}) and R the universal gas constant (8.313 J · mole^{-1} · K^{-1}). The sublimation loss rate coefficient for an ice sphere ψ_s (s^{-1}) is now computed as

$$\Psi_s = \frac{\frac{dm_{sp}}{dt}}{m_{sp}}$$

with m_{sp} (kg) being the particle mass (ρ_i is the ice density = 916.7 kg · m^{-3}):

$$m_{sp} = \frac{4}{3}\pi \cdot \rho_i \cdot r^3$$

The canopy-intercepted load I at time t is given with t–1 being the previous time step, I_{max} the maximum snow interception storage capacity and P the (snow) precipitation (mm) in the current time step (POMEROY et al. 1998):

$$I = I_{t-1} + 0.7 \cdot (I_{\max} - I_{t-1}) \cdot \left(1 - e^{\frac{-P}{I_{\max}}}\right)$$

Liquid precipitation (rain) is assumed to fall through and is added to the ground snow cover; the consideration of rainfall–canopy interaction processes will be the subject of a future model version.

After Hedstrom and Pomeroy (1998), the maximum interception storage capacity I_{max} is equal to 4.4 · LAI. Finally, the sublimation loss rate Q_{cs} (mm) for the snow held within the canopy is:

$$Q_{cs} = C_e \cdot I \cdot \Psi_s dt$$

with C_e being a non-dimensional canopy exposure coefficient, accounting for the fact that sublimation occurs only at the surface of the intercepted snow (Pomeroy and Schmidt 1993):

$$C_e = k_c \cdot \left(\frac{I}{I_{\max}}\right)^{-0.4}$$

k_c = 0.01 is a dimensionless coefficient describing the shape of the intercepted snow deposits (LISTON and ELDER 2006). Apart from sublimation, snow can also be removed from the interception storage by melt unload. The snow masses are hereby assumed to fall down to the ground after a partial melt at the surface. Melt unload L_m (kg · m^{-2}) is estimated for temperatures above freezing using the temperature index melt model of Pellicciotti et al. (2005) (eq. (21)). For the estimation of the load of snow falling to the ground, the following scheme is applied: Using field observations, Liston and Elder (2006) estimated a daily unloading rate of 5 kg · m^{-2} · d^{-1} · K^{-1}. By applying a scaling factor of 3.3, the temperature index melt model was calibrated to fit this estimate. The resulting unloaded mass is calculated in each timestep, and added to the ground snow cover beneath the trees. By means of this snow–canopy interaction model, the processes of interception, snow sublimation, and melt unload are simulated. In a period of heavy snowfall, the interception storage can be filled up to its maximum. From the interception storage, snow is removed by sublimation and melt unload induced by a period of positive temperatures (Fig. 16).

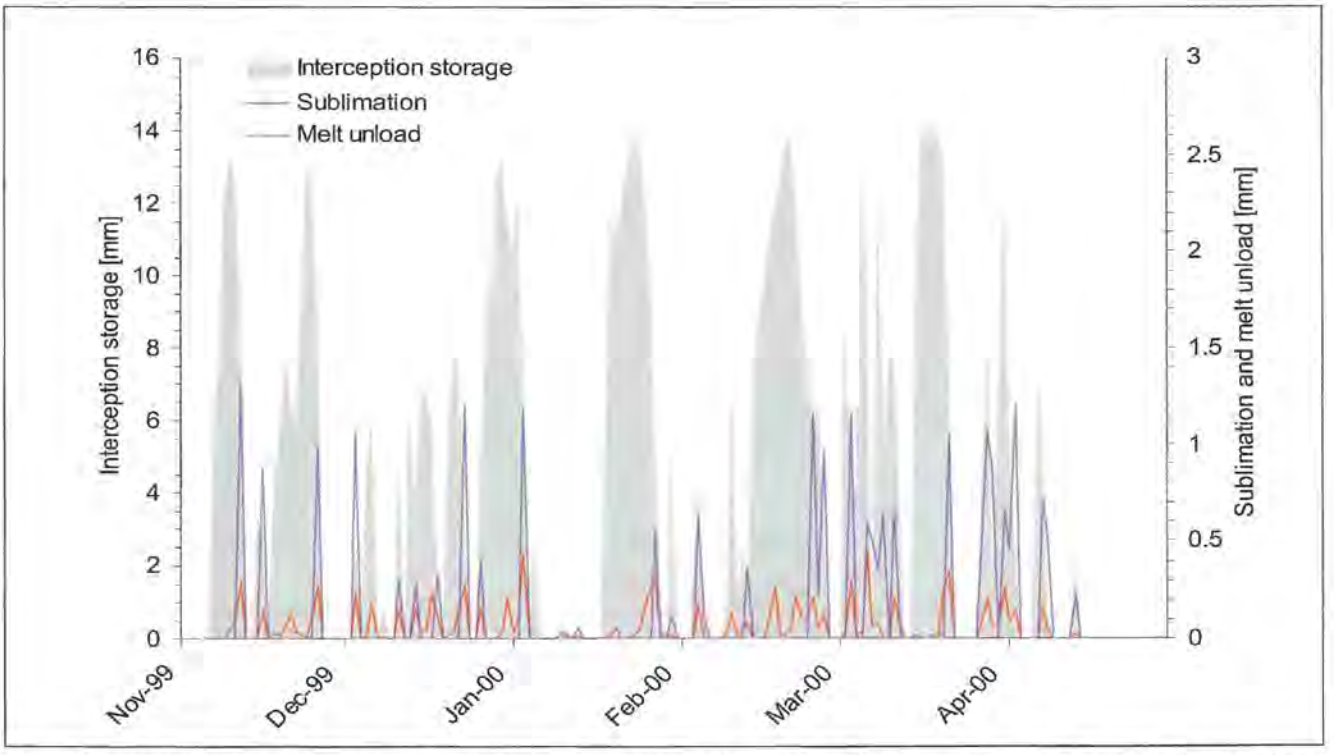

Fig. 16: Modelled canopy interception, sublimation and melt unload of snow for a *pinus mungo* stand (LAI = 3.2) at Reiter Alm III (1615 m a.s.l.) during the winter season 1999/2000.

Both, the simulated rates of sublimation and the combined effect of melt and fall down of intercepted snow strongly depend on the LAI which integratively represents canopy characteristics in the described model: LAI modifies canopy transmissivity for solar radiation, wind speed, canopy density and the maximum interception storage capacity. On top of that, if a relationship between LAI and height of the trees is assumed, tree height could also be replaced with LAI in the formulation of inside-canopy wind speed (eq. (53)), reducing the number of canopy-specific parameters required for the snow-canopy interaction model to only one (LAI). To exhibit the sensitivity of the model on LAI, it was run at the point scale with data from the station Reiter Alm III (1615 m a.s.l., winter season 1999/2000) LAI values ranging from 0 to 14 (Fig. 17). It becomes evident that canopy sublimation (top left) and melt unload (top right) increase with LAI, whereas ground melt (bottom right) decreases with LAI.

An interesting effect is revealed by the illustration of total sublimation at the ground snow surface (Fig. 17, bottom left): for LAI values from one to six, the amount of total sublimation from the surface decreases (due to small wind speeds and consecutive reduced mixing, and higher humidity). However, for LAI values above six total sublimation from the surface increases. This feature is attributable to the later disappearance of the snow cover with increasing LAI, and hence the longer duration of the sublimation process.

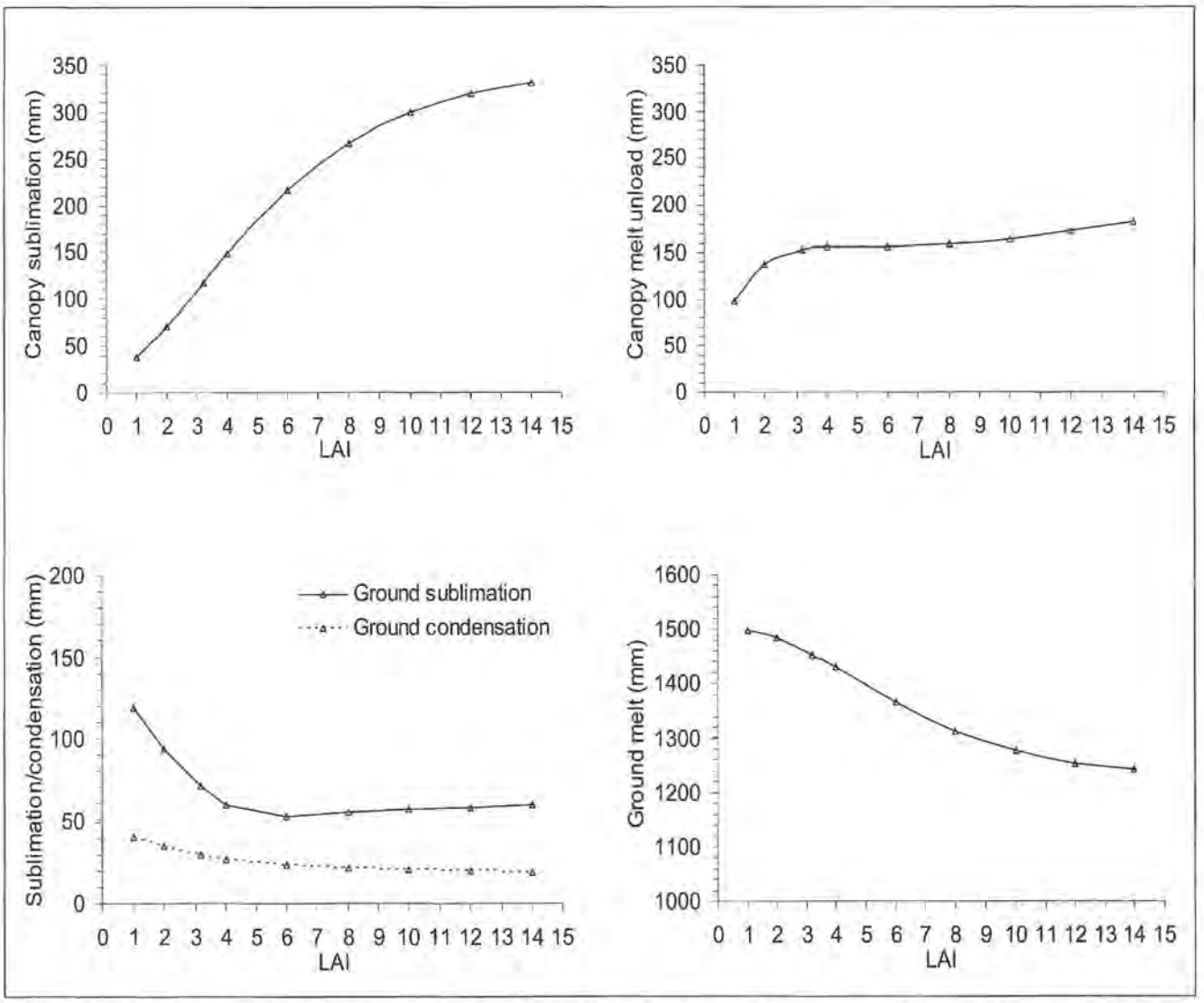

Fig. 17: Sensitivity of the snow-canopy interaction model on LAI: total canopy sublimation (top left) and total canopy melt unload (top right) of snow. Bottom: Total mass exchange related to latent fluxes at the ground snow surface (left) and total melt from the ground snow cover (right). Modelled with data from Reiter Alm III (1615 m a.s.l.) for the winter season 1999/2000.

7 Modelling snow slides

In mountain topography, snow can slide down the steep section of a slope coming to rest at its bottom where it flattens out. This process can lead to a redistribution of snow with the effect that the highest regions of alpine mountains can be a zone which can mostly remain snow–free in winter, whereas thick snowpacks can accumulate in the cirques of the vicinity. In many cases, not only snow sliding off the surrounding rock faces, but, additionally, accumulated wind–blown snow adds even more snow masses to the ground at these locations.

In high alpine terrain, the areas where this gravitationally redistributed snow accumulates preferentially are clearly visible during the melt period since they often represent the last patches of snow in the landscape before the complete disappearance of the snow cover. In the example illustrated in Fig. 18 such areas can be seen in the cirque areas below the steep slopes and at the foot of the vertical rock faces.

If such cirques are well protected against radiation, they can be the source areas for small glaciers at elevations where they normally could not exist. In the center of the photo of Fig. 18, a small, snow–covered glacier located at an elevation of 2190–2340 m a.s.l. is visible (KUHN 1993a). This type of glacier is less sensitive to changing ablation conditions than other types of glaciers, but reacts through a change of ice thickness to changing accumulation conditions (KUHN 1993a, b, KUHN 1995). If the process of gravitational snow transport is not considered in a respective modelling scheme, simulated melt out times of the cirque areas will be too early and melt out times of the slopes and rock faces above much too late (this effect is even more pronounced if a precipitation increase with elevation is assumed and included in the model). A second conclusion is that the mass balance of the snow fields and glaciers in the cirque areas can only be adequately modelled if this lateral redistribution of snow is taken into account. It is therefore an indispensible prerequisite for climate change scenario simulations with a long–term horizon, and for glacier modelling. If not considered in the modelling, snow „towers" will grow on the higher ridges where climatic conditions rarely allow for a regular melt of snow, and eventually existing glaciers in the cirques will rapidly disappear.

The technique used in this study to simulate snow sliding down steep mountain slopes is a mass–conserving, *multiple direction flow propagation* procedure which routes entrained snow masses M_{SWE} along predefined flow couloirs derived from the DEM (GRUBER 2007). Deposition D_{SWE} is controlled by available mass and local maximum deposition. At decreasing inclination, the amount of snow deposited can be quantified with:

$$D_{SWE} = \begin{cases} M_{SWE} & if \quad M_{SWE} < D_{\max} \\ D_{\max} & if \quad M_{SWE} \geq D_{\max} \end{cases}$$

With D_{max} being the maximum snow mass that can be deposited within a single DEM cell during a slide event. Potential surplus is transported into the neighbouring cells, the flow F_{NB} into each neighbour is given by the mass remaining after deposition $M_{SWE} - D_{SWE}$ and the respective draining fraction f_{NB}:

$$F_{NB} = (M_{SWE} - D_{SWE}) \cdot f_{NB}$$

Fig. 18: Eiskarl - (2613 m a.s.l., left) and Spritzkarspitze (2605 m a.s.l., center) in the Karwendel mountains (Tirol/Austria), May 1997. Photo: U. Strasser.

As a result, snow is removed from steep rock faces and accumulated at the foot of the hill slopes in the valleys. In this parameterization both flow and deposition physics are not explicitly described but characterized by simple parameters. Since the effects of kinetic energy are not included, potential uphill flow of fast moving snow masses is neglected. Stability criteria in the layers of the snowpack to be entrained are also not considered. The mass flow is obtained based on the TOPMODEL algorithm developed by QUINN et al. (1991). Regular grids of elevation (the DEM), initial mass (transportable snow on the ground) and the maximum deposition per model cell have to be provided as input data. The model then produces grids of transported and deposited mass of equal size.

The procedure enables a hydrologically plausible redistribution of snow. However, it does not allow the simulation of avalanches. The timing of avalanches on an event basis depends on many factors not considered here, such as layer stability, type of underground, local scale meteorological conditions, external forces etc. If avalanche prediction is the scope of the modelling of gravitational snow slides, all these factors have to be taken into account. For hydrological considerations at the scale of a small mountain catchment, it is sufficient to include the effect of the redistribution at a temporal resolution which is small compared to the duration of accumulation and ablation periods.
The parameterization of the model depends on the model time step, the spatial resolution of the DEM used, and on local terrain characteristics. Some values have to be derived empirically and parameters have to be adapted to produce flow paths which are coherent with visual experience. For the current study, the model was initialized with the following settings: 50 % of the available snow on a slope can be entrained if local inclination i exceeds a limiting inclination angle i_{lim} of 35°. Below that threshold, snow is deposited. The maximum snow mass that can be deposited within a single DEM cell during a slide event D_{max} is mostly determined by local inclination. The following simple function is used to quantify D_{max} (GRUBER 2007):

$$D_{\max} = \begin{cases} \left(1 - \dfrac{i}{i_{\lim}}\right)^{\gamma_s} \cdot D_{\lim} & if \quad i < i_{\lim} \\ 0 & if \quad i > i_{\lim} \end{cases}$$

where D_{lim} is an upper deposition limit, e.g. the maximum amount of snow that would be deposited on horizontal terrain, and γ_s is a shape exponent determining if the increase in maximum deposition is linear ($\gamma_s = 1$) or exponential with decreasing slope angle. D_{lim} is related to the model time step. Accordingly, it has to be varied if the time step changes. Otherwise, e.g. if the time interval between the snow slide calculations doubles, the amount of SWE available for sliding would also double (assuming a constant snowfall rate) which would result in a transport over longer distance if the same D_{lim} were used.

In the current application, the snow slide model is run at the daily scale: All 24 h each cell is checked for snow that is available for transport, and if so, snow is entrained, removed and deposited downhill (Fig. 19). On day 1, half of the SWE situated on slopes steeper > 35° is removed and deposited downhill (where steepness is ≤ 35°). The transition zone at 35° coincides with a model grid cell borderline and, hence, the processes of removal and deposition of snow are sharply delineated from each other in the modelling, as is the case in nature. On day 2, again half of the SWE which has remained on the slope is removed/deposited, and so on. If no additional precipitation occurs, then less than 10 % of initial SWE is left on the slope after day 4 (Fig. 19, right).

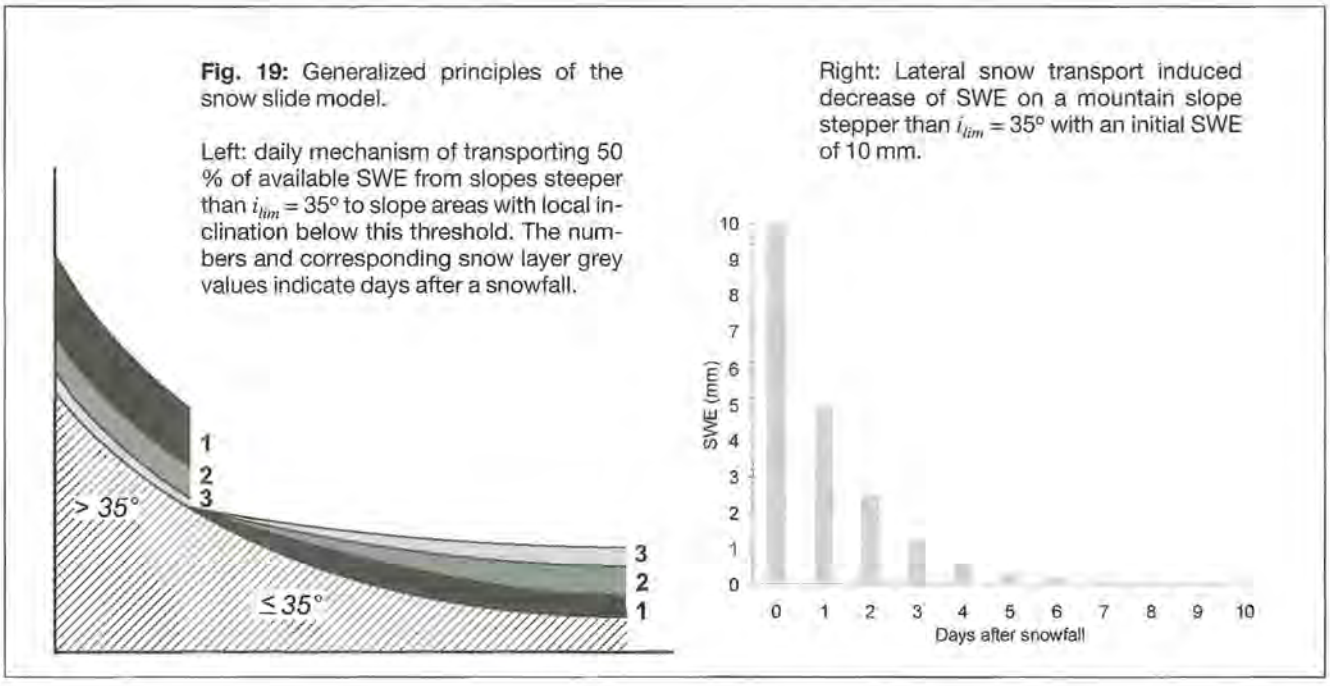

Fig. 19: Generalized principles of the snow slide model.

Left: daily mechanism of transporting 50 % of available SWE from slopes steeper than i_{lim} = 35° to slope areas with local inclination below this threshold. The numbers and corresponding snow layer grey values indicate days after a snowfall.

Right: Lateral snow transport induced decrease of SWE on a mountain slope stepper than i_{lim} = 35° with an initial SWE of 10 mm.

By applying the snow slide module, snow on steep slopes is entrained and deposited in the flat zones underneath. This process is crucial for the understanding and modelling of the snow pattern in high mountain regions, where visual observations confirm that very efficient accumulation can take place at the foot of steep slopes but not on the high crests, even though precipitation amount might be higher there. In the test region, such an area of intensified accumulation even developed into a perennial ice and firn body, the well known Eiskapelle in the Eisbachtal at the foot of the 2000 m high East face of the Watzmann mountain. For the modelling of such phenomena the consideration of gravitational snow transport is indispensable.

Fig. 20 illustrates the simulated masses of snow transported and deposited in each model cell, accumulated for the entire winter season 2003/2004. The Figure shows that snow transport only occurs in cells steeper than the preset threshold. The amount of transported snow follows the expected distribution of total seasonal snowfall amount: maximum values of almost 1280 mm are transported in the uppermost mountain regions. No gravitational snow transport was predicted for the centers of the mostly flat, carstic plateaus of Reiter Alm, Lattengebirge, and Untersberg (NW of the investigation area), and for some small areas at the mountain crests where DEM–derived slope is smaller than the threshold. As expected, the model accumulates snow in the valley bottoms at the foot of steep slopes and beneath the almost vertical rock faces of Reiter Alm, Lattengebirge and Untersberg. Values are generally in the range up to 1000 mm (blue color). Spatially very limited maxima of almost 10.000 mm occur where the fetch area from which the snow slide originates is large and reaches up into areas with a high total seasonal snowfall amount (red color). The Eiskapelle at the base of the Watzmann East face is such an area and is well reproduced by the model.

The model results reproduce the phenomena illustrated in Fig. 18, and visual observations of snow slide deposition areas in the test site well. KUHN (1995) concluded from energy balance considerations at the Hintereisferner (Austrian Alps) that eight m water equivalent must be accumulated for equilibrium conditions at an elevation of 2400 m, corresponding to an accumulation factor of approximately two compared to the total winter precipitation found for several glaciers (Paznauntal/Austria headwatershed, Schwarzmilzferner/Austria (SCHUG and KUHN 1993)). Even higher values for the accumulation factor must be assumed for glaciers that are mainly fed by avalanches from the surrounding rock faces (e.g., Mieminger Schneeferner/Austria, KUHN (1994)).

The consideration of snow slides with the suggested algorithm should actually represent an improvement in the representation of the snow cover heterogeneity in mountainous terrain. Future improvements of the algorithm could include the addition of deposited snow to the local topography, and the recalculation of the (adjacent) flow paths for succeeding snow slides, allowing for even more realistic results of deposition and melt patterns in spring.

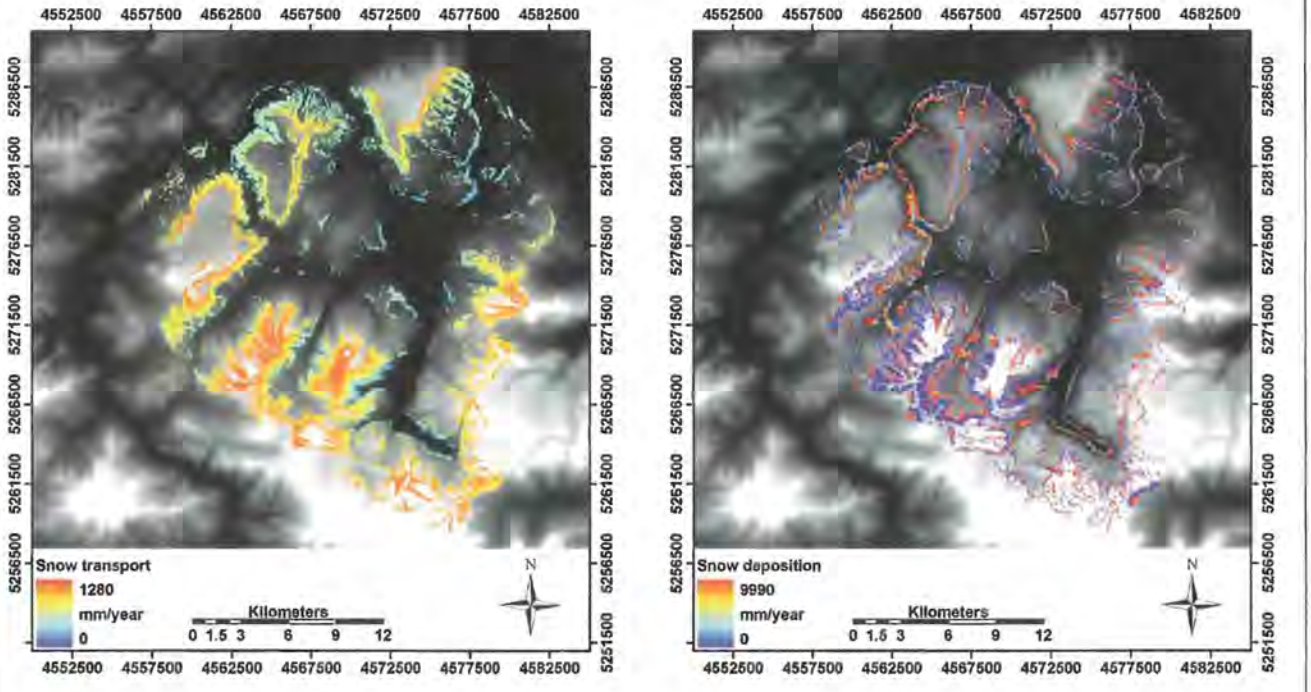

Fig. 20: Total simulated annual transport (left) and deposition (right) of sliding snow in the Berchtesgaden National Park area for the winter season 2003/2004.

8 Modelling wind – induced snow transport

Apart from gravitational snow slides, wind–induced snow transport is the second important process of lateral snow redistribution. The combined effect of these two processes is an entrainment and transport of snow masses away from steep slopes and wind–exposed locations, and a deposition of these masses in wind–sheltered regions. There is also a positive feedback between the two processes as it is common for high alpine topography that wind–blown snow is deposited on leeward slopes from which it can potentially later be entrained and removed by a snow slide. Another factor that needs to be considered is, that during wind transport a certain portion of the amount of snow can undergo sublimation back into the atmosphere and is thereby removed from the transported mass. However, an exact quantification of this effect is hampered by the difficulty in determining the spatial variability of precipitation in high alpine regions. Fig. 21 illustrates how snow is entrained as blowing snow from a mountain crest and sublimates from a layer of turbulent suspension into the air masses above. Sublimation losses during periods of blowing snow can reach amounts of up to 45 % of winter precipitation in undulated terrain or in the Arctic (Marsh 1999). However a similar quantification of this effect has not yet been determined for high alpine areas (Strasser et al. 2008c). Conceptual models describing the effects of blowing snow on the heterogeneity of a snow cover make use of parameters delineated from topography (Winstral and Marks 2002, Hartmann et al. 1999), multivariate statistics (Anderton et al. 2004) or rules (Purves et al. 1998). The more complex, physically based models simulatinig the processes of wind–induced snow transport explicitly describe saltation, turbulent suspension, and related sublimation into the atmosphere (Bowling et al. 2004, Pomeroy 1997, Pomeroy et al. 1993). A proper representation of the wind field is hereby generally the most important factor for an accurate simulation of wind–blown snow and the respective suspension and sublimation processes (Bernhardt et al. 2008a, b, Liston et al. 2007). Consequently, snow transport models like the *Prairie Blowing Snow Model* (PBSM) (Essery et al. 1999, Pomeroy et al. 1993) and SnowTran–3D (Liston et al. 2007, Liston and Sturm 1998) include linkages with methods of estimating the spatial variation in wind speed and the vegetation effect. The latter model is used here to estimate the seasonal effect of the snow transport processes on the water balance in the test site. It is a three–dimensional, physically based model to simulate snow–depth evolution resulting from wind–blown snow (Liston et al. 2007, Liston and Sturm 1998) (Fig. 22).

The model was originally developed and validated in the arctic tundra of Alaska but has been applied to a wide range of landscapes including relatively gentle mountainous terrain since its introduction (Hiemstra et al. 2006, Bruland et al. 2004, Hasholt et al. 2003, Liston and Sturm 2002, Hiemstra et al. 2002, Prasad et al. 2001,

Fig. 21: Wind-induced snow plume on a mountain crest in the Lechtaler Alps (Austria) during blue skies. Photo: P. Neusser.

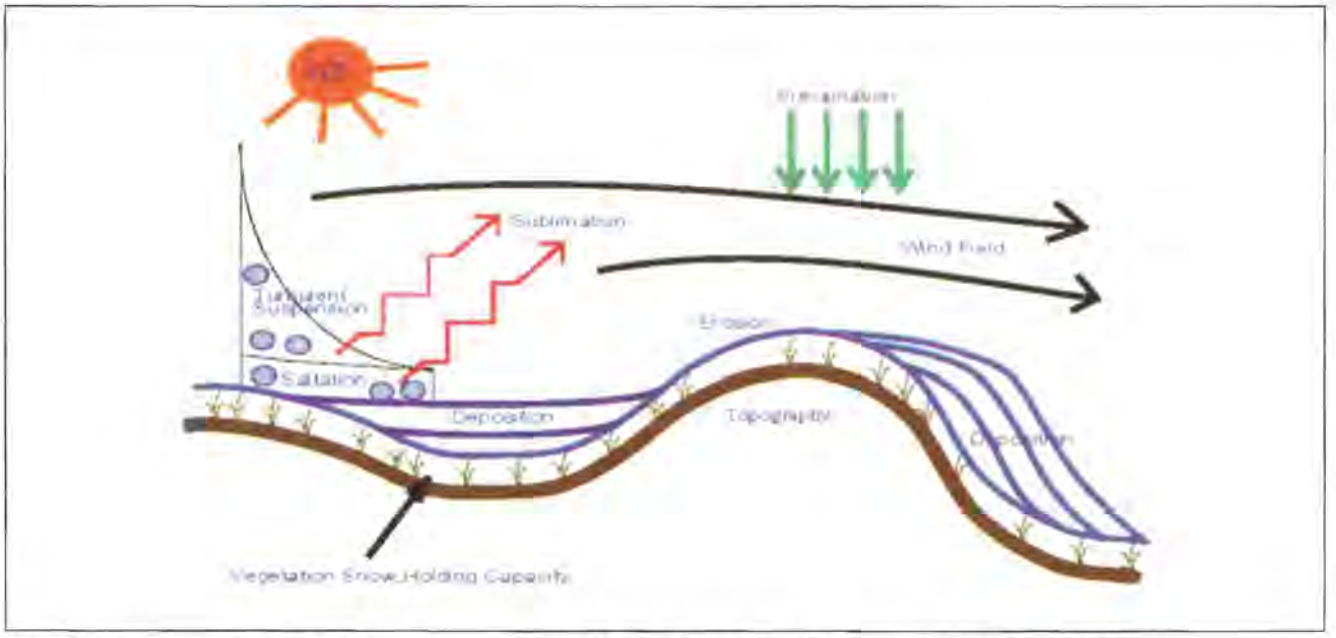

Fig. 22: Processes of windinduced snow transport considered in Snow Tran-3D (from LISTON and STURM 1998).

LISTON et al. 2000, GREEN et al. 1999). Recently, SnowTran–3D has been applied in the high alpine area of the Berchtesgaden National Park in conjunction with a new method to provide the required high resolution wind fields (Bernhardt et al. 2008a, b). The wind field is the key driving force for an accurate, event–based simulation of the erosion, transport and deposition processes of snow.

In general, there are several different strategies of varying complexity to provide a local wind field as input for the snow transport modelling: (i) simple interpolations of wind speed and direction recordings, (ii) interpolation of station recordings in combination with wind–topography relations, (iii) diagnostic atmospheric models without the hydrodynamic equations of motion and (iv) prognostic atmospheric models including all relevant equations of conservation. Attributable to scale–dependent turbulence effects, the conventional methods (i), and to a certain degree (ii), of generating distributed fields of wind speed and direction are of limited applicability in mountainous terrain and should therefore not be used to produce the wind fields for high alpine snow transport modelling. However, the nowadays available high resolution simulations of local wind fields using atmospheric models of type (iii) and (iv) and the coupling of the generated wind fields with a physically based modelling of snow transport enables a vastly improved quantitative determination of the effects of blowing snow in high alpine terrain. In the present study, a two–stage strategy is employed, consisting of the application of an atmospheric model of category (iv) in combination with a semi–empirical approach of category (ii). The method allows the computation of atmospheric wind fields with a resolution of up to 200 m, and consecutive downscaling of these fields to the process scale as represented in AMUNDSEN, i.e. to generate a ground level wind field considering local topography (BERNHARDT et al. 2008a, b). However, both the modelling of wind fields with an atmospheric model as well as distributed wind–induced snow transport simulations, require considerable computational resources. Hence these model runs are computed separately using the following strategy: first a library of high resolution wind fields for all relevant synoptic wind speeds and directions is created for the modelling domain, then the snow transport simulations are conducted, and finally the results are aggregated and integrated for the analysis. The DEM and meteorological data used for SnowTran–3D and AMUNDSEN are identical. With this combination of techniques and models, it becomes feasible for the first time to estimate the combined effect of all processes affecting the heterogeneity of a high alpine snow cover for a common simulation period and domain. Considerable parts of the following sections 8.1 and 8.2 are described in detail in BERNHARD et al. (2008a, b).

8.1. Generation of wind fields

There are only a few applications of wind field modelling in combination with simulations of wind–induced snow transport in high alpine regions. To the best of the author's knowledge, the only ones existing so far were conducted by national avalanche warning services. At the *Centre d'Etudes de la Neige* (CEN) in Grenoble (France) wind fields computed with the atmospheric model *Meso–NH* were used as input for snow transport simulations (DURAND et al. 2004), and at the *Swiss Institute for Snow and Avalanche Research* a snow transport model has been developed (LEHNING et al. 2000) which uses high resolution wind fields of the mesoscale, prognostic model ARPS (XUE et al. 2000) in the *SUBMESO* version for steep terrain (ANQUETIN et al. 1998). In both cases the simulations are event based and spatially limited to a

comparably small area. These simulations show good agreement with local measurements, but for a continuous and distributed application at the catchment scale they are too complex. Therefore, a different strategy is followed here by predicting the wind fields offline, and subsequently use them as available input for the snow transport modelling.

The atmospheric model used in this study is the *PSU/NCAR Mesoscale Model* (known as MM5), which is a mesoscale, non–hydrostatic model with terrain–following coordinates for the simulation and prognosis of the mesoscale atmospheric circulations (GRELL et al. 1995). Due to numerical constraints in the modelling caused by the steepness of the terrain as represented in the DEM, the resolution of the wind fields in the innermost nesting domain is limited to 200 m (Fig. 23). The Figure illustrates how the simulated wind flow follows topography, a feature which could not be reproduced with conventional interpolation of station–recorded wind vectors.

The analysis of wind situations which are potentially relevant for blowing snow events in the study area resulted in a library of 220 wind fields. These were computed offline and then stored in a library of wind fields which can be used in the snow transport modelling. For each timestep, the wind field which corresponds closest with the current situation is selected from the library. The key for choosing the appropriate wind field is given by a synoptic wind vector from DWD *Lokalmodell* simulations which run synchronously (hourly) with the snow transport modelling. The Lokalmodell output allows the determination of the 700 hPa wind vector for each time step, which is then used to find the best–fit 700 hPa wind vector in the library. The associated wind field is then chosen for the snow transport modelling. The original 200 m resolution of the MM5–simulated wind field is downscaled for the process simulations to a 50 m resolution with a conceptual parameterization technique using a high resolution digital terrain model (*Bernhardt* et al. 2008a). The topography–dependent modification of the local wind direction is hereby conducted after Ryan (1977), while the acceleration and deceleration of the wind due to local terrain features is considered using the approach of LISTON and STURM (1998).
With the implementation of the procedure: (i) simulation of all blowing snow relevant wind fields for the domain, (ii) downscaling them to the scale of the processes simulated by the snow transport model and (iii) storing the results in a database which is accessed in each timestep through a key provided by synchronous Lokalmodell simulations, (iv) using the wind fields to force a snow redistribution model, a technique has been established that enables, for the first time, a distributed, continuous and computationally efficient simulation of wind–induced redistribution of snow in a high alpine area.

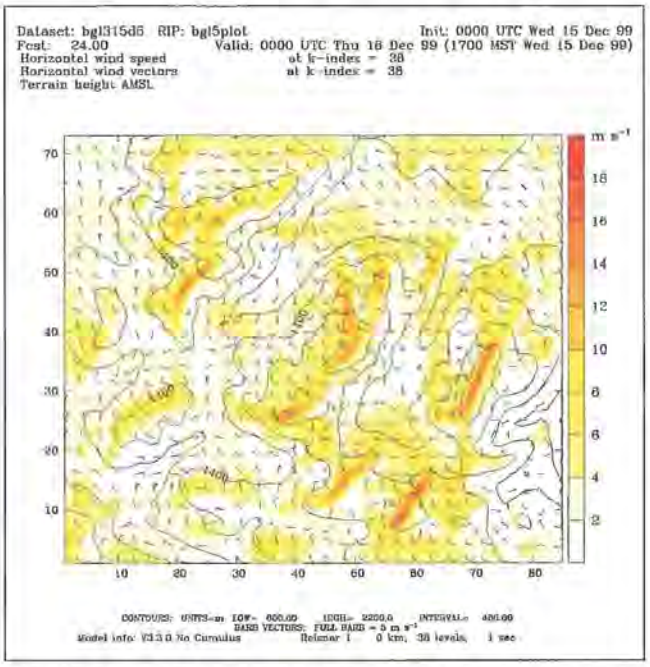

Fig. 23: Example for a MM5-modelled wind field for the central part of the Berchtesgaden National Park domain (synoptic wind flow direction 315°, assumed wind speed at the tropopause level 25 m · s^{-1}).

8.2. Simulation of snow transport

SnowTran–3D includes algorithms to compute the canopy retention capacity, the shear strength and wind–induced shear stress at the snow surface, the transport of snow by saltation and turbulent suspension, the accumulation and erosion of snow, as well as the sublimation of suspended snow (LISTON and STURM, 1998). The shear stress exerted from the wind on the surface is used to compute the amount of snow entrained and transported by saltation and suspension, considering roughness and snow conditions. It is formulated using the friction velocity which is given by wind speed at a reference level and snow surface roughness. Surface roughness itself depends on snow depth and vegetation characteristics. Snow holding retention capacity of each vegetation type determines whether snow is available to be transported at all. Only the surplus amount of snow can be removed and transported. The respective snow holding retention capacity parameters have been derived from the landuse data provided by the National Park administration and tabular values from literature (BERNHARD et al. 2008b). The forcing data required to run SnowTran–3D consist of precipitation, air temperature, humidity, and wind speed and direction. As mentioned, the wind forcing fields are replaced in the current study with the Bernhardt et al. (2008a) modelled library of wind fields (see section 8.1 above). Output of the snow transport modelling are the rates of snow erosion and deposition, sublimation from turbulent suspension and the resulting temporal development of the snow depth in each grid cell of the domain. Details of the numerical formulation of the processes in SnowTran–3D are outlined in Liston and Sturm (1998). Here, only the most important principles relevant for the modelling of sublimation of suspended snow are outlined (and will be interpreted later with respect to the alpine water balance). The spatial characteristics of the resulting simulated erosion and

deposition patterns and their correlation to meteorological conditions and topography are discussed by Bernhard et al. (2008b).

The fundamental calculation in SnowTran-3D is the mass balance (Fig. 24), which is numerically solved in each raster cell of the modelling domain:

$$\frac{dh_s}{dt} = \frac{1}{\rho_s} \cdot \left[\rho_w \cdot P - \left(\frac{dQ_s}{dx} + \frac{dQ_t}{dx} + \frac{dQ_s}{dy} + \frac{dQ_t}{dy} \right) + Q_v \right]$$

with dt being the time between two model timesteps (s), x and y the horizontal coordinates in West–East and North–South (m), ρ_s and ρ_w the densities of snow and water (kg · m^{-3}), Q_S and Q_t the horizontal mass transport rates of saltation and turbulent suspension (kg · (m · s)$^{-1}$), Q_v the sublimation rate of the transported snow particles (kg · (m^2 · s)$^{-1}$), P the rate of precipitation (mm) and hs the snow depth (m).

The model formulations for the sublimation rate of wind-transported snow follow the theories of Pomeroy and Gray (1995), Pomeroy et al. (1993), and Schmidt (1991, 1972). The sublimation rate of transported snow Q_v per unit area of snow cover, is given with x^* being the horizontal coordinate in a reference frame (m), defined by the wind-flow direction (increasing down-wind) (kg · (m^2 · s)$^{-1}$):

$$Q_v(x^*) = \Psi_S \Phi_S h_* + \int_{h_*}^{z_t} \Psi_t(x^*, z)\ \Phi_t(x^*, z)\ dz$$

where ψ_s is the sublimation loss-rate coefficient (1 · s^{-1}) and ϕ_s (kg · m^{-3}) is the vertical mass-concentration distribution. The integration limits range from the snow surface through the saltation and turbulent transport regimes (Liston and Sturm 1998). The subscripts S and t represent saltation $(z = 0\ to\ z = h^*)$ and turbulent suspension $(z = h^*\ to\ z = zt)$ layers, respectively.

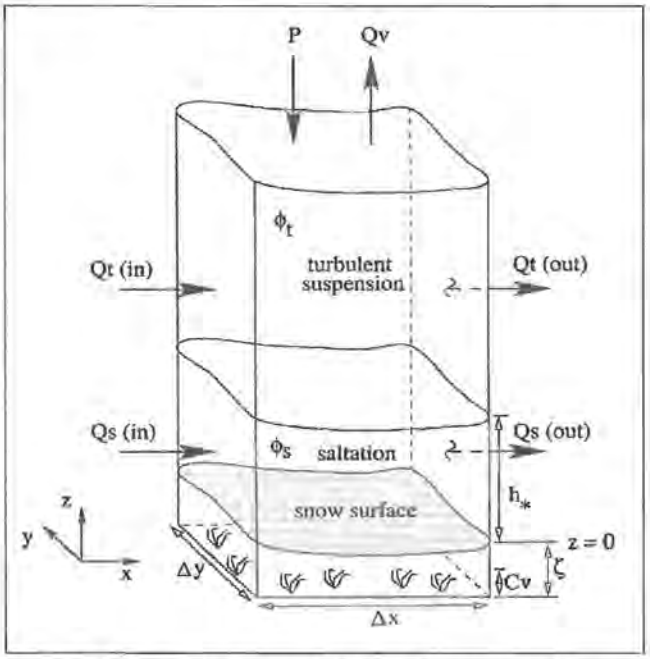

Fig. 24: Scheme of the mass balance of a snow surfacee undergoing wind-induced snow transport as formulated in Snow Tran-3D (from Liston and Sturm 1998).

The sublimation loss rate coefficient, describing the rate of particle mass loss as a function of height within the drifting snow profile, is a function of the temperature-dependent humidity gradients between the snow particle and the atmosphere, conductive as well as advective energy and moisture transfer mechanisms, particle size and solar radiation intercepted by the particle. Thereby, the time rate of mass loss from an ice sphere is calculated based on the same principles as outlined in the modelling of canopy-intercepted snow sublimation (see 6.2). It is assumed that (i) the mean particle size decays exponentially with height, (ii) the relative humidity follows a logarithmic distribution, (iii) the air temperature in the snow-transport layer is well mixed and constant with height, (iv) the variables defined within the saltation layer are constant with height and those in the turbulent suspension layer vary with height, and (v) the solar radiation absorbed by snow particles is a function of the solar elevation angle and fractional cloud cover. The details of this formulation are outlined by Liston and Sturm (1998). In SnowTran-3D, relatively high sublimation rates are predicted during blowing snow events because of the high snow particle surface-area to mass ratios, the high ventilation rates achieved when the particles are in the wind stream (Schmidt 1972), and assuming the existence of a pool of dry air overlying the surface layer with efficient mixing between the two (the model belongs to the Schmidt-type family of sublimation models, Liston and Sturm 2004). Using *Schmidt-type* sublimation models, 15 – 50 % of the snow cover were found to be returned to the atmosphere by sublimation in the Arctic (e.g., Essery and Pomeroy 1999, Pomeroy and Essery 1999, Liston and Sturm 1998), while losses of 15 – 41% were reported for the Canadian prairies (Pomeroy and Gray 1995). In contrast, other studies suggest that during blowing snow events, the air above the surface rapidly saturates with moisture, limiting the amount of snow that can sublimate (e.g., Déry and Yau 2001, King et al. 2001). As thoroughly discussed in Liston and Sturm (2004), there is not necessarily a contradiction between the two types of sublimation: Both regimes may exist depending on the interaction of the surface layer with the overlying air mass. Above inclined snow surfaces, efficient mixing is particularly forced by the frequent katabatic flows and related entrainment of air masses into the shallow surface layer (Smeets et al. 1998). Hence, for the application here, mixing of the surface layer with an overlying mass of dry air is assumed, leading to an efficient removal of moisture from the turbulent suspension layer during blowing snow events.

The specific adaptation of the model to the domain investigated in this study is described in Bernhardt et al. (2008b), including illustrations and detailed discussions of modelled transport and deposition of snow in the study area. For the scale and application considered here, the effects of the blowing snow processes are significant with respect to snow masses being redistributed and sublimated. They are, however, locally limited to the areas close to the mountain crests (Bernhardt et al. 2008b). This is one of the major differences between al-

pine regions and Arctic or Prairie regions where long open fetches allow the extensive redistribution of snow over large distances (POMEROY and GRAY 1995, ESSERY and POMEROY 1999). Analysis has shown that wind related snow transport events mostly occur at wind speeds higher than 4 m · s^{-1}. The resulting, accumulated rates of sublimation due to events of turbulent suspension are the subject of the next section.

The results of a simulation of wind–induced snow transport with emphasis on the balance of erosion and deposition due to the processes of saltation and turbulent suspension are illustrated in Fig. 25. Maximum aggregates of seasonal erosion due to saltation are located on the high ridges which are especially wind–exposed (red areas) with values of almost – 700 mm · $year^{-1}$; respective deposition takes place leeward of the summit crests, in the cirque areas, and in the upper stretches of the valleys with respective amounts of up to 300 mm · $year^{-1}$. The model predicts that redistribution of snow due to turbulent suspension is considerably more efficient. While the resulting pattern for the seasonal aggregate is similar, modelled values for this process are in the range of more than – 1500 (erosion) and up to + 3200 mm · $year^{-1}$ (deposition). Light green areas in both the saltation as well as the suspension patterns of Fig. 25 (valley regions, or the Königssee) represent areas with balances close to Zero. Again it becomes evident that the effects of blowing snow on the heterogeneity of the high alpine snow cover are significant, albeit limited in its spatial extent to the highest regions of a mountain area which is in agreement with personal experience. Only the very wind–exposed ridges undergo considerable erosion of snow, the deposition of which is concentrated to the upmost valley regions and cirques.

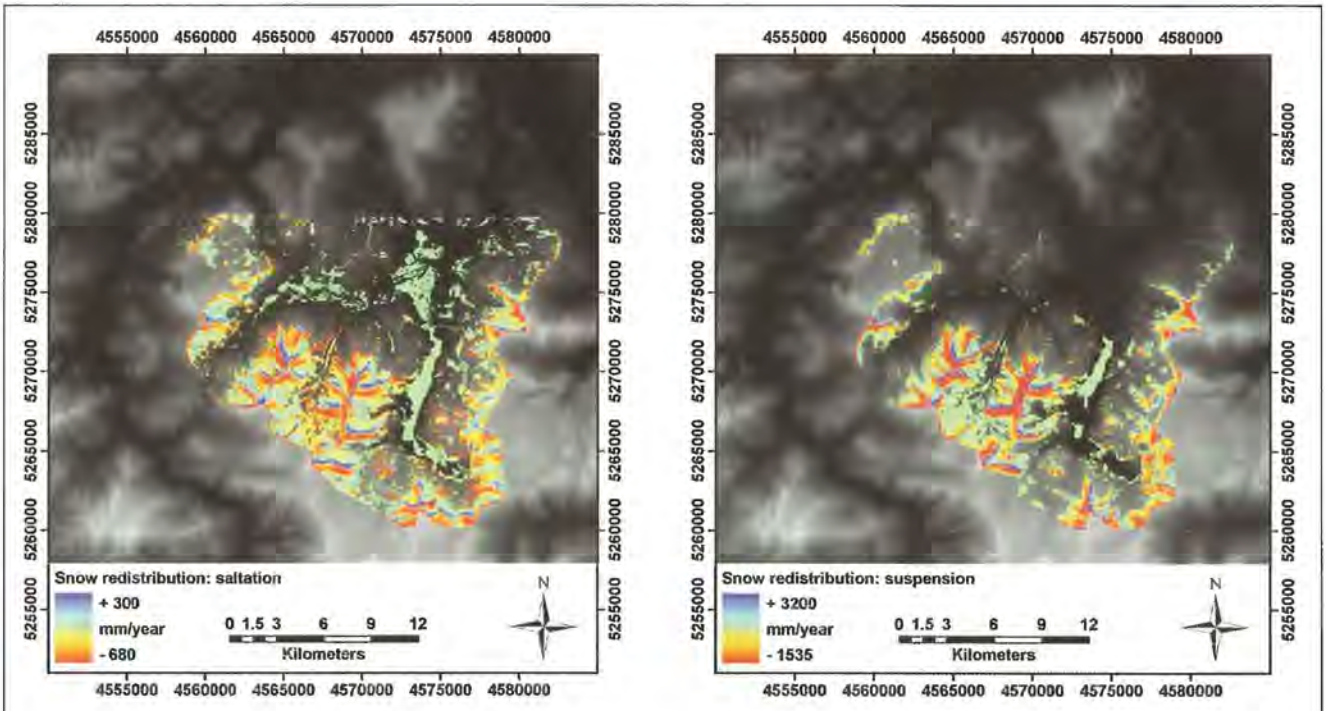

Fig. 25: Simulated values of cumulative erosion (–) and deposition (+) of wind-transported snow due to the processes of saltation (left) and suspension (right) for the Berchtesgaden National Park area for the winter season 2003/2004. The resolution of the wind-induced snow transport modelling shown here is 30 m.

9 The role of snow in the alpine water balance

9.1 Snow precipitation

For the following discussion, snowfall is defined as the portion of solid precipitation which is actually deposited on the ground. Hence, the portion of snowfall that is intercepted in the trees of the canopy and that later sublimates into the above layer of the atmosphere is neglected. However, the small amounts of snow previously intercepted in the canopy and later released by melt-induced unloading to the ground are part of the snowfall in the meaning used here.

For a map of annual snowfall distribution, the hourly snowfall fields as derived with the procedure described in section 4.2 were accumulated for all 8784 timesteps of the modelling period 1 August 2003 to 31 July 2004 (2004 is a leap year). Phase distinction for each individual precipitation event was hereby based on the following consideration: in the critical range between 1 °C and 5 °C, relative humidity triggers the probability with which precipitation is liquid or solid. The dryer it is, the more moisture evaporates from a snowflake, thereby reducing its surface temperature. In contrast, the more humid it is the less effective is the evaporation process, and, hence, the snowflake surface temperature is closer to air temperature and the probability that it melts before reaching the ground increases. A wet temperature of 2 °C proved to be a robust threshold for the phase of the falling hydrometeors (Weber 2005). The resulting annual snowfall distribution is illustrated in Fig. 26 (left). Generally, snow precipitation increases with elevation with the maximum of almost 1400 mm occurring in the summit regions of the highest mountains. In the valleys, accumulated seasonal snowfall is only 250 mm approximately. Where forest covers the mountain slopes, annual snowfall amounts reaching the ground are between 300 and 800 mm, depending on local atmospheric snowfall amount and canopy characteristics. Due to sublimation losses of snow previously intercepted in the canopy, the mountain forests appear as a sharply delineated area of reduced snowfall. The accumulated snowfall visualized in Fig. 26 (left) is also the amount of snow available for spring melt, aside from the generally small modifications of the ground snow mass balance generated by sublimation and condensation. The number of days with snow coverage (Fig. 26, right) ranges from less than 100 in the lower valley areas to more than 200 on the higher plateaus like the Untersberg (upper right corner). Interestingly, the separation of forested and non-forested areas visible in the snowfall Figure is not evident in the illustration of the snow-covered period. This can be attributed to the fact that the lower snow accumulation beneath the trees is compensated for by the melt delaying effect of the forest on the micrometeorological conditions at the ground, mostly shading and reduced wind speed. This analysis suggests that the existence of a forest does neither necessarily shorten, nor prolong the duration of a ground snow cover. This model result coincides with the experience of skiing alpinists that no certain rule can be formulated whether snow depth during spring is higher inside or outside a forest. Rather snow conditions under a forest canopy depend on many factors like local canopy characteristics, exposition, redistribution processes etc., and can vary at a very small scale.

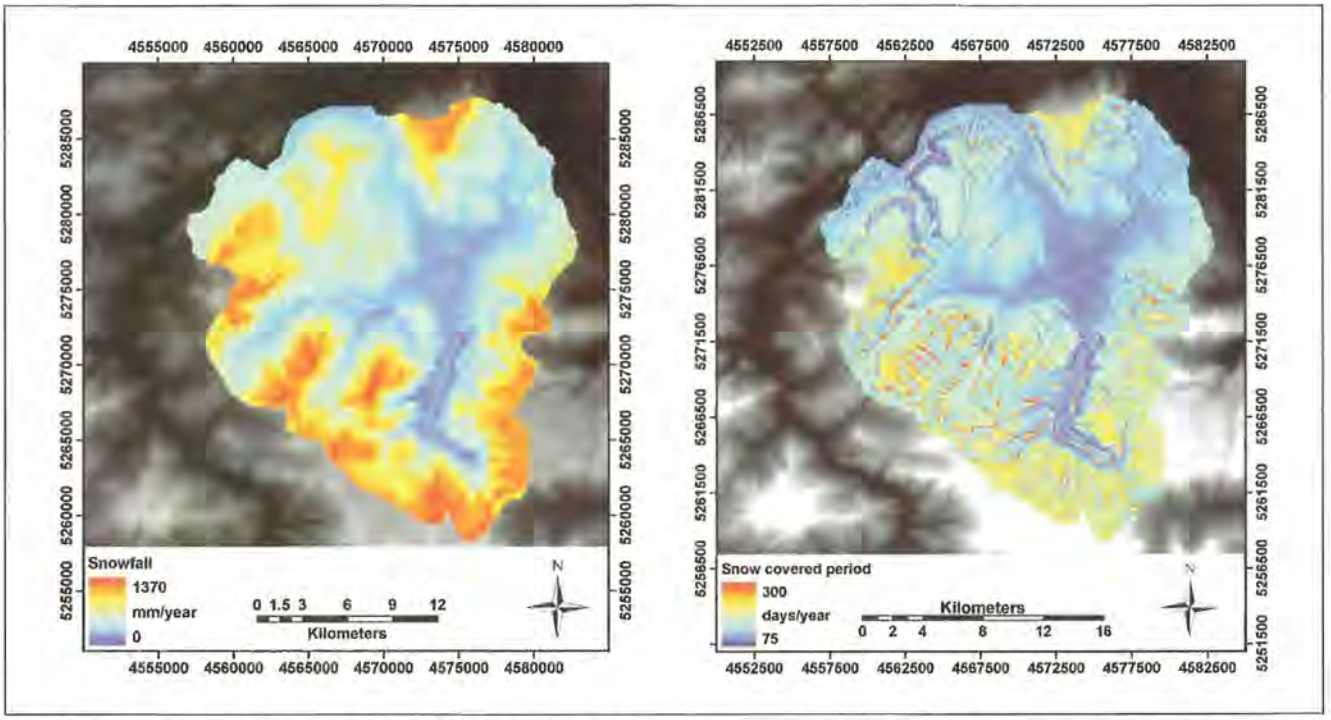

Fig. 26: Cumulative snowfall (left) and modelled duration of the snow-covered period (right) for the Berchtesgaden National Park area for the winter season 2003/2004.

A local but significant modification is caused by the modelled snow slides: In the source areas, snow cover duration is found to be less than 70 days, e.g. the very steep slopes surrounding the southern shore of the Königssee, or the Northwestern edge of the Lattengebirge in the North of the park area. On the other hand, some accumulation areas in the valleys remain snow-covered for more than 300 days particularly in the runout zones of the couloir gullies at the foot of steep mountain slopes. Where local topography effectively shades these regions from solar radiation, they coincide with the locations of existing glaciers (Blaueis glacier and Watzmann glacier).

9.2. Snow sublimation

For a long time, much effort has been invested in the study of snow sublimation processes and its important contribution to the alpine water balance (e.g., LANG 1981). Snow sublimation is the phase transition of water from solid to vaporous. The total energy required for this phase change is the sum of the latent heat of fusion (melting or freezing) and the latent heat of vaporization (evaporation or condensation), for a total of $2.838 \cdot 106\ J \cdot kg^{-1}$ at 0 °C and standard pressure. In this sum, the latent melting heat only represents 12 % of the latent heat of evaporation. The energy and water exchange at the snow–atmosphere interface is constrained by two important factors: The temperature of the (melting) snow surface cannot exceed 0 °C, and, consequently, the water vapour partial pressure at the surface will not exceed 6.11 hPa, limiting the humidity conditions at which evaporation can occur. In the considerations here, meltwater at the surface is assumed to percolate into the deeper layers of the snowpack and then follow the hydrological drainage system of an inclined surface until it eventually reaches the nearest stream. This assumption simplifies the treatment of liquid water inside the layers of the snowpack. Evaporation of liquid water from the snow surface is not considered.
Turbulent motion in the surface layer is driven mechanically during overflow of obstacles, and thermally by buoyancy over small scale surface heterogeneities. Over snow, and in particular above inclined surfaces, the latter effect is typically not very significant. Due to the relatively high amount of energy required for sublimation, related snow mass change rates are generally assumed small compared with melting. However, for cold snow they can represent the only mass loss. *At Niwot ridge, Colorado front range,* Hood et al. (1999) found a total net sublimation of 195 mm snow water equivalent from the ground, which amounts to 15 % of the maximum snow accumulation for the 1994/1995 snow season. The majority of this amount sublimated during the snow accumulation period, while 30 mm net condensation towards the snowpack occurred during the snowmelt period. The 15 % total seasonal snow accumulation lost to sublimation compares well with earlier results, e.g. by Marks et al. (1992) or Kattelmann and Elder (1991). For the Hintereisferner, an alpine glacier in the Ötztal Alps (Austria), annual mass losses due to snow and ice evaporation of approximately 100 mm have been measured with a lysimeter (KASER 1983).

9.2.1. Ground snow sublimation and condensation

The most accurate method for determining latent heat fluxes above a snow surface and direct conversion of the fluxes into millimeters of sublimation or condensation is the *eddy correlation method.* However, this procedure requires high accuracy ultrasonic anemometer and optical water vapour fluctuation measurements, the latter being hampered by poor calibration stability and uncertain long-term accuracy (WEBER 2005). If measurements of wind speed, temperature, and relative humidity at multiple heights above the snow surface are available, latent heat fluxes can also be quite reliably estimated with the *aerodynamic profile method* (*Dyer* 1974). Maximum accuracy is hereby represented by the one of the eddy correlation measurements upon which the method is based. The measurements also serve to provide robust stability functions for a stable stratification of the atmosphere. However, with both procedures long-term measurements are not feasible due to the varying distance between the snow surface and the instrument mounting device. They are, therefore, mostly applied for individual sites and for short periods (e.g., OERLEMANS and GRISOGONO 2002, MARTIN and LEJEUNE 1998, PLUESS and MAZZONI 1994).
In contrast, the *bulk aerodynamic method* requires meteorological measurements at only one height above the snowpack but still gives robust estimates of mechanically-induced turbulent transport (WEBER 2005). This procedure is most applicable for long-term calculations of the latent heat flux, in particular at catchment scale, where typically more than one meteorological station is used to spatially distribute the recordings. Regardless, many models used to simulate seasonal snow cover dynamics neglect mass changes due to sublimation and condensation at the snow surface[19]. In the present study, however, they are considered using the bulk aerodynamic method to derive seasonal, spatially distributed aggregates of sublimation and condensation for snow-covered ground.
The processes of sublimation and condensation at an exposed snow surface are associated with simultaneous adjustment of both the thermal energy and the water content of the affected snow layer. The main mechanism for the transport of latent heat between the surface and the atmosphere is mechanically induced turbulence, its efficiency depending on the irregular and chaotic small scale motion in the surface layer air flow. Generally, the prerequisites for sublimation are a negative saturation deficit and available energy needed for the

[19] http://www.cnrm.meteo.fr/snowmip/

phase transition. At night, sublimation can therefore generally only occur under very dry and warm conditions with stable stratification, usually within a katabatic flow layer when the sensible heat flux compensates for longwave emission (mostly in the range from 0 to –70 W · m^{-2}).

For the scope of this study, the latent heat flux can be adequately parameterized using the bulk formula of eq. (30). It is based on flux–variance relationships and, assuming kinematic latent fluxes, can be calculated from the product of variances of vertical wind speed and water vapour (FOKEN 2003). The variances are estimated using measured mean horizontal wind speeds and calculated water vapour differences. Utilizing this formula together with eq. (41), the mass flux from the snow surface to the atmosphere or vice versa was computed hourly. Required inputs of wind speed and relative humidity at each time step are provided using the same spatial distribution procedure as described in section 4.2 for the other meteorological variables. Resulting rates of sublimation mass loss and condensation mass gain are considered in the hourly modelling of the mass balance of the snow cover. Fig. 27 shows the simulated accumulated seasonal patterns of sublimation and condensation at the ground snow surface in the National Park area (2003/2004). A minimum ground snow sublimation of only a few mm was simulated for the valley areas where the snow cover duration is short (see Fig. 26, right), wind speeds are typically low and, hence, turbulent mixing at the snow surface is limited.

Sublimation losses generally increase for higher elevations, with maxima of approximately 180 mm occurring in the summit regions. Highest sublimation occurs at locations where snow is exposed to relatively high wind speeds (e.g., on the summit crests of Hochkalter (2607 m a.s.l.) and Watzmann (2713 m a.s.l.), both summits being prominent culmination points (see Fig. 7 in which the location of the two peaks is labelled). Forest canopy areas represent local minima for ground snow sublimation (10 to 30 mm). In addition to a reduced amount of snow reaching the ground in these areas, they are also characterized by a reduced amount of incoming radiation, lower wind speeds, and a higher humidity than in the adjacent open areas. Couloirs and very steep slopes where most of the snow is removed by snow slides are also areas of comparably low seasonal sublimation amounts with values in the range of 50 mm. Steep rock faces are represented as bright bands around the mountain massifs indicating high sublimation and condensation amounts (e.g., Reiter Alm or Untersberg). In these areas snow that has slid down accumulates and often lasts until late spring, much longer than at other locations.

The ground condensation picture (Fig. 27, right) reveals small values of 10 to 20 mm in most of the areas. High maximum values of more than 200 mm can be found in the small snow deposition zones where the snow slides are retained and snow is accumulated. There, the snow-covered period lasts until summer (again, see Fig. 26, right), and consequently, frequent warm air and high water vapour pressure conditions in the surface layer enable an efficient latent flux towards the snow surface.

9.2.2. Canopy snow sublimation

In addition to latent fluxes on the ground, snow intercepted in a forest canopy can sublimate back into the atmosphere. Interception efficiency increases with the available deposition surface, increasing size of falling

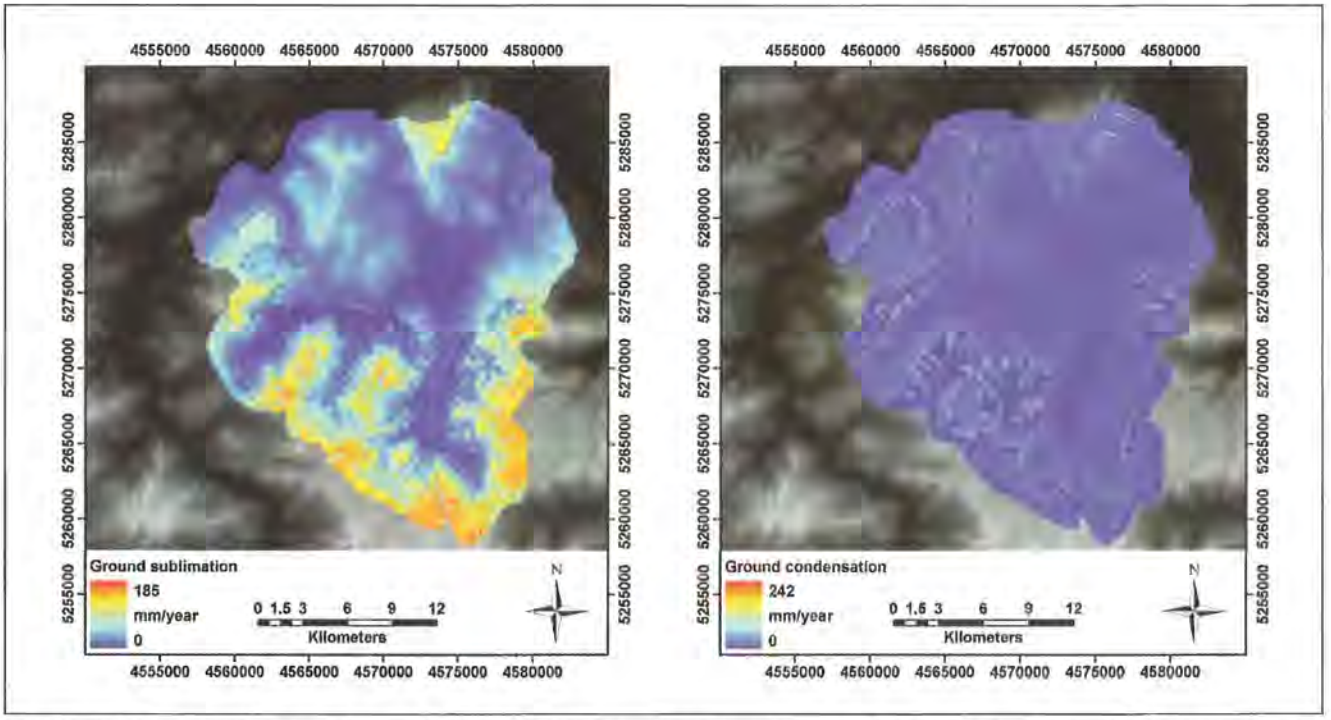

Fig. 27: Total modelled mass exchange due to the latent flux at the ground snow surface in the Berchtesgaden National Park for the winter season 2003/2004. Left: Mass loss due to sublimation. Right: Mass gain due to condensation.

snow crystals, decreasing temperature, decreasing wind speed, and decreasing density of the falling snow (POMEROY and GRAY 1995). Due to the large surface area to mass ratio and the frequent high wind speeds in mountain forest canopies, an efficient turbulent exchange and thus sublimation process is enabled. The resulting proportion of snowfall which sublimates varies depending on interception efficiency, exposure time, and atmospheric conditions.

Consequently, sublimation of snow intercepted in the trees of a mountain canopy increases with (i) larger LAI, (ii) higher air temperature, (iii) more incoming solar radiation, (iv) less atmospheric moisture, and (v) higher wind speed and thus more efficient turbulent mixing, at least up to a certain wind speed threshold. Using the model described in section 6.2, the resulting simulated sublimation rates have been accumulated to a seasonal total of sublimation SWE loss from the canopies in the National Park for Fig. 28.

Resulting total accumulated sublimation ranges between approximately 30 mm (mountain pine stand at the Reiter Alm) and maximum values of more than 250 mm for very dense stands in well ventilated, South-exposed slopes. The higher spruce stands east of the Königsee typically show values of around 200 mm. Generally, frequent smaller snowfall events during winter result in higher total sublimation amounts compared to intensive but singular events, since the interception storage is limited and precipitation surplus falls to the ground. This indicates that the total sublimation amount is dependent upon the frequency and duration of snow intercepted in the forest canopy. Snow that does not sublimate and therefore remains within the interception storage can melt and fall down later. This process is computed in AMUNDSEN using the temperature index model following Pellicciotti et al. (2005) (see eq. (21)).

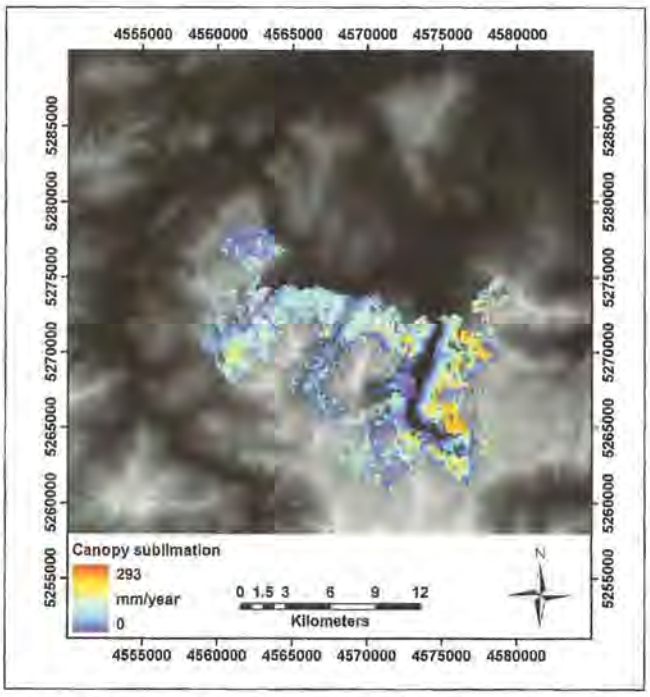

Fig. 28: Total modelled sublimation of previously intercepted snow fromt he canopies in the Berchtesgaden National Park for the winter season 2003/2004.

9.2.3. Sublimation of snow from turbulent suspension

During blowing snow conditions a very efficient exchange of energy and mass between the snow surface and the air masses above can occur (POMEROY and GRAY 1995). During turbulent suspension the suspended snow crystals are mechanically decomposed and eventually sublimate, this process being most efficient where loose snow is available and the wind speed is increased, e.g. at ridges or narrow cols.

Sublimating snow from turbulent suspension can be observed in nature as snow plumes which are blown from high crests into the blue sky atmosphere (Fig. 21), obviously revealing efficient removal of moisture from the near-surface layer of air. During snow storms sublimation may be limited due to higher saturation of the overlying air masses. Although sublimation losses from turbulent suspension of wind-blown snow are limited in their spatial extent in high alpine regions, they can locally reduce accumulated winter precipitation by a remarkable amount.

Simulations of these effects can result in significant portions of winter snowfall being sublimated, with the resulting moisture transport being important as both a source of water vapour to the atmosphere and in reducing the snow depth and snowmelt runoff in spring (MARSH 1999). Of course, there is a justifiable concern about how this effect, when modelled, can be validated. The validation issue in general is discussed with more detail in the respective section hereinafter.

In the current study, SnowTran-3D was run with the same DEM and meteorological forcing data as AMUNDSEN to simulate the total winter snow sublimation losses due to wind-induced snow transport. Wind speed and direction data were provided using the Bernhardt et al. (2008a) library of local wind fields simulated with the Penn State University - National Center for Atmospheric Research MM5 model, applying the procedure described in section 8.1. The efficiency of the sublimation process during blowing snow events depends on the amount of snow in the simulated layers of saltation and turbulent suspension. Accumulated blowing snow sublimation rates for winter 2003/2004 are illustrated in Fig. 29.

Although the areas of considerable sublimation losses due to turbulent suspension are spatially limited (below 1800 m a.s.l. they are negligibly small), the effect can be very significant at the local (pixel) scale. More than 1000 mm of SWE are modelled to sublimate into the atmosphere at the summit crests and ridges of the mountain massifs of Hochkalter and Watzmann. At such wind-exposed locations with frequent occurrences of high wind speeds the processes of snow entrainment and transport are very efficient, leading to an efficient moisture transport across the top of the boundary layer in the air masses above.

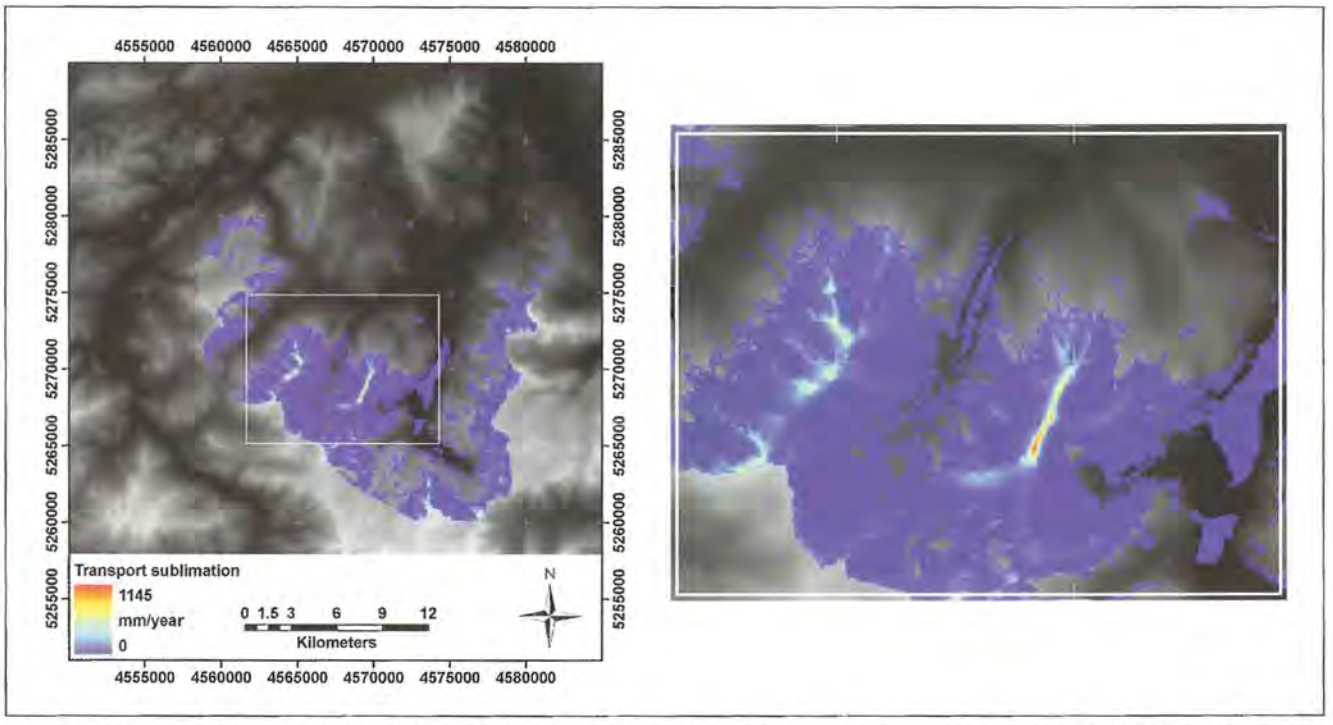

Fig. 29: Total modelled sublimation of wind-induced snow transport from the layer of turbulent suspension in the Berchtesgaden National Park for the winter season 2003/2004 (left), and a close-up of the massifs of Hochkalter and Watzmann (right).

9.2.4. Distribution of total snow sublimation

Total snow sublimation losses from the winter snow cover are given by the sum of the three described processes (Fig. 30, left). Sublimation from the ground and the canopy interception storage are similar in their seasonal efficiency and typically represent a total loss of approximately 100 mm of SWE for quite extensive areas in the test site. Only in a small but exceptionally dense spruce stand east of the Königssee a sublimation loss of almost 300 mm of SWE from the canopy is computed due to the high effective LAI there (see Fig. 8). The general shape of the ground sublimation profile is forced by the exponential expression of the water vapour calculation (eq. (31) and (32)), required for solving eq. (30). Sharp edges are evident in the snow slide erosion/deposition

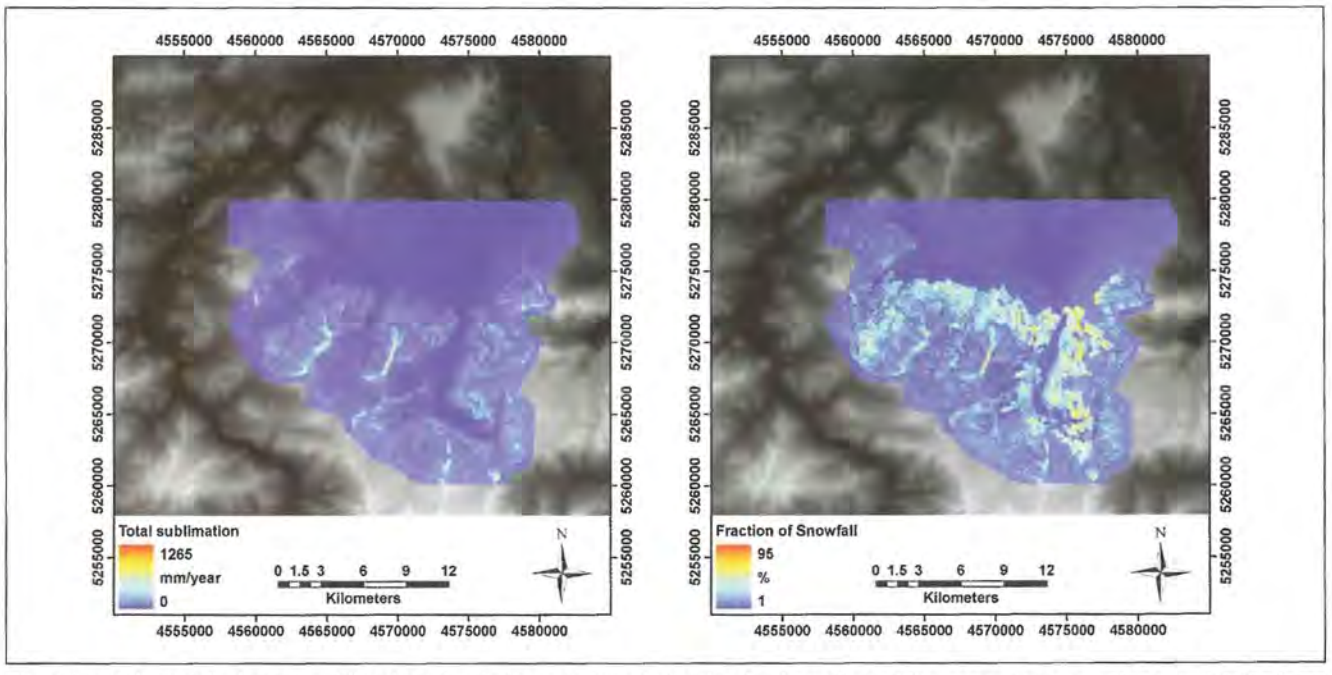

Fig. 30: Total modelled snow sublimation due to the combined effects of sublimation at the ground snow surface, sublation from the canopies, and sublimation from the layer of turbulent suspension (left and the respective fractions of modelled total winter snow sublimation losses of total winter snowfall precipitation (right) for the Berchtesgaden National Park for the winter season 2003/2004.

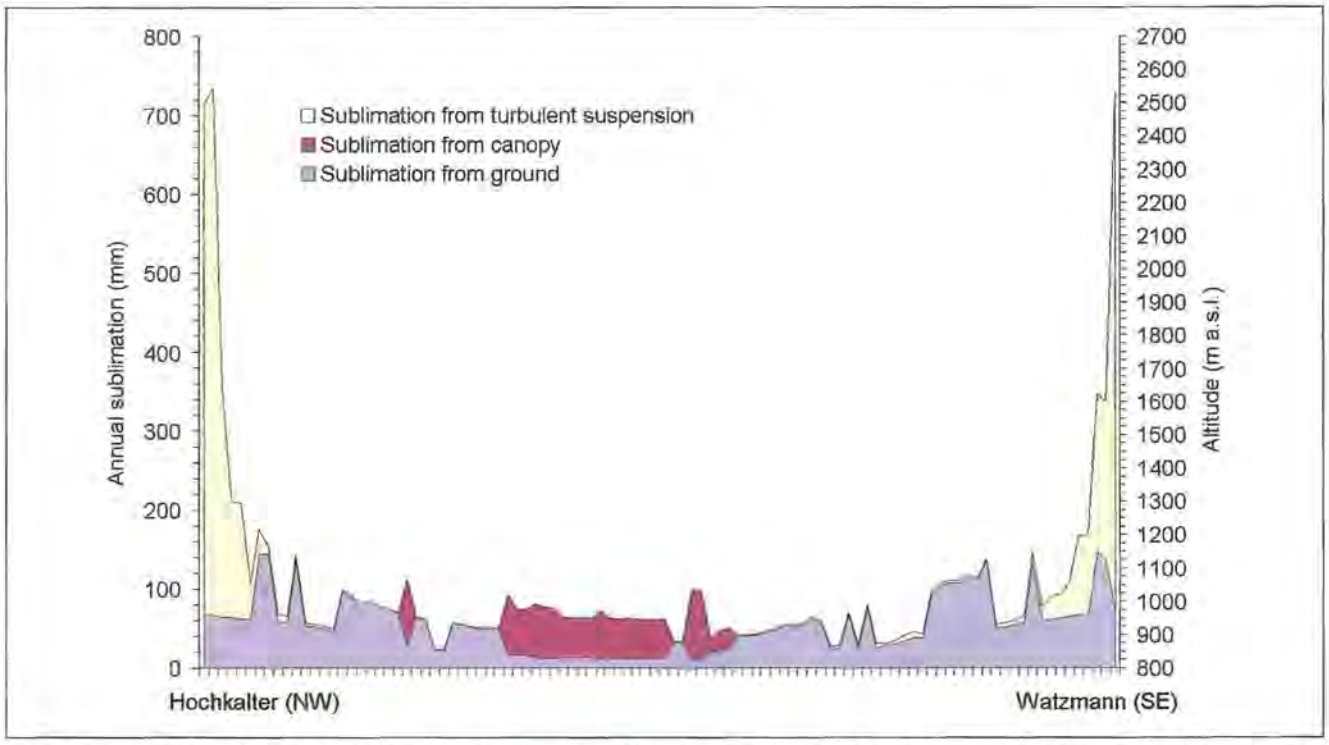

Fig. 31: Simulated contributions to total annual snow sublimation from sublimation from the ground, sublimation of canopy intercepted snow and sublimation of wind-induced, turbulent suspended snow along a cross section from Hochkalter (2607 m a.s.l.) trought the Wimbachtal to Watzmann (2713 m a.s.l.) for the winter season 2003/2004.

areas where the snow cover duration is distinctly different from other regions in the same elevation. Sublimation minima can be predicted for South-exposed areas where the snow cover disappears earlier, in areas where snow is laterally removed, or beneath trees where less snow is accumulated on the ground. Sublimation of snow from turbulent suspension during blowing snow events is generally the most efficient process but limited in its local extent. In Fig. 31, all modelled sublimation losses are illustrated for a profile transect from Hochkalter (2607 m a.s.l.) across the Wimbach valley to the Watzmann (2713 m a.s.l.). At both ends of the profile transect (the high mountain peaks), sublimation rates increase significantly due to the contribution from turbulent suspension during wind-induced snow transport. In the spatial representation (Fig. 30, left) this effect dominates over the other two causing the wind-exposed mountain crests to appear as maximum sublimation areas with total sublimation amount of up to 1200 mm. Dividing the sublimation losses by the seasonal snowfall distribution (Fig. 26, left) results in the fraction of sublimation losses from total seasonal snowfall precipitation as shown in Fig. 30 (right). This fraction amounts to 10 – 20 % in large valley areas and on mountain slopes, up to 50 % in denser, radiation-exposed canopy stands, and up to 90 % at the highest mountain crests.

9.3. Snowmelt

Total seasonal snowmelt can be defined as the amount of snow that has accumulated on the ground, composed of the atmospheric snowfall reaching the ground, rain on snow (the rainwater is stored in the snowpack and later released as melt), previously canopy-intercepted snow that falls to the ground, a potential surplus of the sublimation/condensation balance at the ground, and the effect of lateral redistribution processes. Due to the latter, rain on snow, and the fact that some snow may not melt during summer but remain until the next winter, spatially distributed total seasonal snowmelt cannot be derived by simply subtracting total seasonal sublimation from total seasonal snowfall. Hence, it can only be quantified by means of model simulations. In the present study, snowmelt at the ground was computed with AMUNDSEN for every timestep and then aggregated for the entire period August 2003 to July 2004. The results illustrated in Fig. 32 represent the combined effect of all the processes which modify the heterogeneity of the snow cover. It can be seen that in the valley areas, simulated accumulated snowmelt is below 300 mm. Smaller values of less than 100 mm of annual melt are predicted in areas where snow immediately slides down after a snowfall, namely the steep rock faces of Reiter Alm, Lattengebirge and Untersberg, and the high crests of Hochkalter (1 in the close-up of Fig. 32) and Watzmann (2).

Generally, accumulated melt increases with elevation due to the higher snowfall rates further up. The forest canopies are visible as a relative minimum of snowmelt, compared with the forest-free areas below (about 100 mm less snowmelt, recognizable as sharp line around the canopies) (3). This can be attributed to the fact that less snow is accumulated on the ground beneath a

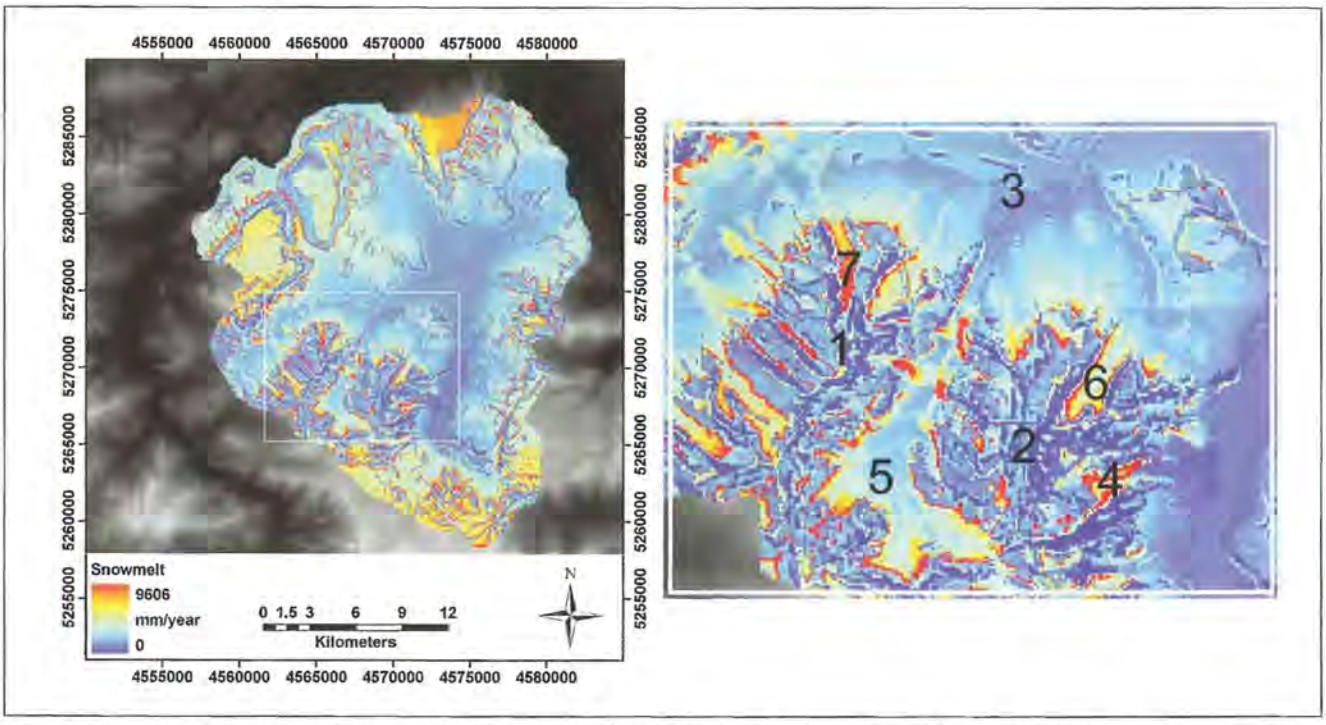

Fig. 32: Total modelled snowmelt in the Berchtesgaden National Park for the winter season 2003/2004 (left), and a close-up of the massifs of Hochkalter and Watzmann (right): Hochkalter (1), Watzmann (2), canopy borderline (3), Eiskapelle (4), Wimbach valley (5), Watzmann glacier (6) and Blaueis glacier (7).

forest canopy. Local maxima are represented by the snow slide couloirs which stretch down from the gullies through the forests, best visible in the mid elevations of the Hochkalter massif, left of (1). On the high plateaus, annual snowmelt is in the range of 1000 – 1600 mm, depending on elevation. This amount represents the storage of atmospheric winter precipitation (both snowfall and rain on snow). Here, snow depth is not modified by canopies or lateral redistribution processes in the modelling. The large maxima in snowmelt amount simulated on these plateaus can therefore be attributed solely to snow accumulating in the deposition zones of snow slides where the snow may remain long into spring or summer. Due to the masses of snow accumulated in these areas during winter, and the long period this snow is exposed to melt conditions in spring and summer (locally even longer), tremendous amounts of meltwater are produced. The small red dot east of the Watzmann mountain is the perennial snowfield Eiskapelle (4) which is fed by avalanches from the Watzmann East face. Here part of the winter snow can remain throughout the summer even though an annual snowmelt of more than 9000 mm is predicted. Other areas of high total melt amounts are the avalanche deposition areas beneath the gullies around the Wimbach valley (5), the deep valleys in the Hochkalter massif and the slopes beneath steep rock faces, e.g. around the massifs of Reiter Alm, Lattengebirge and Untersberg (values above 3000 mm, locally more than 8000 mm).

Finally, the two glaciers in the area – Watzmann glacier (6) and Blaueis glacier (7), both areas of extremely high total snow accumulation – are clearly visible as areas with exceptionally high total snowmelt (up to 6500 mm approximately). The Blaueis glacier collects snow slides from three sides (West, South and East).

Fig. 32 demonstrates the value of the physically based, separate modelling of all processes controlling the heterogeneity of the high alpine sow cover. The AMUNDSEN results provide a detailed spatial distribution map of the snowmelt runoff generation process.

9.4. The alpine winter water balance

The physically based model AMUNDSEN was applied to generate high resolution fields of rain and snowfall distribution, to compute the snow–canopy interaction, and to simulate the energy and mass balance of the ground snow cover in the high mountain region of the Berchtesgaden National Park for the winter season 2003/2004. From the aggregated fields a spatially distributed, detailed map of the winter water balance components can be derived. The winter water balance in each pixel of the domain is computed for each timestep in which either a snow cover already exists or snowfall occurs. Rain on bare ground is removed as runoff. This is then used to check if the mass balance of the snowpack is represented correctly. The total annual water balance is closed for all pixels represented by the results being Zero. Since SnowTran–3D and AMUNDSEN have been applied separately, the rates of wind–induced eroded or deposited snow are not included in this balance.
Hence, the winter water balance is given by (all elements in absolute values):

Winter water balance

= total precipitation
- ground sublimation
- canopy interception storage change
- canopy melt/fall down (canopy)
- entrained snow (slides)
- snowmelt
- ground snow storage change
+ ground condensation
- canopy sublimation
+ canopy melt/fall down (ground)
+ deposited snow (slides)
- rain on bare ground

Annual precipitation generally amounts to values between 1500 mm in the valley to 2600 mm in the highest regions. The fraction of snowfall spans from 17 % in the valleys (250 mm) to 54 % (1400 mm) on the summits. Due to sublimation losses of previously intercepted snow from the canopies, the accumulation of snow beneath the trees is lower than in the open. Depending on forest characteristics, the total amount of snowfall reaching the ground beneath the trees ranges from 300 mm in the valleys to 800 mm in the higher areas.
The results of the snow sublimation modelling from the ground, from the forest canopy, and from turbulent suspension during wind–induced snow transport indicate that the seasonal pattern of accumulated snow sublimation is highly variable. Only the contributions from ground sublimation adding up to about 100 mm of SWE are spatially relatively homogeneous. This process is most efficient for areas with long snow cover duration and generally high wind speeds, i.e. in the highest regions of the domain. Sublimation from canopy–intercepted snow is most efficient in very dense stands which are characterized by high LAI values and large tree heights, and in periods with frequent snowfall events. Results indicate total SWE losses between 100 and 300 mm of SWE in very dense stands. However, the spatial extent of such canopy types is limited. The most efficient sublimation takes place from turbulent transport during blowing snow events. Leeward of the most exposed mountain ridges, total sublimation losses add up to more than 1000 mm of SWE, due to the long availability of snow, an efficient turbulent exchange during the frequent high wind speed situations, and the generally high saturation deficit of the air masses above. The total fraction of these sublimation losses from winter precipitation is between 10 and 90 %. This amount of precipitation is not stored as snow on the ground and does, consequently, not contribute to later melt and meltwater runoff.
Total amount of seasonal snowmelt varies widely within the model area as a consequence of snowfall distribution, local sublimation, and the redistribution processes. In the valley areas where lateral snow redistribution is insignificant, only the amount of snow that has been stored in the ground snow cover melts (approximately 250 mm). From the mid elevation mountain slopes, 300 to 800 mm ground snow cover contribute to total snowmelt in forested areas, with approximately 100 mm more at sites in the same elevations but without a forest. The greatest modification of snowmelt is triggered by the snow slide process: in areas where snow is entrained and removed, namely the steep rock faces, the total annual snowmelt can be as low as 100 mm. This portion of snow is the represents the small amount of snow which is not entrained and hence later melts. However, the amount only represents a rough estimate since it depends highly on the parameterization of the snow slide model which is empirically adapted to best reproduce observed deposition zones. Where topography forces the local accumulation of snow slides from a large fetch the total seasonal snowmelt can exceed 9000 mm, in particular on the Blaueis glacier where snow slides originating from three different directions accumulate.
The spatial pattern for the number of days with snow coverage corresponds closely to the snowmelt map. Minima are the steep rock faces where snow is removed by slides (around 70 days) and the valley areas (around 100 days). The higher mountain slopes are snow–covered for 100 to 200 days, with the duration of the snow cover not being significantly influenced by the existence of a forest canopy. Finally, where snow slides accumulate, the duration of the snow–covered period can be as long as 300 days. Locally, snow may even remain until the following early winter snowfalls as perennial snowfields.

9.5. The annual alpine water balance

In this section, the contributions of the individual terms modelled with AMUNDSEN are quantified with respect to the annual water balance of the catchment. Since no explicit plant development and transpiration module is implemented in the model hitherto, a closed annual water balance cannot be calculated and resulting streamflow cannot be compared to measurements for validation purposes. The value of such a comparison would be moderate anyway, since aside from potential simulation errors, the discrepancy between measured and modelled runoff is also strongly dependent on the error inherent to precipitation estimation. This error can be in the range of 50 % or more in mountain regions especially during winter when questionable local recordings have to be distributed over a high alpine domain (Klemes 1990, Sevruk 1985). Nevertheless, by including observed streamflow recordings an attempt can be made to estimate the residual element of the water balance, actual evapotranspiration, at least in its magnitude.
The elements of the water balance are quantified by deriving the spatial means of the individual maps for the domain of the Berchtesgaden National Park as has been illustrated in the respective figures of this section. This is done for snowfall, rainfall, ground condensation, ground sublimation, and canopy sublimation. As a result of the simulations with AMUNDSEN for 2003/2004, total annual atmospheric precipitation (rainfall plus snowfall), averaged for the domain considered here, amounted to 1923.4 mm, while snowmelt was predicted to be 693.1 mm. To account for sublimation from turbulent

suspension during events of wind-induced snow transport, the respective amount has been subtracted from modelled snowmelt. Hence, the residual amount in the water balance is represented by the different components of mean annual catchment evapotranspiration/condensation, plus the streamflow discharge draining the watershed at its outlet (Table 2).

Inclusion of observed streamflow recordings can now provide a measure of mean annual evapotranspiration amount in the domain. Unfortunately, no gauge recordings for the 2003/2004 season are available at this point. Since the domain is characterized by a very complex karstic drainage system, an accurate calculation of mean annual catchment evapotranspiration is not feasible anyway: it can only be approximated. To do this, the mean annual course of discharge 1965–1999 has been extracted from the literature (DGJ 2003) and converted into mm to at least estimate the magnitude of mean annual catchment evapotranspiration (Table 3). The annual runoff regime is obviously characterized by a summer runoff maximum in May, June and July, attributable to both maximum snowmelt and maximum precipitation. The mean winter discharge is approximately only a third of the mean annual runoff.

Using these estimates, mean annual catchment evapotranspiration for the season 2003/2004 can be approximated, resulting in 1782.9 – 1398.6 mm = 384.3 mm. This amount of water was evaporated from the surfaces (plant and soil, not snow) and transpired by the vegetation in 2003/2004 (approximately). The general magnitude of this amount is in good agreement with distributed, biophysical plant development model simulations computed for this season in the domain (HANK and MAUSER 2007). Finally, it is possible to compare the relative contribution of the simulated components of the winter water balance computed as mean quantities over the domain (Table 4). Snowmelt is by far the dominant element (more than 100 % of snowfall due to rain on snow despite the different losses), while the contribution of the ground and wind-induced transport sublimation fluxes is small (6.9 and 4.1 %, respectively). Sublimation from snow previously intercepted in the canopy can be classified as moderate (13.9 %), due to the efficiency of the process, and the relatively large proportion of forested areas in the catchment. With only 2.4 % of snowfall, ground condensation contribution is the smallest.

Gravitationally driven lateral snow transport (snow slides) only redistributes snow from one location to another but does not add or remove mass to or from the entire system. It is, consequently, not included in the water balance estimation for the catchment area. However, at local scale the processes of entrainment, transport, and deposition of snow all have to be rated as highly significant (see section 8.2).

Table 2: Mean annual water balance components as modelled with AMUNDSEN for the Berchtesgaden National Park area, August 2003 to July 2004. Quantities are absolute accumulated values in mm. The residual of the water balance calculation represents the sum of evapotranspiration from the catchment and streamflow discharge at the catchment outlet.

Rainfall (mm)	Snowfall (mm)	Ground condensation (mm)	Ground sublimation (mm)	Canopy sublimation (mm)	Sublimation from turbulent suspension (mm)	Evapotrans-piration and discharge (mm)
1272.3	651.1	15.8	44.9	84.9	26.5	1782.9

Table 3: Mean streamflow discharge *MQ* 1965-1999 at Berchtesgadener Ache (gauge Kläranlage, 515.6 m a.s.l., catchment size: 367 km²). Quantities are absolute values. Converted from the data in Deutsches Gewässerkundliches Jahrbuch 1999 (DGJ 2003).

MQ (mm)	Aug	Sep	Oct	Nov	Dec	Jan	Feb	Mar	Apr	May	Jun	Jul
Month	157	109	80	64	63	55	47	70	110	207	233	202
Winter (Nov–Apr)						409.4						
Year						1398.6						

Table 4: Contributions relative to total snowfall and scale-dependent significance of the winter water balance components as modelled with AMUNDSEN for 2003/2004.

Water balance component	Seasonal amount (mm)	Relative contribution (%)	Local significance	Regional significance
Snowfall	651.1	100.0	high	high
Ground condensation	15.8	2.4	moderate	small
Ground sublimation	44.9	6.9	moderate	small
Canopy sublimation	84.9	13.0	moderate	moderate
Sublimation from turbulent suspension	26.5	4.1	high	small
Snowmelt	693.1	106.5	high	high

10 Model coupling and validation

In AMUNDSEN, the simulation of all processes implemented as model code is fully coupled, i.e. the interception processes inside the canopy, the modification of the micrometeorological conditions beneath the canopy, the energy balance of the ground snow cover and the lateral transport of sliding snow all mutually interact with each other and exchange variables. Only the SnowTran–3D runs are conducted separately and no update of the ground snow cover mass balance is considered after blowing snow events with respective erosion/deposition of snow. This simplification can be justified by the fact that the spatial extent of the SnowTran–3D simulated snow transport is relatively limited to the model cells on and around the mountain crests, and that the (small) deposition areas of wind–blown snow at the leeward slopes are within the (larger) fetches of the snow slides. Some snow remains on the mountain crests in the modelling (where the DEM–derived slope is small), while snow is removed from both sides of the ridge. Such phenomena are detectable as local maxima of total snowmelt in the model results (Fig. 32, right). In Fig. 18 the respective snow ridges on top of the mountain crests are even visible in nature. This particular phenomenon, however, is an example for model equifinality: a model has produced the right result for a wrong reason. In the classical sense, the term is used to express that various different parameter combinations produce similarly good simulation results with respect to available calibration data (Beven and Freer 2001, Schulz et al. 1999, Beven and Binley 1992). In the present case, the relevant process in nature occurs at a scale which is much smaller than the one considered in the AMUNDSEN simulations. Namely the processes involved are the effects of preferential deposition of precipitation leewards of the crests, and local topography/ turbulence features triggering the redistribution of snow. In the modelling the snow remains on the mountain crests since local slope angles as derived from the DEM for the respective model cell are beneath the threshold value for snow slide entrainment, and, hence, the snow can accumulate to a larger amount without being redistributed.

For the estimation of the winter water balance at the (catchment) scale considered here, both wind erosion of snow on mountain crests as well as deposition of formerly wind–transported snow in leeward slopes can be neglected, since both phenomena are only relevant at the local scale. However, for snowmelt considerations in the crest and snow slide accumulation regions a bidirectional coupling of AMUNDSEN and SnowTran–3D would be required – a challenge for further process studies and model development.

Concerning the validation of the modelled processes discussed here, the study generally followed the strategy to rely on models and model algorithms which have been thoroughly validated already and proved to deliver adequate results when compared with local measurements. In the following section, examples are given where and how the individual submodels of AMUNDSEN have been tested and how the simulation results have been compared to observations.

The parameterization of the shortwave radiative fluxes as described in 4.3.1 has been validated by Strasser et al. (2004) for a high alpine region in Switzerland. Clear sky conditions were selected from a three month time series of hourly recordings of global radiation and compared to the corresponding simulation results (Fig. 33, left). The analysis showed that the model results agreed very well with the measurements ($R^2 = 0.998$).

The parameterization scheme for longwave radiation was compared with measurements at the same site in the Swiss Alps (Strasser et al. 2004). The contribution from surrounding terrain (longwave emission from adjacent slopes depending on their surface characteristics) as well as from clouds was considered separately (Fig. 33, right). The difference of mean incoming longwave ra-

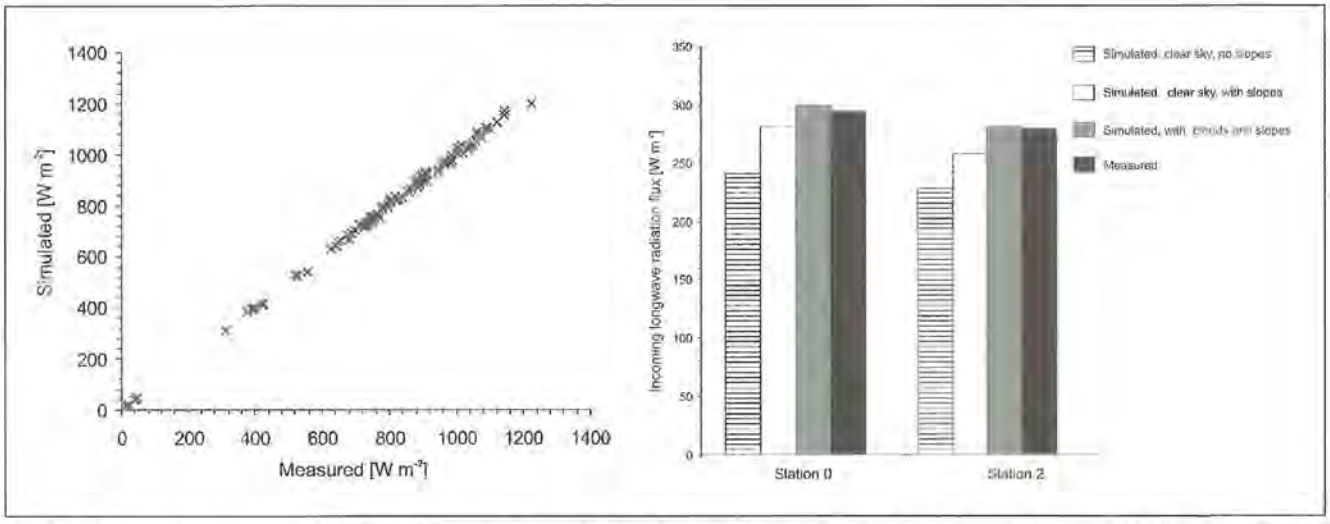

Fig 33: Measured versus simulated shortwave radiative fluxes for clear sky conditions during the melt period 2001 at haut Glacier d'Arolla (Switzerland). n = 122, $R^2 = 0.998$ (left). Right: Mean observed and modelled incoming longwave radiative fluxes at two different sites during the same period at Haut Glacier d' Arolla at 2504 and 2912 m a.s.l., respectiveley. From Strasser et al (2004).

diation between the two sites was 15 W · m^2, attributable to the different boundary layer temperature profile, the effect of surrounding topography, and clouds. The results show only slight overestimation of the flux at the two sites by the model, but can be considered as relatively reliable with respect to the complex terrain and frequent cloudy conditions. Including the effect of longwave emission from adjacent slopes significantly improved the overall results.

The albedo parameterization is of essential importance for the accuracy of energy balance modelling since albedo determines the amount of shortwave radiation absorbed by the snow surface. The scheme applied in AMUNDSEN (eq. (27)) has been compared to measurements using recordings from two *Kipp & Zonen CM7B* albedometers which were installed at two different locations on Haut Glacier d'Arolla in the melt season 2001 (Fig. 34). The results show that the course of the albedo was well reproduced by the model. At both locations, as expected, a decrease of the surface albedo with time due to the ageing of the snow could be observed. The decline is interrupted by peaks in the albedo values which are caused by fresh snowfalls. On 28 June, snowfall occurred at the upper site and thus increased the surface albedo (properly reproduced by the model), but mixed snowfall and rainfall occurred at the lower site, where, consequently, the albedo increase was considerably smaller. This event was reproduced as a pure rainfall event with no consequence for simulated albedo by the model. The sharp decline of albedo due to the ageing of the snow cover is a crucial factor for energy balance considerations. Energy absorption at the snow surface is enhanced by almost 50 % for old snow as compared to fresh snow.
The modelling of the ground snow cover as implemented here has been compared with measurements by several investigators (Zappa et al. 2003, Strasser et al. 2002). One example, out of the many at the point scale, is a comparison of modelled SWE with snow pit measurements as illustrated in Fig. 35 for the Kühroint station site in the National Park area. In 2004/2005, weekly pit recordings of SWE have been conducted which allowed validation of the simulations. On top of that, distributed analyses have been conducted at the regional scale using satellite-data derived snow cover (Strasser and Mauser 2001, Prasch et al. 2008). All comparisons indicated that the described scheme is able to provide robust estimates of the ground snow energy and mass balance.

Model results of sublimation of snow intercepted in an evergreen forest canopy were compared by Liston and Elder (2006) against observations from a continental climate site located within the U.S. Department of Agriculture (USDA) Fraser Experimental Forest (39°53' N, 105°54' W) near Fraser, Colorado, U.S.A. (Fig. 36). In this study, a 2.7 m tall subalpine fir tree *(abies lasiocarpa)* was cut, suspended, and continually weighed at two sites at 2920 and 3230 m a.s.l. from 1 January to 1 May 2001 to estimate sublimation from the tree (Montesi et al. 2004). The validation analysis included 21 storm-free sublimation periods between 9 and 53 hours. The model was driven with hourly observed within-canopy air temperature, relative humidity, and wind speed for both sites. As an example, Fig. 36 (left) shows two diurnal cycles of hourly sublimation rates for the two sites, and the general agreement between observation and simulation. While for individual hours the model over- or underestimated the observed sublimation rates, the errors overall cancelled each other out as the winter progressed and the modelled mass balance was very similar to the measured one for the sublimation period (Fig. 36, right).
The inside-canopy modification of the meteorological parameters has been measured and the respective pa-

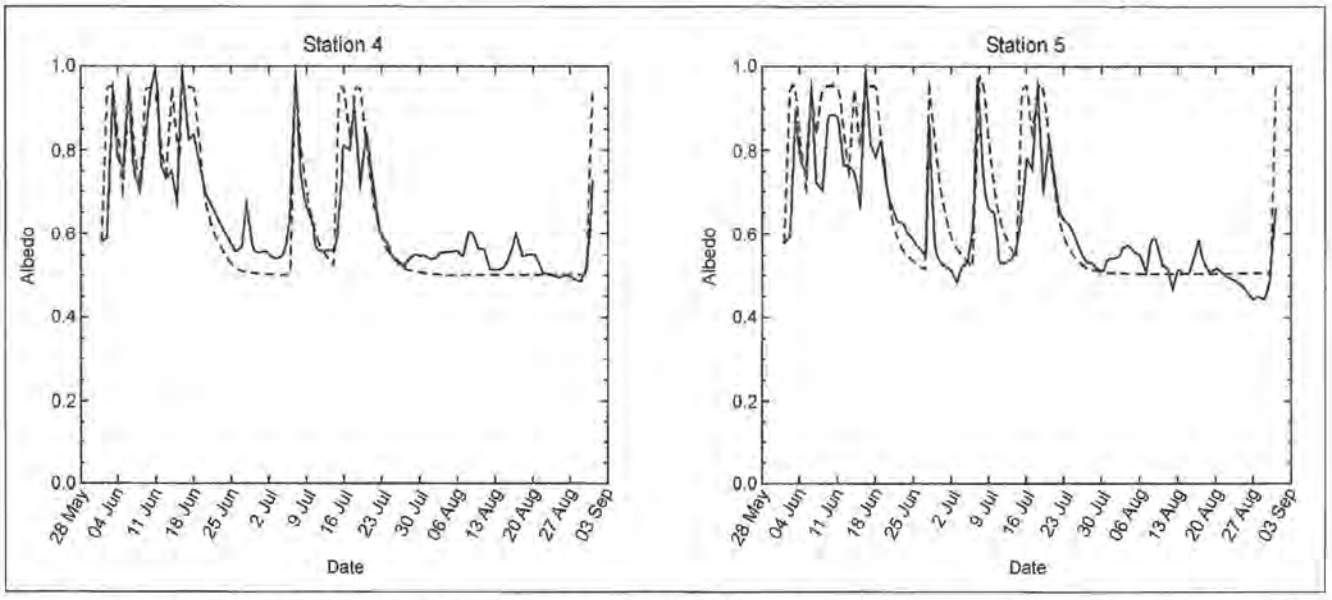

Fig 34: Measured (solid line) and modelled (dotted line) surface albedo for two locations of meteorological recordings at Haut Glacier d' Arolla (Switzerland), 2909 m a.s.l. (left/ and 3005 m a.s.l. (right). To avoid geometrical errors, measurements were made in a surface parallel plane (Mannstein) 1985).

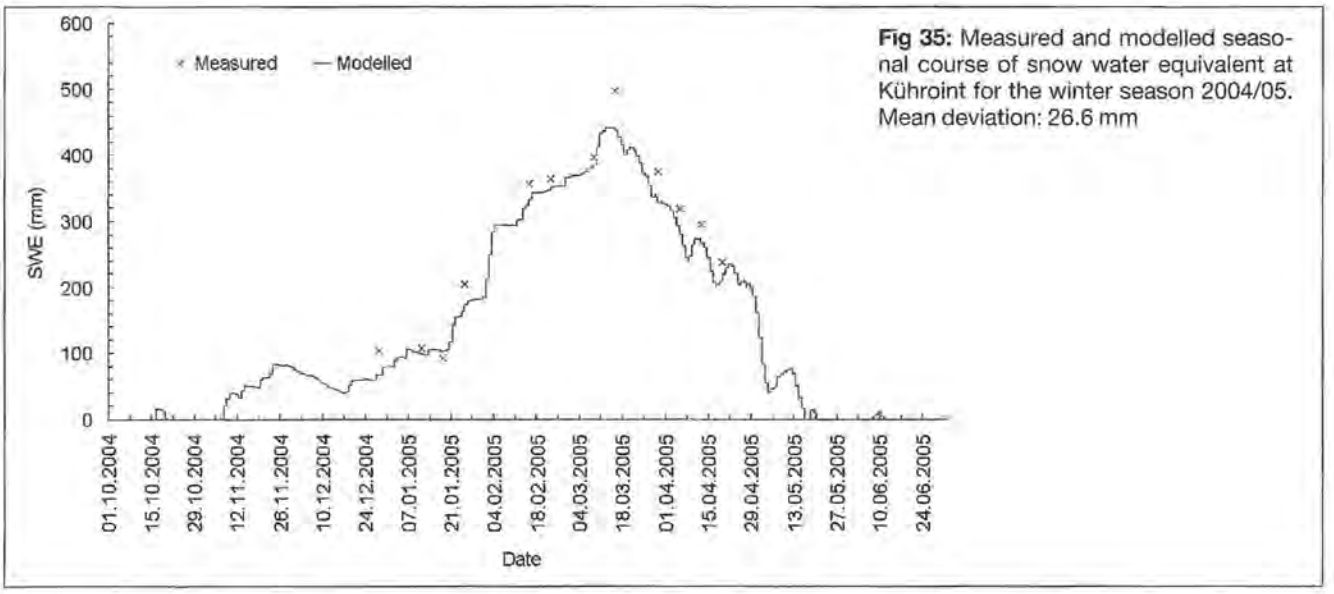

Fig 35: Measured and modelled seasonal course of snow water equivalent at Kühroint for the winter season 2004/05. Mean deviation: 26.6 mm

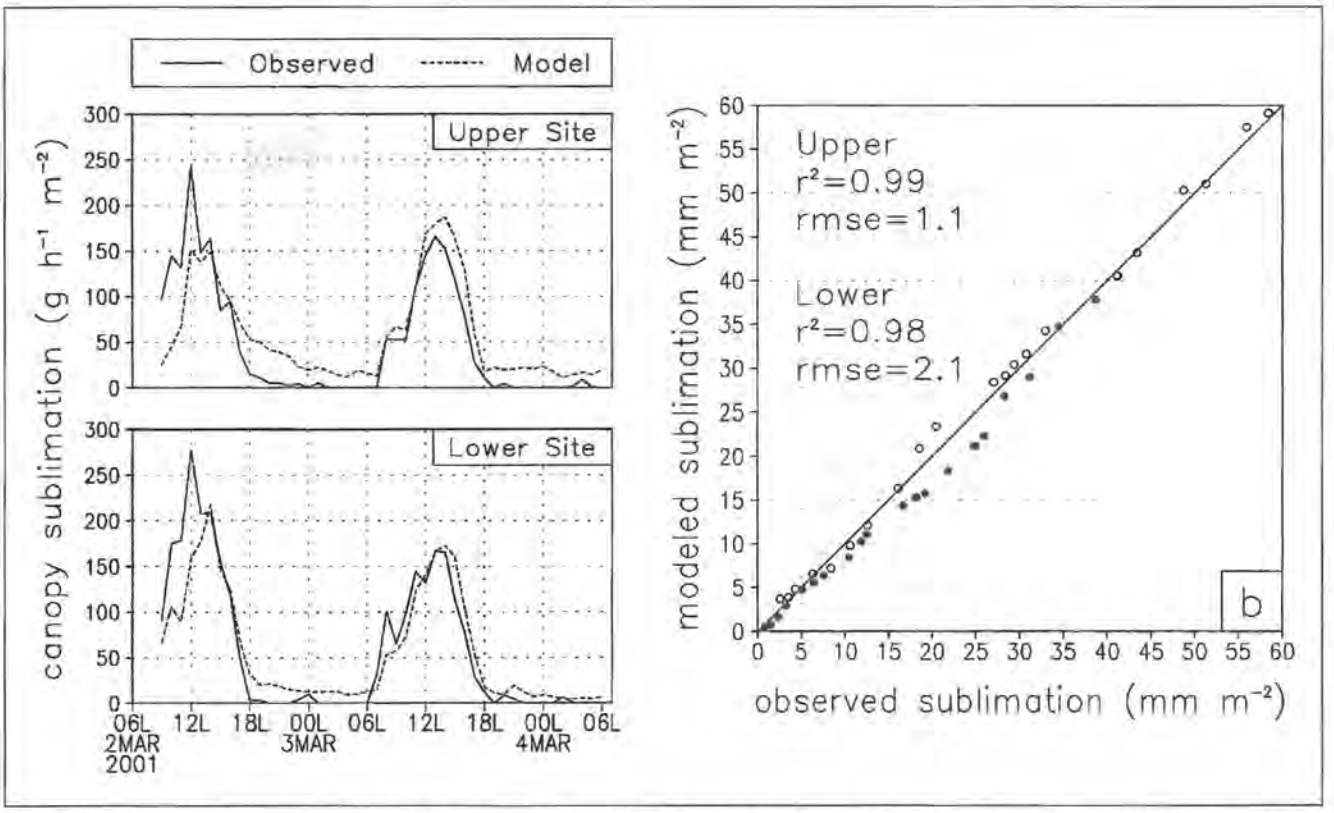

Fig 36: Observed and modelled sublimation rates for intercepted snow in an evergreen forest (left). Right: Total observed and modelled sublimation for two tree sites during a 4-month winter period with 21 sublimation periods. The model was forced to fit the total of observed sublimation at the end of the sublimation season by adjusting the parameter k_c (eq. (67)). From LISTON and ELDER (2006).

rameterization derived for the *Col de Porte observation site* (1420 m a.s.l.) in the French Alps by Durot (1999).

The snow slides module was set up and parameterized using data from the *Pizzac Avalanche* in the Italian Alps (Sovilla 2004) by Gruber (2007).

Finally, SnowTran–3D has been validated for a wide variety of landscapes, including Colorado/USA, Idaho/USA, Wyoming/USA, Svalbard/Norway, Alaska, Greenland, Antarctica, and Siberia (complete references are listed in LISTON et al. 2007). BERNHARDT et al. (2008b) validated the model for the domain investigated here, using snow depth (stake) readings from snow erosion and deposition zones.

All in all, it can be concluded that the validation of the submodels included in the framework AMUNDSEN show that they are robust and mostly versatile tools to reproduce the respective simulated processes. However, the validation at the point scale for any individual modelled processes which greatly depends on input data accuracy and versatility of the used parameterizations, *has only limited value as an estimate for the robustness of the entire framework.* For that purpose, an

integrative comparison of distributed model results would be required, but such a comparison of the entire system has not been performed yet. Consequently, in the following an analysis if the resulting melt pattern is plausible as an integrative measure for the processes which force the accumulation, redistribution, and ablation of the high alpine snow cover will be carried out. The analysis is based on comparisons between the modelled snow cover at a certain model time step with a satellite data derived snow cover acquired for the same date. For that purpose, the model was first run without the snow slides module, the resulting snow cover showing the typical higher snow depth in high elevations. In the second run, the snow slide module was included, inverting the distribution of the modelled snow depths. An improvement of the simulated pattern of snow coverage as compared to „reality" represented by the satellite data derived snow cover map, would be an argument for a generally correct representation of the processes which have produced the simulated snow pattern on that date.

To obtain an observed snow cover map, data recorded by the *Advanced Spaceborne Thermal Emission and Reflection Radiometer* (ASTER), flying onboard the TERRA satellite recorded on 26 May 2005, i.e. at the end of the melt period when a sharp snow line is visible in the above–treeline areas of the test site, was used. The ASTER data *(level 1B)* was color coded (channels 2, 4 and 5 with red, green and blue) to enable the distinction between snow and rock. Now, a visual comparison of the two modelled snow covers, with and without the snow slide routine is possible. These two maps are compared with the snow cover as derived from the satellite data (Fig. 37). The big advantage of this comparison is, that it gives an integrative estimate of model plausibility since the position of the snowline is the result of the accumulation, redistribution and ablation processes. Furthermore, the snowline is an integrated, spatially distributed variable not limited to a local scale. Hence all processes which are modelled and have an effect on the snowline position are considered and checked. Only

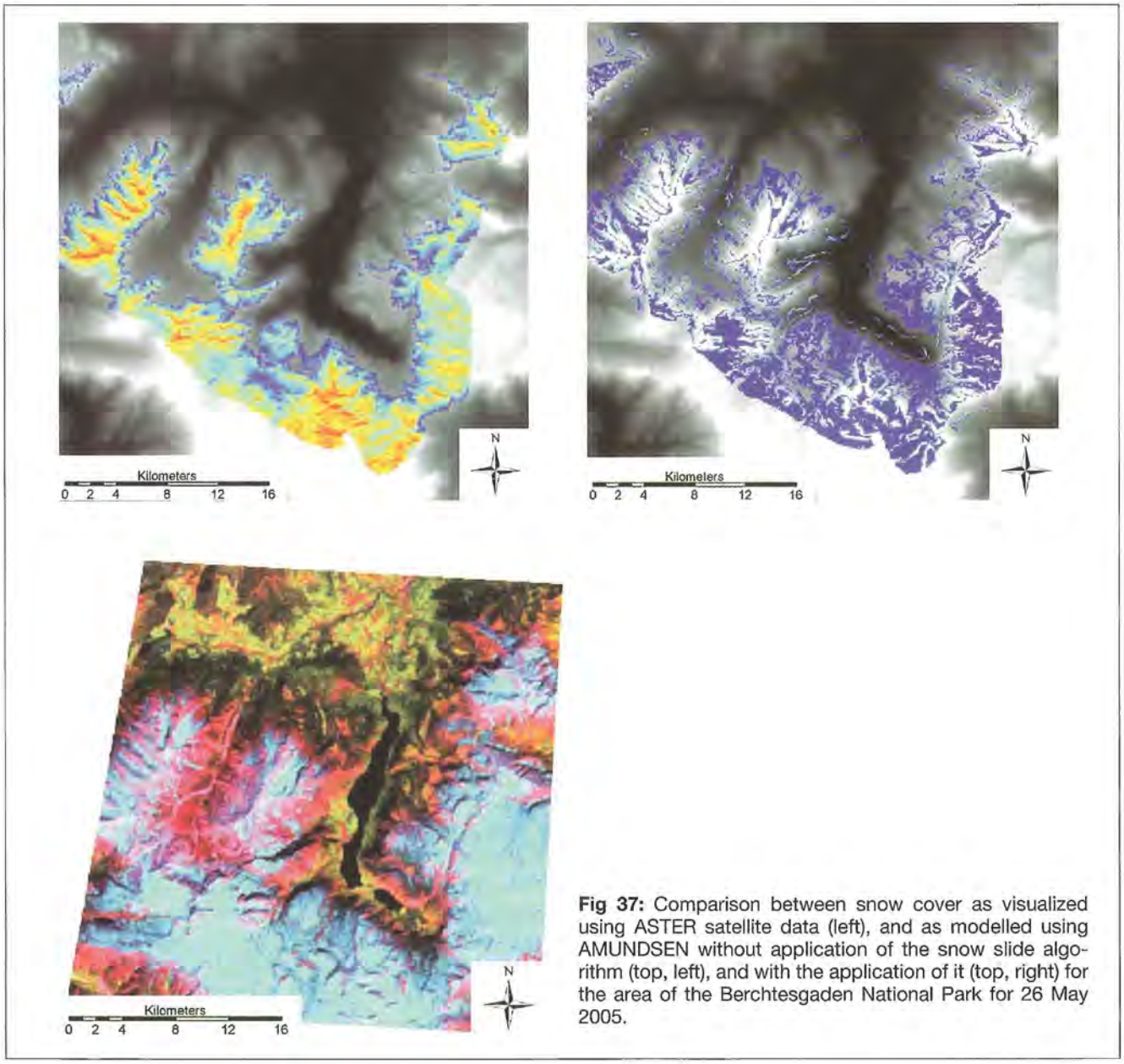

Fig 37: Comparison between snow cover as visualized using ASTER satellite data (left), and as modelled using AMUNDSEN without application of the snow slide algorithm (top, left), and with the application of it (top, right) for the area of the Berchtesgaden National Park for 26 May 2005.

modelled forest canopy processes cannot be validated with this procedure since the forests were already snow–free at the acquisition date (and no appropriate satellite data is available for an earlier date). At least, no snow was left over on or beneath the trees in the model result where in the image data no snow is existent.
The satellite data was acquired for 26 May 2005, corresponding to a time in the melt period when only the upper regions above the treeline were still snow–covered (light blue areas in the image). The general position of the observed snowline coincides well with the one predicted by the model without the snow slides algorithm (upper left in Fig. 37). However, it becomes evident that SWE in this model result is strongly proportional to elevation, clearly visible in the yellow to red areas in the Steinernes Meer (in the South of the park area), and in the ridge structures of Hochkalter and Watzmann mountains. In contrast, the high peaks and ridges are snow–free in the satellite image and remaining snow can be detected in the valley structures stretching from the mountain ridges. Furthermore, at the peaks on the plateau of the Steinernes Meer where the model predicts the highest SWE (Großer Hundstod, Funtenseetauern), only an interrupted, partial snow cover is visible in the satellite image, with some of the underlying limestone rocks completely exposed. This analysis shows that in some parts of the model domain the SWE distribution with elevation is reversed when compared to observations. The removal of snow from the high crests and steep slopes required for a better match between model results and "reality" is accomplished by the snow slide algorithm. In the respective model result (upper right in Fig. 37), the snow cover is much more discontinuous and the peaks on the plateau of the Steinernes Meer are snow–free, as are the ridges stretching from the summits of Hochkalter and Watzmann. In contrast, snow is accumulated in the narrow valleys at the foot of the mountain peaks. This feature is also clearly recognizable in the satellite data (i.e. the far western part of the image). Even a noticeable, large avalanche in the Wimbachtal is reproduced by the model. However, other deposition areas in the modelled image are obviously predicted to be too large, or to stretch down too far into the valleys. Further investigations to fine–tune the snow slide model will be required to address these tendencies.

From the comparison of the images it can be concluded that, in general, the model run that included the snow slide module was able to much better reproduce the snow distribution and the heterogeneous character of the snow cover on the acquisition date. Especially the snow–free summit regions and steep slopes, and the snow–covered valley regions at the foot of the slopes and cirques were simulated more accurately. Future work with respect to model validation by comparing satellite data derived snow cover with simulated ones, will focus on providing a time series of remotely sensed snow cover maps to validate both the spatial as well as the temporal dynamics in the heterogeneity of the simulated snowpack.

11 Alpine snow and climate change - modelling future snow conditions

Alpine mountains are of global importance in providing downstream freshwater, much of it previously stored as snow for several months of the year. This function of a temporal storage of precipitation and its delayed release during melt is one of the key characteristics of a mountain snow cover. In a changing climate, the latter process is assumed to be modified in its temporal dynamics.
Future climate change is generally predicted through the application of *Global Circulation Models* (GCM's) in combination with a given set of boundary conditions, the so–called scenarios. The simulation results are then transferred to the considered (smaller) scale by means of nesting with regional scale climate models and various downscaling techniques. A set of scenarios defining future evolution key factors have been developed in a series of assessment reports by the *Intergovernmental Panel on Climate Change* (IPCC 2007). Consequently, a variety of future global climate predictions exist depending on which model and scenario combination has been used in the simulation. The interpretation of the results is complicated due to the fact that the spatial resolution of the climate predictions is typically not sufficient to be applied in models at a regional or smaller scale, and because the results are highly uncertain particularly in mountainous regions due to the coarse resolution of topography as represented in the climate models.

As an adequate alternative, *stochastic weather generators* can be used to derive time series of future climate evolution if a statistically representative dataset of recorded meteorological variables is available for the domain under investigation. The weather generator proposed in this study belongs to the type of stochastic, non–parametric nearest neighbour resamplers (Yates et al. 2003, Buishand and Brasma 2001, Young 1994). In this procedure, the available historical data is divided into periods which are then statistically re–arranged, with the mean evolution of future temperature following a predetermined trend. This enables the simple and efficient generation of a series of potential future climate conditions which can be used for the subsequent modelling of a potential future snow cover evolution (Strasser et al. 2008a, Mauser et al. 2007, Strasser and Mauser 2006).
In order to investigate the effect of climate change on the snow conditions in the Berchtesgaden National Park area, a baseline scenario is assumed here with a projected global average surface warming of 2.8 °C until the end of the 21st century (mean of 2090–2099 with respect to mean of 1980–1999). This warming trend corresponds to the IPCC A1B scenario (IPCC 2007). A second scenario will be assessed by combining the assumed temperature increase with a shift in precipitation amount from the summer to the winter season, as predicted by several modelling studies that have been carried out for the region of Bavaria (MPI 2007, KLIWA 2007, BayFORKLIM 1996). Analysis will be carried out for a 50 year projection horizon by comparing the periods 2042–2050 and 1998–2006 with respect to (i) the mean seasonal duration of the snow–covered period in the domain, (ii) the mean evolution of the seasonal snow cover at three different local sites, and (iii) the mean annual amount of snowmelt in the domain.

11.1. A stochastic weather generator

With the stochastic weather generator suggested here, projected future climate data is produced with the same temporal resolution as the input data (i.e. as required for input by the snow model). One of the features of the method is, that the physical relations between the meteorological variables are not altered, meaning that the future climate dataset consists of the original recordings which are only re–arranged following a predicted change of temperature and precipitation. The basic assumption of the method is that a climate storyline can be divided into time periods which are characterized by a certain temperature and precipitation, and that these two variables are not independent from each other:

$$P_{tot} = f(T_{mean})$$

with P_{tot} being the total precipitation of a certain time period, P_{mean} its mean temperature and f their functional dependency. In the application here the time periods were chosen to be weeks. A largely similar procedure has already been applied for monthly time periods (Mauser et al. 2007).

In a first step, the typical annual course of the measured meteorological variables is constructed by computing mean temperature and total precipitation for the weekly periods using all years of the historical dataset. The result is a mean annual climate course consisting of 52 weekly periods for the region in which the meteorological stations are located (Fig. 38). Whereas temperature is characterized by a typical seasonal course (warm in summer, cold in winter), the annual course of the weekly precipitation sums is more complex: the local summer maxima (week 5 (early September) and week 50 (mid July), respectively) are separated by generally lower precipitation amounts during the winter. However, the highest maxima of the annual course occur between week 28 (mid February) and week 34 (end of March). As a consequence, there is only a relatively weak relation between temperature and precipitation in this data sample. Potential reasons for the high values of recorded winter precipitation are the following: (i) the reference period 1998–2006 contains the winter 1998–1999, which had a series of extreme snowfalls in February 1999 causing catastrophic avalanche events in the eastern Alps, e.g. in Galtür/Austria, (ii) if the rain gauge is completely covered with snow which later melts and drops into the collector, an „extreme" event is recorded at an unrealistic time, which in reality represents the instantaneous recording of the total sum of precipitation from a certain

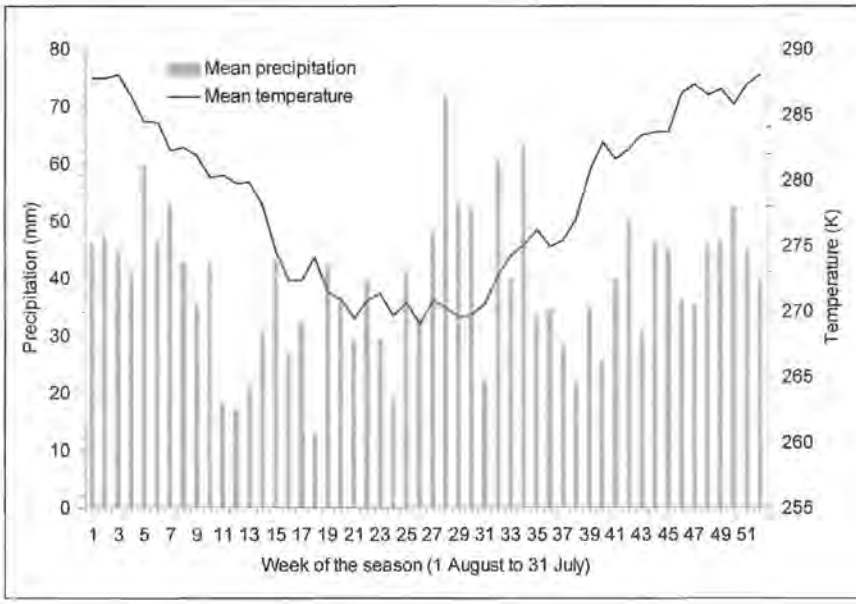

Fig 38: Annual course of mean weekly temperature and precipitation, computed from the recordings of the 11 meteorological stations in the Berchtesgaden National Park area, 1 August 1998 to 31 July 2006.

period before the event, and (iii) in winter the raingauges are frequently not fully functional due to technical failures of the energy supply system.

In the domain considered here, the best equipped and most reliable rain gauges are the ones belonging to the Bavarian Avalanche Warning Service (LWZ) since they were specifically constructed for large snow depths. These gauges are located in the upper regions[20] of the domain. This creates a likely scenario in which the loss of one or more valley stations causes an overestimation of the precipitation average due to the remaining recordings. Reason (i) is a natural phenomenon that can therefore not be corrected. Furthermore, it is very valuable for the scenario generation in terms of including the variability in the recordings for the generation of future climate conditions. Reasons (ii) and (iii) are common difficulties of data recording in mountain regions (see section 1.3.2). With respect to data correction, only simple modifications of implausible values (e.g., negative rainfall or relative humidity of more than 100 %) were performed for the raw data provided by the Bavarian Avalanche Warning Service (LWZ). More sophisticated homogenisation procedures and time series correction are beyond the application considered here. Liston and Elder (2006) describe a system *(MicroMet)* that can be employed to perform such corrections. The data obtained from other sources have been corrected by the respective institutions (Administration of Salzburg and German Weather Service).

The resulting mean annual climate course as illustrated in Fig. 38 is used to construct the future data period by period: firstly, the respective temperature for the weekly period is modified with a random variation factor and the projected trend from the GCM. Then a corresponding precipitation is derived, considering the T_{mean}/P_{tot} relation and, again, a random variation. In the end, the climate of a future week is defined by the so obtained mean temperature and precipitation. In a final step, the period from the historical pool having the most similar temperature and precipitation is selected by applying an *Euclidian nearest neighbour distance measure.* The respective data of the chosen period (air temperature, precipitation, global radiation, relative humidity and wind speed) is then added to the future time series to be constructed. This procedure ensures that the original relationship between temperature and precipitation is preserved in the meteorological time series. It is repeated for all weeks of the year, and all years of the future time series. By modifying the applied random variation, a change in climate variability can be simulated. However, no extremes other than those recorded in the historical data can be reproduced. To allow for more flexibility in the construction of the periods, the basic population from which the measured week is chosen (= the number of weeks available, being equal the number of years for which observational data is available) can be synthetically extended by allowing for one or more weeks before and after the one to be constructed. The principles of the weather generator are illustrated in Fig. 39.

As mentioned, this weather generator is of the stochastic nearest neighbour resampler type. It produces, however, a realistic future climate data series from measurements (and not synthetic weather) for regions with sparse data availability as is the case for the commonly know generators WGEN (Richardson 1981) or LARS-WG (Racksо et al. 1991, Semenov et al. 1998).

The described procedure has a number of specific features. Amongst its advantages is the very efficient applicability: the computation of 50 years of future climate for the 11 stations in the region requires only several minutes on a standard PC. Furthermore, the meteorological input data for the weather generator is physically consistent, as all data were observed in nature. Additionally, the data are in the validated range for the hydrological

[20] http://www.lawinenwarndienst-bayern.de/aktuelle_daten/messstationen/index.php

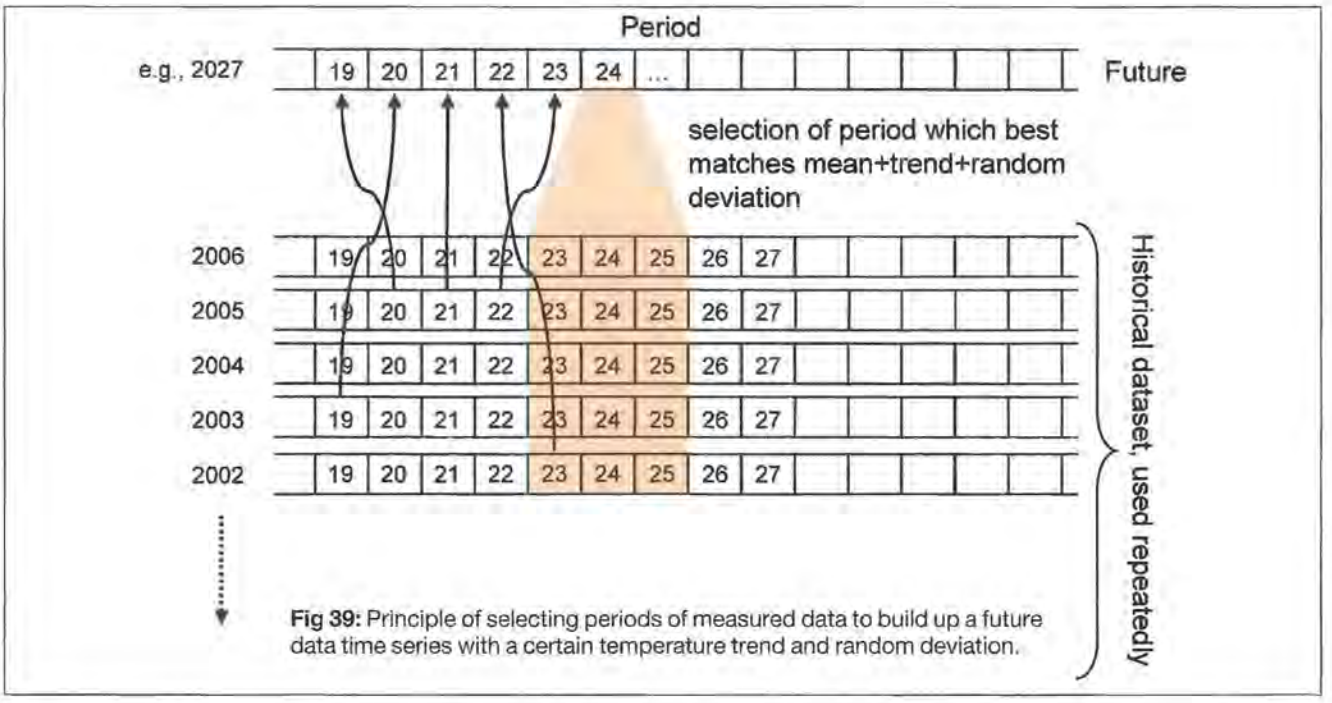

Fig 39: Principle of selecting periods of measured data to build up a future data time series with a certain temperature trend and random deviation.

modelling. A synthetic baseline scenario can easily be constructed by assuming a Zero trend for temperature. Finally, the spatial resolution of the data is preserved as it corresponds exactly to the station locations. However, one significant drawback of the method is that auto-correlation between the single periods is lost and the consideration of changes in the variability of the meteorological variables is limited. Together with the fact that changes in extreme values are not considered it becomes clear that the data resulting from the method cannot be used for modelling variations in probability and extent of hydrological extremes. Furthermore and most crucial, no coupling between the (simulated) characteristics of the land surface, e.g. whether it is snow-covered or not, with the atmosphere is considered, and therefore the important effects of feedback mechanisms are not conserved in the building of the future dataset. This, however, is a drawback that even most physical climate models share.

Consecutive applications of the weather generator produce different climates due to the random deviation which is considered. If this is not desired, the applied random variations can be stored to file and re-used in a consecutive application with modified settings, i.e. to specifically analyze the effects of the selected GCM scenarios.

11.2 Reference period

The reference period for the scenario simulations comprises the time series of data from 1 August 1998 to 31 July 2006 as recorded at the 11 stations situated in the National Park (see Table 1). Missing data (due to a failure in the recording, or simply the fact that the station had not yet been installed at that specific date in the beginning of the reference period) are marked as such with *NaN (Not a Number)* in the dataset. Both, the weather generator as well as AMUNDSEN, treat *NaN* correctly according to the *IEEE standard*[21]. The period comprises 8 winter seasons, including winters with relatively few snow (e.g., 2003/2004) as well very snow-rich winters (e.g., 2005/2006). These eight winter seasons are used for constructing the future climate as well as for comparing the mean modelled snow coverages of the historical and future simulation results. For the latter purpose, AMUNDSEN has been applied for the reference period to produce the spatially distributed mean duration of the snow-covered period for 1998–2006 (Fig. 40). As expected the averaged pattern is similar to that computed for the single winter season 2003/2004 (see Fig. 26). Only the total number of snow-covered days is notably higher as the winter of 2003/2004 was a below that average snow year. The resulting pattern of mean snow coverage duration again clearly shows the effects of elevation (more snowfall and smaller melt rates at higher elevations) and of gravitational snow transport. Locations where snow is entrained and transported show reduced snow cover duration, whereas the snow cover duration can be more than 300 days in areas where transported snow is deposited. As has been elaborated on in section 9.1, the forested and non-forested areas cannot be separated as a distinct line, since accumulation and ablation processes beneath the forest canopy seem to compensate each other. The AMUNDSEN applications using the scenario-dependent future climate datasets will allow the comparison of this pattern with a mean predicted snow cover evolution.

[21] http://standards.ieee.org/

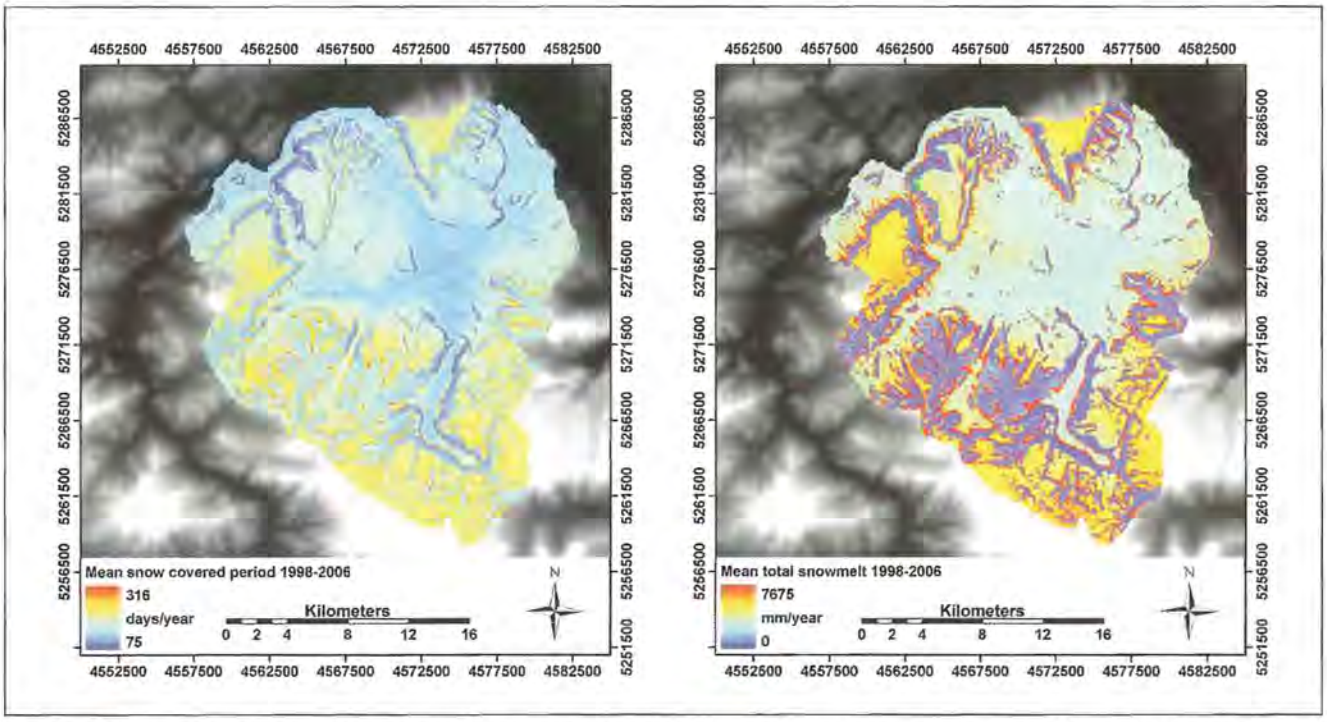

Fig.40: Mean duration of snow-covered period (left) and mean total snowmelt (right) as modelled with AMUNDSEN for the Berchtesgaden National Park area for the winter seasons 1998/1999 to 2005/2006.

11.3 Scenario generation

For this study, the described weather generator was applied to produce time series of hourly air temperature, precipitation, global radiation, relative humidity, and wind speed for the period 1 August 2006 to 31 July 2050. The projecte temperature increase as predicted by the IPCC A1B scenario has an overall slightly concave course. An increase of approximately 1.5 °C is projected until 2050 (IPCC 2007). Two scenarios were produced: one with solely a temperature increase but no modification of precipitation *(scenario I)*, and a second scenario having an identical temperature increase, but including a shift of precipitation from the summer season into the winter *(scenario II)*. For scenario II a linearly increasing amount of mean weekly precipitation, up to a maximum difference of 10 % in 2050, is subtracted from the selection measure of all weeks between May and September and added to it for all weeks between November and April. Consequently, the weather generator selects weeks with more observed precipitation in winter, and weeks with less observed precipitation in summer to build up the scenario II dataset. For reasons of comparability, the same random variations for generating the future data time series have been used for both scenarios (Fig. 41). For the beginning of the future scenario time series, the modification of the selection precipitation can be attributed solely to the random variability, and similar weeks are extracted from the basic population for both the scenarios (samples on the 1:1 lines in Fig. 41). However, as the time series progresses towards the end of the 50 years scenario horizon, the shift of precipitation from summer to winter due to the superimposed trend gets noticeable, and weeks with

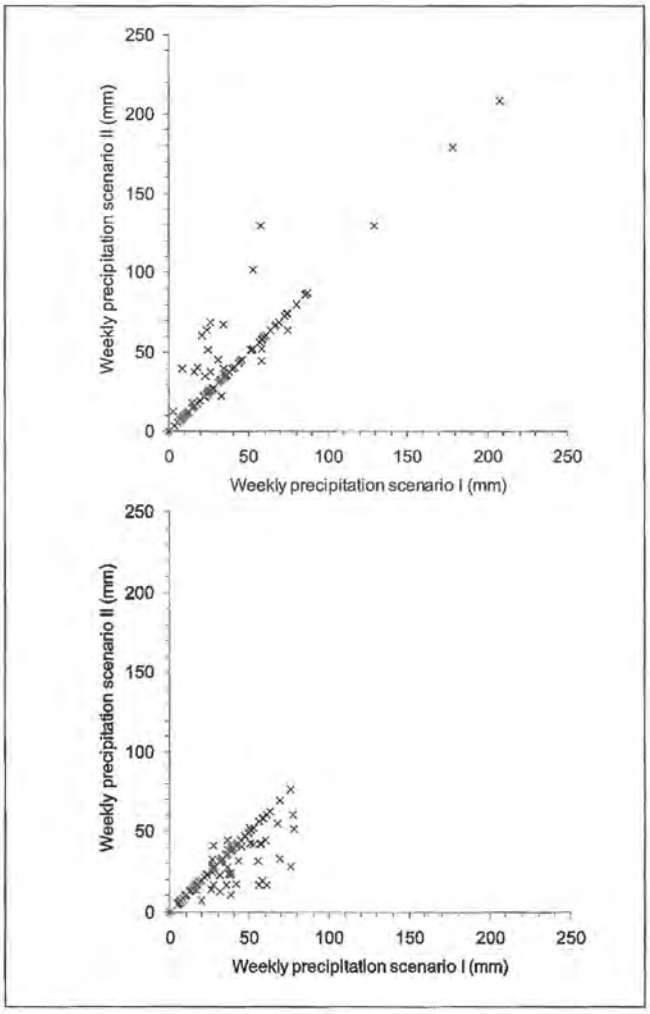

Fig.41: Mean weekly precipitation as selected by the weather generator from the 52 available samples to build up the scenarios I and II for winter (left) and summer (right).

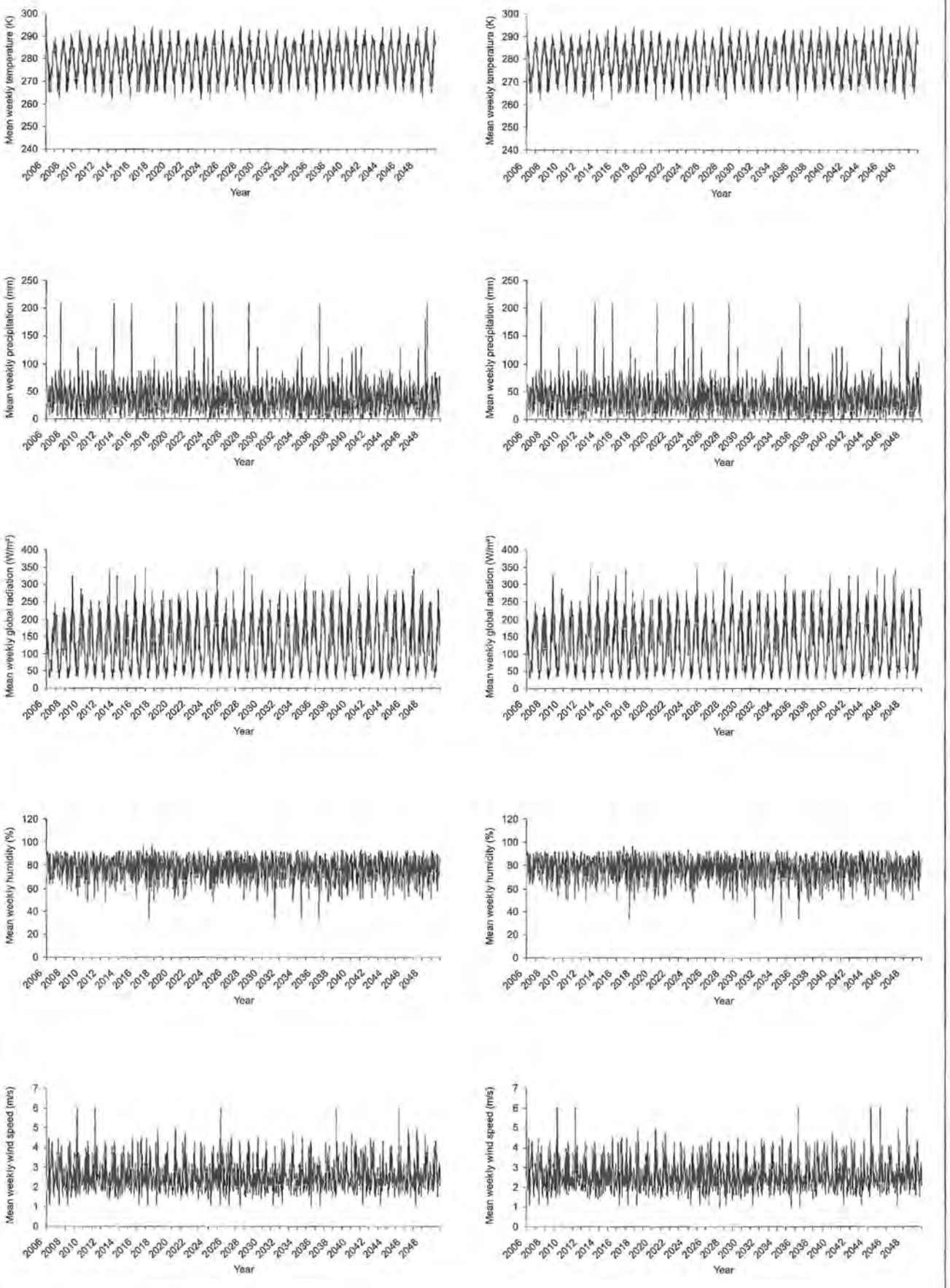

Fig.42: Mean weekly meteorological variables as provided by the weather generator for scenario I (left) and II (right), 2006-2050.

more precipitation are selected in winter (samples above the 1:1 line left in the Figure), while weeks with lower precipitation are selected in summer (samples below the 1:1 line right in the Figure). As an effect of the inclusion of a random variability, the general increase/decrease of precipitation in the future dataset is also characterized with a certain variability, reflecting the characteristics in the change of the natural climate system.

The five high weekly precipitation totals of more than 100 mm in winter (Fig. 41, left) are most likely due to the fact, that the gauges can be completely covered with snow which later drops into the collector and causes an „extreme" event. Such occurrences are left unmodified in the data, since their effect on the long-term simulations of the snow cover as conducted here is likely small.

Applying the weather generator with the described settings results in the two future data time series, illustrated in Fig. 42. The Figure shows the entire course of temperature, precipitation, global radiation, relative humidity, and wind speed as predicted for scenario I and II conditions, respectively, as weekly averages for 2006–2050. The random variations generated by the algorithm for scenario I has been stored to file and was re-used for the creation of scenario II to produce two future meteorological data time series which differ only due to a given seasonal precipitation shift.

There are only few detectable differences between the two scenario datasets (Fig. 42). However, due to enhanced winter precipitation some winter precipitation maxima can be found in scenario II which are missing in scenario I (in 2015, 2018 and 2026). In contrast, the local maximum of precipitation in 2039 in scenario I, not represented in scenario II, occurs during the summer season (August). This again is the result of the given seasonal shift in precipitation timing from summer to winter in scenario II. Another noticeable difference can be seen for summer global radiation. In scenario II, the lower precipitation amounts in summer are accompanied by higher mean weekly global radiation, due to the more frequent sunshine situations (such local maxima can be detected in 2015, 2045, 2046, and 2049). Accordingly, summer mean weekly humidity in scenario II slightly decreased (visible e.g. in 2029). High mean weekly wind speeds can be detected occurring only in scenario I (in 2025), but also occurring solely in scenario II (in 2044 and 2048), with all these phenomen happening during December.

Different strategies exist to discuss the effective mean changes of future climate data series. A numerical trend analysis may be performed (Strasser and Mauser 2006, Mauser et al. 2007), answering the question whether the data follows a linear or any other trend. Depending on the variability inherent in the recorded historical dataset, the projected course of the future data differs sooner or later from what a linear trend would suggest, and consequently, the trend analysis results depend on the temporal extent of the future climate scenario.

Another suitable method to analyze the change in the future climate data is a comparison of averages between the reference and the scenario periods. For that purpose, the annual and seasonal (winter and summer) means of the meteorological variables, temperature, precipitation, relative humidity, global radiation, and wind speed are computed for the period 2042–2050 (for both scenarios) and compared to the respective means of these variables for the reference period 1998–2006, providing a quantification of the effective change of the meteorological conditions affecting the mean evolution of the snow cover today and in the future. The mean characteristic meteorological values for the reference period (1998–2006) are listed in Table 5, with the corresponding numbers for scenarios I and II listed in Table 6 and Table 7, respectively.

Table 5: Mean characteristic meteorological variables for the reference period (1998-2006).

Meteorological variable	Annual mean	Winter mean	Summer mean
Temperature (K)	278.5	272.7	284.3
Precipitation (mm)	2037.0	980.4	1056.6
Relative humidity (%)	77.3	76.1	78.5
Global radiation ($W \cdot m^2$)	138.0	93.8	182.2
Wind speed ($m \cdot s^{-2}$)	2.6	2.7	2.4

Table 6: Mean characteristic meteorological variables for scenario I (2042-2050).

Meteorological variable	Annual mean	Winter mean	Summer mean
Temperature (K)	279.5	273.6	285.5
Precipitation (mm)	1907.4	1000.2	906.1
Relative humidity (%)	76.7	76.8	76.6
Global radiation ($W \cdot m^2$)	141.7	94.7	189.8
Wind speed ($m \cdot s^{-2}$)	2.6	2.8	2.4

Table 7: Mean characteristic meteorological variables for scenario II (2042-2050).

Meteorological variable	Annual mean	Winter mean	Summer mean
Temperature (K)	279.5	273.5	285.5
Precipitation (mm)	1859.0	1052.0	804.4
Relative humidity (%)	76.4	77.3	75.6
Global radiation ($W \cdot m^2$)	144.4	94.1	195.8
Wind speed ($m \cdot s^{-2}$)	2.6	2.9	2.4

For both scenarios I and II, the resulting mean change of annual temperature until 2050 is +1 K, with the increase being larger in summer (+1.2 K) than in winter (+0.9 and +0.8 K). This difference originates from the intrinsic variability of the measured data available.
For both scenarios, mean annual precipitation decreases (–129.6 and –178.0 mm, respectively), due to the generally increasing temperature and related more frequent sunny high pressure situations.

However, the picture is different for the seasonal course of precipitation: whereas summer precipitation is considerably decreased (–150.5 and –252.2 mm), winter precipitation increases in both scenarios (+19.8 and + 71.6 mm). The increased winter precipitation can be explained by the fact that most snowfalls occur at temperatures around the freezing point. For high mountain regions, these temperatures are higher temperatures than the winter average. Therefore, a projected increase in temperature will make these conditions more likely in resulting in a shift of seasonal precipitation from summer to winter even in scenario I, although only temperature has been altered for its generation. Mean annual relative humidity is decreased in both scenarios (–0.6 and –0.9 %), whereby again, the decrease is caused by the seasonal mean for summer (–1.9 and –2.9 %). For winter the mean relative humidity actually increases slightly (+0.7 and +1.2 %). The changes again are attributable to the more frequent clear sky situations in summer and more precipitation events in winter. Mean annual global radiation is generally increased (+3.7 and +6.4 $W \cdot m^{-2}$), considerably for summer (+7.6 and +13.6 $W \cdot m^{-2}$) and modestly for winter (+0.9 and +0.3 $W \cdot m^{-2}$). Finally, mean annual wind speed is increased slightly during winter for both scenarios due to the more frequent precipitation events.

This data was subsequently used to simulate the mean annual snow cover evolution for 2042–2050 for both scenarios I and II. All snow in the domain considered here is assumed to melt during spring and summer, and hence the simulated snow storage is built up every winter independently from the previous one. Therefore it is not necessary to continuously model the future scenario for all years. Identical results for the analysis period are obtained if the years are modelled individually, remarkably improving processing speed in the present application. The results are discussed in the next section.

11.4 Future seasonal snow cover model results

11.4.1 Mean future seasonal snow cover duration

As a first indicator for the effect of a changing climate on the simulated snow cover, the mean future seasonal snow cover duration was analyzed. For this purpose, the obtained continuous hourly climate datasets for the reference period 1998–2006 and the period 2042–2050 for scenarios I and II have been used to compute the three sets of seasonal snow cover evolution, and averages for the annual duration of the snow cover (e.g., number of days with snow on the ground) were derived. The results are spatially distributed and covering the entire area of the National Park.
Generally, the spatial pattern of the modelled mean annual duration of the snow-covered period for 2042–2050 under scenario I conditions is similar to the one for the reference period (see Fig. 40), i.e. more snowfall and smaller melt rates in higher elevations, and a clearly visible effect of gravitational snow transport. Where snow is entrained and transported, the snow cover duration is reduced, while where transported snow is deposited, the snow cover duration is relatively long, even though the maximum snow cover duration being 15 days shorter than for the reference period. Again, forested and non-forested areas cannot be separated as a sharp line since accumulation and ablation processes beneath the forest canopy obviously compensate for each other leading to similar snow cover duration values than in the adjacent non-forested areas.
The map of the mean annual differences in the duration of the snow-covered period between 2042–2050 under scenario I conditions and the reference period 1998–2006 is characterized by a complex pattern (Fig. 43, right). The following structures can be detected: (i) a general decrease in the duration of the snow-covered period in the valley regions from NE towards SW, (ii) a separation of the forested areas (significant decrease in the number of snow days) from non-forested areas (moderate decrease in the number of snow days), (iii) the maximum reduction of the period of snow coverage can be seen in the snow slide deposition zones, and (iv) a moderate increase in the number of snow days in areas where snow is entrained and gravitationally transported by means of the snow slide model.
As has been pointed out in the previous section, scenario I is characterized by a moderate increase of winter

temperature (+0.9 K in the average), accompanied by a related increase in winter precipitation (+19.8 mm in the average). A warming in combination with an increased precipitation can have different effects on to the energy- and resulting mass balance of the modelled snow cover, leading to either a prolongation of the snow-covered period (at locations where more precipitation now falls as snow), or a shortening of the period (in areas where more precipitation now falls as rain). Additional, very crucial effects in that respect are the protection against melt through the high albedo of new snow, and an enhanced turbulent mixing during storms with associated rainfalls.

The complex pattern in the change of the number of snow days from NE towards SW is the result of a combination of these processes. On the plateau of the Untersberg in the very North of the domain, the warming and increased precipitation in winter compensate for each other (change in the duration of the snow-covered period ≈ Zero), whereas on the plateau of the Reiter Alm (in the same elevation), the change equals approximately -14 days (non-forested areas) to -18 days (forested areas). The yellow-reddish coloring for the valleys corresponds to -10 days, approximately.

In the forested areas, the reduction of the snow-covered period, generally, amounts to around 20 days. The sublimation of previously intercepted snow in the canopy is an efficient process remarkably reducing the duration of the period of snow coverage beneath the canopy. This process is strongly dependent on radiation input, and therefore considerably more efficient during the changed climate. A maximum reduction of the snow-covered period (35 days) can be detected in the snow slide deposition zones. Here, the effect of additional winter precipitation is compensated most efficiently by the higher temperature, additional increase of global radiation (+7.6 W · m^{-2}), and reduced relative humidity (-1.9 %) during summer (see Table 5 and Table 6), all supporting a more efficient melting process.

Finally, the duration of the snow-covered period is moderately increased in the steep zones of entrainment and gravitational transport of snow. Whereas in other regions the mass balance of the snow cover is controlled by precipitation input and the energy balance, it is mainly forced by precipitation input and consecutive gravitational removal of snow in the transport zones. As a consequence, snow is efficiently removed after each snowfall event, and the remaining snow layer quickly becomes thin enough (see Fig. 19) to completely melt out the next time the energy balance becomes positive, even in mid winter. The absolute number of snow days in the transport zones is considerably smaller than in non-transport zones of the same elevation, clearly visible at the mountain ridges. Consequently, an increase in winter precipitation (mostly snowfall at these elevations) results in more days with snow coverage.

Next, the mean annual duration of the snow-covered period for 2042-2050 under scenario II conditions is considered (Fig. 44). The resulting pattern looks fairly similar to the one derived for scenario I conditions. However, since precipitation in winter is increased even further in this scenario, and obviously most of this precipitation falls as snow, the decrease in the duration of the snow-covered period is generally less than for scenario I (legend of Fig. 44 (right)). This analysis indicates that increased winter precipitation compensates to a certain degree for a general warming trend. The extent of this effect can be further analyzed by subtracting the map of

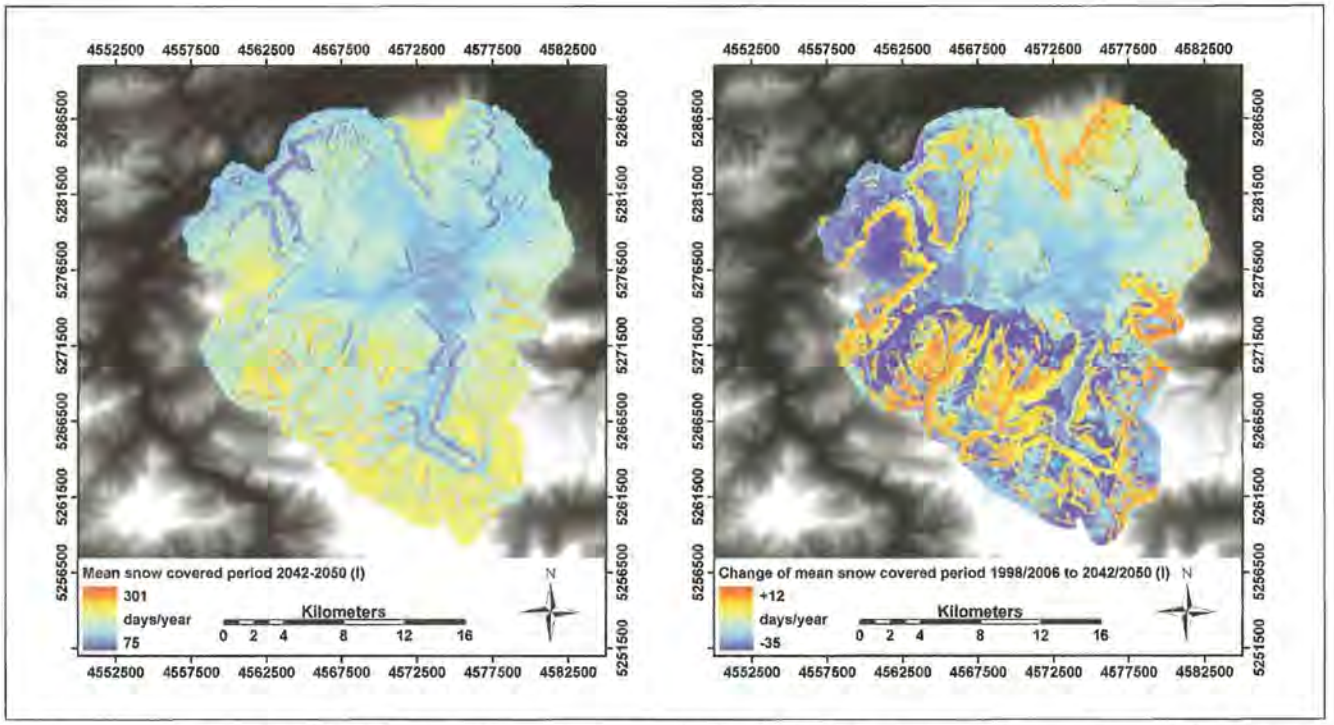

Fig.43: Left: mean annual modelled duration of snow-covered period for 2042-2050 under scenario I conditions. Right: Mean annual difference in the duration of the snow-covered period between 2042-2050 under scenario I conditions and the reference period 1998-2006.

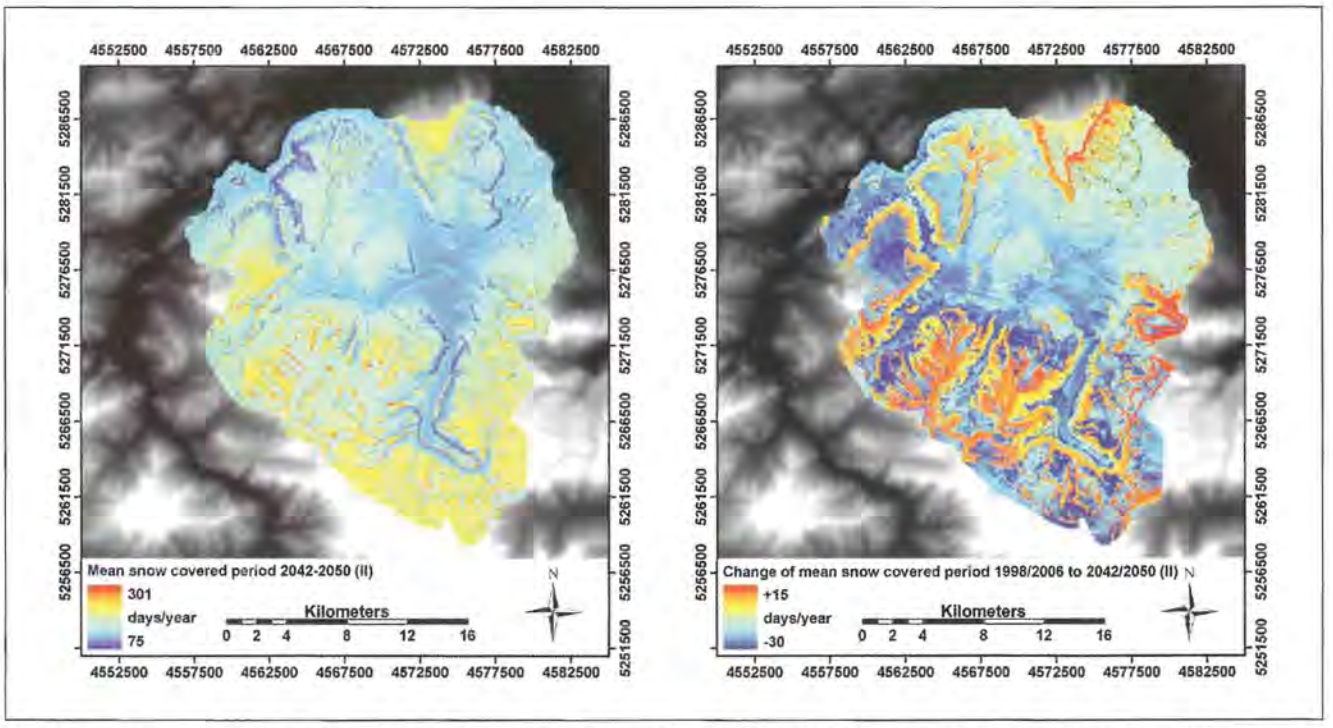

Fig.44: Left: Mean annual duration of the snow-covered period for 2042-2050 under scenario II conditions. Right: Mean annual difference in the duration of the snow-covered period between 2042-2050 under scenario II conditions and the reference period 1998-2006.

the mean annual duration of the snow–covered period obtained for scenario I from the one obtained for scenario II (Fig. 45).

In most areas, the snow–covered period is longer for scenario II due to the increased snow precipitation in winter. The effect is especially visible in the sharply delineated forested areas where the additional snowfall events remarkably increase the duration of the ground snow cover beneath the trees, more than they do in the open areas.

A reduction of mean annual duration of the snow–covered period in scenario II compared to scenario I can be detected in the accumulation zones of the gravitational snow slides (blue areas in Fig. 45). Here, the effect of additionally accumulated snow is compensated for by the increased energy available for melt during late spring and summer under scenario II conditions (see Table 6 and Table 7). Since the snow in these zones remains until summer, its duration is mainly regulated by the energy supply available for melt during the summer.

For the distributed patterns of snow cover duration it can be concluded from the simulations, that a general warming will lead to shorter snow–covered period, the effect being most pronounced in forested areas. On steep rock faces, snow might remain longer due to the more frequent precipitation events (with precipitation still falling as snow). If precipitation increases in winter, the increased air temperatures will be compensated for to a certain extent, and again the forested areas react most sensitive to the change.

The snow cover duration in the snow slide accumulation zones seems to depend more on the melt energy supply rather than on accumulation amount.

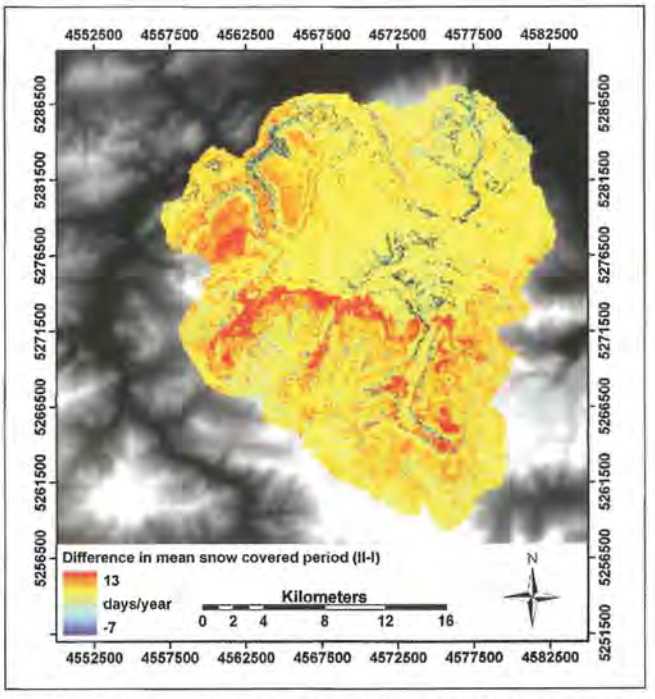

Fig. 45: Difference of mean annual duration of the snow-covered period for 2042-2050 between scenario I and II.

11.4.2 Mean future seasonal snow cover evolution

In the following, the mean annual durations of the snow–covered period are investigated for the valley site Schönau (617 m a.s.l.), for the subalpine site Kühroint (1407 m a.s.l.) and for the high alpine site Funtenseetau-

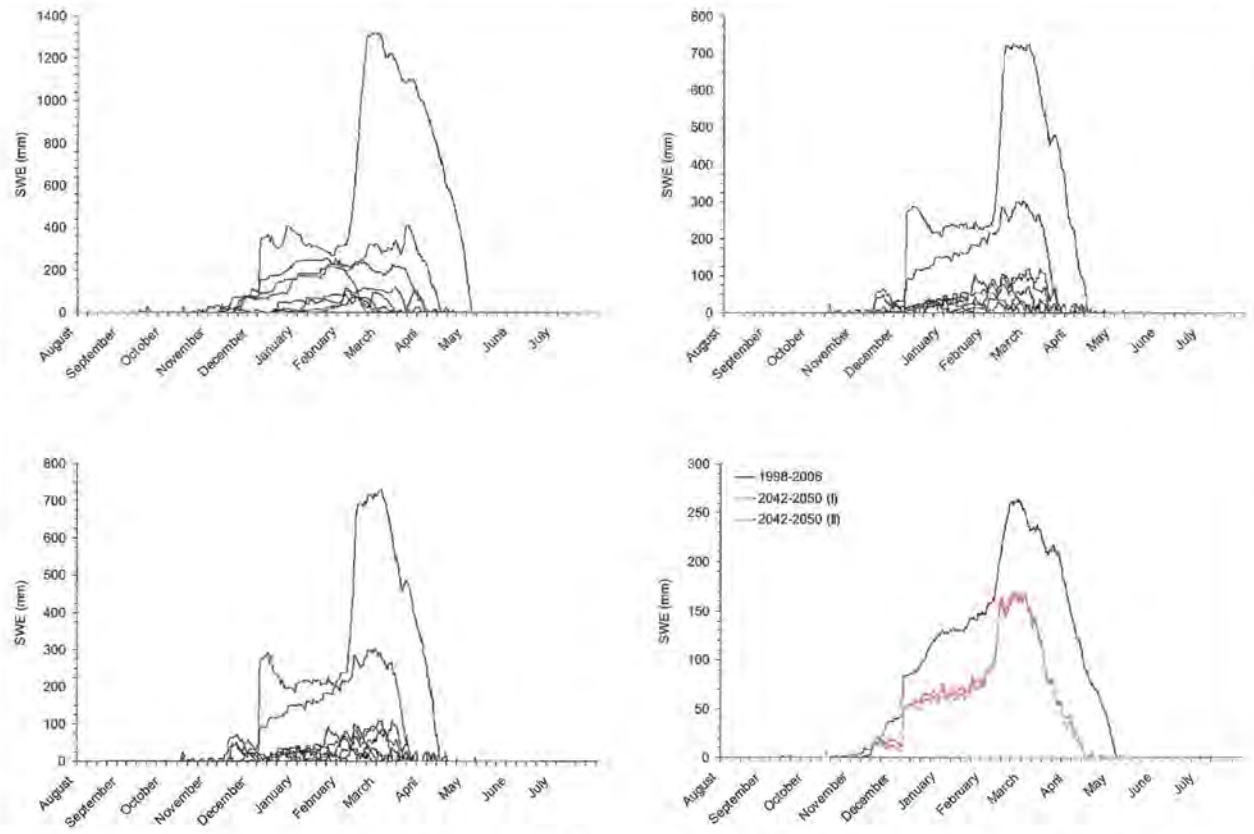

Fig. 46: Seasonal snow cover evolution for a valley site at Schönau (628 m a.s.l.) for the winter seasons 1998-2006 (reference period, top left), 2042-2050 (scenario I, top right) and 2042-2050 (scenario II, bottom left). Bottom right: Comparison of the respective mean snow cover evolution for the periods.

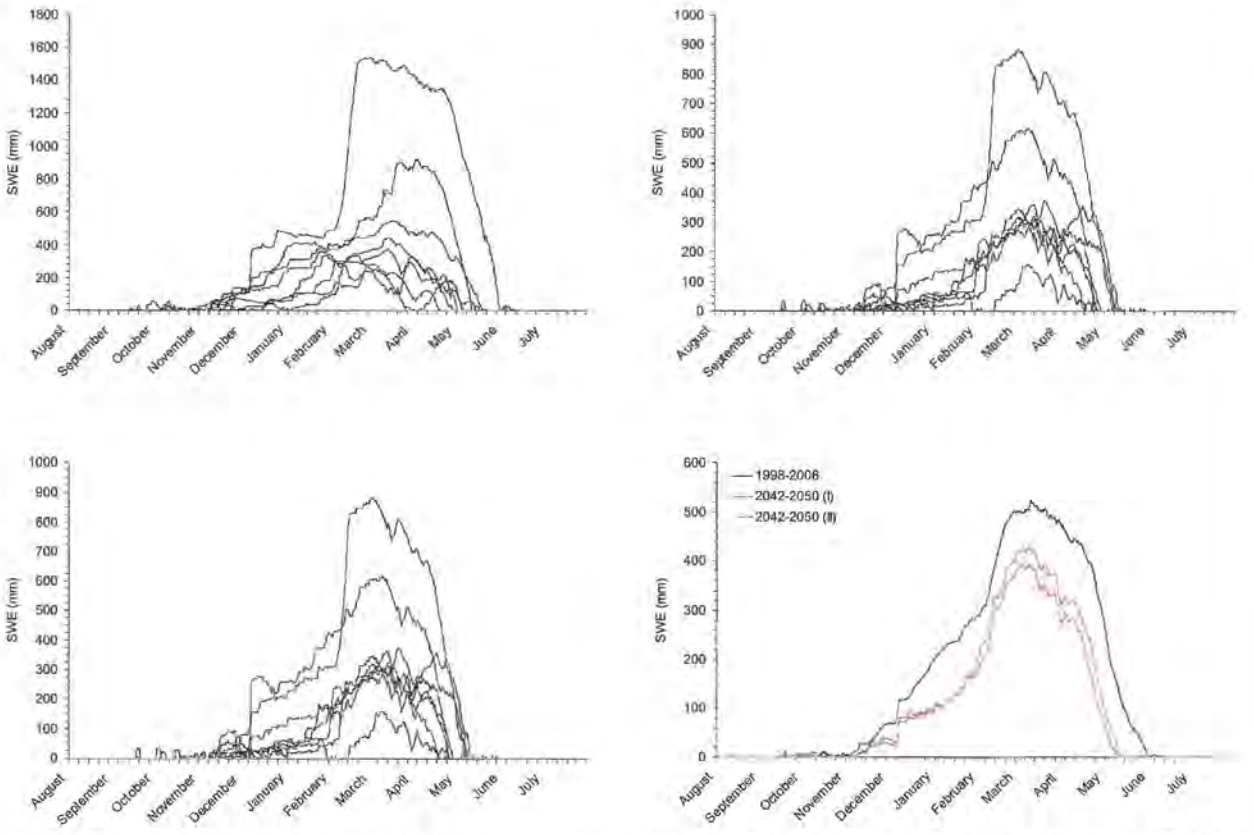

Fig. 47: Seasonal snow cover evolution for a subalpine site at Kühroint (1404 m a.s.l.) for the winter seasons 1998-2006 (reference period, top left), 2042-2050 (scenario I,top right) and 2042-2050 (scenario II, bottom left). Bottom right: Comparison of the respective mean snow cover evolution for the periods.

ern (2445 m a.s.l.). The results will be analyzed as a further indicator for the effects of a changing climate on the snow cover.

Schönau is an undisturbed valley site characterized by a very variable snow cover from season to season (Fig. 46), the avalanche winter of 1998/1999 being a remarkable example of a season with an extraordinary thick and long lasting snow cover (the significant increase of SWE visible in the Figure occurred in February 1999).

Both scenarios are relatively similar with respect to both shape and depth of the simulated SWE courses, with only the maximum extent being lower than in the reference period (Fig. 46, bottom right). At Schönau, the mean snow cover duration is 127 days for 1998–2006 (Table 8). For scenario I, this duration is reduced by nine days, whereas for scenario II the reduction is only seven days. The difference of two days can be attributed to the additional snowfall precipitation in scenario II. As indicated in Fig. 46 (bottom right), reductions of the snow-covered period occur at the end of the melt period in spring.

For Kühroint, a subalpine site without gravitational snow transport, a similar illustration can be deduced (Fig. 47). The variability of the annual snow cover evolution for the reference period is moderately less than in the valley, mostly due to the lower temperatures and consequently less frequent melt conditions in this elevation range during winter. The February 1999 snowfall event is again significant, but less different from the other seasons. Again, for both scenarios the mean seasonal courses are very similar with the main reduction of the snow-covered period occurring at the end of the melt period in spring (Fig. 47, bottom right). Compared to the reference period, the mean annual snow-covered period is seven days shorter in scenario I conditions, two of which are compensated for if precipitation is increased as in scenario II.

Finally, Funtenseetauern is a site where snow is frequently entrained and removed, e.g. slides down from the slopes around the summit onto the surrounding areas. In Fig. 48, the frequent alterations between snow coverage and periods when snow is removed in the modelling become evident. Consequently, at this location both maximum SWE is less and mean snow cover duration is shorter than at Kühroint, even though the snowfall amount is higher (see Fig. 26). For both future scenarios, modelled SWE is less than for the seasons in the reference period, but differences are much smaller than for Kühroint or Schönau. On the high mountain, snowfalls can occur even in summer and the build-up of the winter snow cover depends more on accumulation than on melt. Therefore, under scenario I conditions the mean duration of the snow cover at Funtenseetauern is increased by six days. For scenario II, the effect of more frequent snowfalls becomes even more evident, resulting in a snow cover period that is nine days longer.

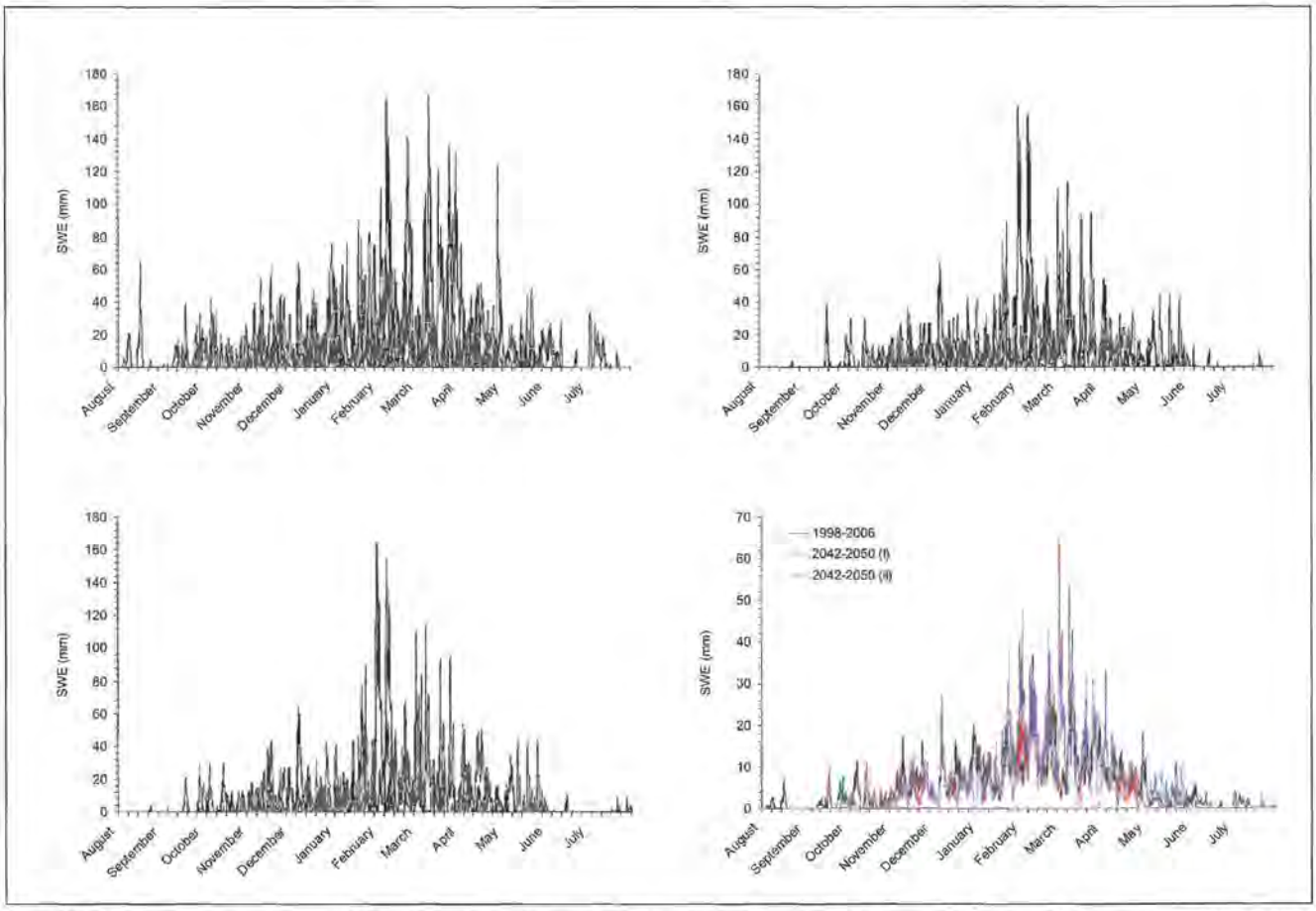

Fig. 48: Seasonal snow cover evolution for a high alpine site on Funtenseetauern (2340 m a.s.l.) for the winter seasons 1998-2006 (reference period, top left), 2042-2050 (scenario I, top right) and 2042-2050 (scenario II, bottom left). Bottom right: Comparison of the respective mean snow cover evolution for the periods.

Table 8: Mean annual duration of the snow-covered period (in days) for a valley site (Schönau), a subalpine site (Kühroint) and a high alpine site (Funtenseetauern) in the Berchtesgaden National Park for the reference period 1998-2006 and the future period 2042-2050 for conditions of scenario I and II, respectively. Elevations are derived from the DEM and therefore slightly differ from the actual ones of the station locations (see Table 1).

Model location	Reference period (1998–2006)	Scenario I (2042–2050)	Scenario II (2042–2050)
Schönau (628 m a.s.l.) E4574000 N5275600	127	118	120
Kühroint (1404 m a.s.l.) E4572300 N5270650	188	181	183
Funtenseetauern (2340 m a.s.l.) E4572950 N5261750	153	159	162

For the point scale simulations and their inter-seasonal differences it can be concluded that the variability decreases with elevation and in the warmer conditions in the future climate scenarios.

The maximum SWE mainly decreases in the valleys. Generally, the snow cover duration in areas where snow is entrained and gravitationally removed is shorter than in flat regions. It is, however, predicted to increase under both future climate scenarios due to the more frequent snowfall events. Apart from the mean future seasonal duration and the mean future seasonal evolution of the modelled snow cover, the amount of snowmelt which is supplied as meltwater to the streamflow system is utilized in the following as a third indicator for the effect of a changing climate on the snow cover conditions. The scheme to analyze the simulation results remains the same.

11.4.3. Mean future seasonal snowmelt

The amount of snow that melts and contributes to runoff is computed for each time step with the water balance equation (eq. (73)), and the results are aggregated in AMUNDSEN for each annual season to provide a picture of the corresponding spatial distribution. In Fig. 49, the mean seasonal snowmelt for the period 2042–2050 under scenario I conditions is illustrated, as well as the resulting difference compared to the reference period.

Where the evolution of the snow cover is not disturbed by lateral transport, the snowmelt amount increases with elevation, with the maxima occurring on the flat areas of the highest plateaus of Steinernes Meer (yellow areas). Including the lateral transport processes shifts the areas of absolute maximum snowmelt to areas, where the snow slides accumulate and deposit masses

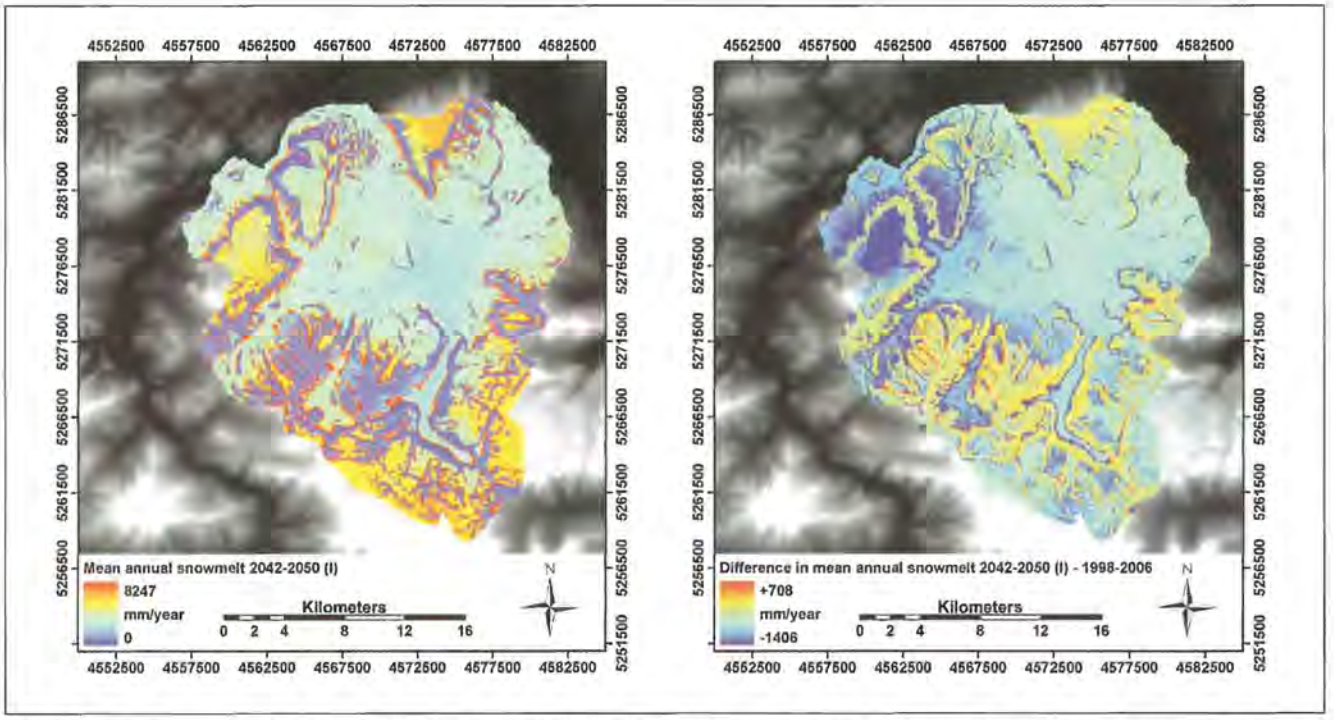

Fig.49: Left: Mean annual snowmelt for the period 2042-2050 under scenario I conditions. Right: Mean annual difference of snowmelt between 2042-2050 under scenario I conditions and the reference period 1998-2006.

of snow from the upper regions (red coloring). Areas with entrainment and removal of snow by gravitational slides are areas of minimum snowmelt (blue areas). This distribution is typical and similar to what has been computed for the single season 2003/2004 (see Fig. 32).

With respect to the difference between snowmelt in scenario I conditions and the reference period the following can be derived from Fig. 49. In warmer conditions, mean annual snowmelt is less in the forested areas of the mountain slopes and on the plateaus (blue areas), but remains similar to historical conditions on plateaus without forests (Untersberg and Steinernes Meer, yellow coloring) and in steep snow slide areas. Maxima of increased mean annual snowmelt can be located in the snow accumulation zones of the slides (red coloring). In the flat valley regions, the mean total amount of snowmelt is moderately reduced (light blue areas).

For scenario II conditions, the map of mean annual snowmelt is very similar to the one obtained for scenario I (Fig. 50). The increased amounts of precipitation falling as snow and therefore available for melt, become most clearly visible in the higher maximum of snowmelt from regions of snow accumulation by snow slide deposition (red areas, 8247 and 8370 mm · year^{-1} for scenario I and II respectively). The map of the difference in mean annual snowmelt between scenario II conditions and the reference period is similar to what was stated for scenario I. Only the reduction of snowmelt at the ground of the forest canopies is less significant under scenario II conditions. The warmer inside–canopy temperatures and their effect on the snow cover at the ground has been

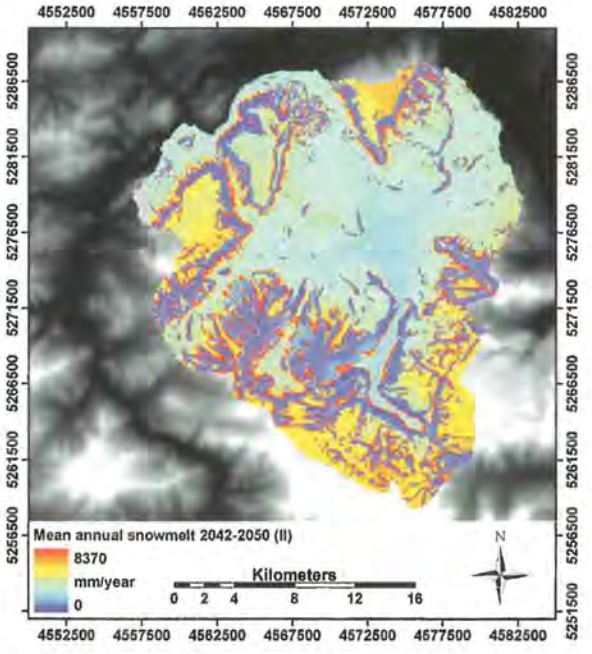

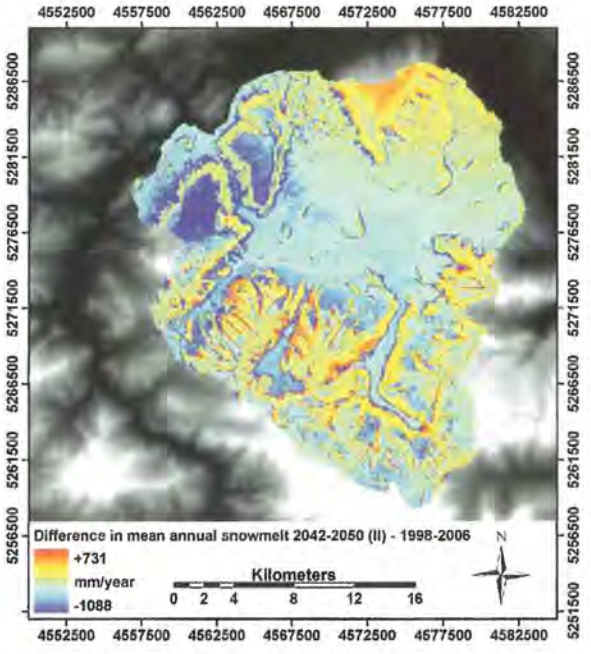

Fig. 50: Left: Mean annual snowmelt for the period 2042-2050 under scenario II conditions. Right: Mean annual difference of snowmelt between 2042-2050 under scenario II conditions and the reference period 1998-2006.

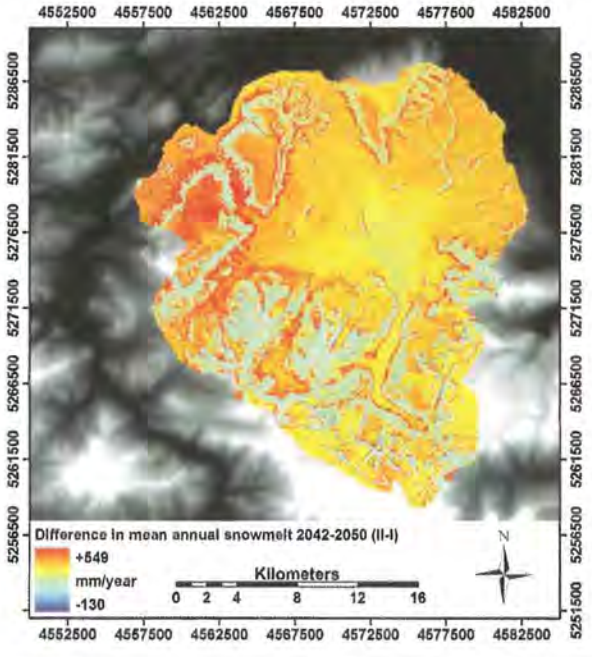

Fig. 51: Difference of mean annual snowmelt for 2042-2050 between scenario I and II.

largely compensated for by additional snowfall precipitation. According to the model results as described here, the canopy is the land surface type which reacts most sensitive to a warmer climate and a changing precipitation regime.

In Fig. 51, the simulated total annual snowmelt amounts for the two scenario simulations are subtracted from each other. Forest canopies become again visible as areas with considerable more snow available and melting in scenario II conditions, together with the snow slide accumulation zones (red areas). The yellow areas in the valleys are characterized by moderately increased total annual snowmelt amount in scenario II conditions, compared to scenario I conditions. Changes are very small in the steep slopes where snow is entrained and laterally removed.

Finally, some artefacts occur in some pixels close to the areas of maximum difference between scenario I and II (red areas) where accumulated snow remains all summer and is not melted by the end of July (small dark blue areas). In these locations, the mean annual snowmelt is smaller in scenario II than in scenario I, but only because the melt process is not finished in July in the modelling. Such effects can occur in the small areas where the DEM has sinks which lead to unrealistically high local accumulation of snow that has previously slid off adjacent slopes. This could be eliminated by either respective correction of the DEM, or by adding deposited snow to terrain elevation (and hence filling the sinks), causing subsequent snow slides to pass a completely filled sink.

However, the detailled modelling of such processes is probably only appropriate at finer scales.

Next, mean hourly melt rates for the eight seasons are discussed at the point scale for the three locations Schönau, Kühroint, and Funtenseetauern (Fig. 52). Firstly, it it has to be noted that the mean hourly melt rates are in the range of up to two mm · h^{-1} (Schönau and Kühroint), and up to 1 mm · h^{-1} (Funtenseetauern), considerably less than the maximum hourly melt rate which can occur on clear sky radiation days (which can be in the range of 7–8 mm · h^{-1}). This reduction is due to the averaging over the eight seasons. Secondly, while the melt rates at Kühroint compared to Schönau are less in the early winter, they are higher in spring in Kühroint despite its higher elevation. This can be explained by the fact that, in the higher elevation, early winter is generally colder, but more snow is available for snowmelt in spring leading to a melt period that extends further into the late spring early summer period.

The main difference between the reference period and the future scenario melt rates is the earlier end of the melt period in the future in May and June, respectively. This corresponds to what has been elaborated on for the mean future snow cover duration in the previous section. At Funtenseetauern, snowmelt rates are generally lower because of the limited energy available. Furthermore, no thick snowpack is built up there due to the continuous gravitational removal of freshly fallen snow. As a result, low snowmelt rates can occur in that summit loction throughout the year from August to July.

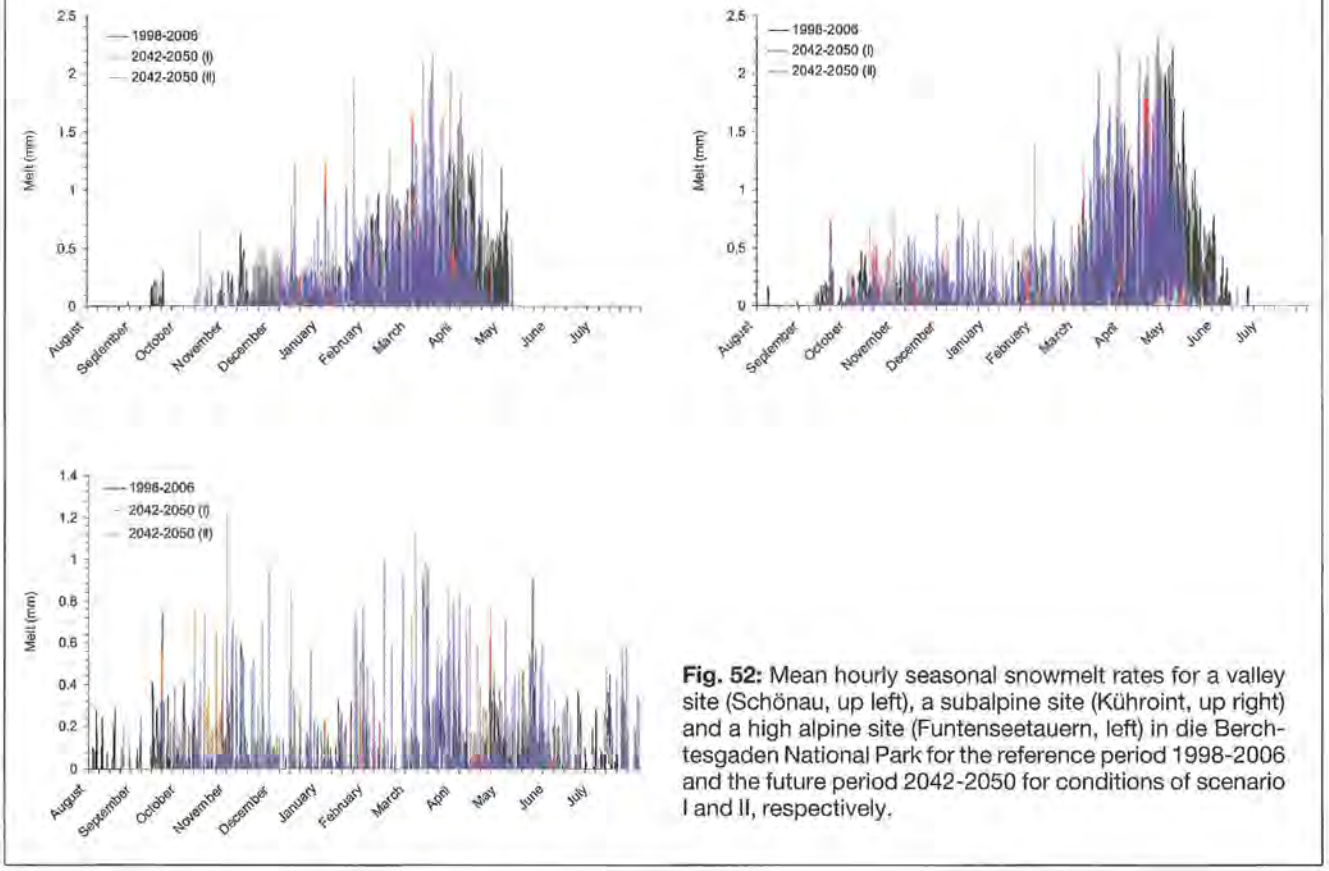

Fig. 52: Mean hourly seasonal snowmelt rates for a valley site (Schönau, up left), a subalpine site (Kühroint, up right) and a high alpine site (Funtenseetauern, left) in die Berchtesgaden National Park for the reference period 1998-2006 and the future period 2042-2050 for conditions of scenario I and II, respectively.

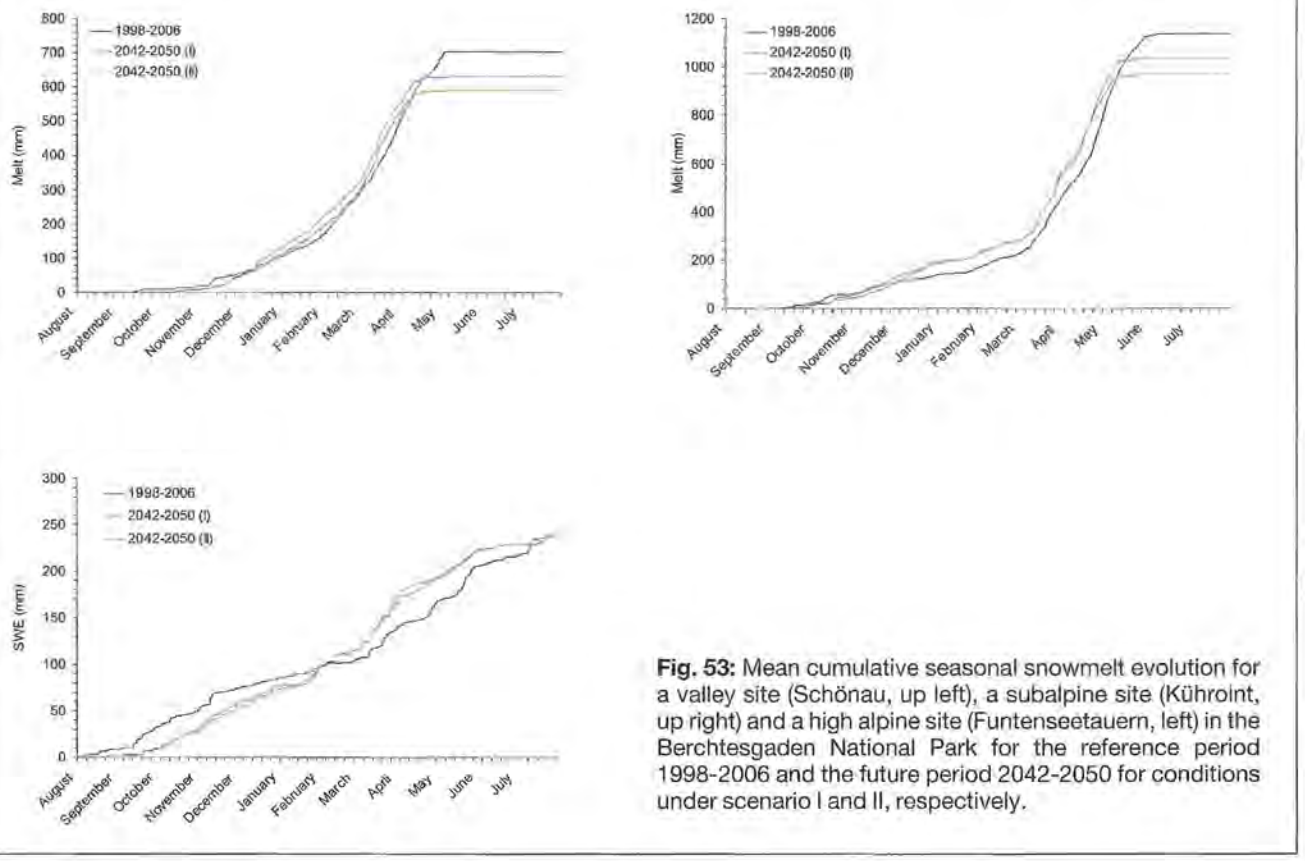

Fig. 53: Mean cumulative seasonal snowmelt evolution for a valley site (Schönau, up left), a subalpine site (Kühroint, up right) and a high alpine site (Funtenseetauern, left) in the Berchtesgaden National Park for the reference period 1998-2006 and the future period 2042-2050 for conditions under scenario I and II, respectively.

The mean cumulative seasonal snowmelt evolution for the three local sites is discussed in the following section by analyzing the mean accumulated melt for the reference period, as well as for the two future scenario periods (Fig. 53).

At Schönau, the accumulated mean annual melt for the reference period amounts to 701.6 mm · a^{-1}, approximately. This amount is reduced by 15.8 % for the simulations using scenario I conditions, while the reduction is only 10.2 % in scenario II due to its increased winter precipitation (Table 9). It does not matter for this analysis whether this additional precipitation is snow or rain on snow, since the latter also contributes to snowmelt. The pattern is similar for Kühroint: Mean annual melt for the reference period amounts to 1137.3 mm · a^{-1}, reduced by 14.6 % (scenario I) and 8.9 % (scenario II), the latter again due to enhanced winter precipitation. For Funtenseetauern, the accumulated snowmelt course for all periods is different from what has been observed at the other two locations. The mean total amount of snowmelt is 236.8 mm · a^{-1}, increased by 0.2 % in scenario I, and

Table 9: Mean annual snowmelt amounts (in mm SWE) for a valley site (Schönau), a subalpine site (Kühroint) and a high alpine site (Funtenseetauern) in the Berchtesgaden National Park for the reference period 1998-2006 and the future period 2042-2050 for conditions under scenario I and II, respectively. Elevations are derived from the DEM and differ slightly from the ones of the station locations (see Table 1).

Model location	Reference period (1998–2006)	Scenario I (2042–2050)	Scenario II (2042–2050)
Schönau (628 m a.s.l.) E4574000 N5275600	701.6	590.6	630.0
Kühroint (1404 m a.s.l.) E4572300 N5270650	1137.3	970.7	1035.7
Funtenseetauern (2340 m a.s.l.) E4572950 N5261750	236.8	237.2	242.5

2.4 % in scenario II, respectively. The courses of snowmelt are fairly similar for all three periods. Some minor differences can, however, be observed with snowmelt being less effective in the first winter half (until February) for the future scenarios, while being more effective in the second winter half (from February to melt out in July). This is due to the increase of temperature in summer which lasts until end of October (with corresponding reduction of precipitation), i.e. some early snowfalls are rain in the future scenarios. The total amount of snowmelt is much less on Funtenseetauern compared with the other two sites since a large portion of snowfall is removed by means of the snow slides and not available for snowmelt anymore. This snow is transported down to the accumulation zones and contributes to spring snowmelt there.

Overall, the analysis of the point scale simulations of accumulated snowmelt revealed, that it increases with elevation (if snow is not laterally removed), but it decreases with the warmer conditions of the scenarios. Part of this effect is compensated for by the increasing precipitation in scenario II. In high alpine regions the effects of the additional precipitation outweigh the higher temperatures and lead to a slightly higher mean annual snowmelt than at present.

Conclusion and outlook

In this report, the physically based and distributed snow cover model system AMUNDSEN is described, and its application for continuous historical and future meteorological input data series. The test site is the high alpine central area of the National Park Berchtesgaden (Bavarian Alps, Germany).

The model has been particularly designed to realize long–term simulations of snow cover dynamics in high mountain regions from small to regional scales. It enables the adequate reproduction of the characteristic patterns of a mountain snow cover by considering the specific processes affecting observed heterogeneities of accumulation, redistribution, and ablation of snow in high alpine terrain.

AMUNDSEN computes hourly meteorological fields from time series of scattered point observations collected at station locations most representative in space and elevation. By means of this meteorological forcing, distributed fields of accumulation, lateral redistribution, and ablation of snow are modelled. The processes and effects of wind–induced snow transport are simulated with the blowing–snow model SnowTran–3D.

The unique meteorological conditions of high mountain areas are addressed in detail for the provision of the meteorological input variable fields. The respective parameterizations include dynamic, elevation–dependent lapse rates of the meteorological input variables, the effect of topography on the shortwave and longwave radiative fluxes, and their modification by shadows, multiple and terrain reflections, and clouds. Radiation distribution in mountainous terrain produces a very complex pattern of available melt energy for ablation and plays an important role for the understanding and simulation of the high alpine snow cover heterogeneity.

In many lower alpine regions, mountain forest is the predominant type of land cover. Snow¬vegetation interaction is explicitly modelled, resulting in a modification of the micrometeorological conditions affecting the snow on the ground inside a canopy. Sublimation of previously intercepted snow from the canopy back into the upper air masses is considered, as well as melting and falling down of snow from the trees down to the ground. The energy balance at the ground snow surface is simulated with a physically based scheme including an explicit formulation for the related exchange of mass. Both, the mass and the energy balances are closed for the considered snow storage system between the atmosphere and to the soil.

In the upper regions of many high alpine domains, steep slopes and rock faces with sharp ridges are predominant landscape elements. For these regions, the processes of lateral redistribution of snow are the main cause of the observed snow patterns typical for high mountain regions. To realistically reproduce them in the simulations, a specific model is included and applied to gravitationally redistribute snow from the steeper slopes of mountain summit regions downwards to the valley cir-

ques. It must be concluded from visual observations that these regions generally have the highest snow accumulations and that the snow coverage duration in spring is longest. Wind–induced snow erosion, transport and deposition as well as sublimation from a layer of turbulent suspension are quantified by means of a separate numerical model and by utilizing the most plausible fields of wind speed and direction, simulated in advance using a regional atmospheric model. However, due to the computational expenses these wind fields can only be provided for limited areas, at least at the time being. For applications of larger areas, an empirical parameterization derived from the process modelling results will have to be provided until computing efficiency allows for the complex, physically based schemes to be applied for large areas at a still fine enough spatial resolution. Successful attempts to represent lateral redistribution of snow with either empirical or rule–based models in mountain catchments have been undertaken already (Kuhn 2003, Purves et al. 1998). A corresponding, adequate parameterization will be developed for AMUNDSEN.

By means of a stochastic weather generator coupled with AMUNDSEN, a very efficient computation of potential future climate data series is enabled. Historical datasets are partitioned into periods of predeterminated length, and statistically re–arranged in such a way that the resulting future data time series reproduces a given climatic trend. The procedure will benefit greatly from the continuous extension of the available meteorological time series, increasing the data pool from which the periods are chosen to build up the future climate. The analysis of more downscaled climate model scenario outputs will enhance the formulation of the expected trends. Such regional climate model applications for high alpine areas will come up soon in current international joint projects[22] in which parts of the presented model algorithms are applied. The scales of the GCM output are, however, still mostly inadequate for producing proper input data for process models such as the one presented here. First efforts to overcome this and to link a high resolution representation of the land surface to a regional climate model have been recently undertaken (Marke and Mauser 2007). Meanwhile, the ensemble–type simulations of the snow cover evolution utilizing a broader variety of weather generator generated climate scenarios will be a promising strategy to estimate the range of potential future snow cover dynamics change and their impact on the related water resources availability. One drawback of this method is, however, that the inherent feedback effects of the surface type, snow or bare ground, on the surface climate is not always represented. It seems feasible to include an adequate adaptation to consider this important aspect as a next step of model improvement.

The validation of the energy balance and snowmelt parts of the model is fairly good, though performed at the point scale only in the first instance. The location where the snow pillow device was installed is well equipped with a meteorological station. There the meteorological input data is measured and not spatially distributed (i.e., not affected by the interpolation uncertainty). A pattern comparison between satellite derived maps of snow coverage at a regional scale shows a good general correspondence between the AMUNDSEN simulation and observation. It also confirms that the inclusion of the gravitational snow slides model greatly improves the representativeness and plausibility of the spatial heterogeneity of the modelled snow cover. However, with regard to the number and interdependence of the represented processes, the comparison of simulated versus observed snow distribution for a single model time step is only a poor indicator for the general performance of such a complex model. Future attempts to validate the model results will therefore have to include the acquisition of a continuous time series of remotely sensed snow cover distributions, e.g. by means of an operational terrestrial sensor. Such a time series comparison of distributed model results versus observations will represent an important step towards a comprehensive assessment of model uncertainty. On top of that, it can furthermore serve to provide a time series of distributed model parameters to be assimilated into the modelling, e.g. precipitation phase information.

The analysis of the results of the model presented in this study is conducted by determining distributed seasonal quantities of snow cover mass balance elements, and discussing the specific features of the spatial pattern with regard to the high alpine topography in the study domain of the Berchtesgaden National Park. The mean annual contribution of the individual water balance components is quantified, and a mean annual evapotranspiration amount is estimated by including observed streamflow recordings. The analysis indicates that at the local scale, interpolated precipitation, as well as modelled snowmelt and sublimation during wind–induced snow transport are important water balance quantities, whereas the importance of condensation and sublimation of snow at the ground and from the canopy is moderate. At the regional scale, precipitation and snowmelt still represent important water balance quantities, whereas the contributions of sublimation from the canopy are moderate, while the ones of condensation and sublimation of snow at the ground as well as from wind–induced snow transport are small. Lateral redistribution of snow does not affect the water balance of the entire snow storage system, but locally the amount of snow affected may be highly significant.

Applying the stochastic weather generator two future climate change scenarios were constructed and used for prognostic model runs to estimate the potential sea-

[22] GLOWA-Danube: Integrative techniques, scenarios and strategies for the future of water in the upper Danube basin (www.glowa-danube.de). Brahmatwinn: Twinning European and South Asian river rasins to enhance capacity and implement adaptive management approaches (www.brahmatwinn.uni-jena.de)

sonal evolution of the mountain snow cover under changed climatic conditions. For an assumed moderate trend towards higher temperatures, the results show a rapid but spatially very differentiated decline of snow cover duration. This also applies for the second scenario, in which the warming was combined with a shift of precipitation from summer to winter. Overall it becomes evident that although the increased winter precipitation still predominantly falls as snow, the additional accumulation of the snowpack is compensated for by the higher temperatures.

There is still plenty of room for a further improvement of AMUNDSEN. On the input side, there is still a lot of work to be done with respect to the installation of networks of autonomous stations providing continuous meteorological recordings in high alpine areas, and the development of adequate parameterizations for the respective surface layer processes. Generally, in high mountain areas the precipitation amount is considered to be the most inaccurate model input quantity particularly for snowfall which is extremely difficult to measure. New devices such as the laser distrometer *Ott Parsivel*[23] are continuously developed and currently tested to provide improved recordings of rainfall and snowfall rates. The generally assumed precipitation undercatch in the measurements is, in reality, even larger by the respective sublimation amount as quantified in this study, if it is not considered in the modelling. If the relevant water exchange processes between the snow surface and the atmosphere can be accurately calculated, atmospheric precipitation distributions could be estimated using an inverse *modelling approach* (e.g., after Liston and Sturm, 2002). For that purpose, it is intended to couple the snow processes models with a hydrological model (including evaporation and transpiration), which would make comparisons between simulated and observed streamflow possible. This kind of model enhancement will also facilitate to quantify the important effects of snowmelt on streamflow in a changing climate. However, the investigation domain of the Berchtesgaden National Park is not well suited for that purpose due to its very complex karstic drainage system.

At the process level, many details still await improved consideration. To facilitate the application of the model in pre-alpine regions and in lowlands, a liquid water storage component with potential refreezing will be developed, including the comparison of model results with measurements at different scales. Promising attempts in this respect have already been undertaken (Mauser et al. 2007). To enable the validation of model results with observed snow heights (which are commonly available), a SWE-snow height relationship will be included into AMUNDSEN, through a modelling of snow density. The new parameterization of the turbulent fluxes, which is specifically appropriate for the frequent high wind speed situations in high mountain regions will be compared with the existing simpler scheme using measurements including data from other mountain sites than the one investigated here. Energy transfer at the snow-soil interface is still treated in a very simple way. A physically based model for the consideration of varying soil temperatures and the respective energy exchange at the snow-soil interface has proved succesful in improving the snow simulation (Muerth and Mauser 2007). Finally, the interaction of rainfall with snow previously intercepted in the canopy is not yet considered; this process becomes more importance with respect to the expected increase in winter precipitation, and predicted higher temperatures.

Much work is still required to adequately parameterize the different forest stands and produce reliable, validated snow cover patterns in forested areas. In the SnowMIP2[24] project much effort has been invested to compare the existing model approaches, including the one implemented in AMUNDSEN, with measurements from different sites. The advances developed in modelling snow-forest processes will be of particular importance at regional to global scales to improve our knowledge and understanding of the land surface characteristics with respect to the energy exchange with the atmosphere under conditions of climate change and related bidirectional effects for global warming.

When transferring the model to other study sites, the parameters of the snow slide submodel will have to be slightly adapted to local terrain characteristics. Related experience in determining the location of typical avalanche stretches and the patterns of snow cover disappearance in spring will be valuable expert knowledge needed for proper model parameter adjustment.

In addition to what has been mentioned here, there are many other details with promising scientific potential for further development of the modelling. Examples are: the derivation and assimilation of remotely sensed model parameters, the consideration of redistributed snow deposits as local modifications of topography for succeeding snow slide events, or a bidirectional coupling of AMUNDSEN with the blowing snow model SnowTran-3D. A parameterization of the resulting patterns of wind-induced erosion and deposition with terrain characteristics (e.g., elevation, curvature, exposition) and prevailing wind direction will be the first step to directly integrate the transport processes into the model and enable a plausible redistribution of blowing snow, enabling long-term scenario simulations without the requirement of an explicit SnowTran-3D simulation.

Despite all potential for future development, the current AMUNDSEN version still facilitates an improvement in the theoretical understanding and numerical representation of the long-term snow cover dynamics in high mountain regions. This is absolutely crucial to investigate the influence of changing climatic conditions on the mountain water resources. The high sublimation losses

[23] www.ott-hydrometrie.de/web/ott_de.nsf/id/pa_parsivel_e.html
[24] http://xweb.geos.ed.ac.uk/~ressery/SnowIP2.html

from turbulent suspension at mountain crests are limited to comparably small areas and may not affect the overall alpine water balances significantly. However, if not considered in long-term simulations, snow may accumulate unrealistically high in those areas (especially the summits of high mountains), since snowmelt processes are relatively inefficient or limited in their seasonal duration there. The snow slide submodel facilitates the removal of snow from the high and steep zones of a mountain site and, hence, produces a more realistic snow redistribution in complex, high alpine terrain. Additionally, the consideration of gravitational snow transport is required in the modelling to consistently remove the snow from higher ridge crests and deposit it in the transition zones at the foot of mountain slopes and in the cirques which are accumulation areas for mountain glaciers. In that respect, both the inclusion of wind-induced redistribution and sublimation processes of snow, as well as of gravitational transport by slides are indispensible prerequisites for obtaining realistic results in the simulated snow cover patterns and for an adequate representation of accumulation and ablation in the long-term modelling of high mountain snow cover dynamics and glacier response to climate change.

When successfully implemented, the bi-directional coupling of atmosphere and land surface modelling applied to entire mountain regions will enable an improved, more realistic prediction of seasonal snow cover development under future climate conditions, the consequences of which are manifold from hydrological, ecological, economical and other perspectives. As a result of higher temperatures, winter precipitation and related snowmelt and, hence, spring runoff will increase. On the other hand, the available water resources in summer will decrease (Zierl and Bugman 2005), with implicit consequences for hydropower and in-stream hydraulic plants, irrigation as well as the for the use of stream water as cooling water (Barnett et al. 2005). The management of this specific use of mountain waters most likely will have to change. The changes in water supply to be expected due to climate change, and the related effect on land and water resources design and management practices are an important topic of recent hydrological research (e.g., Bronstert et al. 2002, Menzel and Bürger 2002, Middlekoop et al. 2001).

The retreat of the alpine glaciers considerably affects mountain hydrology (Strasser et al. 2008b, IPCC 2007, ICIMOD 2000a, b). Firstly, the existence of glaciers in the headwatersheds ensures a supply of stream water, originating from ice melt during the typically dry summer periods. This effect is even pronounced under the predicted changing climate, attributable to more frequent warm radiation days during summer. However, as soon as ice resources diminish below a certain threshold, the amount of ice melt contribution to the streamflow will decrease as well. This reduction of runoff during a period with the most water demand is expected to considerably affect downstream water resources management practices. However, the expected effect is locally extremely variable and strongly depends on scale, often being over-estimated at the regional and larger scales (Strasser et al. 2008b). Remarkable advances in physically based, distributed glacier mass balance modelling have been achieved recently (Weber et al. 2008). Other predictions of the effects of a changing cryosphere in a warmer climate include a higher risk of floods and natural hazards due to thawing of permafrost, loss of slope stability, and lake outburst events (Frauenfelder et al. 2005, Kääb et al. 2005, Haeberli et al. 1997, Haeberli and Beniston 1998, Haeberli 1994).

The habitats of many plants and animals depend on climate. The consequences of changing temperature, precipitation or radiation will effectively lead to the migration and extinction of species, threatening biodiversity in high alpine areas (WWF 2007). Vegetation zones will geographically shift due to a change of ecological factors, the composition of the mixed mountain forests will alter, and the carbon cycle will change. Some test sites of a world-wide project[25] to investigate such effects over a long time period are situated in the Berchtesgaden National Park.

From an economical point of view, recreational activities are deeply rooted in the cultural identity of the alpine region, and much of the winter tourism focuses on snow-dependent alpine and cross-country skiing (Elsasser and Messerli 2001). Even today, snow conditions have already been deteriorating as a result of higher winter temperatures, and the number of days with sufficient snow for cross-country and alpine skiing is declining (Breiling and Charamza 1999). Changes are also expected for the current winter traffic patterns – some ski resorts might lose their profitability, at least for certain periods, while others might benefit from their higher location and attract even more guests (Tepfenhart et al. 2008). A long-term survival of ski resorts can be assumed if at least 70 % of the ski seasons (1 December until 15 April) have at least 100 days with good snow condition, i.e. at least 30 to 50 cm of snow depth (Bürki et al. 2003). In the Swiss Alps, an upward-shift in elevation of approximately 500 m for the long-term survival of ski resorts (as determined by snow conditions) has been projected for a variety of IPCC scenarios with a 100 year horizon (Verbunt and Gurtz 2004).

The field of generating future climate scenarios for land surface modelling in mountain areas is one of the most prominent research issues in today's snow sciences. Due to their high sensitivity to environmental change, mountain ecosystems can be considered as „early warning systems" for climate change[26]. Thereby the temporal storage of water resources in the snow cover is an important element in mountain water systems. Extreme hydrological events likely to result from climate change may have major consequences in both mountain areas, and downstream.

[25] GLORIA: GLobal Observation Research Initiative in Alpine environments (www.gloria.ac.at)
[26] http://epaedia.eea.europa.eu/page.php?pip=569

The mentioned aspects are central issues of several joint international research initiatives currently proposed to the EC in which the presented model is supposed to be applied, transferred and further developed[27]. In the EC's Green Paper "Adapting to climate change in Europe – options for EU action" Europe's mountain areas are identified as being one of the most vulnerable regions with respect to climate change[28]. The policy–relevant dimension of climate change in mountain regions and its effect on the water resources and supply for the population is expressed by the many relevant international commitments[29], protocols[30], and initiatives[31] concluded by the European Union as well as by the emerging EU environmental legislation and policies[32], implementation of the 6th Environmental Action Programme[33], associated thematic strategies[34] and action plans[35]. Based on these statements, various recommendations for mitigation and adaptation to the effects of climate change on the water resources are derived[36].

On the global level, AMUNDSEN and the Berchtesgaden National Park meteorological database currently represent the scientific platform in terms of alpine snow modelling within the international framework of the IP3[37] network, funded by the *Canadian Foundation for Climate and Atmospheric Sciences* (CFCAS).

In all the mentioned respects, the presented model is an important step forward in the development of a land surface scheme able to represent mountain specific snow processes for long–term climate change scenario simulations, and a realistic modelling of snow accumulation on glaciers.

The process descriptions are mostly physically based, hence local calibration is not required and the model is generally transferable in space and time. Therefore it facilitates applications in other domains than the one selected here. Additionally, this enables the applicability for future scenario simulation experiments, and a prediction of distribution and availability of water resources stored as snow. The most important model parameters which have to be specifically provided for a certain model domain comprise of hourly recordings of meteorological variables, a DEM, the sky view factor, and the LAI as well as tree height for the canopy.

With today's computing power, and the tremendous speed of technological development, it will soon be possible to extend and transfer physically based snow cover simulations for high mountain regions, such as the one presented here, to the regional scale of entire mountain ranges. Then an expedient coupling of the land surface processes representation with regional climate models will be enabled, and hence an adequate prediction of future water resources distribution, availability, and release in mountain water systems.

---

[27] AlpS: The Alpine Observing System for Climate and Environmental Change
NetDynaom: NETwork for Integrated Assessment of the DYNAmics of MOuntain Catchments under Global Change
AMORES: Alpine MOnitoring Services with REmote Sensing

[28] COM 2007 (http://ec.europa.eu/environment/climat/adaptation/index_en.htm)

[29] United Nations Framework Convention on Climate Change (http://unfccc.int/2860.php)

[30] Kyoto (http://unfccc.int/kyoto_protocol/items/2830.php)
Montreal (http://ozone.unep.org/Publications/MP_Handbook/Section_1.1_The-Montreal_Protocol/)

[31] World Summit on Sustainable Development (http://www.un.org/events/wssd/)
GEOSS: Global Earth Observation System of Systems (http://www.epa.gov/geoss/)

[32] IPCC: Intergovernmental Panel on Climate Change (http://www.ipcc.ch/)
EU Water Initiative (http://ec.europa.eu/research/water-initiative/index_en.html)
EU Water Framework Directive (http://ec.europa.eu/environment/water/water-framework/index_en.html)
European Climate Change Programme (http://ec.europa.eu/environment/climat/eccp.htm)

[33] 6th Environment Action Programme (http://ec.europa.eu/environment/newprg/index.htm)

[34] http:/europa.eu/scadplus/leg/en/s15012.htm

[35] Environmental Technologies Action Plan (http://ec.europa.eu/environment/etap/index_en.htm)

[36] E.g., ESPACE (http://www.espace-projekt.org/)

[37] Improved Processes and Parameterisation for Prediction in Cold Regions (www.usak.ca/ip3/)

Zusammenfassung und Ausblick

In dieser Arbeit wird das physikalisch basierte und flächenverteilte Schneedeckenmodell AMUNDSEN beschrieben, und seine Anwendung für kontinuierliche historische und zukünftige meteorologische Eingabedaten. Das Testgebiet ist der hochalpine Zentralbereich des Nationalparks Berchtesgaden (Bayerische Alpen, Süddeutschland).
Das Modell wurde speziell für Langfrist–Simulationen der Schneedeckendynamik in Hochgebirgsregionen kleiner bis regionaler Skala konzipiert. Es ermöglicht eine verbesserte Reproduktion der charakteristischen Muster der Gebirgsschneedecke durch Berücksichtigung der spezifischen Prozesse, welche die beobachteten Heterogenitäten von Akkumulation, Umverteilung und Ablation von Schnee in hochalpinem Terrain bewirken.

AMUNDSEN berechnet stündliche meteorologische Felder von Zeitreihen verteilter Punktmessungen, welche an möglichst repräsentativ in Raum und Höhe verteilten Standorten erhoben wurden. Mit diesem meteorologischen Antrieb werden verteilte Felder von Akkumulation, lateraler Umverteilung und Ablation von Schnee modelliert. Die Prozesse und Auswirkungen von wind-induziertem Schneetransport werden mit einem separaten Modell simuliert. Die Prozessbeschreibungen sind möglichst physikalisch formuliert, so dass eine lokale Kalibrierung nicht notwendig ist und das Modell prinzipiell in Raum und Zeit übertragbar ist. Dadurch ermöglicht es langfristige Simulationen zukünftiger Schneedeckenentwicklung in einem sich wandelnden Klima, und eine Vorhersage der Verteilung und Verfügbarkeit der Wasserressourcen, welche temporär als Schnee gebunden sind.
Die einzigartigen meteorologischen Bedingungen in Hochgebirgsregionen werden zur Aufbereitung der meteorologischen Eingabedatenfelder detailliert berücksichtigt. Die entsprechenden Parameterisierungen beinhalten dynamische, höhenabhängige Gradienten der meteorologischen Eingabevariablen, den Einfluß der Topographie auf die kurz– und langwelligen Strahlungsflüsse und deren Modifikation durch Schatten, multiple und Geländereflexionen sowie Wolken. Die Strahlungsverteilung in Gebirgsregionen produziert ein sehr komplexes Muster der verfügbaren Schmelzenergie und spielt eine wichtige Rolle für das Verständnis und die Simulation der Heterogenität der hochalpinen Schneedecke.
In vielen alpinen Regionen gemäßigter Höhenlage ist Bergwald der dominante Landnutzungstyp. Mit AMUNDSEN wird die Wechselwirkung zwischen Schnee und Vegetation explizit modelliert, was zu einer Modifikation der mikrometeorologischen Bedingungen führt, welche in einem Bestand auf die Schneedecke am Boden wirken. Darüberhinaus wird die Sublimation von Schnee, welcher zuvor in den Kronen des Bestandes interzipiert ist, zurück in die darüberliegenden Luftschichten der Atmosphäre berücksichtigt, sowie Schmelze und Herunterfallen von Schnee auf den Boden modelliert.
Die Energiebilanze der Schneedecke am Boden wird mit einem physikalisch basierten Ansatz modelliert, einschließlich einer expliziten Formulierung des beteiligten Massenaustausches. Sowohl die Energie–, als auch die Massenbilanz des betrachteten Schneespeichers zwischen Boden und Atmosphäre sind geschlossen.
In den höhergelegenen Regionen vieler hochalpiner Gebiete stellen steile Hänge und Felswände mit scharfen Felsgraten die dominierenden Landschaftselemente dar. In diesen Regionen sind die Prozesse lateraler Umverlagerung von Schnee die wesentlichen Ursachen für die beobachteten, für das Hochgebirge typischen Schneemuster. Um sie in Modellrechnungen realistisch wiedergeben zu können, wird ein spezifisches Modell integriert und angewendet, das den Schnee von den Steilhängen der Gipfelbereiche gravitativ in die darunterliegenden, flacheren Karböden transportiert. Diese Gebiete stellen Zonen höchster Akkumulation dar, und dort bleibt die Schneedecke im Frühjahr am längsten liegen.

Wind–induzierte Erosion, Transport und Deposition, sowie Sublimation von Schnee aus einer Schicht turbulenter Suspension werden mit einem separaten numerischen Modell quantifiziert. Dabei finden möglichst plausible Felder von Windgeschwindigkeit und –richtung Verwendung, welche zuvor mit einem regionalen Atmosphärenmodell simuliert wurden. Solche Windfelder können wegen der beträchtlichen Anforderungen an die Rechenzeit derzeit nur für räumlich begrenzte Gebiete bereitgestellt werden. Bevor die komplexen, physikalisch basierten Ansätze mit hinreichender Auflösung auch für größere Gebiete angewendet werden können, werden für entsprechende Anwendungen noch empirische Parameterisierungen benötigt. Erfolgreiche Ansätze, die laterale Umverteilung von Schnee mit empirischen oder regelbasierten Modellen in Gebirgseinzugsgebieten wiederzugeben, gibt es z.B. schon von Kuhn (2003) oder Purves et al. (1998). Eine entsprechende Parameterisierung wird auch für AMUNDSEN entwickelt werden.
Durch Einsatz eines stochastischen Wettergenerators, welcher mit AMUNDSEN gekoppelt ist, wird eine sehr effiziente Berechnung einer Zeitreihe meteorologischer Daten für zukünftiges Klima ermöglicht. Dabei werden historische Datensätze in Perioden vorgegebener Länge aufgeteilt und statistisch derart umsortiert, so dass die zukünftige Datenreihe einen gegebenen Klimatrend reproduziert. Das Verfahren wird sehr vom kontinuierlichen Ausbau des Messnetzes automatischer meteorologischer Stationen im Nationalparkgebiet profitieren: dadurch wird nämlich der Datenpool vermehrt, aus welchem die Perioden zur Konstruktion des zukünftigen Klimas ausgewählt werden können. Die Analyse von weiteren, down–gescalten Klimamodellausgaben für bestimmte Szenarien wird die Formulierung der erwarteten Trends verbessern. Entsprechende Kopplungen mit regionalen Klimamodellen finden in internationalen Ver-

bundprojekten[38] Anwendung, in welchen auch Teile der hier dargestellten Modellalgorithmen verwendet werden. Der Maßstab der GCM–Ausgaben jedoch ist meist zu grob, um geeignete Eingabedaten für Prozessmodelle wie das hier beschriebene zu produzieren. Erste erfolgreiche Ansätze, dies zu bewerkstelligen und eine hochaufgelöste Darstellung der Landoberfläche mit einem regionalen Klimamodell zu verbinden, wurden jüngst unternommen (MARKE and MAUSER 2007). Für die Zwischenzeit ist es eine vielversprechende Strategie, mit Hilfe von Ensemble–Simulationen der Schneedeckenentwicklung und unter Verwendung von vielfältigen, mit Klimageneratoren erzeugten Szenarien den Bereich potentieller zukünftiger Schneedeckendynamik und der entsprechenden Auswirkungen auf die Verfügbarkeit der Wasserressourcen abzuschätzen. Ein Nachteil dieser Methode jedoch ist, dass die innewohnenden Feedback–Effekte des Landoberflächen–Typs, nämlich Schnee oder nackter Boden, auf das Grenzschichtklima nicht immer berücksichtigt sind. Eine entsprechende Parameterisierung zur Berücksichtigung dieses Effekts ist ein wichtiger Schritt zukünftiger Modellverbesserungen.

Die Validierung der Energiebilanz und Schneeschmelze auf der Punktskala zeigt gute Ergebnisse. Der Ort zur Validierung, wo das Schneekissen installiert ist, ist mit einer sehr genau messenden meteorologischen Station ausgestattet. Dort sind in der Modellierung die meteorologischen Daten gemessen, d.h. nicht räumlich interpoliert (und damit nicht mit entsprechenden Unsicherheiten behaftet). Auf regionaler Skala zeigt ein Mustervergleich zwischen aus Satellitendaten abgeleiteter Schneebedeckung und der AMUNDSEN–Simulation eine gute Übereinstimmung. Insbesondere bestätigt der Vergleich, dass die Modellierung der gravitativ bedingten Schneerutsche die Repräsentativität und Plausibilität der räumlichen Heterogenität der modellierten Schneedecke bedeutend verbessert. Unter Berücksichtigung der Anzahl und vielfältigen Wechselwirkungen der berücksichtigten Prozesse ist der Vergleich zwischen modellierter und beobachteter Schneeverteilung zu nur einem Modell–Zeitschritt allerdings als nur wenig signifikanter Indikator für die Güte eines so komplexen Modells anzusehen. Zukünftige Schritte zur Modellvalidierung werden daher die Akquise einer kontinuierlichen Zeitreihe fernerkundeter Schneedeckenmuster mit einbeziehen, z.B. unter Verwendung eines operationellen, terrestrischen Sensors; dieser würde auch die Assimilation von flächenverteilten Modellparametern erlauben, etwa die Phase des Niederschläge. Ein derartiger Zeitreihenvergleich von flächenverteilten Modellergebnissen mit Beobachtungen wird einen wichtigen Schritt hin zu einer vollständigen Untersuchung der Modellunsicherheiten sein.

Die Analyse der Modellergebnisse wird durch Ableitung verteilter, saisonaler Größen von Schneedecken–Massenbilanzelementen durchgeführt, sowie durch Diskussion der spezifischen Eigenschaften des räumlichen Musters der Schneedecke unter Bezug auf die hochalpine Topographie im Untersuchungsgebiet des Nationalparks Berchtesgaden. Dabei wird der mittlere jährliche Beitrag der einzelnen Wasserbilanzkomponenten quantifiziert, und durch Einbezug gemessener Abflussmesswerte ein mittlerer jährlicher Betrag der Evapotranspiration abgeschätzt. Die Ergebnisse zeigen, dass auf lokaler Skala die interpolierten Niederschläge und die modellierte Schneeschmelze sowie Sublimation während wind–induziertem Schneetransport wichtige Wasserbilanzgrößen darstellen, während die Bedeutung von Kondensation und Sublimation von Schnee am Boden und aus dem Bestand mäßig sind. Auch auf regionaler Skala repräsentieren Niederschlag und Schneeschmelze bedeutende Bilanzgrößen, während die Beiträge von Sublimation aus dem Bestand mäßig und diejenigen von Kondensation und Sublimation am Boden, wie auch die von wind–induziertem Transport, gering sind. Laterale Umverteilung von Schnee beeinflusst nicht die Wasserbilanz des Einzugsgebietes, aber lokal kann die Menge Schnee, die von diesem Prozess erfasst wird, beträchtlich sein.

Unter Verwendung des stochastischen Klimagenerators wurden zwei Szenarien zukünftigen Klimawandels generiert und für prognostische Modell–Läufe verwendet, um die potentielle, saisonale Entwicklung der Gebirgsschneedecke unter veränderten klimatischen Bedingungen abzuschätzen. Für einen angenommenen mäßigen Trend zu höheren Temperaturen zeigen die Ergebnisse eine rapide und räumlich stark differenzierte Abnahme der Schneedeckendauer. Dies gilt auch für das zweite Szenario, für welches die Erwärmung mit einer Verschiebung der Niederschläge vom Sommer in den Winter kombiniert wurde. Insgesamt ergibt sich, dass die zusätzliche Akkumulation durch die höheren Temperaturen kompensiert werden, obwohl die vermehrten Winterniederschläge überwiegend als Schnee fallen.
Es gibt noch viele Verbesserungsmöglichkeiten. Eine große Herausforderung für sich stellt die Messtechnik im Hochgebirge dar. Prinzipiell gilt nicht nur dort der Niederschlag als die am ungenauesten bekannte Modelleingabe–Größe, was ganz besonders für Schneefall gilt. Neue Geräte wie der Laser–Distrometer *Ott Parsivel*[39] werden laufend weiterentwickelt und getestet, um verbesserte Messungen von Regen und Schneefall bereitzustellen. Wenn nicht in den Modellrechnungen berücksichtigt, ist die prinzipiell angenommene Unterschätzung der Niederschläge in den Messungen wegen der entsprechenden Verdunstungsverluste in Wirklichkeit sogar noch größer als angenommen.

[38] GLOWA-Danube: Integrative techniques, scenarios and strategies for the future of water in the upper Danube basin (www.glowa-danube.de)
Brahmatwinn: Twinning European and South Asian river rasins to enhance capacity and implement adaptive management approaches (www.brahmatwinn.uni-jena.de)

[39] www.ott-hydrometrie.de/web/ott_de.nsf/id/pa_parsivel_e.html

Wenn man die relevanten Wasseraustausch–Prozesse zwischen der Schneeoberfläche und der Atmosphäre genau berechnet, könnte man die Verteilung der atmosphärischen Niederschläge mit einem inversen Modellansatz abschätzen (z.B. wie LISTON und STURM, 2002). Es ist vorgesehen, zu diesem Zweck die Schneedeckenmodellierung mit einem hydrologischen Modell zu koppeln (welches Evaporation und Transpiration mit berücksichtigt), und damit Vergleiche zwischen modelliertem und gemessenen Abfluss vorzunehmen. Eine solche Modellverbesserung wird auch ermöglichen, die bedeutenden Auswirkungen der Schneesschmelze auf den Gerinneabfluss in einem sich wandelnden Klima zu quantifizieren. Das Untersuchungsgebiet des Nationalparks Berchtesgaden ist hierfür wegen seiner komplexen Karsthydrologie allerdings nur bedingt geeignet.

Auf der Eingabedatenseite des Modells ist noch viel zu tun im Hinblick auf die Entwicklung von geeigneten Parameterisierungen für die relevanten Prozesse in der Grenzschicht. Um die Anwendung des Modells in voralpinen Regionen und im Unterland zu ermöglichen, wird eine Flüssigwasserkomponente mit potentiellem Wiedergefrieren entwickelt, einschließlich eines Vergleichs von Modellergebnissen mit Messungen auf verschiedenen Skalen. Vielversprechende Ansätze diesbezüglich wurden schon unternommen (MAUSER et al. 2007). Um eine Modellvalidierung mit beobachteten Schneehöhen zu ermöglichen (welche üblicherweise vorhanden sind), wird eine SWE–Schneehöhenbeziehung durch Modellierung der Schneedichte in AMUNDSEN integriert. Die neue Parameterisierung der turbulenten Flüsse, welche spezifisch für die im Hochgebirge häufigen hohen Windgeschwindigkeiten geeignet ist, wird mit dem bestehenden, einfacheren Verfahren auch unter Verwendung von Daten aus einem anderen als dem hier vorgestellten Untersuchungsgebiet verglichen werden. Der Energietransfer an der Schnee–Boden–Grenzschicht wird noch recht einfach behandelt. Ein physikalisch basiertes Modell für die Berücksichtigung variierender Bodentemperaturen und entsprechender Energie–Austauschvorgänge an der Schnee–Boden–Grenzschicht hat bereits Verbesserungen in der Simulation der Schneedecke ergeben (MUERTH and MAUSER 2007). Die Wechselwirkung von flüssigem Regen mit Schnee, der zuvor im Bestand interzipiert ist, ist noch nicht berücksichtigt. Dieser Prozess gewinnt zusätzliche Bedeutung im Hinblick auf den erwarteten Klimawandel, wenn die Winterniederschläge bei steigender Temperatur zunehmen.
Viel Arbeit ist noch nötig, die verschiedenen Waldbestände angemessen zu parameterisieren und verlässliche, validierte Schneemuster für Wälder zu modellieren. Im Rahmen des SnowMIP2[40] – Projektes wurde bereits ein Vergleich bestehender Modellansätze initiiert, einschließlich des in AMUNDSEN implementierten und hier verwendeten. Die bei der Modellierung der Schnee–Vegetation Wechselwirkung erzielten Fortschritte werden von spezifischer Bedeutung auf regionaler bis globaler Skala sein im Hinblick auf unser Wissen und unser Verständnis der Landoberflächeneigenschaften, was den Energieaustausch mit der Atmosphäre und sich verändernden Klimabedingungen und entsprechenden, bidirektionalen Auswirkungen für die globale Erwärmung anbelangt.
Bei der Übertragung des Modells in andere Untersuchungsgebiete wird eine geringfügige Anpassung der Parameter des Schneerutsch–Modells an die lokalen Geländeeigenschaften notwendig sein. Entsprechende Erfahrung in der räumlichen Bestimmung typischer Lawinenzüge und frühjährlicher Schneeschmelzmuster wird hierbei wertvolles Expertenwissen darstellen, welches für eine geeignete Anpassung der Modellparameter erforderlich ist.
Zusätzlich gibt es noch viele andere Details mit vielversprechendem wissenschaftlichen Potential für die Weiterentwicklung der Modellierung. Beispiele sind: die Ableitung und Assimilation fernerkundeter Modellparameter, die Berücksichtigung verlagerten Schnees als lokale Modifikation der Topographie für nachfolgende Schneerutsche, oder eine bidirektionale Kopplung von AMUNDSEN mit dem Triebschneemodell SnowTran–3D. Eine Parameterisierung der resultierenden Muster von wind–induzierter Erosion und Deposition mit Geländeeigenschaften (z.B. Höhe, Wölbung und Exposition) und vorherrschender Windrichtung wird ein erster Schritt sein, die Berücksichtigung der Transportprozesse direkt in das Modell zu integrieren und eine plausible Umverteilung von Triebschnee zu ermöglichen. Diese schafft die Voraussetzung, langfristige Szenarienrechnungen ohne explizite Modellierung mit SnowTran–3D durchführen zu können.
Abgesehen von allem zukünftigen Entwicklungspotential, ermöglicht auch die derzeitige Version von AMUNDSEN bereits eine Verbesserung im theoretischen Verständnis und in der numerischen Modellierung der langfristigen Schneedeckendynamik in Hochgebirgsregionen. Dies ist entscheidend für die Untersuchung des Einflusses sich verändernder klimatischer Bedingungen auf die Wasserressourcen im Gebirge.
Die hohen Sublimationsverluste aus turbulenter Suspension an Graten sind auf relativ kleine Flächen begrenzt und dürften die gesamte alpine Wasserbilanz nur gering beeinflussen. Wenn sie allerdings in Langfristsimulationen nicht berücksichtigt werden, kann Schnee auf diesen Flächen (v.a. den Gipfeln hoher Berge) unrealistisch hoch akkumulieren, da dort Schneeschmelzprozesse relativ wenig effizient sind oder zeitlich begrenzt in ihrer saisonalen Dauer. Obwohl es keine Modellierung individueller Lawinenereignisse erlaubt, ermöglicht das Schneerutsch–Modell die laterale Verlagerung von Schnee von den hohen und steilen Bereichen eines Berges und produziert damit eine realistischere Umverteilung von Schnee in komplexem, hochalpinen Relief. Zusätzlich wird die Berücksichtigung von gravitativem Schneetransport in der Modellierung benötigt, um den Schnee von hochgelegenen Graten konsisten wegzu-

[40] http://xweb.geos.ed.ac.uk/~ressery/SnowIP2.html

verlagern, d.h. und ihn in den Übergangsbereichen am Fuß der Berghänge und in den Karen, welche oft Nährgebiete für Gebirgsgletscher darstellen, zu deponieren. In dieser Hinsicht sind die Berücksichtigung von windinduzierter Umverlagerung und Sublimationsprozessen sowie von gravitativem Schneetransport durch Rutsche unverzichtbare Voraussetzungen, um realistische Ergebnisse in den simulierten Schneedeckenmustern zu erhalten und für eine sinnvolle Wiedergabe von Akkumulation und Ablation in der Langfristsimulation von Schneedeckendynamik und Gletscherreaktion auf sich wandelndes Klima im Hochgebirge.
Eine erfolgreich implementierte, bidirektionale Kopplung von Atmosphären- und Landoberflächenmodellierung wird bei Anwendung auf ganze Gebirgsregionen eine verbesserte, realistischere Vorhersage von saisonaler Schneedeckenentwicklung unter zukünftigen Klimabedingungen ermöglichen, deren Konsequenzen aus hydrologischer, ökologischer und anderen Perspektiven vielfältig sind. Als Ergebnis höherer Temperaturen wird der Winterniederschlag und damit die entsprechende Schneeschmelze und damit der Abfluss, zunehmen. Auf der anderen Seite werden die verfügbaren Wasserressourcen im Sommer abnehmen (Zierl and Bugman 2005), mit damit einhergehenden Konsequenzen für Wasserkraft, Laufkraftwerke, Bewässerung und für die Nutzung von Gerinneabfluss zu Kühlzwecken (Barnett et al. 2005). Das Management dieser spezifischen Nutzung von Gebirgswasser wird sich höchstwahrscheinlich ändern müssen. Die Veränderungen der Wasserversorgung, welche mit dem Klimawandel zu erwarten sind, und die entsprechenden Auswirkungen auf die Gestaltung und die Managementpraxis der Land- und Wasserressourcen sind wichtige Themen heutiger hydrologischer Forschung (e.g., Bronstert et al. 2002, Menzel and Bürger 2002, Middlekoop et al. 2001).

Der Rückgang alpiner Gletscher beeinflusst beträchtlich die Gebirgshydrologie (Strasser et al. 2008b, IPCC 2007, ICIMOD 2000a, b). Zum einen gewährt die Existenz von Gletschern in den Kopfeinzugsgebieten einen Nachschub von Gerinneabfluss aus Eisschmelze, welche typischerweise in trockenen Sommerperioden auftritt. Dieser Effekt wird durch den vorhergesagten Klimawandel sogar noch verstärkt, hervorgerufen durch die öfter auftretenden warmen Strahlungstage im Sommer. Sobald die Eisressourcen unter eine gewisse Grenze zurückgehen wird der Anteil von Eisschmelze jedoch auch zurückgehen. Diese Verringerung des Abflusses während einer Periode mit der größten Wassernachfrage wird vermutlich die Managementpraktiken flussabwärts deutlich verändern. Der erwartete Effekt ist jedoch lokal extrem variabel und hängt stark von der Skala ab, wobei der auf regionaler und größerer Skala oft überschätzt wird (Strasser et al. 2008b). Bemerkenswerte Fortschritte in physikalisch basierter, flächenverteilter Gletschermassenbilanz-Modellierung sind kürzlich erzielt worden (Weber et al. 2008). Weiter Vorhersagen der Auswirkungen einer sich wandelnden Kryosphäre in wärmeren Klimabedingungen umfassen größere Risiken von Hochwasser und Naturkatastrophen durch den tauenden Permafrost, Verlust an Hangstabilität und Ausbrüche von Gletscherseen (Frauenfelder et al. 2005, Kääb et al. 2005, Haeberli et al. 1997, Haeberli and Beniston 1998, Haeberli 1994).
Die Lebensräume vieler Pflanzen und Tiere hängen vom Klima ab. Die Auswirkungen von sich verändernden Temperaturen, Niederschlägen und Strahlungsverhältnissen werden in wirksamer Weise zu Migration und Aussterben von Arten führen und damit die Biodiversität in hochalpinen Regionen bedrohen (WWF 2007). Vegetationszonen werden sich durch die Veränderung von ökologischen Faktoren geographisch verlagern, die Zusammensetzung des Berg-Mischwaldes wird sich umstellen, und der Kohlenstoffkreislauf wird sich verändern. Einige Testflächen eines weltweiten Projekts[41] zur Untersuchung solcher Effekte über längere Zeiträume liegen im Gebiet des Nationalparks.

Aus ökonomischer Sicht sind Erholungsaktivitäten tief in der kulturellen Identität der alpinen Region verwurzelt, und ein großer Anteil des Wintertourismus ist auf schneeabhängiges, alpines Skifahren und Langlaufen ausgerichtet (Elsasser and Messerli 2001). Schon heute haben sich vielerorts die Schneeverhältnisse verschlechtert als Resultat von höheren Wintertemperaturen, und die Anzahl der Tage mit genügend Schnee für Langlauf und Skifahren geht zurück (Breiling and Charamza 1999). Veränderungen werden auch für die derzeitigen Winterverkehrsmuster erwartet – einige Skigebiete werden wohl ihre Profitabilität verlieren, zumindest für bestimmte Phasen, während andere von ihrer höheren Lage profitieren und dann sogar mehr Gäste anziehen werden (Tepfenhart et al. 2008). Ein längerfristiges Bestehen von Skigebieten kann angenommen werden wenn zumindest 70 % der Skifahr-Perioden (1. Dezember bis 15. April) wenigstens 100 Tage mit guten Schneebedingungen aufweisen, d.h. mindestens 30 bis 50 cm Schneehöhe (Bürki et al. 2003). In den schweizer Alpen wurde für eine Reihe von IPCC-Szenarien mit einem Horizont von 100 Jahren eine Höherwanderung von Skigebieten um ungefähr 500 m (abgeleitet aus entsprechenden Schneebedingungen) für ein längerfristiges Bestehen vorhergesagt (Verbunt and Gurtz 2004).
Der Bereich der Aufbereitung zukünftiger Klimaszenarien für die Modellierung der Landoberfläche in Gebirgsregionen ist eines der wichtigsten Forschungsthemen in der heutigen Schneeforschung. Gebirgs-Ökosysteme können wegen ihrer hohen Sensitivität auf Umweltveränderungen dabei als „Frühwarnsysteme" für den Klimawandel angesehen werden[42]. Dabei ist die temporäre Speicherung von Wasserressourcen in der Schneedecke ein wichtiges Element des Wassersystems im Gebirge. Extreme hydrologische Ereignisse, welche

[41] GLORIA: GLOBAL Observation Research Initiative in Alpine environments (www.gloria.ac.at)
[42] http://epaedia.eea.europa.eu/page.php?pip=569

wahrscheinlich als Konsequenz des Klimawandels auftreten, dürften größere Auswirkungen sowohl auf die Gebirgsareale selbst, als auch auf die flussabwärtigen Flachländer haben.
Die genannten Aspeke sind zentrale Themen einer Reihe von internationalen Verbundvorhaben, welche zur Zeit bei der Europäischen Kommission beantragt sind und wo das vorgestellte Modell angewendet, übertragen und weiter entwickelt werden soll[43]. Im Bericht der EC „Adapting to climate change in Europe – options for EU action" werden die Europäischen Gebirge als am stärksten vulnerable Gebiete im Hinblick auf den Klimawandel identifiziert[44]. Die Politikrelevante Dimension des Klimawandels in Gebirgsregionen und seiner Auswirkungen auf die Wasserressourcen und –versorgung der Bevölkerung wird auch durch die vielen internationalen Übereinkünfte[45], Protokolle[46] und Initiativen[47] ausgedrückt, welche von der Europäischen Union beschlossen wurden, sowie durch die entstehende EU–Umweltgesetzgebung und Politik[48], Umsetzung des 6. Umweltaktionsprogrammes[49] sowie entsprechende thematische Strategien[50] und Aktionspläne[51].
Basierend auf diesen Erklärungen werden eine Vielzahl von Empfehlungen für Vermeidung und Anpassung an Klimawandel–Auswirkungen auf die Wasserressourcen abgeleitet[52]. Auf globaler Ebene repräsentieren AMUNDSEN und die Datenbank meteorologischer Messwerte des Nationalparks Berchtesgaden eine wissenschaftliche Plattform für alpine Schneemodellierung im internationalen Rahmen des IP3[53] Netzwerkes, welches von der *Canadian Foundation for Climate and Atmospheric Sciences* (CFCAS) gefördert wird. In all den genannten Aspekten sind die vorgestellten Algorithmen ein wichtiger Schritt weiter in Richtung Entwicklung eines Landoberflächenmodells zur Simulation gebirgsspezifischer Prozesse für Langfristrechenläufe von Klimawandel–Szenarien, und einer realistischen Modellierung der Schneeakkumulation auf Gletschern. Das Modell beruht auf der Philosophie, die Kalibrierung von Parametern zu vermeiden und statt dessen auf robuste Parameterisierung mit möglichst physikalischem Hintergrund zurückzugreifen. Dies ermöglicht die Übertragbarkeit des Modells in Raum und Zeit, und damit auch die Anwendbarkeit für Szenario–Simulationen in anderen als dem hier ausgewählten Testgebiet. Die wichtigsten Eingabeparameter, welche für ein bestimmtes Gebiet spezifisch zur Verfügung stehen müssen, umfassen stündliche Aufzeichnungen meteorologischer Variablen, ein DEM, den sky view factor, und LAI bzw. Wuchshöhe der Bäume im Bestand.

Mit der heutigen Rechenleistung und der gewaltigen Geschwindigkeit der technologischen Entwicklung wird es bald möglich sein, physikalisch basierte Schneedeckensimulationen für Hochgebirgsregionen wie die hier vorgestellte auszudehnen und auf die regionale Skala ganzer Gebirgszüge zu übertragen. Dann wird eine sinnvolle Kopplung der Landoberflächenprozesse mit regionalen Klimamodellen ermöglicht, und somit eine verlässlichere Vorhersage der Verteilung, Verfügbarkeit und Abgabe zukünftiger Wasserressourcen in Gebirgseinzugsgebieten.

---

[43] AlpS: The Alpine Observing System for Climate and Environmental Change
NetDynamo: NETwork for Integrated Assessment of the DYNAmics of MOuntain Catchments under Global Change
AMORES: Alpine MOnitoring Services with REmote Sensing
[44] COM 2007 (http://ec.europa.eu/environment/climat/adaptation/index_en.htm)
[45] United Nations Framework Convention on Climate Change (http://unfccc.int/2860.php)
[46] Kyoto (http://unfccc.int/kyoto_protocol/items/2830.php)
Montreal (http://ozone.unep.org/Publications/MP_Handbook/ Section_1.1_The_Montreal_Protocol/)
[47] World Summit on Sustainable Development (http://www.un.org/events/wssd/)
GEOSS: Global Earth Observation System of Systems (http://www.epa.gov/geoss/)
[48] IPCC: intergovernmental Panel on Climate Change (http://www.ipcc.ch/)
EU Water Initiative (http://ec.europa.eu/research/water-initiative/index_en.html)
EU Water Framework Directive (http://ec.europa.eu/environment/water/water-framework/index-en.html)
European Climate Change Programme (http://ec.europa.eu/environment/climat/eccp.htm)
[49] 6th Environment Action Programme (http://ec.europa.eu/environment/newprg/index.htm)
[50] http://europa.eu/scadplus/leg/en/s15012.htm
[51] Environmental Technologies Action Plan (http://ec.europa.eu/environment/etap/index_en.htm)
[52] E.g., ESPACE (http://www.espace-project.org/)
[53] Improved Processes and Parameterisation for Prediction in Cold Regions (www.usak.ca/ip3)

List of figures

List of tables

List of abbreviations and acronyms

ALPINE3D	Distributed model for alpine surface processes
AMUNDSEN	Alpine MUltiscale Numerical Distributed Simulation ENgine
ARPS	Mesoscale, prognostic atmospheric model
ASCII	American Standard Code for Information Interchange
ASTER	Advanced Spaceborne Thermal Emission and Reflection Radiometer
bmb+f	Bundesministerium für Bildung und Forschung
C	Imperative, procedural programming language
CAI	Cortex Area Index
CET	Central European Time
CFCAS	Canadian Foundation for Climate and Atmospheric Sciences
CROCUS	One-dimensional snow model for avalanche forecasting
DANUBIA-Light	Transdisciplinary modelling system to investigate regional climate change effects on the water balance
DEM	Digital Elevation Model
DGJ	Deutsches Gewässerkundliches Jahrbuch
DWD	Deutscher Wetterdienst
EC	European Community
ESCIMO	Energy balance Snow Cover Integrated MOdel
ETH	Eidgenössische Technische Hochschule
FORTRAN	Procedural programming language, mainly for numerical computations
Gauß-Krüger	Cartesian coordinate system
GCM	Global Circulation Model
GIS	Geographical Information System
HBV	Temperature-index snowmelt model
IAHS	International Association for Hydrological Sciences
IDL	Interactive Data Language
IDW	Inverse Distance Weighting
IEEE	Institute of Electrical and Electronics Engineers
IPCC	Intergovernmental Panel on Climate Change
LAI	Leaf Area Index
LINUX	Free, multi-platform, multi-user operating system
LARS-WG	Stochastic weather generator
LWZ	Lawinenwarnzentrale Bayern
Mac OS	Operating system for Apple Macintosh computers
Meso-NH	Mesoscale, prognostic atmospheric model
MM5	Mesoscale, non-hydrostatic atmospheric model
MPEG-4	Standard for the compression of video and audio data
NaN	Not a Number, used for representation of invalid floating numbers
PBSM	Prairie Blowing Snow Model
PC	Personal Computer
PREVAH	Distributed hydrological modelling system
PROMET	Processes of Radiation, Mass and Energy Transfer
RAM	Random Access Memory
ROI	Region of Interest
RWT	Correlation coefficient for the fluctuations of vertical wind component and potential temperature
SI	International System of Units
Snowmodel	Physically based framework for snow processes modelling
SNOWPACK	One-dimensional snow cover model
SNTHERM	One-dimensional energy and mass balance model for snow and soil
SnowTran-3D	Three-dimensional model for wind-induced snow transport simulation
SRM	Snowmelt Runoff Model
SVAT	Soil Vegetation Atmosphere Transfer
SWE	Snow Water Equivalent
TERRA	Multi-national, multi-disciplinary space mission
TIFF	Tagged Image File Format
TOMS	Total Ozone Mapping Spectrometer
UNIX	Multi-user operating system
UTC	Universal Time Coordinated
UTM	Universal transversal mercator projection
WGEN	Weather generator (weather simulation model)
WINDOWS	Graphical operating system for personal computers

Symbols

A	advective energy	$W \cdot m^{-2}$
a	snow albedo	
a_a	atmospheric albedo	
a_g	ground albedo	
a_f	empirical snow albedo factor for melt	$0.0094\ m^2 \cdot mm \cdot h^{-1} \cdot W^{-1}$
a_{min}	minimum snow albedo	0.5
$a_{min} + a_{add}$	maximum snow albedo	0.75 – 0.95
a_{t-1}	snow albedo of the previous timestep	
B	soil heat flux	$2.0\ W \cdot m^{-2}$
β	scaling factor	0.9
β_e	elevation correction	
C	cloudiness	
C_e	non–dimensional canopy exposure coefficient	
C_p	specific heat capacity of moist air	$J \cdot kg^{-1}\ K^{-1}$
$C_{p,dry}$	specific heat capacity of dry air	$1004.67\ J \cdot kg^{-1}\ K^{-1}$
c	excentricity correction factor	
cF	cloud factor	
c_i	melting heat of ice	$3.375 \cdot 10^5\ J \cdot kg^{-1}$
c_{ss}	specific heat of snow (at 0 °C)	$2.10 \cdot 10^3\ J \cdot kg^{-1} \cdot K^{-1}$
c_{sw}	specific heat of water (at 5 °C)	$4.18 \cdot 10^3\ J \cdot kg^{-1} \cdot K^{-1}$
D	day number	
D_{SWE}	deposition of gravitationally transported snow	mm
D_{lim}	upper limit of deposition per model cell and slide event	350 mm
D_{max}	maximum deposition per model cell and slide event	mm
D_v	water vapour diffusivity in the atmosphere	$m^2 \cdot s^{-1}$
dm/dt	mass loss rate	$kg \cdot s^{-1}$
δ	declination	radian
E	latent heat flux	$W \cdot m^{-2}$
e	base of the natural exponential function	2.71828
e_l	water vapour partial pressure	hPa
e_s	saturated vapour pressure	hPa
e_w	saturated vapour pressure for wet temperature	hPa
δe	mass flux by sublimation or resublimation	mm
Δe	water vapour pressure difference	hPa
ε	longwave emissivity of snow	0.98 – 1
ε_{sky}	mean longwave emissivity of the sky	
ε_{cs}	clear sky emissivity	
ε_{oc}	overcast sky emissivity	
F_c	canopy density	
F_{NB}	snow transported to a neigbour cell	mm
f_{NB}	draining fraction for a neigbour cell	
Φ_S	vertical mass–concentration distribution	$kg \cdot m^{-3}$
G	incoming shortwave (global) radiation	$W \cdot m^{-2}$
G_{dir}	incoming direct radiation	$W \cdot m^{-2}$
G_{ref}	reflected radiation	$W \cdot m^{-2}$
G^*	clear sky solar radiation	W · m–2

g	gravitational constant	9.81 $m \cdot s^{-2}$
g_a	mean atmospheric temperature gradient	–0.0098 $K \cdot m^{-1}$ (no rain)
		–0.0065 $K \cdot m^{-1}$ (rain)
g_s	surface layer temperature gradient	$K \cdot m^{-1}$
Γ	day angle	radian
γ	psychrometric constant	$hPa \cdot K^{-1}$
γ_s	shape exponent	1
H	sensible heat flux	$W \cdot m^{-2}$
H_S	snow height	m
h	canopy height	m
h_e	elevation above sea level (a.s.l.)	m
h_s	snow depth	m
h_*	height of saltation layer	m
I	snow interception	mm
I_{max}	snow interception storage capacity	mm
i	inclination angle	°
i_{lim}	limiting inclination angle	35°
J	julian day	
j	empirical factor for rock temperature	$K \cdot W^{-1} \cdot m^2$
k	recession factor	0.12 ($T > 0$°C) and 0.05 ($T < 0$ °C)
k_E	dimensionless shape coefficient	0.01
k	von Karman constant	0.35
L_v	latent heat of vaporization	$J \cdot kg^{-1}$
L_m	melt unload of intercepted snow	$kg \cdot m^{-2}$
LAI	leaf area index	$m^2 \cdot m^{-2}$
l	vertical ozone layer thickness	m
l_s	sublimation/resublimation heat of snow (at –5 °C)	$2.838 \cdot 10^6 J \cdot kg^{-1}$
λ_t	thermal conductivity of the atmosphere	$0.024 J \cdot m^{-1} \cdot s^{-1} \cdot K^{-1}$
M	energy potentially available for melt	$W \cdot m^{-2}$
M_a	molecular mass of dry air	$28.97 kg \cdot kmol^{-1}$
M_W	molecular weight of water	$0.018 kg \cdot mole^{-1}$
M_{SWE}	gravitationally transported snow	mm
MQ	mean discharge	mm
m	relative optical path length	m
m_{sp}	snow particle mass	kg
m_r	increase factor for radiative fluxes	
N_u	Nusselt number	
ν	kinematic viscosity of air	$1.3 \cdot 10^{-5} m^2 \cdot s^{-1}$
P	precipitation	mm
P_{tot}	total precipitation	mm
p	atmospheric pressure	hPa
		3.14159
Q	radiation balance	$W \cdot m^{-2}$
$Q_{l\uparrow}$	longwave emission from the snow surface	$W \cdot m^{-2}$
$Q_{l\downarrow}$	longwave radiation	$W \cdot m^{-2}$
$Q_{lc\downarrow}$	longwave radiation at the ground of the canopy	$W \cdot m^{-2}$
$Q_{s\downarrow}$	solar radiation	$W \cdot m^{-2}$
$Q_{sc\downarrow}$	solar radiation at the ground of the canopy	$W \cdot m^{-2}$
Q_{cs}	sublimation loss rate	mm

Q_s	horizontal mass transport rates of saltation	$kg \cdot (m \cdot s)^{-1}$
Q_t	horizontal mass transport rates of turbulent suspension	$kg \cdot (m \cdot s)^{-1}$
Q_v	sublimation rate of transported snow particles	$kg \cdot m \cdot s)^{-1}$
R	universal gas constant	$8.313\ J \cdot mole^{-1} \cdot K^{-1}$
R_c	dimensionless scaling parameter	$0.8\ s \cdot m^{-1}$
R_d	gas constant for dry air	$287\ J \cdot K^{-1} \cdot kg^{-1}$
R_e	Reynolds number	
RH	relative humidity in the open	%
RH_c	relative humidity inside a forest canopy	%
RWT	correlation coefficient for turbulent mixing	
r	radius of an ice sphere	$500 \cdot 10\text{–}6$ m
ρ_a	density of dry air	$kg \cdot m^{-3}$
ρ_s	density of snow	$kg \cdot m^{-3}$
ρ_i	density of ice (at 0 °C)	$916.7\ kg \cdot m^{-3}$
ρ_v	saturation density of water vapour	$kg \cdot m^{-3}$
ρ_w	density of water	$1025\ kg \cdot m^{-3}$
S_h	Sherwood number	
$S_{f/t}$	ratio of forward scattering to total scattering	
SH	specific humidity	
SH_s	specific humidity for saturation conditions	
SR_{abs}	solar radiation absorbed by a snow particle	$W \cdot m^{-2}$
SS	sunshine duration	h
σ	Stefan Boltzmann constant	$5.67 \cdot 10^{-8}\ W \cdot m^{-2} \cdot K^{-4}$
T_a	air temperature (2 m)	K
T_{a005}	air temperature (0.05 m)	K
T_c	canopy air temperature	K
T_s	snow surface temperature	K
T_{s0}	snow temperature (a the ground)	K
T_{s20}	snow surface temperature (at 0.2 m)	K
T_{s40}	snow surface temperature (at 0.4 m)	K
T_{s60}	snow surface temperature (at 0.6 m)	K
T_{mean}	mean daily air temperature	K
T_r	temperature of rocks	K
T_w	wet temperature	K
T_+	temperature between air temperature and rocks	K
T_{mean}	mean weekly temperature	K
t	local time in hours	h
dt	time between two model timesteps	s
tf	empirical temperature factor for melt	$0.00021\ h^{-1} \cdot °C^{-1}$
δt	temperature offset	K
τ_a	aerosol transmittance	
τ_{aa}	diffuse scattered direct radiation transmittance	
τ_{as}	diffuse aerosol scattering transmittance	
τ_g	trace gases transmittance	
τ_r	Rayleigh scattering transmittance	
τ_{rr}	diffuse Rayleigh scattering transmittance	
τ_w	water vapour transmittance	
τ_o	ozone scattering transmittance	
θ_z	solar zenith angle	radian

ψ_a	sublimation loss rate coefficient	s^{-1}
v	clear sky atmospheric visibility	25000 m
W	wind speed	$m \cdot s^{-1}$
W_{max}	maximum wind speed	$m \cdot s^{-1}$
W_c	wind speed inside the canopy	$m \cdot s^{-1}$
WD	wind direction	degree
w	precipitable water	mm
x	West–East horizontal coordinate in the domain	m
x^*	horizontal coordinate in a reference frame	m
y	North–South horizontal coordinate in the domain	m
z	height above ground	m
z_t	upper limit of turbulent suspension layer	m
ω	hour angle	radian
w_0	single scattering albedo	

References

ANDERSON, E.A. (1973): National Weather Service River Forecast System – Snow Accumulation and Ablation Model. NOAA Tech. Memo. NWS, US. Dept. of Commerce, Silver Spring.

ANDERTON, S.P., WHITE, S.M. and ALVERA, B. (2004): Evaluation of Spatial Variability in Snow Water Equivalent for a High Mountain Catchment. In: *Hydrol. Process., 18,* 435–453.

ÅNGSTRÖM, A. (1916): Über die Gegenstrahlung der Atmosphäre. In: *Meteorolog. Zeitschr., 33,* 529–538.

ANKER, D. and ROBERTS, D. (1999): The lost explorer. Simon and Schuster, New York.

ANQUETIN, S., GUILBAUD, C. and CHOLLET, J. (1998): The formation and destruction of inversion layers within a deep valley. In: *J. Appl. Meteor., 37,* 1547–1560.

ARNOLD, N.S., WILLIS, I.C., SHARP, M.J., RICHARDS, K.S. and LAWSON, W.J. (1996): A distributed surface energy–balance model for a small valley glacier. I. Development and testing for Haut Glacier d'Arolla, Valais, Switzerland. In: *J. Glaciol., 42(140),* 77–89.

BARNETT, T.B., ADAM, J.C. and LETTENMAIER, D.P. (2005): Potential impacts of a warming climate on water availability in snow–dominated regions. In: *Nature, 438(17),* doi: 10.1038/nature04141, 303–309.

BARTELT, P. and LEHNING, M. (2002): A physical SNOWPACK model for the Swiss avalanche warning. Part I: numerical model. In: *Cold Reg. Sci. Tech., 35,* 123–145.

BAYFORKLIM (1996): Klimaatlas von Bayern. Bayerischer Klimaforschungsverbund (BayFORKLIM).

BERGSTRÖM, S. (1992): The HBV model – its structure and applications. SMHI Reports RH, No. 4, Norrköping.

BERNHARDT, M., ZÄNGL, G., LISTON, G.E., STRASSER, U. and MAUSER, W. (2008a): Using wind fields from a high resolution atmospheric model for simulating snow dynamics in mountainous terrain. In: *Hydrol. Process.* (in press).

BERNHARDT, M., STRASSER, U., LISTON, G.E. and MAUSER, W. (2008b): High resolution modelling of snow transport in complex terrain using simulated wind fields. In: *The Cryosphere Discuss.*, (accepted).

BEVEN, K.J. and FREER, J. (2001): Equifinality, data assimilation, and uncertainty estimation in mechanistic modelling of complex environmental systems. In: *J. Hydrol., 249,* 11–29.

BEVEN, K.J. and BINLEY, A.M. (1992): The future of distributed models: model calibration and uncertainty prediction. In: *Hydrol. Process., 6,* 279–298.

BINTANJA, R. (1996): The parameterization of shortwave and longwave radiative fluxes for use in zonally averaged climate models. In: *J. Clim., 9,* 439–454.

BIRD, R.E. and HULSTROM, R.L. (1981): A simplified clear sky model for direct and diffuse insolation on horizontal surfaces. Tech. Rep. SERI/TR–642–761, Solar Research Institute. Golden, Colorado.

BLÖSCHL, G. (1999): Scaling issues in snow hydrology. In: *Hydrol. Process., 13(14–15),* 2149–2175.

BLÖSCHL, G. (1996): Scale and Scaling in Hydrology. Wiener Mitteilungen „Wasser, Abwasser, Gewässer", Bd. 132. Technische Universität Wien, Institut für Hydraulik, Gewässerkunde und Wasserwirtschaft, Wien.

BLÖSCHL, G. and SIVAPALAN, M. (1995): Scale issues in hydrological modelling – a review. In: *Hydrol. Process., 9,* 251–290.

BOLZ, H. (1949): Die Abhängigkeit der infraroten Gegenstrahlung von der Bewölkung. In: *Z. f. Met., 3,* 97–100.

BOURGES, B. (1985): Improvement in solar declination computation. In: *Solar energy, 35,* 367–369.

BOWLING, L.C., POMEROY, J.W. and LETTENMAIER, D.P. (2004): Parameterization of Blowing–Snow Sublimation in a Macroscale Hydrology Model. In: *J. Hydrometeor., 5(5),* 745–762.

BREILING, M. and CHARAMZA, P. (1999): The impact of global warming on winter tourism and skiing: a regionalised model for Austrian snow conditions. In: *Reg. Env. Change, 1(1),* 4–14.

BROCK, B.W. and ARNOLD, N.S. (2000): A spreadsheet–based (Microsoft Excel) point surface energy balance model for glacier and snow melt studies. In: *Earth Surf. Proc. Landf., 25,* 649–658.

BROCK, B.W., WILLIS, I.C., SHARP, M.J. and ARNOLD, N.S. (2000): Modelling seasonal and spatial variations in the surface energy balance of Haut Glacier d'Arolla, Switzerland. In: *Ann. Glaciol., 31,* 53–62.

BRONSTERT, A., NIEHOFF, D. and BÜRGER, G. (2002): Effects of climate and land–use change on storm runoff generation: present knowledge and modelling capabilities. In: *Hydrol. Process., 16,* 509–529.

BRUBAKER, K., RANGO, A. and KUSTAS, W. (1996): Incorporating radiation inputs into the Snowmelt Runoff Model. In: *Hydrol. Process., 10,* 1329–1343.

BRULAND, O., LISTON, G.E., VONK, J., SAND, K. and KILLINGTVEIT, A. (2004): Modelling the snow distribution at two high arctic sites at Svalbard, Norway, and at an Alpine site in central Norway. In: *Nord. Hydrol., 35,* 191–208.

BRUN E., DAVID P., SUDUL M. and BRUNOT G. (1992): A numerical model to simulate snow–cover stratigraphy for operational avalanche forecasting. In: *J. Glaciol, 38(128),* 13–22.

BRUNT, D. (1932): Notes on radiation in the atmosphere. In: *Quart. J. Royal Meteor. Soc., 58,* 389–420.

BRUTSAERT, W. (1975): On a derivable formula for long–wave radiation from clear skies. In: *Water Resour. Res., 11,* 742–744.

BUCK, A.L. (1981): New equations for computing vapour pressure and enhancement factor. In: *J. Appl. Meteor., 20,* 1527–1532.

BÜRKI, R., ELSASSER, H. and ABEGG, B. (2003): Climate change – Impacts on Tourism Industry in Mountain Areas. 1st Conference on Climate Change and Tourism. Djerba, April 2003.

BUISHAND, T.A. and BRANDSMA, T. (2001): Multisite simulation of daily precipitation and temperature in the Rhine Basin by nearest–neighbour resampling. In: *Water Resour. Res., 37(11),* 2761–2776.

BURLANDO, P., PELLICCIOTTI, F. and STRASSER, U. (2002): Modelling Mountainous Water Systems Between Learning and Speculating, Looking for Challenges. In: *Nord. Hydrol., 33(1),* 47–74.

CAMPBELL, C., JAMIESON, B. and HÄGELI, P. (2004): Small–scale mapping of snow stability: If not, why not? (http://www.schulich.ucalgary.ca/Civil/Avalanche/Papers/SmallScaleStabilityMapping_Nov04.pdf).

CHEN, J.M., RICH, P.M., GOWER, S.T., NORMAN, J.M. and PLUMMER, S. (1997): Leaf area index of boreal forests: Theory, techniques, and measurements. In: *J. Geophys. Res., 102,* 29429–29443.

CIONCO, R.M. (1978): Analysis of canopy index value for various canopy densities. In: *Bound. Lay. Met., 15,* 81–93.

CLINE, D., ELDER, K. and BALES, R. (1998): Scale effects in a distributed snow water equivalence and snowmelt model for mountain basins. In: *Hydrol. Process., 12,* 1527–1536.

CORRIPIO, J.G. (2003): Vectorial algebra algorithms for calculating terrain parameters from DEMs and solar radiation modelling in mountainous terrain. In: *Int. J. Geogr. Inf. Sci., 17(1),* 1–23.

DERY, S.J. and YAU, M.K. (2001): Simulation of blowing snow in the Canadian Arctic using a double–moment model. In: *Bound. Lay. Met., 99,* 297–316.

DGJ (2003): Deutsches Gewässerkundliches Jahrbuch, Donaugebiet, 1999. Bayer. Landesamt für Wasserwirtschaft (ed.), München.

DURAND, Y., GUYOMARC'H, G., MÉRINDOL, L. and CORRIPIO, J.G. (2004): 2D numerical modelling of surface wind velocity and associated snowdrift effects over complex mountainous topography. In: *Ann. Glaciol., 38,* 59–70.

DUROT, K. (1999): Modélisation hydrologique distribuée du bassin versant nivo-pluvial de Sarennes. Validation des données d'entrée et dévelopement d'un module de fonte nivale sous forêt. Ph.D. dissertation, LTHE, 332 p, Grenoble.

DYER, A.J. (1974): A Review of Flux-Profile Relationships. In: *Bound. Lay. Met., 7,* 363–372.

EBERHARDT, R. (2002): Ökologisch orientierte Modellbildung zur potenziellen Schneedeckenverteilung im Biosphärenreservat Berchtesgaden. In: Nationalpark Berchtesgaden (ed.): Forschung im Nationalpark Berchtesgaden von 1978 bis 2001, Forschungsbericht, 46, 95–108.

ELSASSER, H. and MESSERLI, B. (2001): The Vulnerability of the Snow Industry in the Swiss Alps. In: *Mountain Res. and Dev., 21(4),* 335–339.

ENDERS, G. (1994): Theoretische Topoklimatologie, Forschungsbericht 1, Nationalpark Berchtesgaden.

ESCHER-VETTER, H. (2000): Modelling meltwater production with a distributed energy balance method and runoff using a linear reservoir approach – results from Vernagtferner, Oetztal Alps, for the ablation seasons 1992 to 1995. In: *Z. Gletscherkd. Glazialgeol., 36(1),* 19–50.

ESSERY, R.L.H., POMEROY, J.W., PARVIANEN, J. and STORCK, P. (2003): Sublimation of snow from boreal forests in a climate model. In: *J. Clim., 16,* 1855–1864.

ESSERY, R.L.H., LI, L. and POMEROY, J.W. (1999): A Distributed Model of Blowing Snow over Complex Terrain. In: *Hydrol. Process., 13,* 2423–2438.

ETCHEVERS, P., MARTIN, E., BROWN, R., FIERZ, C., LEJEUNE, Y., BAZILE, E., BOONE, A., DAI, Y.-J., ESSERY, R.L.H., FERNANDEZ, A., GUSEV, Y., JORDAN, R., KOREN, V., KOWALCZYK, E., NASONOVA, N.O., PYLES, R.D., SCHLOSSER, A., SHMAKIN, A.B., SMIRNOVA, T.G., STRASSER, U., VERSEGHY, D., YAMAZAKI, T. and YANG, Z.-L. (2004): Validation of the surface energy budget simulated by several snow models (SnowMIP project). Papers from the International Symposium on Snow and Avalanches, June 2003, Davos, Switzerland. In: *Ann. Glaciol., 38,* 150–158.

ETCHEVERS, P., MARTIN, E., BROWN, R., FIERZ, C., LEJEUNE, Y., BAZILE, E., BOONE, A., DAI, Y.-J., ESSERY, R.L.H., FERNANDEZ, A., GUSEV, Y., JORDAN, R., KOREN, V., KOWALCZYK, E., PYLES, R.D., SCHLOSSER, A., SHMAKIN, A.B., SMIRNOVA, T.G., STRASSER, U., VERSEGHY, D., YAMAZAKI, T. and YANG, Z.-L. (2002): SnowMIP, an intercomparison of snow models: first results. Proceedings of the International Snow Science Workshop (ISSW 2002), October 2002, Penticton, British Columbia, Canada.

ETCHEVERS, P., DURAND, Y., HABETS, F., MARTIN, E. and NOILHAN, J. (2001a): Impact of spatial resolution on the hydrological simulation of the Durance high alpine catchment. In: *Ann. Glaciol., 32,* 87–92.

ETCHEVERS, P., HABETS, F. and GOLAZ, C. (2001b): Simulation of the water budget and the river flows of the Rhône basin from 1981 to 1994. In: *J. Hydrol., 224,* 60–85.

FERGUSON, R.I. (1999): Snowmelt Runoff Models. In: *Prog. Phys. Geogr., 23(2),* 205–227.

FLEAGLE, R.G. and BUSINGER, J.A. (1980): An Introduction to Atmospheric Physics. 432 p, Academic Press.

FOKEN, T. (2003): Angewandte Meteorologie – Mikrometeorologische Methoden. Springer Verlag, ISBN 3540003223, 289 p, Berlin.

FRANZ, H.P. (1995): Das Geographische Informationssystem der Nationalparkverwaltung Berchtesgaden: Entwicklung, Stand, Trends. In: *Salzb. Geogr. Mat., 22,* 72–78.

FRAUENFELDER, R., ZEMP, M., HAEBERLI, W. and HOELZLE, M. (2005): Worldwide glacier mass balance measurements: trends and first results of an extraordinary year in Central Europe. In: *Ice and Climate News, 6,* 9–10.

GARNIER, B. and OHMURA, A. (1968): A method of calculating the direct shortwave radiation income on slopes. In: *J. Appl. Meteorol., 7,* 796–800.

GEORGES, C. and KASER, G. (2002): Ventilated and unventilated air temperature measurements for glacier-climate studies on a tropical high mountain site. In: *J. Geophys. Res., 107(D24),* doi:10.1029/2002JD002503.

GREENE, E.M., LISTON, G.E. and PIELKE, R.A. (1999): Simulation of above treeline snowdrift formation using a numerical snow-transport model. In: *Cold Reg. Sci. Tech., 30,* 135–144.

GRELL, G.A., DUDHIA, J. and STAUFFER, D.R. (1995): Tech. Note NCAR/TN-398+STR, Boulder, Colorado.

GREUELL, W. and BÖHM, R. (1998): 2 m temperatures along melting mid-latitude glaciers, and implications for the sensitivity of the mass balance to variations in temperature. In: *J. Glaciol., 44*(146), 9–20.

GREUELL, W., KNAP, W. and SMEETS, P. (1997): Elevational changes in meteorological variables along a midlatitude glacier during summer. In: *J. Geophys. Res., 102(22),* 25941–25954.

GRUBER, S. (2007): A mass-conserving fast algorithm to parameterize gravitational transport and deposition using digital elevation models. In: *Water Resour. Res., 43,* W06412, doi:10.1029/2006WR004868.

GURTZ, J., ZAPPA, M., JASPER, K., LANG, H., VERBUNT, M., BARDOUX, A. and VITVAR, T. (2003): A comparative study in modelling runoff and its components in two mountainous catchments. In: *Hydrol. Process., 17,* 297–311.

GURTZ, J., BALTENSWEILER, A. and LANG, H. (1999): Spatially distributed hydrotope-based modelling of evapotranspiration and runoff in mountainous basins. In: *Hydrol. Process., 13,* 2751–276.

HAEBERLI, W. (1994): Accelerated glacier and permafrost changes in the Alps. In: Beniston, M. (ed.): *Mountain Environments in Changing Climates,* Routledge, 91–107.

HAEBERLI, W., WEGMANN, M. and VONDER MÜHLL, D. (1997): Slope stability problems related to glacier shrinkage and permafrost degradation in the Alps. In: *Eclogae Geologicae Helvetiae, 90,* 407–414.

HAEBERLI W. and BENISTON M. (1998): Climate change and its impact on glaciers and permafrost in the Alps. In: *Ambio, 27,* 258–265.

HAMMEL, K. and KENNEL, M. (2001): Charakterisierung und Analyse der Wasserverfügbarkeit und des Wasserhaushaltes von Waldstandorten in Bayern mit dem Simulationsmodell BROOK90. Forstliche Forschungsberichte, 185, 148 p, Munich.

HANK, T. and MAUSER, W. (2007): Modelling the Impact of Climate Change on the Phenological Development of Forest Trees in the Upper Danube Basin. In: Proceedings of the International Congress „Managing Alpine Future – strategies for sustainability in times of change", Innsbruck.

HARDY, J., MELLOH, R., ROBINSON, P. and JORDAN, R. (2000): Incorporating effects of forest litter in a snow process model. In: *Hydrol. Process., 14(18),* 3227–3237.

HARTMANN, M.D., BARON, J.S., LAMMERS, R.B., CLINE, D.W., BAND, L.E., LISTON, G.E. and TAGUE, C. (1999): Simulations of snow distribution and hydrology in a mountain basin. In: *Water Resour. Res. 35(5),* 1587–1603.

HASHOLT, B., LISTON, G.E. and KNUDSEN, N.T. (2003): Snow-distribution modelling in the Ammassalik region, south east Greenland. In: *Nord. Hydrol., 34,* 1–16.

HECHT, P. and HUBER, D. (2002): Potentielle Verbreitung von Pflanzenarten im Nationalpark Berchtesgaden, ermittelt mit Hilfe eines Geographischen Informationssystems. Abschlussbericht. Im Auftrag der Nationalparkverwaltung Berchtesgaden.

HEDSTROM, N.R. and POMEROY, J.W. (1998): Measurements and modelling of snow interception in the boreal forest. In: *Hydrol. Process., 12,* 1611–1625.

HELLSTRÖM, R.Å. (2000): Forest cover algorithms for estimating meteorological forcing in a numerical snow model. In: *Hydrol. Process., 14,* 3239–3256.

HIEMSTRA, C.A., LISTON, G.E. and REINERS, W.A. (2006): Observing, modelling, and validating snow redistribution by wind in a Wyoming upper treeline landscape. In: *Ecol. Mod., 197,* 35–51.

HIEMSTRA, C.A., LISTON, G.E. and REINERS, W.A. (2002): Snow redistribution by wind and interactions with vegetation at upper treeline in the Medicine Bow Mountains, Wyoming, USA. In: *Arct., Antarct. and Alp. Res., 34,* 262–273.

HOCK, R. (1998): Modelling glacier melt and discharge. Zuer. Geogr. Schriften, 70, 126 p, Department of Geography, ETH Zurich.

HOOD, E., WILLIAMS, M. and CLINE, D. (1999): Sublimation from a seasonal snowpack at a continental, mid-latitude alpine site. In: *Hydrol. Process., 13,* 1781–1797.

ICIMOD (2000a): Inventory of Glaciers, Glacial Lakes and Glacial Lake Outburst Floods – Monitoring and Early Warning Systems in the Hindu Kush Himalayan Region – Bhutan. In: Mool et al. (eds.) 2001: International Centre for Integrated Mountain Development, 227 p, Kathmandu.

ICIMOD (2000b): Inventory of Glaciers, Glacial Lakes and Glacial Lake Outburst Floods – Monitoring and Early Warning Systems in the Hindu Kush Himalayan Region – Nepal. In: Mool et al. (eds.) 2001: International Centre for Integrated Mountain Development, 363 p, Kathmandu.

IPCC (2007): IPCC Fourth Assessment Report. Working group I: The Physical Science Basis of Climate Change (http://ipcc-wg1.ucar.edu/wg1/wg1-report.html).

IQBAL, M. (1983): An introduction to solar radiation. Academic Press, 390 p, London.

JORDAN, R. (1991): A one-dimensional temperature model for a snow cover, technical documentation for SNTHERM.89. Special Report 91-16, U.S. Army Cold Regions Research and Engineering Laboratory, Hanover, N.H.

KÄÄB, A., REYNOLDS, J.M. and HAEBERLI, W. (2005): Glacier and permafrost hazards in high mountains. In: Huber, U.M., Bugmann, H.K.M. and Reasoner, M.A. (eds.): Global Change and Mountain Regions (A State of Knowledge Overview). Advances in Global Change Research, Springer, Dordrecht, 225–234.

KASER, G. (1983): Über die Verdunstung auf dem Hintereisferner. In: *Ztschr. f. Gletschk. Glazialgeol., 19(2),* 149–162.

KASTEN, F. (1966): A New Table and Approximation Formula for the Relative Optical Air Mass. In: *Arch. Meteor. Geophys. Bioklimatol., Ser. B, 14,* 206–223.

KATTELMANN, R. and ELDER, K. (1991): Hydrologic characteristics and water balance of an alpine basin in the Sierra Nevada. In: *Water Resour. Res., 27,* 1553–1562.

KING, J.C., ANDERSON, P.S. and Mann, G.W. (2001): The seasonal cycle of sublimation at Halley, Antarctica. In: *J. Glaciol., 47,* 1–8.

KLEMES, V. (1990): The modelling of mountain hydrology: the ultimate challenge. In: *IAHS Publ., 190,* 29–43.

KLIWA (2007): Klimaveränderung und Konsequenzen für die Wasserwirtschaft. Fachvorträge des KLIWA-Symposiums am 25.–26. September (Stuttgart). Kliwa-Berichte, 10, 256 p, Karlsruhe.

KLOK, E.J. and OERLEMANS, J. (2002): Model study of the spatial distribution of the energy and mass balance of the Morteratschgletscher, Switzerland. In: *J. Glaciol., 48(163),* 505–518.

KOBOLTSCHNIG, G. (2007): Mehrfachvalidierung hydrologischer Eis- und Schneeschmelzmodelle in hochalpinen, vergletscherten Einzugsgebieten. Dissertation, University of Natural Resources and Applied Life Sciences, Vienna.

KÖNIG, M., WINTHER, J.-G., ISAKSSON, E. (2001): MEASURING SNOW and GLACIER ICE PROPERTIES from Satellite. In: *Reviews of Geophysics, 39(1),* 1–27.

KONDRATYEV, K.Y. (1969): Radiative heat exchange in the Atmosphere. 411 p, Academic Press. New York, San Francisco, London.

KONNERT, V. (2006): pers. comm.

KONNERT, V. (2004): Standortkarte Nationalpark Berchtesgaden. Forschungsbericht 49, Nationalpark Berchtesgaden.

KUCHMENT, L.S. and GELFAN, A.N. (1996): The determination of the snowmelt rate and the meltwater outflow from a snowpack for modelling river runoff generation. In: *J. Hydrol., 179,* 23–36.

KUHN, M. (2003): Redistribution of snow and glacier mass balance from a hydrometeorological model. In: *J. Hydrol., 282,* 95–103.

KUHN, M. (1995): The mass balance of very small glaciers. In: *Z. Gletscherkd. Glazialgeol., 31,* 171–179.

KUHN, M. (1993a): Zwei Gletscher im Karwendelgebirge. In: *Z. Gletscherkd. Glazialgeol., 29(1),* 85–92.

KUHN, M. (1993b): Der Mieminger Schneeferner, ein Beispiel eines lawinenernährten Kargletschers. In: *Z. Gletscherkd. Glazialgeol., 29(2),* 153–171.

LANG, H. (1985): Höhenabhängigkeit der Niederschläge. In: Der Niederschlag in der Schweiz. Beiträge zur Geologie und Hydrologie der Schweiz, 31, 149–157, Bern.

LANG, H. (1981): Is evaporation an important component in high alpine hydrology? In: *Nord. Hydrol., 12,* 217–224.

LEE, L.W. (1975): Sublimation of snow in a turbulent atmosphere. Ph.D. dissertation, 162 p, University of Wyoming.

LEHNING, M., VÖLKSCH, I., GUSTAVSON, D., NGUYEN, T.A., STÄHLI, M. and ZAPPA, M. (2006): ALPINE3D: a detailed model of mountain surface processes and its application to snow hydrology. In: *Hydrol. Process., 20,* 2111–2128.

LEHNING, M., BARTELT, P., BROWN, B., FIERZ, C. and SATYAWALI, P. (2002a): A physical SNOWPACK model for the Swiss avalanche warning. Part II. Snow microstructure. In: *Cold Reg. Sci. Tech., 35,* 147–167.

LEHNING, M., BARTELT, P., BROWN, B. and FIERZ, C. (2002b): A physical SNOWPACK model for the Swiss avalanche warning. Part III: meteorological forcing, thin layer formation and evaluation. In: *Cold Reg. Sci. Tech., 35,* 169–184.

LEHNING, M., DOORSCHOT, J. and RADERSCHALL, N. (2000): Combining snowdrift and snowpack models to estimate snow loadings in avalanche slopes. In: Hjorth-Hansen, E., Holland, D., Loset, S. and Norem, H. (eds.): Snow Engineering, 113–122, Balkema.

LINK, T. and MARKS, D. (1999a): Point simulation of seasonal snow cover dynamics beneath boreal forest canopies. In: *J. Geophys. Res, 104(22),* 27841–27857.

LINK, T. and MARKS, D. (1999b): Distributed simulation of snowcover mass- and energy-balance in the boreal forest. In: *Hydrol. Process., 13,* 2439–2452.

LISTON, G.E. (2004): Representing subgrid snow cover heterogeneities in regional and global models. In: *J. Climate, 17(6),* 1381–1397.

LISTON, G.E. and ELDER, K. (2006): A Distributed Snow-Evolution Modeling System (SnowModel). In: *J. Hydromet., 7(2),* 217–234.

LISTON, G.E. and STURM, M. (2004): The role of winter sublimation in the Arctic moisture budget. In: *Nord. Hydrol., 35(4),* 325–334.

LISTON, G.E. and STURM, M. (2002): Winter precipitation patterns in Arctic Alaska Determined from a Blowing-Snow Model and Snow-Depth Observations. In: *J. Hydromet., 3,* 646–659.

Liston, G.E. and STURM, M. (1998): A snow-transport model for complex terrain. In: *J. Hydromet., 3,* 646–659.

LISTON, G.E., HAEHNEL, R.B., STURM, M., HIEMSTRA, C.A., BEREZOVSKAYA, S. and TABLER, R.D. (2007): Simulating complex snow distributions in windy environments using SnowTran-3D. In: *J. Glaciol., 53(181),* 241–256.

LISTON, G.E., WINTHER, J.G., BRULAND, O., ELVEHOY, H., SAND, K. and KARLOF, L. (2000): Snow and blue-ice distribution patterns on the coastal Antarctic Ice Sheet. In: *Antarc. Sci., 12,* 69–79.

LUDWIG, R., MAUSER, W., NIEMEYER, S., COLGAN, A., STOLZ, R., ESCHER-VETTER, H., KUHN, M., REICHSTEIN, M., TENHUNEN, J., KRAUS, A., LUDWIG, M., BARTH, M. and HENNICKER R. (2003): Web-based modelling of energy, water and matter fluxes to support decision making in mesoscale catchments – The integrative perspective of GLOWA-Danube. In: *Phys. Chem. Earth, 28,* 621–634.

MACHGUTH, H., PAUL, F., HÖLZLE, M. and HAEBERLI, W. (2007): Distributed glacier mass balance modelling as important component of modern multi-level glacier monitoring. In: *Ann. Glaciol., 43(9),* 335–43.

MANNSTEIN, H. (1985): The interpretation of albedo measurements on a snow covered slope. In: *Arch. Meteorol. Geophys. Bioklimatol., Ser. B, 36,* 73–81.

MARKE, T. and MAUSER, W. (2008): SCALMET – a tool for bidirectional coupling of climate models with physically-based simulations of land surface processes. In: Abstracts of the International Congress Managing Alpine Future – strategies for sustainability in times of change 2007, Innsbruck, Austria.

MARKS, D., DOZIER, J. and DAVIS, R.E. (1992): Climate and energy exchange at the snow surface in the alpine region of the Sierra Nevada: 1. Meteorological measurements and monitoring. In: *Water Resour. Res., 17,* 609–627.

MARSH, P. (1999): Snowcover formation and melt: recent advances and future prospects. In: *Hydrol. Process., 13,* 2117–2134.

MARTIN, E. and LEJEUNE, Y. (1998): Turbulent fluxes above the snow surface. In: *Ann. Glaciol., 26,* 179–183.

MARTINEC, J., RANGO, A. and ROBERTS, R. (1998): Snowmelt runoff model (SRM) user's manual. Edited by M.F. Baumgartner and G.M Apfl. Geographica Bernensia, P 35, 84 p, University of Bern.

MAUSER, W. (2003): GLOWA-Danube: Integrative hydrologische Modellentwicklung zur Entscheidungsunterstützung beim Einzugsgebietsmanagement. In: *Peterm. Geogr. Mitt., 147(6),* 68–75.

MAUSER, W. and BACH, H. (2008): PROMET – a Physical Hydrological Model to Study the Impact of Climate Change on the Water Flows of Medium Sized, Complex Watersheds. In: *J. Hydrol.* (submitted).

MAUSER, W. and LUDWIG, R. (2002): GLOWA-DANUBE – A research concept to develop integrative techniques, scenarios and strategies regarding global changes of the water cycle. In: Beniston, M. (ed.) (2002): Climatic Change: Implications for the Hydrological Cycle and for Water Management. Advances in Global Change Research. 10. Kluwer Academic Publishers, Dordrecht and Boston, 171–188.

MAUSER, W. and SCHÄDLICH, S. (1998): Modelling the spatial distribution of evapotranspiration on different scales using remote sensing data. In: *J. Hydrol., 212–213,* 250–267.

MAUSER, W., PRASCH, M. and STRASSER, U. (2007): Physically based Modelling of Climate Change Impact on Snow Cover Dynamics in Alpine Regions using a Stochastic Weather Generator. Proceedings of the International Congress on Modelling and Simulation MODSIM07, 2007, Christchurch, New Zealand.

MELLOH, R.A., HARDY, J.P., DAVIS, R.E. and ROBINSON, P.B. (2001): Spectral albedo/reflectance of littered forest snow during the melt season. In: *Hydrol. Process., 15,* 3409–3422.

MENZEL, L. and BÜRGER, G. (2002): Climate change scenarios and runoff response in the Mulde catchment (Southern Elbe, Germany). In: *J. Hydrol., 267,* 53–64.

MICHLMAYR, G., HOLZMANN, H., KOBOLTSCHNIG, G., LEHNING, M., MOTT, R., SCHÖNER, W. and ZAPPA, M. (2008): Validation of the physically based mountain surface processes model ALPINE3D for glacier mass balance and glacier hydrology studies at Goldbergkees, Austria. In: Hydrol. Process. (in print).

MIDDLEKOOP, H., DAAMEN, K., GELLENS, D., GRABS, W., KWADIJK, J.C.J., LANG, H., PARMET, B.W.A.H., SCHÄDLER, B., SCHULLA, J. and WILKE, K. (2001): Impact of climate change on hydrological regimes and water resources management in the Rhine basin. In: *Clim. Change, 62,* 105–128.

MONTESI, J., ELDER, K., SCHMIDT, R.A. and DAVIS, R.E. (2004): Sublimation of intercepted snow within a subalpine forest canopy at two elevations. In: *J. Hydrometeor., 5,* 763–773.

MPI (2007): http://www.mpimet.mpg.de/wissenschaft/ueberblick/atmosphaere-im-erdsystem/ regionale-klimamodellierung/remo-uba/abbildungen.html.

MUERTH, M. and MAUSER, W. (2007): Implications of a regional scale soil temperature and freezing model in the Upper Danube Basin based on Climate Change scenarios. In: Proceedings of the International Congress „Managing Alpine Future – strategies for sustainability in times of change", Innsbruck.

NIEMELÄ, S., RÄISÄNEN, P. and SAVIJÄRVI, H. (2001): Comparison of surface radiative flux parameterizations. Part II: Shortwave radiation. In: *Atmos. Res., 58,* 141–154.

NUNEZ, M. (1980): The calculation of solar and net radiation in mountainous terrain (Risdon, Tasmania). In: *J. Biogeogr., 7(2),* 173–186.

OBLED, CH. (1971): Modèle mathématique de la fusion nivale. Ph.D. dissertation, Institut de mécanique de Grenoble, 170 p, Grenoble.

OERLEMANS, J. and GRISOGONO, B. (2002): Glacier winds and parameterisation of the related surface heat fluxes. In: *Tellus, 54,* 440–452.

OERLEMANS, J., ANDERSON B., HUBBARD, A., HUYBRECHTS P., JOHANNESSON, T., KNAP, W.H., SCHMEITS, M., STROEVEN, A.P., VAN DE WAL, R.S.W., WALLINGA, J. and ZUO, Z. (1998): Modelling the response of glaciers to climate warming. In: *Clim. Dyn., 14,* 267–274.

OHMURA, A. (2001): Physical basis for the temperature-based melt-index method. In: *J. Appl. Meteor., 40,* 753–761.

PELLICCIOTTI, F., BROCK, B., STRASSER, U., BURLANDO, P., FUNK, M. and CORRIPIO, J.G. (2005): An enhanced temperature-index glacier melt model including shortwave radiation balance: development and testing for Haut Glacier d'Arolla, Switzerland. In: *J. Glaciol., 51(175),* 573–587.

PLUESS, C. and MAZZONI, R. (1994): The Role of Turbulent Heat Fluxes in Energy Balance of High Alpine Snow Cover. In: *Nord. Hydrol., 25,* 25–28.

POMEROY, J.W. (1997): Application of a Distributed Blowing Snow Model to the Arctic. In: *Hydrol. Process., 11,* 1451–1464.

POMEROY, J.W. and ESSERY, R.L.H. (1999): Turbulent fluxes during blowing snow: field test of model sublimation prediction. In: *Hydrol. Process., 13,* 2963–2975.

POMEROY, J.W. and DION, K. (1996): Winter radiation extinction and refection in a boreal pine canopy: measurements and modelling. In: *Hydrol. Process., 10,* 1591–1608.

POMEROY, J.W. and GRAY, D.M. (1995): Snowcover: Accumulation, Relocation, and Management. National Hydrology Research Institute, Saskatoon, Canada. NHRI Science Report, 7, 144 p, Saskatoon.

POMEROY, J.W. and SCHMIDT, R.A. (1993): The Use of Fractal Geometry in Modelling Intercepted Snow Accumulation and Sublimation. Proceedings of the 50th Annual Eastern Snow Conference, Honour Paper, 1–10.

POMEROY, J.W., GRAY, D.M., HEDSTROM, N. and JANOWICZ, J.R. (2002): Prediction of seasonal snow accumulation in cold climate forests. In: *Hydrol. Process., 16,* 3543–3558.

PRASAD, R., TARBOTON, D.G., LISTON, G.E., LUCE, C.H. and SEYFRIED, M.S. (2001): Testing a blowing snow model against distributed snow measurements at Upper Sheep Creek, Idaho. In: *Water Resour. Res., 37(5),* 1341–1356.

POMEROY, J.W., GRAY, D.M., SHOOK, K.R., TOTH, B., ESSERY, R.L.H., PIETRONIERO, A. and HEDSTROM, N. (1998): An evaluation of snow accumulation and ablation for land surface modelling. In: *Hydrol. Process. 12,* 2339–2367.

POMEROY, J.W., GRAY, D.M. and LANDINE, P.G. (1993): The Prairie Blowing Snow Model – characteristics, validation, operation. In: *J. Hydrol., 144,* 165–192.

PRASCH, M., STRASSER, U. and MAUSER, W. (2008): Validation of a physically based snow model for the simulation of the accumulation and ablation of snow (ESCIMO). In: Strasser, U. and Vogel M. (eds.) (2008): Proceedings of the Alpine*Snow*Workshop (www.alpinesnowworkshop.org), Munich, October 5–6, 2006, Germany. Forschungsbericht 53, Nationalpark Berchtesgaden.

PRATA, A.J. (1996): A new long-wave formula for estimating downward clear-sky radiation at the surface. In: *Quat. J. Roy. Met. Soc., 122,* 1127–1151.

PURVES, R.S., BARTON, J.S., MACKANESS, W.A. and SUGDEN, D.E. (1998): The development of a rule-based spatial model of wind transport and deposition of snow. In: *Ann. Glaciol., 26,* 197–202.

QUINN, P., BEVEN, K., CHEVALLIER, P. and PLANCHON, O. (1991): The prediction of hillslope paths for distributed hydrological modelling using digital terrain models. In: *Hydrol. Process., 5,* 59–79.

RACSKO, P., SZEIDL, L. and SEMENOV, M.A. (1991): A serial approach to local stochastic weather models. In: *Ecol. Mod., 57,* 27–41.

RICHARDSON, C.W. (1981): Stochastic simulation of daily precipitation, temperature and solar radiation. In: *Water Resour. Res., 17,* 182–190.

ROBINSON, N. (ed.) (1966): Solar radiation, American Elsevier, New York.

ROHRER, M.B. (1992): Die Schneedecke im Schweizer Alpenraum und ihre Modellierung. Zuer. Geogr. Schriften, 49, 178 p, Zurich.

RYAN, B.C. (1977): A mathematical model for diagnosis and prediction of surface wind in mountainous terrain. In: *J. Appl. Meteor., 16(6),* 571–584.

SCHMIDT, R.A. (1991): Sublimation of snow intercepted by an artificial conifer. In: *Agric. For. Meteor., 54,* 1–27.

SCHMIDT, R.A. (1972): Sublimation of wind-transported snow – a model. U.S. Forest Service. Research Paper 90, Rocky Mountain Forest and Range Experiment Station.

SCHUG, J. and KUHN, M. (2003): Der Schwarzmilzferner in den Allgäuer Alpen: Massenbilanz und klimatische Bedingungen. In: *Z. Gletscherkd. Glazialgeol., 29,* 55–74.

SCHULZ, K., BEVEN, K. and HUWE, B. (1999): Equifinality and the problem of robust calibration in nitrogen budget simulations. In: *Soil Sci. Soc. Am. J., 63,* 1934–1941.

SCHWARB, M. (2001): The Alpine Precipitation Climate. Zuericher Klima-Schriften 80. Institut für Klimaforschung der ETH, Zurich.

SEMENOV, M.A., BROOKS, R.J., BARROW, E.M. and RICHARDSON, C.W. (1998): Comparison of WGEN and LARS-WG stochastic weather generators for diverse climates. In: *Clim. Res.,10,* 95–107.

SEVRUK, B. (1985): Systematischer Niederschlagsmessfehler in der Schweiz. In: Sevruk, B. (ed.): Der Niederschlag in der Schweiz. Geogr. V. Bern, 65–75.

Slater, A.G., Schlosser, C.A., Desborough, C.E., Pitman, A.J., Henderson-Sellers, A., Robock, A., Vinnikow, K.Y., Mitchell, K. and the PILPS 2(d) contributors (2001): The representation of Snow in Land-surface Schemes; Results from the PILPS 2(d). In: *J. Hydrometeor., 2,* 7–25.

SMEETS, C.J., DYNKERKE, P.G. and VUGTS, H.F. (1998): Turbulence Characteristics of the Stable Boundary Layer over a Mid-Latitude Glacier. Part 1: A Combination of Katabatic and Large-Scale Forcing. In: *Bound. Lay. Met., 87,* 117–145.

SOVILLA, B. (2004): Field experiments and numerical modelling of mass entrainment and deposition in snow avalanches. Ph.D. dissertation, ETH Zurich.

SPENCER, J.W. (1971): Fourier series representation of the position of the sun. In: *Search, 2(5),* 171-201.

STRASSER, U. (2002): AMUNDSEN – a Scientific Modelling Tool for the Interpolation, Simulation and Visualization of Variable Fields in Alpine Terrain. ICE Bulletin (http://www.slf.ch/ice/ice-bulletin-2002.html).

STRASSER, U. (1998): Regionalisierung des Wasserkreislaufs mit einem SVAT-Modell am Beispiel des Weser-Einzugsgebiets. Münchener Geographische Abhandlungen, Reihe B, Band 28, 146 p, ISBN 3 925 308 88 1, Munich.

STRASSER, U. and MAUSER, W. (2006): Using a stochastic climate generator for simulating global warming effects on the water resources in a mountain basin. Geophysical Research Abstracts, abstracts of the European Geosciences Union General Assembly 2006, Vienna, Austria.

STRASSER, U. and ETCHEVERS, P. (2005): Simulation of Daily Discharges for the Upper Durance Catchment (French Alps) Using Subgrid Parameterization for Topography and a Forest Canopy Climate Model. In: *Hydrol. Process., 19,* 2361–2373.

STRASSER, U. and MAUSER, W. (2001): Modelling the Spatial and Temporal Variations of the Water Balance for the Weser Catchment 1965–1994. In: *J. Hydrol., 254(1–4),* 199–214.

STRASSER, U., FRANZ, H. and MAUSER, W. (2008a): Distributed modelling of snow processes in the Berchtesgaden National Park (Germany). In: Strasser, U. and Vogel M. (eds.) (2008): Proceedings of the Alpine*Snow*Workshop (www.alpinesnowworkshop.org), Munich, October 5–6, 2006, Germany. Forschungsbericht 53, Nationalpark Berchtesgaden.

STRASSER, U., WEBER, M. and PRASCH, M. (2008b): How important is glacier melt in the water balance? In: Abstracts of the Alpine Glaciological Meeting 2008, Chamonix, France.

STRASSER, U., BERNHARDT, M., WEBER, M., LISTON, G.E., and MAUSER, W. (2008c): Is snow sublimation important in the alpine water balance? In: *The Cryosphere, 2,* 53–66.

STRASSER, U., CORRIPIO, J.G., BROCK, B., PELLICCIOTTI, F., BURLANDO, P. and FUNK, M. (2004): Spatial and Temporal Variability of Meteorological Variables at Haut Glacier d'Arolla (Switzerland) During the Ablation Season 2001: Measurements and Simulations. In: *J. Geophys. Res., 109(3),* doi:10.1029/2003JD003973.

STRASSER, U., ETCHEVERS, P. and LEJEUNE, Y. (2002): Intercomparison of two Snow Models with Different Complexity Using Data from an Alpine Site. In: *Nord. Hydrol., 33(1),* 15–26.

TASCHNER, S., STRASSER, U. and MAUSER, W. (1998): Modelling the Spatial Snow Water Equivalent Using NOAA-AVHRR Data for Mesoscale Catchments. SPIE Proc. Series, Proceedings of the EUROPTO 1998 Conference, Barcelona.

TEPFENHART, M., MAUSER, W. and SIEBEL, F. (2008): Climate change and the competition among ski areas for day tourists. In: Strasser, U. and Vogel M. (eds.) (2008): Proceedings of the Alpine*Snow*Workshop (www.alpinesnowworkshop.org), Munich, October 5–6, 2006, Germany. Forschungsbericht 53, Nationalpark Berchtesgaden.

THORPE, A.D. and MASON, B.J. (1966): The evaporation of ice spheres and ice crystals. In: *Brit. J. Appl. Phys., 17,* 541–548.

TOMS-EP (2001): Total Ozone Mapping Spectrometer-Earth Probe data sets. (http://toms.gsfc.nasa.gov/eptoms/ep.html).

TRIBBECK, M.J., GURNEY, R., MORRIS, E.M. and PEARSON, D.W.C. (2004): A new Snow-SVAT to simulate the accumulation and ablation of seasonal snow beneath a forest canopy. In: *J. Glaciol., 50*(169), 171–182.

U.S. ARMY CORPS OF ENGINEERS (1956): Snow Hydrology, U.S. Army Corps of Engineers. North Pacific Division, 437 p, Portland, Oregon.

VERBUNT, M. and GURTZ, J. (2004): The use of hydrological models for socio-economic decisions in view of climate change. In: Herrmann, A. and Schröder, U. (eds.): Studies in Mountain Hydrology, IHB/HWRP-reports, H 2, Koblenz.

WEBER, M. (2008): A parameterization for the turbulent fluxes over melting surfaces derived from eddy correlation measurements. In: Strasser, U. and Vogel M. (eds.) (2008): Proceedings of the Alpine*Snow*Workshop (www.alpinesnowworkshop.org), Munich, October 5–6, 2006, Germany. Forschungsbericht 53, Nationalpark Berchtesgaden.

WEBER, M. (2007): pers. comm.

WEBER, M. (2005): Mikrometeorologische Prozesse bei der Ablation eines Alpengletschers. Ph.D. dissertation, Institute for Meteorology and Geophysics, University of Innsbruck.

WEBER, M., PRASCH, M., STRASSER, U. and MAUSER, W. (2008): Embedded grid–modelling of 506 glaciers in the upper Danube basin. In: Geophysical Research Abstracts, abstracts of the European Geosciences Union General Assembly 2008, Vienna, Austria.

WEBER, M., PRASCH, M., STRASSER, U. and KUHN, M. (2007): Embedded sub– grid modelling of glacier change within the DANUBIA–system. Poster for the International Workshop „Glaciers in Watershed and Global Hydrology", 2007, Obergurgl.

WINKLER, D. (2005): Der Blaueisgletscher in Not. Berchtesgadener Heimatkalender 2006, 45–48.

WINSTRAL, A. and MARKS, D (2002): Simulating wind fields and snow redistribution using terrain based parameters to model snow accumulation and melt over semi–arid mountain catchment. In: *Hydrol. Process., 16,* 3585–3603.

WMO (1986): Intercomparison of models of snowmelt runoff. Operational Hydrology Report 23. World Meteorological Organization, Geneva.

WOOD, E.F., SIVAPALAN, M., BEVEN, K. and BAND, L. (1988): Effects of spatial variability and scale with implications to hydrologic modeling. In: *J. Hydrol., 102,* 29–47.

WWF (2005): An Overview of Glaciers, Glacier Retreat, and Subsequent Impacts in Nepal, India and China. World Wildlife Fund Nepal Programme, March 2005, 70 p.

XUE, M., DROEGEMEIER, K.K. and WONG, V. (2000): The advanced regional prediction system (ARPS) – a multi–scale nonhydrostatic atmospheric simulation model. Part I: Model dynamics and verification. In: *Meteor. Atmos. Phys., 75,* 161–193.

YATES, D., GANGOPADHAY, S., RAJAGOPALAN, B. and STRZEPEK, K. (2003): A technique for generating regional climate scenarios using a nearest neighbour algorithm. In: *Water Resour. Res., 39(7),* SWC 7–1 – 7–14.

YOUNG, K.C. (1994): A mulitvariate chain model for simulating climatic parameters with daily data. In: *J. Appl. Meteor., 33,* 661–671.

ZAPPA, M., POS, F., STRASSER, U., WARMERDAM, P. and GURTZ, J. (2003): Seasonal water balance of an Alpine catchment as evaluated by different methods for spatially distributed snowmelt modelling. In: *Nordic Hydrol., 34(3),* 179–202.

ZIERL, B. and BUGMAN, H. (2005): Global change impacts on hydrological processes in Alpine catchments. In: *Wat. Res. Res., 41,* 1–13.

Last access to all websites named in this report: 25 March 2008.

Roald Amundsen

(1872 - 1928)

Photo: Steve Nicklas, NOAA Photo Library Collection[54]
(copyright license in the public domain).

Roald Amundsen (1872–1928) was a Norwegian polar explorer and the first person to reach the South Pole. He served as first mate on the *Belgica* (1897–1899) in an expedition to the Antarctic, and he commanded the *Gjøa* which was the first ship to complete the route through the Northwest Passage (1903–1906). He then purchased Fridtjof Nansen's *Fram* and prepared to drift toward the North Pole and then finish the journey by sledge. The news that R.E. Peary had anticipated him in reaching the North Pole caused Amundsen to consider going South. He was successful in reaching the South Pole on 14 December 1911, just 35 days before R.F. Scott. In the course of these expeditions, he added much valuable scientific and geological information to the knowledge of Antarctica. In 1918, back in the arctic regions, Amundsen set out to negotiate the Northeast Passage with the *Maud.* After two winters he arrived at *Nome,* as first after N.A.E. Nordenskjöld to sail along the whole northern coast of Europe and Asia. Amundsen then turned to air exploration. In 1925, he and L. Ellsworth failed to complete a flight across the North Pole, but the next year in the dirigible *Norge,* built and piloted by U. Nobile, they succeeded in flying over the pole and the hitherto unexplored regions of the Arctic Ocean north of Alaska. Yet in 1928, Amundsen set out on a rescue attempt that cost him his life.

[15] http://www.nationalpark-berchtesgaden.bayern.de/

In der Reihe der Forschungsberichte sind erschienen:

Nr. 1 G. Enders
Theoretische Topoklimatologie

Nr. 2 R. Bochter, W. Neuerburg, W. Zech
Humus und Humusschwund im Gebirge

Nr. 3 Herausgeber Nationalparkverwaltung
Zur Situation der Greifvögel in den Alpen

Nr. 4 G. Enders
Kartenteil: Theoretische Topoklimatologie

Nr. 5 O. Siebeck
Der Königssee – Eine limnologische Projektstudie

Nr. 6 R. Bochter
Böden naturnaher Bergwaldstandorte auf carbonatreichen Substraten

Nr. 7 Herausgeber Nationalparkverwaltung
Der Funtensee

Nr. 8 H. Schmid-Heckel
Zur Kenntnis der Pilze in den Nördlichen Kalkalpen

Nr. 9 R. Boller
Diplopoden als Streuzersetzer in einem Lärchenwald

Nr. 10 E. Langenscheidt
Höhlen und ihre Sedimente in den Berchtesgadener Alpen

Nr. 11 Herausgeber Nationalparkverwaltung
Das Bärenseminar

Nr. 12 H. Knott
Geschichte der Salinenwälder von Berchtesgaden

Nr. 13 A. Manghabati
Einfluß des Tourismus auf die Hochgebirgslandschaft

Nr. 14 A. Spiegel-Schmidt
Alte Forschungs- und Reiseberichte aus dem Berchtesgadener Land

Nr. 15 H. Schmid-Heckel
Pilze in den Berchtesgadener Alpen

Nr. 16 L. Spandau
Angewandte Ökosystemforschung im Nationalpark Berchtesgaden

Nr. 17 W. Berberich
Das Raum-Zeit-System des Rotfuchses

Nr. 18 U. Mäck, R. Bögel
Untersuchungen zur Ethologie und Raumnutzung von Gänse- und Bartgeier

Nr. 19 B. Dittrich, U. Hermsdorf
Biomonitoring in Waldökosystemen

Nr. 20 F. Kral, H. Rall
Wälder – Geschichte, Zustand, Planung

Nr. 21 M. Klein, R.-D. Negele, E. Leuner, E. Bohl, R. Leyerer
Fischbiologie des Königssees: Fischereibiologie und Parasitologie

Nr. 22 W. Traunspurger
Fischbiologie des Königssees: Nahrungsangebot und Nahrungswahl, Bd. I

Nr. 23 R. Gerstmeier
Fischbiologie des Königssees: Nahrungsangebot und Nahrungswahl, Bd. II

Nr. 24 W. Hecht, M. Förster, F. Pirchner
R. Hoffmann, P. Scheinert, H. Rettenbeck
Fischbiologie des Königssees: Ökologisch-genetische Untersuchungen am Seesaibling und Gesundheitsstatus der Fische

Nr. 25 G. Hofmann
Klimatologie des Alpenparks

Nr. 26 K. Rösch
Einfluß der Beweidung auf die Vegetation des Bergwaldes

Nr. 27 H. Remmert, P. G. Rey, W. R. Siegfried,
W. Scherzinger, S. Klaus
Kleinstmögliche Populationen bei Tieren

Nr. 28 B. Müller, W. Berberich, A. David
Schalenwild

Nr. 29 J. Köppel
Beitrag der Vegetation zum Wasserhaushalt

Nr. 30 H. Zierl et al.
Die Wallfahrt über das Steinerne Meer

Nr. 31 P. Pechacek
Spechte im Nationalpark Berchtesgaden

Nr. 32 Chr. Dommermuth
Beschleunigte Massenabtragung im Jennergebiet

Nr. 33 R. Bögel
Untersuchungen zur Flugbiologie und Habitatnutzung von Gänsegeiern

Nr. 34 A. Schuster
Singvögel im Biosphärenreservat Berchtesgaden

Nr. 35 M. Höper
Moose – Arten, Bioindikation, Ökologie

Nr. 36 T. Barthelmeß
Die saisonale Planktonsukzession im Königssee

Nr. 37 W. Lippert, S. Springer, H. Wunder
Die Farn- und Blütenpflanzen des Nationalparks

Nr. 38 G. Gödde
Die Holzbringung um den Königssee

Nr. 39 A. Stahr
Bodenkundliche Aspekte der Blaikenbildung auf Almen

Nr. 40 R. Braun
Die Geologie des Hohen Gölls

Nr. 41 F. Gloßner, R. Türk
Die Flechtengesellschaften im Nationalpark Berchtesgaden und dessen Vorfeld

Nr. 42 R. Türk, H. Wunder
Die Flechten des Nationalparks Berchtesgaden und angrenzender Gebiete

Nr. 43 V. Konnert, J. Siegrist
Waldentwicklung im Nationalpark Berchtesgaden von 1983 bis 1997

Nr. 44 S. Schmidtlein
Aufnahme von Vegetationsmustern auf Landschaftsebene

Nr. 45 U. Brendel, R. Eberhardt, K. Wiesmann-Eberhardt,
W. d'Oleire-Oltmanns
Der Leitfaden zum Schutz des Steinadlers in den Alpen

Nr. 46 Herausgeber Nationalparkverwaltung
Forschung im Nationalpark Berchtesgaden von 1978 bis 2001

Nr. 47 Th. Rettelbach
Die Antagonisten des Buchdruckers im Nationalpark Berchtesgaden

Nr. 48 P. Pechacek, W. d'Oleire-Oltmanns
International Woodpecker Symposium

Nr. 49 V. Konnert
Standortkarte Nationalpark Berchtesgaden

Nr. 50 K. Fischer
Geomorphologie der Berchtesgadener Alpen

Nr. 51 R. Gerecke, H. Franz
Quellen im Nationalpark Berchtesgaden

Nr. 52 Thomas Kudernatsch
Auswirkungen des Klimawandels auf alpine Pflanzengesellschaften im Nationalpark Berchtesgaden

Nr. 53 U. Strasser
Proceedings Alpine*Snow*Workshop

Nr. 54 C. Küfmann
Flugstaubeintrag und Bodenbildung im Karst der Nördlichen Kalkalpen

Zu beziehen über die Nationalparkverwaltung Berchtesgaden, Doktorberg 6, D-83471 Berchtesgaden